(Not so) Hyperbolic models for complex flows
Applications to environmental flows

Nina Aguillon[1,2,3] & Jacques Sainte-Marie[1,2,3]

1- Sorbonne Université, Laboratoire J.-L. Lions, F-75005, Paris
2- Inria, EPC ANGE, Rocquencourt - B.P. 105, F78153 Le Chesnay cedex
3- CNRS, UMR 7598, Laboratoire Jacques-Louis Lions, F-75005, Paris

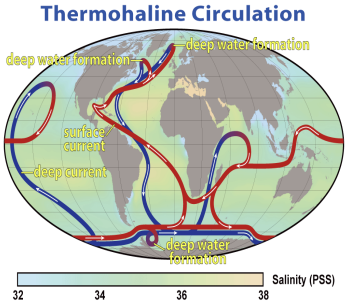

January 15, 2024[1]

[1]N'hésitez pas à me contacter si vous trouvez des erreurs ou coquilles, ou si vous avez des suggestions d'améliorations : Jacques.Sainte-Marie@inria.fr.

Abstract

In this course, we study models describing free surface complex flows in the context of natural hazards, oceanography and marine energies. The models encountered in this domain are mainly hyperbolic systems or at least with hyperbolic features.

The objectives of the course are threefold

- to present a rigorous derivation process of models in fluid mechanics,
- to describe typical analysis techniques for hyperbolic systems,
- to build numerical schemes for the approximation of the considered systems.

The document is organized as follows. First, starting from the free surface incompressible Navier-Stokes equations, we give a rigourous derivation of the most popular model for geophysical flows i.e. the Saint-Venant system. Then we study its main properties. The numerical techniques allowing to discretize the Saint-Venant system are then presented. A special emphasis is given to the treatment of the source terms (topography, friction,...). In the last part of the document we present more complex models where unfortunately few rigourous results are available. In such situations, we propose guidelines for the analysis and the discretization of the systems.

WARNING This document present several aspects of modelling in fluid mechanics that will be tackled during the course. The course mainly focus on chapters II and IV of this document.

Contents

Chapter I

Models & numerical methods for hydraulic energies

1 Presentation

The modeling, the analysis and the simulation of geophysical flows are complex and challenging topics and these issues have been given an extensive coverage in applied research and engineering.

Among all the aspects of geosciences, we mainly focus on gravity driven flows arising in many situations as

- hazardous flows (flooding, rogue waves, landslides...),
- oceanography (long term simulations, impact of climate change...)
- sustainable energies (hydrodynamics-biology coupling, biofuel production, marine energies...),
- risk management and land-use planning (morphodynamic evolutions, early warning systems...)

As suggested by the preceding list, this is an extensive field. For these multi-scale and multi-physics systems, the difficulty is often to isolate a reduced-size problem for which mathematical modeling and simulation can bring significant benefits.

There exists a strong demand from scientists and engineers for models and numerical tools able to simulate not only the water depth and the velocity field but also the distribution and evolution of external quantities such as pollutants or biological species and the interaction between flows and structures (seashores, erosion processes...). One of the key point of the researches is to answer this demand by the development of efficient, robust and validated models and numerical tools.

Models and numerical tools resulting from these researches are useful for the analysis of past events, for the understanding of complex phenomena and for risk management...

1.1 Motivations and context

The geophysical flows studied here are free surface flows and the fluid considered, usually water, can be considered as incompressible (even if the density variations of water is a key point in oceanography e.g. thermohaline stratification). But because of the free surface, we will see that the encountered models share common points with compressible fluids.

The modeling, the analysis and the simulation of free surface flows are complex and challenging topics and this issue has been given extensive coverage in applied research and engineering. The difficulties arising in geophysics are threefold:

- The models and equations encountered in fluid mechanics (typically the Navier-Stokes equations) are complex to analyse and solve.
- This first feature is reinforced by the fact that the considered phenomena often take place over large domains and time periods e.g. coastal erosion, elevation of temperature in oceans, propagation of a tsunami,...
- Last but not least, these problems are multiphysics with strong couplings and nonlinearities.

Efficient models and numerical tools are necessary to tackle these problems. Notice that the objective of the continuous and discrete models is not only to represent known events but to be predictive. This means they should have a wide range of validity.

Geophysical flows are often described by conservation laws and characterized by

- non smooth solutions (shock waves, dam break) to capture,
- drying and flooding leading to topological modifications of the fluid domain.

Since the above mentioned difficulties can hardly be satisfied using finite elements type discretizations, finite volume schemes [59, 24, 85, 62] are often used for their numerical approximation.

1.2 Models of reduced complexity

The difficulties coming from the discretization and the simulation of the Navier-Stokes equations and also from the scales – in space and time – of the considered problems in geophysics encourage to look for models of reduced complexity but able to represent complex flows.

The Saint-Venant system [17] is a well known and efficient approximation of the Navier-Stokes system for Shallow Water flows. For a large class of problems (dam break, flooding, debris flow) the Saint-Venant system is a very good approximation of the Navier-Stokes system [126, 57, 98, 55, 28]. For decades, it has been the cornerstone of river hydrodynamics studies. Even if the Saint-Venant system is widely used, its discretization remains tricky and this is an important part of this course.

The derivation of the Saint-Venant system from the Navier-Stokes equations is based on two main approximations – valid because of the Shallow Water assumption – namely

- the pressure is hydrostatic or equivalently the vertical acceleration of the fluid can be neglected compared to the gravitational effects,
- the horizontal fluid velocity is well approximated by its vertical mean.

The Saint-Venant system is able to tackle a wide range of physical problems but considering density-stratified flows or flows with large friction coefficients, with significant water depth, with complex rheology, the two preceding approximations become questionable. So in the last chapter of this document, we present models of minimal complexity – especially at the computational point of view – adapted to flows where these two assumptions are no more valid. Of course these new models mean more accurate approximations of the Navier-Stokes system but also more sophisticated models than the Saint-Venant system.

1.3 Need for efficient numerical techniques

Because of the free surface, the models considered in this course and approximating the Navier-Stokes equations often have the form of conservation laws with source terms and exhibit hyperbolic features. Finite volume techniques are mostly used for their discretization but the numerical approximation of the proposed models is not in the scope of this course.

Notice when starting from a model that has not been derived using a rigorous process or that does not satisfy any stability property such as entropy inequality it is, of course, not possible to derive an efficient numerical technique for its discretization.

In numerical analysis of PDEs, the stability properties of a scheme are often examined or proved when the discretization in space Δx and the discretization in time δt tend to 0. Unfortunately, in oceanography, the considered scales in space and time require to work with rather coarse meshes. And hence, the derivation of efficient numerical schemes with $\Delta x, \Delta t = \mathcal{O}5(1)$ is a big challenge.

2 Eulerian/lagrangian description

There are two ways to describe fluid flows

- The Lagrangian description is one in which individual fluid particles are tracked, it consists in following each fluid particle along its displacement in the fluid domain.

  In the Lagrangian description of a fluid flow, individual fluid particles are "marked" and their positions, velocities, ... are described as a function of time. The physical laws, such as Newton's laws and conservation of mass and energy, apply directly to each particle. If there were only a few particles to consider, as in a high school physics experiment with billiard balls, the Lagrangian description would be desirable. However, fluid flow is a continuum phenomenon, at least down to the molecular level. It is not possible to track each "particle" in a complex flow field. Thus, the Lagrangian description is rarely used in fluid mechanics.

- In the Eulerian description, a control volume is defined, within which fluid flow properties of interest are expressed as fields.

  In the Eulerian description, individual fluid particles are not identified. Instead, a control volume is defined, pressure, velocity, acceleration, and all other flow properties are described as fields within the control volume. In other words, each property is expressed as a function of space and time. In the Eulerian description of fluid flow, one is not concerned about the location or velocity of any particular particle, but rather about the velocity, acceleration, ... of whatever particle happens to be at a particular location of interest at a particular time. Since fluid flow is a continuum phenomenon, the Eulerian description is usually preferred in fluid mechanics. Note, however, that the physical laws such as Newton's laws and the laws of conservation of mass and energy apply directly to particles in a Lagrangian description. Hence, some translation or reformulation of these laws is required for use with an Eulerian description.

Hence, the model and equations presented all along this document are written using the eulerian description.

The correlation between these two descriptions can be illustrated as follows. Let us consider an Eulerian velocity field $\underline{u} = \underline{u}(x,y,z,t) \in \mathscr{R}^3$, then the Lagrangian trajectory of a particle $M(t) = (x(t),y(t),z(t))^T \in \mathscr{R}^3$ in the fluid is defined by

$$\frac{dM}{dt} = \underline{u}(M(t),t). \tag{I.1}$$

Starting from the Eulerian description $u = u(x,y,z,t)$, one can recover the Lagrangian description by solving the ordinary differential equation (I.1). The flow of the trajectories is the function

$$\begin{aligned} \varphi_t : \mathscr{R}^3 &\longrightarrow \mathscr{R}^3 \\ M(t_0) &\mapsto M(t) \end{aligned}$$

The calculus of derivation in the Lagrangian/Eulerian approach are related by the following formula. For any scalar quantity f we have

$$\hat{f} = \frac{Df}{Dt} = \frac{d}{dt} f(M(t),t) = \frac{\partial f}{\partial t} + \underline{u}.\nabla f,$$

with the notation

$$\nabla f = \begin{pmatrix} \frac{\partial f}{\partial x} \\ \frac{\partial f}{\partial y} \\ \frac{\partial f}{\partial z} \end{pmatrix}.$$

The quantity

$$\frac{Df}{Dt},$$

is denoted the particle derivative of f or the material derivative.

3 The incompressible Navier-Stokes system

When dealing with free surface geophysical flows, the assumption of shallow water or shallow layer is often helpful, unfortunately these assumptions can hardly be justified using the Euler system. For this reason, we start from the Navier-Stokes equations and the Euler system will be obtained as the limit of the Navier-Stokes system when the viscosity and bottom friction vanish.

3.1 The Navier-Stokes equations

The Navier-Stokes equations restricted to two dimensions have the following general formulation

$$\frac{\partial u}{\partial x}+\frac{\partial w}{\partial z}=0, \tag{I.2}$$

$$\rho_0\left(\frac{\partial u}{\partial t}+u\frac{\partial u}{\partial x}+w\frac{\partial u}{\partial z}\right)+\frac{\partial p}{\partial x}=\frac{\partial \sigma_{xx}}{\partial x}+\frac{\partial \sigma_{xz}}{\partial z}, \tag{I.3}$$

$$\rho_0\left(\frac{\partial w}{\partial t}+u\frac{\partial w}{\partial x}+w\frac{\partial w}{\partial z}\right)+\frac{\partial p}{\partial z}=-\rho_0 g+\frac{\partial \sigma_{zx}}{\partial x}+\frac{\partial \sigma_{zz}}{\partial z}, \tag{I.4}$$

where ρ_0 is the fluid density – supposed constant here – and the z axis represents the vertical direction. We consider this system for

$$t>t_0, \quad x\in\mathscr{R}, \quad z_b(x,t)\leqslant z\leqslant \eta(x,t),$$

where $\eta(x,t)$ represents the free surface elevation, $\mathbf{u}=(u,w)^T$ is the fluid velocity with u (resp. w) the horizontal (resp. vertical) component, g is the gravity constant and p the fluid pressure. The water depth is $H=\eta-z_b$, see Fig. I.1. We consider the bathymetry z_b can vary with respect to abscissa x and also with respect to time t. The system (I.2)-(I.4) will be completed by boundary conditions (paragraph 3.2) and initial conditions.

The chosen form of the viscosity tensor σ is symetric

$$\sigma_{xx}=2\mu\frac{\partial u}{\partial x}, \qquad \sigma_{xz}=\mu\left(\frac{\partial u}{\partial z}+\frac{\partial w}{\partial x}\right), \tag{I.5}$$

$$\sigma_{zz}=2\mu\frac{\partial w}{\partial z}, \qquad \sigma_{zx}=\mu\left(\frac{\partial u}{\partial z}+\frac{\partial w}{\partial x}\right), \tag{I.6}$$

with μ the viscosity that is supposed constant. For a more general form of the viscosity tensor, see Ref. [51, 87]. We define the total stress tensor σ_T

$$\sigma_T=-pI_d+\sigma.$$

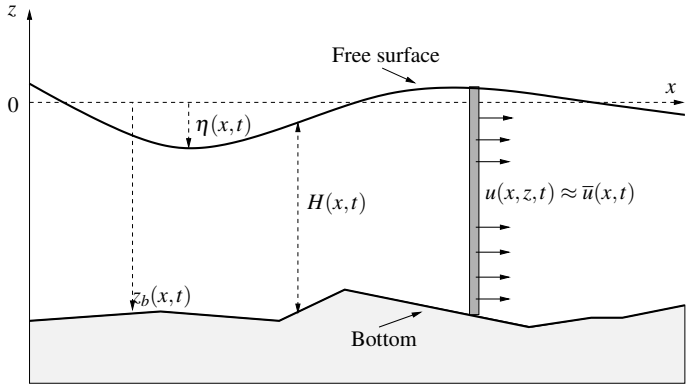

Figure I.1: Notations: water depth $H(x,t)$, free surface $\eta(x,t)$ and bottom $z_b(x,t)$.

As in Ref. [57], we introduce the indicator function for the fluid region

$$\varphi(x,z,t)=\begin{cases}1 & \text{for } z_b\leqslant z\leqslant\eta,\\ 0 & \text{otherwise.}\end{cases} \tag{I.7}$$

The fluid region is advected by the flow, which can be expressed, thanks to the incompressibility condition, by the relation

$$\frac{\partial \varphi}{\partial t}+\frac{\partial \varphi u}{\partial x}+\frac{\partial \varphi w}{\partial z}=0. \tag{I.8}$$

The solution φ of this equation takes the values 0 and 1 only but it may not be of the form (I.7) for all times. The analysis below is limited to the conditions where this form is preserved. For a more complete presentation of the Navier-Stokes system and its closure, the reader can refer to Ref. [89]. Notice that in the fluid domain, equation (I.8) reduces to the divergence free condition whereas accross the upper and lower boundaries it is equivalent to the kinematic boundary conditions defined in the following.

3.2 Boundary conditions

The system (I.2)-(I.4) is completed with boundary conditions. The outward and upward unit normals to the free surface $\mathbf{n}_s$ and to the bottom $\mathbf{n}_b$ are given by

$$\mathbf{n}_s = \frac{1}{\sqrt{1+\left(\frac{\partial \eta}{\partial x}\right)^2}} \begin{pmatrix} -\frac{\partial \eta}{\partial x} \\ 1 \end{pmatrix}, \quad \mathbf{n}_b = \frac{1}{\sqrt{1+\left(\frac{\partial z_b}{\partial x}\right)^2}} \begin{pmatrix} -\frac{\partial z_b}{\partial x} \\ 1 \end{pmatrix} \equiv \begin{pmatrix} -s_b \\ c_b \end{pmatrix},$$

respectively. We use here the same definition for $s_b(x)$ and $c_b(x)$ as in [28], $c_b(x) > 0$ is the cosine of the angle between $\mathbf{n}_b$ and the vertical.

3.2.1 At the free surface

Classically at the free surface we have the kinematic boundary condition

$$\frac{\partial \eta}{\partial t} + u_s \frac{\partial \eta}{\partial x} - w_s = 0, \tag{I.9}$$

where the subscript s denotes the value of the considered quantity at the free surface. The dynamical condition at the free surface takes into account the equilibrium with the atmospheric pressure. Considering the air viscosity is negligible, the continuity of stresses at the free boundary imposes

$$\sigma_T \mathbf{n}_s = -p^a(x, \eta(x,t), t)\mathbf{n}_s, \tag{I.10}$$

where $p^a = p^a(x,z,t)$ is a given function corresponding to the atmospheric pressure.

3.2.2 At the bottom

Since we consider the bottom can vary with respect to time t, the kinematic boundary condition is

$$\frac{\partial z_b}{\partial t} + u_b \frac{\partial z_b}{\partial x} - w_b = 0, \tag{I.11}$$

where the subscript b denotes the value of the considered quantity at the bottom and $(x,t) \mapsto z_b(x,t)$ is a given function. Notice that we shall consider

$$\frac{\partial z_b}{\partial t} = 0, \tag{I.12}$$

and therefore Eq. (I.11) reduces to a classical no-penetration condition

$$\mathbf{u}_b.\mathbf{n}_b = 0. \tag{I.13}$$

For the stresses at the bottom we consider a wall law under the form

$$\sigma_T \mathbf{n}_b - (\mathbf{n}_b.\sigma_T \mathbf{n}_b)\mathbf{n}_b = \kappa \mathbf{u}_b. \tag{I.14}$$

If $\kappa = \kappa(\mathbf{u}_b, H)$ is a positive constant then we recover a Navier friction condition as in [57]. For $\mathbf{t}_b = (c_b, s_b)^t$, using (I.13) we have

$$\mathbf{t}_b.\sigma_T \mathbf{n}_b = \kappa c_b u_b = \kappa \sqrt{1+\left(\frac{\partial z_b}{\partial x}\right)^2} u_b. \tag{I.15}$$

When the slope of the bottom is small, relation (I.15) writes

$$\mathbf{t}_b.\sigma_T \mathbf{n}_b = \kappa u_b. \tag{I.16}$$

3.3 Initial conditions

For the variables u, w, H and z_b initial conditions have to be prescribed.

3.4 Non negativity of the pressure

We also suppose in each point of the fluid region – including at the bottom – we have

$$p - p^a \geqslant 0.$$

The analysis below is restricted to this situation. Notice that in the case of hydrostatic Euler or Navier-Stokes equations (see paragraph 1.1, page 20) since we have

$$p - p^a = \rho_0 g(\eta - z),$$

this assumption reduces to the non-negativity of the water height H. Notice also that $p - p^a < 0$ means vaccum appears. Such a situation is not realistic for geophysical flows.

3.5 The incompressible Euler system

When the viscous and friction terms can be neglected, the Navier-Stokes system (I.2)-(I.4) can be replaced by the Euler system

$$\frac{\partial u}{\partial x} + \frac{\partial w}{\partial z} = 0, \tag{I.17}$$

$$\rho_0 \left(\frac{\partial u}{\partial t} + u\frac{\partial u}{\partial x} + w\frac{\partial u}{\partial z} \right) + \frac{\partial p}{\partial x} = 0, \tag{I.18}$$

$$\rho_0 \left(\frac{\partial w}{\partial t} + u\frac{\partial w}{\partial x} + w\frac{\partial w}{\partial z} \right) + \frac{\partial p}{\partial z} = -\rho_0 g, \tag{I.19}$$

that is also completed with initial and boundary conditions. described in paragraphs 3.2 and 3.3. Of course, for the Euler system only the kinematic boundary conditions (I.9) and (I.11) are necessary and the dynamical boundary condition (I.10) reduces to

$$p|_s = 0. \tag{I.20}$$

We recall the fondamental stability property related to the fact that the Euler system admits an energy

$$E = \rho_0 \frac{u^2 + w^2}{2} + \rho_0 g z, \tag{I.21}$$

leading to the following equation

$$\frac{\partial}{\partial t} \int_{z_b}^{\eta} (E + p^a)\, dz + \frac{\partial}{\partial x} \int_{z_b}^{\eta} u\big(E + p\big)\, dz = H \frac{\partial p^a}{\partial t} + (p|_b - p^a) \frac{\partial z_b}{\partial t}, \tag{I.22}$$

where $p|_b$ denotes the value at the bottom i.e. $p|_b = p(x, z_b(x), t)$.

Remark 1. Do not mix up the *compressible* and *incompressible* Euler system. Geophysical fluids such as water are usually incompressible BUT because of the free surface, the models used in practice (see the following paragraphs) share common features with models encountered in compressible fluid mechanics (gaz dynamics).

4 Origins of the Euler equation

Let us consider a fluid with density $\rho(x,y,z,t)$. A particle located in (x,y,z) at time t will have at time $t+dt$ the position

$$(x+udt, y+vdt, z+wdt).$$

The variation of density will be

$$d\rho = \rho(x+udt, y+vdt, z+wdt, t+dt) - \rho(x,y,z,t) = \frac{\partial \rho}{\partial x}udt + \frac{\partial \rho}{\partial y}vdt + \frac{\partial \rho}{\partial z}wdt + \frac{\partial \rho}{\partial t}dt. \quad \text{(I.23)}$$

And hence, considering the fluid density does not vary w.r.t. time t i.e. $d\rho = 0$ leads to

$$\frac{\partial \rho}{\partial t} + u\frac{\partial \rho}{\partial x} + v\frac{\partial \rho}{\partial y} + w\frac{\partial \rho}{\partial z} = 0. \quad \text{(I.24)}$$

Now let V be a volume of fluid with surface S. The mass contained in V is defined by

$$m = \iiint_V \rho dv,$$

and the mass flux leaving V is defined by

$$\oiint_S \rho \underline{u}.\underline{ds} = \oiint_S \rho \left(uds_x + vds_y + wds_z\right).$$

In absence of source or sink, the mass conservation within V reads

$$\frac{dm}{dt} = \iiint_V \frac{\partial \rho}{\partial t} dv + \oiint_S \rho \underline{u}.\underline{ds} = 0,$$

and using the Green-Ostrogradsky formula

$$\oiint_S \rho \underline{u}.\underline{ds} = \iiint_V \mathrm{div}(\rho \underline{u}) dv,$$

we obtain the local mass conservation equation

$$\frac{\partial \rho}{\partial t} + \frac{\partial (\rho u)}{\partial x} + \frac{\partial (\rho v)}{\partial y} + \frac{\partial (\rho w)}{\partial z} = 0. \quad \text{(I.25)}$$

Considering $\rho = \rho_0 = cst$, the preceding relation gives the divergence free condition

$$\frac{\partial u}{\partial x} + \frac{\partial v}{\partial y} + \frac{\partial w}{\partial z} = 0. \quad \text{(I.26)}$$

As in (I.23), a variation of velocity will be

$$d\underline{u} = \underline{u}(x+udt, y+vdt, z+wdt) - \underline{u}(x,y,z,t) = \frac{\partial \underline{u}}{\partial x}udt + \frac{\partial \underline{u}}{\partial y}vdt + \frac{\partial \underline{u}}{\partial z}wdt + \frac{\partial \underline{u}}{\partial t}dt,$$

leading to the following expression for the material acceleration

$$\underline{a} = \frac{\partial \underline{u}}{\partial t} + u\frac{\partial \underline{u}}{\partial x} + v\frac{\partial \underline{u}}{\partial y} + w\frac{\partial \underline{u}}{\partial z}. \quad \text{(I.27)}$$

Applying the fundamental law of dynamics we obtain

$$\rho \underline{a} - \mathrm{div}(\sigma_T) = \underline{g}, \quad \text{(I.28)}$$

where $\underline{g}$ is the external forcing due to the gravity effects and σ_T is the total stress tensor with

$$\sigma_T = -pI_d + \sigma.$$

In case of the "perfect fluid", one has $\sigma = 0$. Finally, when $\rho = \rho_0 = cst$, Eqs (I.26) and (I.28) give the incompressible Euler system.

5 Models for compressible fluids

Compressible flow (gas dynamics) is the branch of fluid mechanics that deals with flows having significant changes in fluid density. Gases, but not the liquids considerred here, display such behavior.

The study of gas dynamics is often associated with the flight of modern high-speed aircraft and atmospheric reentry of space-exploration vehicles; however, its origins lie with a simpler machine. At the beginning of the 19^{th} century, investigation into the behavior of fired bullets led to improvement in the accuracy and capabilities of guns and artillery. As the century progressed, inventors such as Gustaf de Laval advanced the field, while researchers such as Ernst Mach sought to understand the physical phenomenon involved through experimentation.

As mentioned above, on the contrary of gases, fluids are usually incompressible. But in geosciences, we will see that some media such as granular materials, multi-phase flows behave as compressible fluids.

The Euler equation for compressible gas dynamics is formed by the complete equation for conservation of mass, momentum and energy

$$\frac{\partial \rho}{\partial x} + \frac{\partial (\rho u)}{\partial x} + \frac{\partial (\rho w)}{\partial z} = 0, \tag{I.29}$$

$$\frac{\partial (\rho u)}{\partial t} + \frac{\partial (\rho u^2)}{\partial x} + \frac{\partial (\rho uw)}{\partial z} + \frac{\partial p}{\partial x} = 0, \tag{I.30}$$

$$\frac{\partial (\rho w)}{\partial t} + \frac{\partial (\rho uw)}{\partial x} + \frac{\partial (\rho w^2)}{\partial z} + \frac{\partial p}{\partial z} = 0, \tag{I.31}$$

$$\frac{\partial E}{\partial t} + \frac{\partial u(E+p)}{\partial x} + \frac{\partial w(E+p)}{\partial z} = 0, \tag{I.32}$$

where the pressure law $p(\rho, e)$ is given (for polytropic gas) by

$$p = (\gamma - 1)\rho e,$$

with $1 \leqslant \gamma \leqslant 3$ and

$$E = \frac{1}{2}\rho(u^2 + w^2) + \rho e,$$

is the total energy (kinetic energy + internal energy). The system (I.29)-(I.32) is a non-linear hyperbolic system which structure has been widely studied, see [24, 60].

6 Multi-phase flows

In practice and especially in geosciences, the fluid can be a mixture of several liquids, several species, several phases. A typical case is a landslide, in such a case the fluid may contain water, rock, sand. In other situations the fluid only contain a liquid but whose density can vary e.g. the water density is a function of temperature, salinity and in oceans the flows are stratified with respect to the fluid density.

When trying to model multi-phase flows, the first approcah consists in coupling models describing the behavior of each phase. This means we are able to define the interfaces of each phase and to calculate the interaction between them. Due to the scales of the considered phenomena, it is hardly possible. A simpler approach is to consider the fluid as a mixture and to derive equations governing the motion of only the mixture and not the distinct phases.

6.1 A typical two-phase model

More precisely, a two-phase fluid – each phase being immiscible and incompressible – with denstities and velocities $(\rho_i, \underline{u}_i)$, $i = 1, 2$ can be modeled by two conservation mass equations

$$\frac{\partial \rho_1 \varphi}{\partial t} + \frac{\partial (\rho_1 \varphi u_1)}{\partial x} + \frac{\partial (\rho_1 \varphi w_1)}{\partial z} = 0,$$

$$\frac{\partial \rho_2 (1-\varphi)}{\partial x} + \frac{\partial (\rho_2 (1-\varphi) u_2)}{\partial x} + \frac{\partial (\rho_2 (1-\varphi) w_2)}{\partial z} = 0,$$

where φ is the volumic fraction of the first component in the mixture. completed with momentum equations

$$\frac{\partial(\rho_1\varphi\underline{u}_1)}{\partial t}+(\underline{u}_1.\nabla)(\rho_1\varphi\underline{u}_1)+\nabla.\sigma_{2,1}=\rho_1\varphi\underline{g},$$

and

$$\frac{\partial\rho_2(1-\varphi)\underline{u}_2}{\partial t}+(\underline{u}_2.\nabla)(\rho_2(1-\varphi)\underline{u}_2)+\nabla.\sigma_{1,2}=\rho_2(1-\varphi)\underline{g}.$$

The quantities $\sigma_{1,2}$ and $\sigma_{2,1}$ denotes the stress tensor depending on the interaction between the two fluids. The definition $\sigma_{1,2}$ and $\sigma_{2,1}$ is often a very complex problem. In general, the system has to be completed with a closure relation adding a constraint on the two phases dynamics

$$F(\varphi,\sigma_{1,2},\sigma_{2,1})=0,$$

and ensuring the thermo-mechanical compatibility.

6.2 The Navier-Stokes system with variable density

In many situations such as lakes and estuarine waters, the geophysical water flows typically exhibit a significant density stratification related to vertical variations of temperature and chemical composition. In these water bodies effects related to small density gradients may strongly affect the hydrodynamics. Density stratification processes are therefore often important in environmental flows, and in particular they are a key feature in the biogeochemical mechanisms occurring in natural aquatic systems.

With the same notations as in paragraph 3.1, the system has the form:

$$\frac{\partial\rho}{\partial t}+\frac{\partial\rho u}{\partial x}+\frac{\partial\rho w}{\partial z}=0, \tag{I.33}$$

$$\frac{\partial\rho u}{\partial t}+\frac{\partial\rho u^2}{\partial x}+\frac{\partial\rho uw}{\partial z}+\frac{\partial p}{\partial x}=\frac{\partial\sigma_{xx}}{\partial x}+\frac{\partial\sigma_{xz}}{\partial z}, \tag{I.34}$$

$$\frac{\partial\rho w}{\partial t}+\frac{\partial\rho uw}{\partial x}+\frac{\partial\rho w^2}{\partial z}+\frac{\partial p}{\partial z}=-\rho g+\frac{\partial\sigma_{zx}}{\partial x}+\frac{\partial\sigma_{zz}}{\partial z}. \tag{I.35}$$

The fluid density $\rho(x,t)$ is assumed to depend on the spatial and temporal distribution of a given tracer $T(x,t)$, namely

$$\rho=\rho(T), \tag{I.36}$$

and T is governed by a transport-diffusion equation

$$\frac{\partial\rho T}{\partial t}+\frac{\partial\rho uT}{\partial x}+\frac{\partial\rho wT}{\partial z}=\mu_T\frac{\partial^2T}{\partial x^2}+\mu_T\frac{\partial^2T}{\partial z^2}, \tag{I.37}$$

where μ_T is the tracer diffusivity.

Notice that assuming $\mu_T=0$ – that is not fully relevant in the situations we considered – Eqs. (I.33), (I.36) and (I.37) leads to the divergence free condition **[EX]**

$$\frac{\partial u}{\partial x}+\frac{\partial w}{\partial z}=0.$$

7 Fluid with complex rheology

In continuum mechanics, a Newtonian fluid is a fluid in which the viscous stresses arising from its flow, at every point, are linearly proportional to the local strain rate, the constant of proportionality being the viscosity coefficient. This corresponds to the definitions (I.5)-(I.6). In other words,we say that the forces are proportional to the rates of change of the fluid's velocity vector as one moves away from the point in question in various directions. If the fluid is also isotropic (that is, its mechanical properties are the same along any direction), the viscosity tensor reduces to two real coefficients –

Lamé coefficients – describing the fluid's resistance to continuous shear deformation and continuous compression or expansion, respectively.

Newtonian fluids are the simplest mathematical models of fluids that account for viscosity. While no real fluid fits the definition perfectly, many common liquids and gases, such as water and air, can be assumed to be Newtonian for practical calculations under ordinary conditions.

Obviously a non-Newtonian fluid is a fluid that does not follow the previous definition. In a non-Newtonian fluid, the relation between the shear stress and the shear rate is not linear and can even be time-dependent (Time Dependent Viscosity). Although the concept of viscosity is commonly used in fluid mechanics to characterize the shear properties of a fluid, it can be inadequate to describe non-Newtonian fluids. They are best studied through several other rheological properties that relate stress and strain rate tensors under many different flow conditions–such as oscillatory shear or extensional flow–which are measured using different devices or rheometers. The properties are better studied using tensor-valued constitutive equations, which are common in the field of continuum mechanics. Ketchup, toothpaste, paint, blood, and shampoo are typical non-Newtonian fluids.

A number of geophysical flows involve rapid gravity-driven mass movements of solid particles within a fluid. Typical examples include snow avalanches, debris flows, lava flows, and submarine avalanches. These flows usually take the appearance of viscous fluids flowing down a slope but the rheology within these fluids cannot be modeled by a Newtonian fluid. Indeed, the interaction between the fluid and the solid particles it contains is very difficult to describe and leads to complex constitutive laws with viscosity, plasticity, hysteresis....

There are many occurences of free-surface non-Newtonian flows over an inclined topography in nature, for instance geophysical flows: mud flows, landslides, debris avalanches... Their mathematical prediction is important, typically for safety reasons in connection with land use planning in the case of geophysical flows. But their modelling is still difficult, as one can conclude from the continuing intense activity in that area (see the reviews [4, 47] e.g. plus the numerous references cited therein.

We describe hereafter some well-known constitutive law for non-Newtonian fluids.

7.1 The Mohr-Coulomb criterion

In the case of a visco-plastic behavior, the flow only begins when the stress is greater than a threshold called the yield stress. The most famous example is the Mohr-Coulomb criterion.

The Mohr-Coulomb [46] failure criterion represents the linear envelope that is obtained from a plot of the shear strength of a material versus the applied normal stress. This relation is expressed as

$$\sigma_T = \sigma_N \tan(\varphi) + c, \tag{I.38}$$

where σ_T is the shear strength, σ_N is the normal stress, c is the intercept of the failure envelope with the σ_T axis, and φ is the slope of the failure envelope. The quantity c is often called the cohesion and the angle φ is called the angle of internal friction.

7.2 The Drucker-Prager criterion

The Drucker-Prager yield criterion [54] is a pressure-dependent model for determining whether a material has failed or undergone plastic yielding. The criterion was introduced to deal with the plastic deformation of soils. It and its many variants have been applied to rock, concrete, polymers, foams, and other pressure-dependent materials.

This criterion generalizes the Mohr-Coulomb criterion and has a more regular mathematical formulation than (I.38). Several formulation are available, we propose the following one

$$\begin{cases} \sigma = \sigma_v + \kappa \frac{\sigma_v}{\|\sigma_v\|} & \text{if } \|\sigma_v\| \neq 0, \\ \|\sigma\| \leqslant \kappa & \text{else} \end{cases} \tag{I.39}$$

where σ_v corresponds to the viscous effects i.e. in 2d

$$\sigma_{v,xx} = 2\mu\frac{\partial u}{\partial x}, \qquad \sigma_{v,xz} = \mu\left(\frac{\partial u}{\partial z} + \frac{\partial w}{\partial x}\right),$$
$$\sigma_{v,zz} = 2\mu\frac{\partial w}{\partial z}, \qquad \sigma_{v,zx} = \mu\left(\frac{\partial u}{\partial z} + \frac{\partial w}{\partial x}\right),$$

with μ the viscosity that is supposed constant. The plasticity coefficient κ is related to the pressure thought the relation

$$\kappa = \sqrt{2}\lambda[p]_+,$$

where λ is a friction coefficient and $[p]_+$ is the positive part of the pressure.

Notice that replacing κ by a simple constant coefficient leads to the Bingham law [19].

7.3 Herschel-Bulkley fluid

The Herschel-Bulkley fluid [72, 120] is a generalized model of a non-Newtonian fluid, in which the strain experienced by the fluid is related to the stress in a complicated, non-linear way. The viscous stress tensor is given, in the usual way, as a viscosity, multiplied by the rate-of-strain tensor σ_v defined in (I.40) but in contrast to the Newtonian fluid, the viscosity is itself a function of the strain tensor. This is constituted through the formula [3]

$$\mu = \begin{cases} \mu_0, & \Pi \leqslant \Pi_0 \\ k\Pi^{n-1} + \sigma_0\Pi^{-1}, & \Pi \geqslant \Pi_0 \end{cases},$$

where Π is the second invariant of the rate-of-strain tensor

$$\Pi = \sqrt{\frac{1}{2}\left((\mathrm{tr}\Sigma_v)^2 - \mathrm{tr}(\Sigma_v\Sigma_v)\right)},$$

with $\sigma_v = 2\mu\Sigma_v$.

If $n = 1$ and $\sigma_0 = 0$, this model reduces to the Newtonian fluid. If $n < 1$ the fluid is shear-thinning, while $n > 1$ produces a shear-thickening fluid. The limiting viscosity μ_0 is chosen such that $\mu_0 = k\Pi_0^{n-1} + \sigma_0\Pi_0^{-1}$. A large limiting viscosity means that the fluid will only flow in response to a large applied force. This feature captures the Bingham-type behaviour of the fluid.

This equation is also commonly written as

$$\sigma = \sigma_0 + K\gamma^n,$$

where σ is the shear stress, γ the shear rate, σ_0 the yield stress, and K and n are regarded as model factors.

Chapter II

The Saint-Venant system - Derivation and properties

In this chapter, we first present the shallow water assumption that is the corner stone of the modeling of geophysical flows. Then we derive the Saint-Venant system including viscosity and friction effects. Finally, we give the main properties – at the continuous level – of the Saint-Venant system.

1 The shallow water approximation

Let us introduce the quantities

- h and λ, two characteristic dimensions along the z and x axis respectively,
- $C = \sqrt{gh}$ the typical horizontal wave speed.

We also define the small parameter

$$\varepsilon = \frac{h}{\lambda}, \tag{II.1}$$

and we assume $\varepsilon \ll 1$. Notice that such an assumption is valid for rivers, lakes or coastal flows.

The objective is now, departing from the Navier-Stokes equations (I.2)-(I.4) and using the assumption of shallow water flows, to obtain an error estimate for the quantities

$$u - \overline{u}, \quad \text{and} \quad \overline{u^2} - \overline{u}^2,$$

where the vertical average $\overline{A}$ of a given quantity A is defined by

$$\overline{A} = \frac{1}{H}\int_{z_b}^{\eta} A \, dz. \tag{II.2}$$

For that purpose, the equations (I.2)-(I.4),(I.9),(I.10),(I.11) and (I.14) will be rescaled using characteristic quantities.

More precisely, we introduce : $T = \lambda/C$ for time, $W = h/T = \varepsilon C$ for the vertical velocity, $U = \lambda/T = C$, for the horizontal velocity and $P = C^2$ for the pressure. This leads to the following dimensionless quantities

$$\tilde{x} = \frac{x}{\lambda}, \quad \tilde{z} = \frac{z}{h}, \quad \tilde{\eta} = \frac{\eta}{h}, \quad \tilde{t} = \frac{t}{T},$$
$$\tilde{p} = \frac{p}{P}, \quad \tilde{p}^a = \frac{p^a}{P}. \quad \tilde{u} = \frac{u}{U}, \quad \text{and} \quad \tilde{w} = \frac{w}{W}.$$

We denote the inverse of the Reynolds number

$$\tilde{\nu} = \frac{\mu}{U\lambda},$$

the inverse of the square of the Froude number

$$\tilde{g} = \frac{gh}{U^2},$$

and the rescaled bottom friction coefficient

$$\tilde{\kappa} = \frac{\kappa}{U}.$$

Using the divergence free condition, after rescaling and dropping the $\tilde{}$, the dimensionless 2D Navier-Stokes equations (I.2)-(I.4) reads

$$\frac{\partial u}{\partial x} + \frac{\partial w}{\partial z} = 0, \tag{II.3}$$

$$\frac{\partial u}{\partial t} + \frac{\partial u^2}{\partial x} + \frac{\partial uw}{\partial z} + \frac{\partial p}{\partial x} = \frac{\partial}{\partial x}\left(2\nu\frac{\partial u}{\partial x}\right) + \frac{\partial}{\partial z}\left(\frac{\nu}{\varepsilon^2}\frac{\partial u}{\partial z} + \nu\frac{\partial w}{\partial x}\right), \tag{II.4}$$

$$\varepsilon^2\left(\frac{\partial w}{\partial t} + \frac{\partial uw}{\partial x} + \frac{\partial w^2}{\partial z}\right) + \frac{\partial p}{\partial z} = -1 + \frac{\partial}{\partial x}\left(\nu\frac{\partial u}{\partial z} + \varepsilon^2\nu\frac{\partial w}{\partial x}\right) + \frac{\partial}{\partial z}\left(2\nu\frac{\partial w}{\partial z}\right). \tag{II.5}$$

The system (II.3)-(II.5) is completed with the boundary conditions presented in paragraph 3.2 and applied to the dimensionless system. On the free surface, the two no stress conditions (I.10) read

$$\frac{\nu}{\varepsilon}\left(\left.\frac{\partial u}{\partial z}\right|_s+\varepsilon^2\left.\frac{\partial w}{\partial x}\right|_s\right)-\varepsilon\frac{\partial \eta}{\partial x}\left(2\nu\left.\frac{\partial u}{\partial x}\right|_s-p_s\right)=0, \tag{II.6}$$

$$2\nu\left.\frac{\partial w}{\partial z}\right|_s-p_s-\varepsilon\nu\frac{\partial \eta}{\partial x}\left(\left.\frac{\partial u}{\partial z}\right|_s+\varepsilon^2\left.\frac{\partial w}{\partial x}\right|_s\right)=0, \tag{II.7}$$

and the kinematic boundary condition (I.9) is not modified. On the bottom the Navier condition (I.16) reads

$$\begin{aligned}\frac{\nu}{\varepsilon}&\left(\varepsilon^2\left.\frac{\partial w}{\partial x}\right|_b+\left.\frac{\partial u}{\partial z}\right|_b\right)-\varepsilon\frac{\partial z_b}{\partial x}\left(2\nu\left.\frac{\partial u}{\partial x}\right|_b-p_b\right)\\&+\varepsilon\frac{\partial z_b}{\partial x}\left(2\nu\left.\frac{\partial w}{\partial z}\right|_b-p_b-\nu\frac{\partial z_b}{\partial x}\left(\left.\frac{\partial u}{\partial z}\right|_b+\varepsilon^2\left.\frac{\partial w}{\partial x}\right|_b\right)\right)=\kappa\left(1+\varepsilon^2\left(\frac{\partial z_b}{\partial x}\right)^2\right)^{3/2}u_b,\end{aligned}$$

or

$$\frac{\nu}{\varepsilon}\left.\frac{\partial u}{\partial z}\right|_b=\kappa u_b+\mathscr{O}(\varepsilon). \tag{II.8}$$

and the no penetration condition at the bottom (I.11) is not modified.

There are many ways to introduce a scaling in the viscosity and friction coefficients, see Ref. [18, 87]. Here we shall suppose we are in the following asymptotic regime

$$\nu=\varepsilon\nu_0,\quad \kappa=\varepsilon\kappa_0. \tag{II.9}$$

1.1 The hydrostatic system

Neglecting (temporarily) the viscous terms and taking the formal limit as ε vanishes in the system (II.3)-(II.5) gives the proposition

Proposition II.1. *The hydrostatic system*

$$\begin{aligned}&\frac{\partial u}{\partial t}+\frac{\partial u^2}{\partial x}+\frac{\partial uw}{\partial z}+\frac{\partial p}{\partial x}=0,\\&w=-\frac{\partial}{\partial x}\int_{z_b}^{z}u\,dz,\\&p=p^a+(\eta-z),\end{aligned} \tag{II.10}$$

completed with kinematic boundary condition (I.9) is a formal approximation as ε *tends to* 0 *of the free surface incompressible Euler system.*

Proof. The proof of this proposition uses only very simple calculations **[EX]**. □

Thus the hydrostatic assumption consists in neglecting the vertical acceleration of the fluid and this strongly modifies the properties of the model. Indeed, for the hydrostatic model, the pressure p is a linear function of H, z_b and z instead of being a Lagrange multiplier of the divergence free condition.

It is important to notice that with the hydrostatic assumption, the vertical acceleration is neglected but it does not mean the vertical velocity is neglected, see (II.10).

1.2 Estimates

Using the boundary conditions (I.9),(I.11),(II.6)-(II.8) an integration of equations (II.3), (II.4) from the bottom to the free surface gives

$$\frac{\partial H}{\partial t}+\frac{\partial}{\partial x}\int_{z_b}^{\eta} u dz=0, \tag{II.11}$$

$$\frac{\partial}{\partial t}\int_{z_b}^{\eta} u\,dz+\frac{\partial}{\partial x}\left(\int_{z_b}^{\eta} u^2 dz+\int_{z_b}^{\eta} p\,dz\right)=-p_b\frac{\partial z_b}{\partial x}+\varepsilon\frac{\partial}{\partial x}\int_{z_b}^{\eta} 2\nu_0\frac{\partial u}{\partial x}dz$$
$$+\frac{\partial z_b}{\partial x}2\nu_0\varepsilon^2\left.\frac{\partial u}{\partial x}\right|_b-\nu_0\varepsilon\left(\left.\frac{\partial u}{\partial z}\right|_b+\varepsilon^2\left.\frac{\partial w}{\partial x}\right|_b\right). \tag{II.12}$$

Likewise, an integration from the bottom to the free surface of Eq. (II.4) gives

$$p_b=H-\frac{\partial z_b}{\partial x}\nu_0\varepsilon^2\left(\left.\frac{\partial u}{\partial z}\right|_b+\varepsilon^2\left.\frac{\partial w}{\partial x}\right|_b\right)+2\nu_0\varepsilon\left.\frac{\partial w}{\partial z}\right|_b,$$

and replacing the previous expression for p_b into Eq. (II.12) gives

$$\frac{\partial H}{\partial t}+\frac{\partial}{\partial x}\int_{z_b}^{\eta} u dz=0, \tag{II.13}$$

$$\frac{\partial}{\partial t}\int_{z_b}^{\eta} u\,dz+\frac{\partial}{\partial x}\left(\int_{z_b}^{\eta} u^2 dz+\int_{z_b}^{\eta} p\,dz\right)=-H\frac{\partial z_b}{\partial x}+\varepsilon\frac{\partial}{\partial x}\int_{z_b}^{\eta} 2\nu_0\frac{\partial u}{\partial x}dz$$
$$-\kappa_0\varepsilon\left(1+\varepsilon^2\left(\frac{\partial z_b}{\partial x}\right)^2\right)^{3/2}u_b, \tag{II.14}$$

where the boundary condition (II.8) has been used.

Now we use the shallow water assumption i.e. $\varepsilon\ll 1$ and the equation (II.4) leads to

$$\frac{\partial}{\partial z}\left(\nu_0\frac{\partial u}{\partial z}\right)=\mathscr{O}(\varepsilon).$$

Since the boundary conditions (II.6),(II.8) give

$$\left.\frac{\partial u}{\partial z}\right|_s=\mathscr{O}(\varepsilon^2),\quad\text{and}\quad\left.\frac{\partial u}{\partial z}\right|_b=\mathscr{O}(\varepsilon), \tag{II.15}$$

after an integration in z it comes

$$u=\overline{u}+\mathscr{O}(\varepsilon),\qquad\overline{u^2}=\overline{u}^2+\mathscr{O}(\varepsilon), \tag{II.16}$$

and we recover the so-called motion by slices of usual shallow water systems. Likewise, integrating in z Eq. (II.5), the pressure p satisfies

$$p=p^a+(\eta-z)+\mathscr{O}(\varepsilon). \tag{II.17}$$

We look for a more accurate estimate of the quantity $\overline{u^2}$. So we come back to Eq. (II.4) and using relations (II.14),(II.16) and (II.17) it comes

$$\begin{aligned}\frac{\partial}{\partial z}\left(\frac{\nu_0}{\varepsilon}\frac{\partial u}{\partial z}\right) &= \frac{\partial u}{\partial t}+\frac{\partial u^2}{\partial x}+\frac{\partial uw}{\partial z}+\frac{\partial p}{\partial x}-\varepsilon\frac{\partial}{\partial x}\left(\nu_0\frac{\partial u}{\partial x}\right)\\ &= \frac{\partial\overline{u}}{\partial t}+\overline{u}\frac{\partial\overline{u}}{\partial x}+\frac{\partial\eta}{\partial x}+\frac{\partial p^a}{\partial x}+\mathscr{O}(\varepsilon)\\ &= -\frac{\kappa_0}{H}u_b+\mathscr{O}(\varepsilon).\end{aligned} \tag{II.18}$$

Integrating from z_b to z and taking the boundary condition (II.8) into account, we deduce

$$\frac{\partial u}{\partial z} = \frac{\varepsilon \kappa_0}{\nu_0}\left(1 - \frac{z-z_b}{H}\right) u_b + \mathscr{O}(\varepsilon^2), \tag{II.19}$$

and we obtain the following formula which gives an expression of the vertical velocity through a parabolic correction

$$u = \left(1 + \frac{\varepsilon \kappa_0}{\nu_0}\big(z - z_b - \frac{(z-z_b)^2}{2H}\big)\right) u_b + \mathscr{O}(\varepsilon^2). \tag{II.20}$$

Then integrating from z_b to η, we obtain

$$\bar{u} = \left(1 + \frac{\varepsilon \kappa_0}{3\nu_0} H\right) u_b + \mathscr{O}(\varepsilon^2), \tag{II.21}$$

that gives

$$u = \left(1 + \frac{\varepsilon \kappa_0}{\nu_0}\left(z - z_b - \frac{(z-z_b)^2}{2H} - \frac{H}{3}\right)\right) \overline{u} + \mathscr{O}(\varepsilon^2). \tag{II.22}$$

Then we recover

$$u = \overline{u} + \mathscr{O}(\varepsilon). \tag{II.23}$$

From relation (II.23), one can write $u = \overline{u} + u'$ with $u' = \mathscr{O}(\varepsilon)$ and $\overline{u'} = 0$ so it comes

$$u^2 = \overline{u}^2 + 2\overline{u}u' + \mathscr{O}(\varepsilon^2),$$

leading to

$$\overline{u^2} = \overline{u}^2 + O(\varepsilon^2). \tag{II.24}$$

2 Derivation of the Saint-Venant system

The hydrostatic assumption in the Navier-Stokes system (I.2)-(I.4) that means the contribution of the vertical acceleration in the pressure p can be neglected, leads to the classical model,

$$\frac{\partial u}{\partial x} + \frac{\partial w}{\partial z} = 0, \tag{II.25}$$

$$\frac{\partial u}{\partial t} + \frac{\partial u^2}{\partial x} + \frac{\partial uw}{\partial z} + \frac{\partial p}{\partial x} = \frac{\partial}{\partial x}\left(2\nu \frac{\partial u}{\partial x}\right) + \frac{\partial}{\partial z}\left(\nu \frac{\partial u}{\partial z} + \nu \frac{\partial w}{\partial x}\right), \tag{II.26}$$

$$\frac{\partial p}{\partial z} = -g + \frac{\partial}{\partial x}\left(\nu \frac{\partial u}{\partial z}\right) + \frac{\partial}{\partial z}\left(2\nu \frac{\partial w}{\partial z}\right). \tag{II.27}$$

Notice such a model can be obtained by an asymptotic expansion of the rescaled Navier-Stokes system (II.3)-(II.5) retaining only the terms up to $\mathscr{O}(\varepsilon^2)$. This hydrostatic model – or some variants with horizontal and vertical viscosity or other specific terms – is very used in geophysical flows studies and its averaging along the vertical direction leads to the classical Saint-Venant system [55, 57, 98] described by the following proposition

Proposition II.2. *Up to $\mathscr{O}(\varepsilon)$ terms, the solutions of the Navier-Stokes equations (I.2)-(I.4) satisfies the Saint-Venant system defined by*

$$\frac{\partial H}{\partial t} + \frac{\partial}{\partial x}\big(H\bar{u}\big) = 0, \tag{II.28}$$

$$\frac{\partial (H\bar{u})}{\partial t} + \frac{\partial (H\bar{u}^2)}{\partial x} + \frac{g}{2}\frac{\partial H^2}{\partial x} = -H\frac{\partial p^a}{\partial x} - gH\frac{\partial z_b}{\partial x} - \kappa \bar{u}. \tag{II.29}$$

The smooth solutions of (II.28)-(II.29) satisfy the energy equality

$$\frac{\partial E_h}{\partial t} + \frac{\partial}{\partial x}\left(\bar{u}\big(E_h + g\frac{H^2}{2}\big)\right) = -\kappa \bar{u}^2 + H\frac{\partial p^a}{\partial t},$$

with the energy

$$E_h = \frac{H\bar{u}^2}{2} + \frac{gH(\eta + z_b)}{2} + Hp^a. \tag{II.30}$$

Proof of proposition II.2. We use the rescaled Navier-Stokes system (II.3)-(II.5) coupled with the estimates (II.23) and (II.24). It is very important to notice that a rigorous proof of this proposition can hardly be obtained using only the Euler system. Indeed, the estimates (II.23),(II.24) are derived from the shallow water assumption applied to the viscous terms in the Navier-Stokes system.

Using the boundary condition (II.7), the vertical integration of Eq. (II.5) from z to $\eta = H + z_b$ gives

$$p = p^a + (\eta - z) + \mathscr{O}(\varepsilon). \tag{II.31}$$

Then using (II.24) and the kinematic boundary conditions (I.9)-(I.11) (written in the dimensionless variables), a vertical integration of Eq. (II.4) gives

$$\frac{\partial(H\bar{u})}{\partial t} + \frac{\partial(H\bar{u}^2)}{\partial x} + \frac{1}{2}\frac{\partial H^2}{\partial x} = -H\frac{\partial p^a}{\partial x} - H\frac{\partial z_b}{\partial x} - \kappa\bar{u} + \mathscr{O}(\varepsilon).$$

Likewise a vertical integration of the divergence free condition (II.25) coupled with the boundary conditions (I.9)-(I.11) leads to

$$\frac{\partial H}{\partial t} + \frac{\partial}{\partial x}\big(H\bar{u}\big) = 0.$$

Notice that in order to obtain the two previous equations, the Leibniz rule

$$\int_a^b \frac{\partial f}{\partial y} dz = \frac{\partial}{\partial y}\int_a^b f\, dz - \frac{\partial b}{\partial y} f(b) + \frac{\partial a}{\partial y} f(a),$$

is used.

The energy balance can be obtain multiplying Eq. (II.29) by $\bar{u}$ and performing simple manipulations **[EX]**. It can also be obtained using a vertical integration of Eq. (II.4) mutiplied by u **[EX]**(see paragraph 3.5 for the case of non-smooth solutions).

In terms of the initial variables the preceding model becomes (II.28)-(II.29) and that completes the proof. □

When the viscosity effects cannot be neglected, we have the following proposition

Proposition II.3. *The viscous Saint-Venant system defined by*

$$\frac{\partial H}{\partial t} + \frac{\partial}{\partial x}\big(H\bar{u}\big) = 0, \tag{II.32}$$

$$\frac{\partial(H\bar{u})}{\partial t} + \frac{\partial(H\bar{u}^2)}{\partial x} + \frac{g}{2}\frac{\partial H^2}{\partial x} = -H\frac{\partial p^a}{\partial x} - gH\frac{\partial z_b}{\partial x} + \frac{\partial}{\partial x}\big(4\nu H\frac{\partial \bar{u}}{\partial x}\big) - \frac{\kappa\bar{u}}{1 + \frac{\kappa}{3\nu}H}, \tag{II.33}$$

results formally from an hydrostatic approximation in $\mathscr{O}(\varepsilon^2)$ of the Navier-Stokes equations. The smooth solutions satisfy the equality

$$\frac{\partial E_h}{\partial t} + \frac{\partial}{\partial x}\left(\bar{u}\big(E_h + g\frac{H^2}{2} - 4\nu H\frac{\partial \bar{u}}{\partial x}\big)\right) = H\frac{\partial p^a}{\partial t} - \frac{\kappa\bar{u}^2}{1 + \frac{\kappa}{3\nu}H} - 4\nu H\left(\frac{\partial \bar{u}}{\partial x}\right)^2,$$

with E_h given by (II.30).

Proof of proposition II.3. The proof is similar to the one given in proposition II.2 but uses more accurate estimates derived from the shallow water assumption. Using the boundary conditions (I.9),(I.11),(II.6)-(II.8) an integration of equations (II.3), (II.4) from the bottom to the free surface gives (II.13)-(II.14). We have

$$\frac{\partial u_s}{\partial x} = \left.\frac{\partial u}{\partial x}\right|_s + \left.\frac{\partial \eta}{\partial x}\,\frac{\partial u}{\partial z}\right|_s = \left.\frac{\partial u}{\partial x}\right|_s + \mathscr{O}(\varepsilon^2), \tag{II.34}$$

and using the relations (II.7), (II.34) and the Leibniz rule, we can write

$$\varepsilon \int_z^\eta \frac{\partial}{\partial x}\left(\nu_0 \frac{\partial u}{\partial z}\right) dz - 2\varepsilon\nu_0 \frac{\partial w}{\partial z} = \varepsilon\nu_0 \frac{\partial u}{\partial x} + \varepsilon\nu_0 \frac{\partial u}{\partial x}\bigg|_s + \mathscr{O}(\varepsilon^3).$$

This leads to the following expression for the pressure p

$$\begin{aligned} p &= p^a + (\eta - z) - \varepsilon\nu_0 \frac{\partial u}{\partial x} - \varepsilon\nu_0 \frac{\partial u}{\partial x}\bigg|_s + \mathscr{O}(\varepsilon^2), \\ &= p^a + (\eta - z) - 2\varepsilon\nu_0 \frac{\partial u}{\partial x} + \mathscr{O}(\varepsilon^2). \end{aligned} \tag{II.35}$$

Finally, using (II.21),(II.35) in (II.14) and returning to the initial variables completes the proof. □

2.1 Vertical velocity

Because of the hydrostatic assumption, the vertical velocity w no more appears in the Saint-Venant system but can be obtained from the divergence free condition. Namely, an integration from z_b to η of relation (II.25) coupled with the kinematic boundary conditions (I.9),(I.11) gives (up to $\mathscr{O}(\varepsilon^2)$ terms)

$$H\overline{w} = -\frac{H^2}{2}\frac{\partial \overline{u}}{\partial x} + H\frac{\partial z_b}{\partial x}\overline{u}.$$

After simple manipulations and using the continuity equation (II.32), we can obtain that the preceding relation is equivalent to the equation

$$\frac{\partial}{\partial t}\left(\frac{\eta^2 - z_b^2}{2}\right) + \frac{\partial}{\partial x}\left(\frac{\eta^2 - z_b^2}{2}\overline{u}\right) - H\overline{w} = 0, \tag{II.36}$$

that is more convenient in practice since it is written in a conservative form. Relation (II.36) can also be obtained calculating **[EX]**

$$\int_{z_b}^\eta z\left(\frac{\partial u}{\partial x} + \frac{\partial w}{\partial z}\right) dz = 0.$$

2.2 The Saint-Venant system with a passive tracer

The water can also advect external quantities. Indeed, in lakes, rivers, coastal regions the water contains/carries components such as : biological species, pollutant, sediment,... Let us consider a passive tracer whose concentration is defined by T. The word *passive* means the tracer concentration does not modify the water density. First we assume the tracer is only advected by the flow and does not react within the fluid.

Then the conservation of the tracer T is governed by the equation

$$\frac{\partial T}{\partial t} + \frac{\partial uT}{\partial x} + \frac{\partial wT}{\partial z} = 0,$$

and using the shallow water assumption, the preceding equation becomes (with obvious notations)

$$\frac{\partial HT}{\partial t} + \frac{\partial H\bar{u}T}{\partial x} = 0. \tag{II.37}$$

So the Saint-Venant system with a passive tracer consists in the set of equations (II.32)-(II.33),(II.37).

Let us suppose the evolution of the tracer T is governed by an advection-diffusion equation. What is the modified version of Eq. (II.37) ? **[EX]**

2.3 Classical friction laws

In props. II.2 and II.3 we have considered a Navier type friction law (linear) corresponding to the friction law used in the definition of the boundary condition (I.14) but in practice more complex laws – often empirical – can be used, see [126]. We denote S_f the source term due to friction.

Classical friction laws :

- Navier $S_f = \kappa \overline{u}$,
- Manning-Strickler $S_f = C_f \frac{\overline{u}|\overline{u}|}{H^{\frac{1}{3}}}$,
- Darcy-Weisbach $S_f = C_f \overline{u}|\overline{u}|$

Notice that it is sometimes necessary to impose $H = 0 \Rightarrow \overline{u} = 0$ to ensure the dissipative effect at rest.

2.4 The Saint-Venant system in 2d

Starting from the 3d incompressible Navier-Stokes (or Euler) equations with free surface, a 2d version of the Saint-Venant system can be obtained **[EX]**. Its formulation is given by

$$\frac{\partial H}{\partial t} + \nabla_{x,y}(H\mathbf{u}) = 0, \tag{II.38}$$

$$\frac{\partial H\mathbf{u}}{\partial t} + \nabla_{x,y} \cdot (H\mathbf{u} \otimes \mathbf{u}) + \nabla_{x,y} \frac{g}{2} H^2 = -H\nabla_{x,y} p^a - gH\nabla_{x,y} z_b - S_f(H, H\mathbf{u}), \tag{II.39}$$

where H is the water depth and the horizontal velocity vector $\mathbf{u} = (\overline{u}, \overline{v})$ and $\nabla_{x,y} = (\partial_x, \partial_y)^T$. The friction effects are modeled by $S_f(H, H\mathbf{u})$ with S_f a function from $\mathbb{R}^+ \times \mathbb{R}$ to $\mathbb{R}^2$ satisfying

$$\forall \mathbf{n} \in \mathbb{S}^1, \forall (H, \mathbf{u}) \in \mathbb{R}^+ \times \mathbb{R}^2, \quad \text{sgn}(H\mathbf{u} \cdot \mathbf{n}) = \text{sgn}(S_f(H, H\mathbf{u}) \cdot \mathbf{n})$$

and where $\mathbb{S}^1$ is the unit sphere and the sgn function satisfies $\text{sgn}(0) = 0$. Such an assumption ensures the friction effects are dissipative.

Other sources terms can be added to the Saint-Venant system such as Coriolis forces, wind stress, evaporation, rain,... In most of the cases the derivation can be obtained rigorously [57, 98, 107].

2.5 Another derivation of the Saint-Venant system

We start form the incompressible and hydrostatic Euler system with free surface (see prop. II.1) written under the form

$$\begin{aligned} &\frac{\partial u}{\partial x} + \frac{\partial w}{\partial z} = 0, \\ &\frac{\partial u}{\partial t} + \frac{\partial u^2}{\partial x} + \frac{\partial uw}{\partial z} + g\frac{\partial \eta}{\partial x} = 0, \end{aligned} \tag{II.40}$$

and completed with the boundary conditions (I.9) and (I.11). We assume $p^a = 0$.

As already mentioned, using the two kinematic boundary conditions, a vertical integration of the divergence free condition leads to

$$\frac{\partial H}{\partial t} + \frac{\partial}{\partial x}\left(H\overline{u}\right) = 0,$$

whereas the vertical integration of the momentum equation (II.40) gives

$$\frac{\partial (H\overline{u})}{\partial t} + \frac{\partial}{\partial x} \int_{z_b}^{\eta} u^2 \, dz + \frac{g}{2} \frac{\partial H^2}{\partial x} = -gH \frac{\partial z_b}{\partial x}.$$

And in order to obtain a closure relation defining the quantity

$$\int_{z_b}^{\eta} u^2 \, dz,$$

we proceed as follows.

The goal is to transpose the entropy-based moment closures proposed by Levermore in [86] for kinetic equations to our framework, the approach we propose is detailed in paragraph 2.1 but for a more complex model.

If u' is defined as the deviation of u with respect to its depth-average, then it comes

$$u = \frac{1}{H}\int_{z_b}^{\eta} u\, dz + u' = \overline{u} + u'.$$

We study the minimization problem

$$\min_{u'} \int_{z_b}^{\eta} E(z;u)\, dz, \tag{II.41}$$

with $E(z;u)$ corresponding to (I.21) in the hydrostatic framework i.e.

$$E(z;u) = \frac{u^2}{2} + gz.$$

The energy $E(z;u)$ being quadratic with respect to u we notice

$$\int_{z_b}^{\eta} u^2\, dz = H\overline{u}^2 + 2\int_{z_b}^{\eta} \overline{u}u'\, dz + \int_{z_b}^{\eta} (u')^2\, dz = H\overline{u}^2 + \int_{z_b}^{\eta} (u')^2\, dz \geqslant H\overline{u}^2. \tag{II.42}$$

Equation (II.42) means that the solution of the minimization problem (II.41) is given by

$$\int_{z_b}^{\eta} E(z;\overline{u}) = \min_{u'} \int_{z_b}^{\eta} E(z;u)\, dz,$$

and

$$\int_{z_b}^{\eta} E(z;\overline{u}) = \frac{H}{2}\overline{u}^2 + \frac{g}{2}(\eta^2 - z_b^2).$$

Since the only choice leading to an equality in relation (II.42) corresponds to

$$u = \overline{u}, \tag{II.43}$$

this allows to precise the closure relation associated to a minimal energy, namely

$$\int_{z_b}^{\eta} u^2\, dz = H\overline{u}^2, \tag{II.44}$$

and we have obtained a derivation of the Saint-Venant system saying it is the model with minimal kinetic energy included in the hydrostatic Euler system.

3 Properties of the Saint-Venant system (continuous level)

The main properties are presented below. For complementary informations, the reader can refer to Bouchut [24].

To begin with, some vocabulary :

- the *gravity waves* speed is $c = \sqrt{gH}$ and corresponds to the sound speed in the Euler (gaz) equations. A tsunami propagates at the speed $\sqrt{gH}$,
- when $|\overline{u}| < c$ (resp. $|\overline{u}| > c$), the flow regime is *subcritic* or *fluvial* (resp. *supercritic* or *torrential*), and if $|\overline{u}| \simeq c$, the flow regime is said to be *transcritic*,
- the flow regime is often characterized by the Froude number defined by

$$Fr = \frac{|\overline{u}|}{\sqrt{gH}}, \tag{II.45}$$

  $Fr < 1$ corresponds to a fluvial regime and $Fr > 1$ coresponds to a torrential flow,

- a stationary entropic shock is called an *hydraulic jump*, cf. Figures below.

In rivers, near the mouth and because of the tides you can see hydraulic jumps (also called mascaret), see Fig II.1-*(a)*. Another example is depicted over Fig. II.1-*(b)*, determine the torrential and fluvial areas **[EX]**.

(a) *(b)*

Figure II.1: Two typical hydraulic jumps : *(a)* a mascaret and *(b)* an hydraulic jump in a sink.

3.1 Conservative form

In the following, we often write the Saint-Venant system (II.28)-(II.29) under the conservative and condensed form

$$\frac{\partial X}{\partial t} + \frac{\partial}{\partial x} F(X) = S_b(X) + S_{f,v}(X), \tag{II.46}$$

where

$$F(X) = \begin{pmatrix} H\bar{u} \\ H\bar{u}^2 + \frac{g}{2}H^2 \end{pmatrix},$$

and $X \in \Omega := (H \geqslant 0, H\bar{u} \in \mathbb{R})$. S_b accounts for the topography source term and $S_{f,v}$ represents the dissipative effects (friction and viscosity). But the Saint-Venant system – without viscosity – can also be written in a quasilinear form i.e.

$$\begin{aligned} &\frac{\partial H}{\partial t} + \bar{u}\frac{\partial H}{\partial x} + H\frac{\partial \bar{u}}{\partial x} = 0, \\ &\frac{\partial \bar{u}}{\partial t} + \bar{u}\frac{\partial \bar{u}}{\partial x} + g\frac{\partial H}{\partial x} = -g\frac{\partial z_b}{\partial x} - \kappa\frac{\bar{u}}{H}, \end{aligned}$$

or equivalently

$$\frac{\partial Y}{\partial t} + A(Y)\frac{\partial Y}{\partial x} = \tilde{S}_b(Y) + \tilde{S}_f(Y), \tag{II.47}$$

with $Y = (H, \bar{u})^T$ and

$$A(Y) = \begin{pmatrix} \bar{u} & H \\ g & \bar{u} \end{pmatrix}.$$

But it is well-known that for quasilinear systems, the solution Y naturally developps discontinuities (shock waves). The main difficulty in such systems is therefore to give a sense to (II.47). This difficulty is somehow solved when considering conservative systems. For this reason, in the following and when possible, we single out the conservative form of the equations.

3.2 Hyperbolicity and Riemann invariants

3.2.1 A very simple case

The Riemann invariants play an important role in the analysis and the discretization of an hyperbolic system. We illustrate this in the case of a linear hyperbolic system.

Let us consider the hyperbolic linear system

$$\frac{\partial Y}{\partial t} + A_0 \frac{\partial Y}{\partial x} = 0, \tag{II.48}$$

where A_0 is a square matrix with constant coefficients and $Y \in \mathscr{R}^d$. The system being hyperbolic, the matrix A_0 can be diagonalized over $\mathscr{R}$ so there exist an invertible square matrix P_0 and d eigenvalues of A_0 denoted $\{\lambda_{0,i}\}_{1\leqslant i\leqslant d}$ such that

$$\Lambda_0 = \mathrm{diag}(\lambda_{0,1}, \ldots, \lambda_{0,d}) = (P_0)^{-1} A_0 P_0.$$

Multiplying (II.48) on the left by $(P_0)^{-1}$, we obtain the diagonalized system

$$\frac{\partial}{\partial t}((P_0)^{-1}Y) + (P_0)^{-1}A_0P_0\frac{\partial}{\partial x}((P_0)^{-1}Y) = 0,$$

or equivalently

$$\frac{\partial Z}{\partial t} + \Lambda_0 \frac{\partial Z}{\partial x} = 0,$$

with $Z = (P_0)^{-1}Y$. The previous system is easy to solve and each component of the vector Z is given by

$$Z_i = f_{0,i}(x - \lambda_{0,i}t),$$

where the functions $\{f_{0,i}\}_{1\leqslant i\leqslant d}$ are defined by the initial conditions. Finally $Y = P_0 Z$ gives the solution of the system (II.48).

3.2.2 Riemann invariants for the Saint-Venant system

In practice We consider the Saint-Venant system without friction nor viscosity and written in the quasilinear form for a float bottom i.e.

$$\begin{aligned}
&\frac{\partial H}{\partial t} + \bar{u}\frac{\partial H}{\partial x} + H\frac{\partial \bar{u}}{\partial x} = 0,\\
&\frac{\partial \bar{u}}{\partial t} + \bar{u}\frac{\partial \bar{u}}{\partial x} + g\frac{\partial H}{\partial x} = 0.
\end{aligned}$$

Defining

$$c = \sqrt{gH},$$

the two previous equations can be rewritten under the form

$$\begin{aligned}
&\frac{\partial (2c)}{\partial t} + \bar{u}\frac{\partial (2c)}{\partial x} + c\frac{\partial \bar{u}}{\partial x} = 0,\\
&\frac{\partial \bar{u}}{\partial t} + \bar{u}\frac{\partial \bar{u}}{\partial x} + c\frac{\partial (2c)}{\partial x} = 0,
\end{aligned}$$

and the sum of the two equations gives

$$\frac{\partial (\bar{u}+2c)}{\partial t} + (\bar{u}+c)\frac{\partial (\bar{u}+2c)}{\partial x} = 0, \tag{II.49}$$

whereas the difference of the two equations leads to

$$\frac{\partial (\bar{u}-2c)}{\partial t} + (\bar{u}-c)\frac{\partial (\bar{u}-2c)}{\partial x} = 0. \tag{II.50}$$

The equations (II.49) and (II.50) corresponds to the two characteristic curves of the Saint-Venant system.

Abstract version For $H > 0$, the Saint-Venant system (II.28)-(II.29) is hyperbolic since it admits two distinct eigenvalues $\lambda_\pm = u \pm \sqrt{gH}$ with the associated eigenvectors

$$l_\pm = \begin{pmatrix} \sqrt{H} \\ \pm\sqrt{g} \end{pmatrix}.$$

In particular this implies the eigenvalues cannot cross. Then the eigenvalues $\lambda_\pm$ are genuinely nonlinear since

$$\lambda'_\pm . l_\pm \neq 0.$$

Definition II.4. We say that a scalar function $w(Y)$ is a (weak) λ_+-Riemann invariant if for all Y,

$$\nabla w(Y).r_+(Y) = 0.$$

Let us consider the right eigenvector of matrix A i.e.

$$r_\pm^T A = \lambda_\pm r_\pm^T.$$

Since the two eigenvalues $\lambda_\pm$ are distinct, we obtain calculating $r_+^T A l_-$ that

$$r_-^T l_+ = r_+^T l_- = 0,$$

and therefore

$$\nabla w(Y) = \frac{\partial w(Y)}{\partial Y},$$

is colinear to l_- and hence is a right eigenvector associated with λ_- i.e.

$$\frac{\partial w(Y)}{\partial Y} A = \lambda_- \frac{\partial w(Y)}{\partial Y}.$$

The following definition holds.

Definition II.5. We say that a scalar function $w(Y)$ is a (strong) λ_+-Riemann invariant if for all Y,

$$\nabla w(Y) A = \lambda_+ w(Y).$$

The interest of this notion lies in the fact that it can be characterized by the property that a smooth solution Y to the homogenous system (II.47) satisfies

$$\frac{\partial w(Y)}{\partial t} + \lambda_+ \frac{\partial w(Y)}{\partial x} = 0.$$

Indeed, let us consider the homogenous system (II.47) and multiplying it on the left by $l_\pm$ gives

$$l_\pm \frac{\partial Y}{\partial t} + \lambda_\pm l_\pm \frac{\partial Y}{\partial x} = 0, \tag{II.51}$$

A rewritting of (II.51) gives **[EX]**

$$\frac{\partial w_\pm}{\partial t} + \lambda_\pm \frac{\partial w_\pm}{\partial x} = 0,$$

where the two Riemann invariants $w_\pm$ are defined by

$$w_\pm = \overline{u} \pm 2\sqrt{gH}, \tag{II.52}$$

and we recover the two equations (II.49) and (II.50).

The link between strong and weak Riemann invariants is given by the following proposition (written in the specific case of the 2×2 Saint-Venant system).

Proposition II.6. *A function $w(Y)$ is a strong λ_+ Riemann invariant if and only if $w(Y)$ is a weak λ_- Riemann invariant.*

3.2.3 The full system

Consider the Saint-Venant system – without viscosity nor friction – with its energy equality

$$\begin{aligned}
&\frac{\partial H}{\partial t} + \frac{\partial}{\partial x}\big(H\bar{u}\big) = 0,\\
&\frac{\partial (H\bar{u})}{\partial t} + \frac{\partial (H\bar{u}^2)}{\partial x} + \frac{g}{2}\frac{\partial H^2}{\partial x} = -gH\frac{\partial z_b}{\partial x},\\
&\frac{\partial E_h}{\partial t} + \frac{\partial}{\partial x}\left(\bar{u}\big(E_h + g\frac{H^2}{2}\big)\right) = 0,
\end{aligned}$$

i.e. for smooth solutions. What are the eigenvalues/eigenvectors of this system ? Is it hyperbolic ? **[EX]**

3.2.4 The topography as an unknown

When $z_b(x,t) = z_b(x)$, it is possible to consider the topography as an unknown associated with a distributed parameter and governed by the equation

$$\frac{\partial z_b}{\partial t} = 0.$$

Then the Saint-Venant system can be rewritten under the form

$$\begin{aligned}
&\frac{\partial z_b}{\partial t} = 0,\\
&\frac{\partial H}{\partial t} + \frac{\partial H\bar{u}}{\partial x} = 0,\\
&\frac{\partial H\bar{u}}{\partial t} + \frac{\partial}{\partial x}\left(H\bar{u}^2 + gH^2/2\right) + gH\frac{\partial z_b}{\partial x} = 0.
\end{aligned} \tag{II.53}$$

The eigenvalues associated with $\lambda_\pm = \bar{u} \pm \sqrt{gH}$ still are genuinely nonlinear whereas $\lambda_0 = 0$ is linearly degenerated. In such a situation, the two wave speeds λ_- and λ_+ are not ordered with respect to the eigenvalue λ_0. This also raises the question what happens when $\lambda_- = \lambda_0$ or $\lambda_- = \lambda_0$.

Proposition II.7. *If $|\bar{u}| \neq \sqrt{gH}$ then the system (II.53) is strictly hyperbolic. Else, two of the eigenvalues coincide and the system is said to be* resonant.

Proof. The system (II.53) reads

$$\frac{\partial}{\partial t}\begin{pmatrix} z_b \\ H \\ H\bar{u} \end{pmatrix} + \begin{pmatrix} 0 & 0 & 0 \\ 0 & 0 & 1 \\ gH & gH - \bar{u}^2 & 2\bar{u} \end{pmatrix} \frac{\partial}{\partial x}\begin{pmatrix} z_b \\ H \\ H\bar{u} \end{pmatrix} = \mathbf{0}.$$

Simple calculus (**[EX]**) gives the eigenvectors

$$l_\pm = \begin{pmatrix} 0 \\ 1 \\ \bar{u} \pm \sqrt{gH} \end{pmatrix} \text{ and } l_0 = \begin{pmatrix} gH - \bar{u}^2 \\ -gH \\ 0 \end{pmatrix},$$

that concludes the proof. □

In case of resonance, the eigenvectors are no more a basis of $\mathbb{R}^3$. And the analogy with the linear case is no more valid for the study of the Riemann problem.

Another difficulty is that (II.53) is a non conservative system. Indeed

$$gH\frac{\partial z_b}{\partial x},$$

consists in the product of two distributions and hence non defined. Nevertheless, the following result is helpful.

Proposition II.8. *Let us consider a strictly hyperbolic non conservative system with a linearly degenerated field. Then the associated wave is a contact discontinuity and any Riemann invariant associated with this wave is constant throughout this wave.*

This result ensures that for a linearly degenerated field (the stationary wave here), the fact that the system is non conservative does not modify its usual characterization – that is not the case for a genuinely nonlinear field. For the system (II.53), the Riemann invariants of the stationary wave are given by **[EX]**

$$w_0^1(X) = H\overline{u} \quad \text{and} \quad w_0^2(X, z_b) = \frac{\overline{u}^2}{2} + g(H + z_b).$$

The Riemann invariants have to be compared with the stationary states of the Bernouilli theorem, see paragraph 3.7.1 (page 34).

3.3 Domain invariant

The notion of invariant domain plays an important role in the resolution of a system of conservation laws. We say that a convex set $\mathscr{X}$ is an invariant domain for (II.46) if it has the property that

$$\mathscr{X}^0(x) \in \mathscr{X} \text{ for all } x \;\Rightarrow\; \mathscr{X}(t,x) \in \mathscr{X} \text{ for all } x,t. \tag{II.54}$$

There is a full theory that enables to determine the invariant domains of a system of conservaion laws, see [123].

For the Saint-Venant system, the set

$$\{(H, H\overline{u}), H \geqslant 0\},$$

is an invariant domain.

The property for a scheme to preserve an invariant domain is an important issue of stability, as can be easily understood. In particular, the occurence of negative values for the water depth H (or the density in gas dynamics) leads rapidly to breakdown in the computation.

3.4 Shocks

A shock with speed U is a solution having the form

$$X(x,t) = \begin{cases} X_l & \text{if } \frac{x}{t} < U \\ X_r & \text{if } \frac{x}{t} > U \end{cases}$$

see Fig. II.2.

Let us consider the functions $X = (H, H\overline{u})^T$ defined by

$$H = H_l + H_e(x - Ut)(H_r - H_l), \tag{II.55}$$
$$H\overline{u} = (H\overline{u})_l + H_e(x - Ut)\big((H\overline{u})_r - (H\overline{u})_l\big), \tag{II.56}$$

where H_r, H_l, $(H\overline{u})_r$ and $(H\overline{u})_l$ are four constants. H_e denotes the Heaviside function. Then $X = (H, H\overline{u})^T$ are solutions of the homogenous Saint-Venant system (II.32)-(II.33) if

$$F(X_r) - F(X_l) = U(X_r - X_l). \tag{II.57}$$

Relation (II.57) is the so called Rankine-Hugoniot condition.

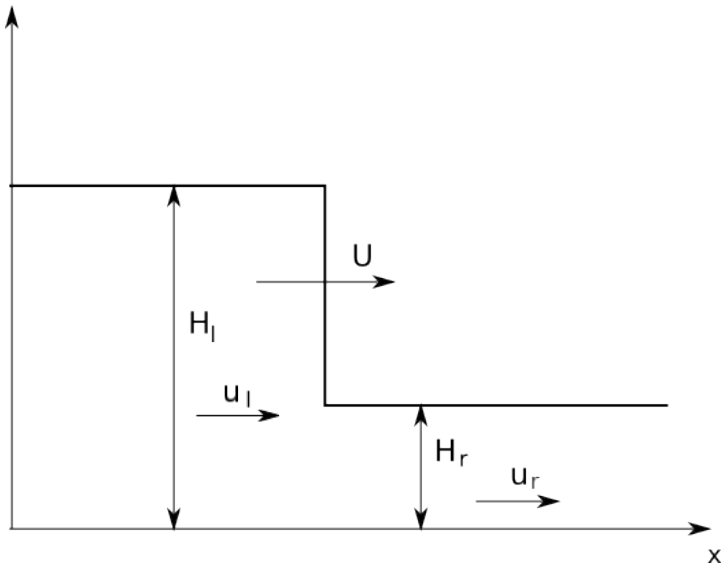

Figure II.2: A simple shock propagating with velocity U.

3.5 Entropy and non smooth solutions

The notion of entropy is fundamental. By definition, an entropy for the (homogenous) quasilinear system is a function $\zeta(Y)$ with real values such that it exists another real valued function $G(Y)$, called the entropy flux, satisfying

$$G'(Y) = \zeta'(Y)A(Y).$$

In other words, $\zeta' A$ needs to be an exact differential form. This property enables, by multiplying (II.47) by $\zeta'(Y)$, to establish another conservation law

$$\frac{\partial \zeta(Y)}{\partial t} + \frac{\partial G(Y)}{\partial x} = 0.$$

However the preceding equality cannot be satisfied when considering discontinuous solutions and it is replaced by

$$\frac{\partial \zeta}{\partial t} + \frac{\partial G}{\partial x} \leqslant 0. \tag{II.58}$$

A weak solution $X(t,x)$ to (II.46) is said to be entropy satisfying if (II.58) holds. This property is indeed a criteria to select a unique solution to the system, that can have many weak solutions otherwise.

For the Saint-Venant system, there exists a natural entropy/entropy flux pair and we call entropy solution to the Saint-Venant system, a weak solution which satisfies the entropy inequality given in the following theorem (we assume $p^a = 0$).

Theorem II.9. *The system (II.28)-(II.29) is strictly hyperbolic for $H > 0$. It admits a mathematical entropy E_h defined by (II.30) (which is also the energy) and satisfying*

$$\frac{\partial E_h}{\partial t} + \frac{\partial}{\partial x}\left(\overline{u}\big(E_h + g\frac{H^2}{2}\big)\right) = -\mathscr{D}, \tag{II.59}$$

with $\mathscr{D} \geqslant 0$ being the dissipation energy corresponding to the discontinuities.

We do not prove this theorem which relies on the classical theory of hyperbolic equations and simple algebraic calculation, see Dafermos [49]. We just recall that for smooth solutions $\mathscr{D} = 0$. Notice that E_h is convex with respect to H and $H\bar{u}$ **[EX]**.

To illustrate the notion of dissipation for non smooth solutions, we have the following proposition

Proposition II.10. *Let us consider a solution of the system (II.28)-(II.29),(II.59) (with flat bottom) containing a stationary shock. Then if H_l and H_r denote the water depth around the discontinuity then we have the relation*

$$\mathscr{D} = \frac{g}{4}|H_l - H_r|^3 \sqrt{\frac{g(H_l + H_r)}{2H_l H_r}}.$$

Proof of proposition II.10. We recall that around the shock, the Rankine-Hugoniot relations (II.57)

$$\begin{aligned} -U[H] + [H\bar{u}] &= 0, \\ -U[H\bar{u}] + \left[H\bar{u}^2 + \frac{g}{2}H^2\right] &= 0, \end{aligned}$$

holds with $U = 0$. The rest of the proof is left to the reader, see [22]. □

3.6 Existence of solutions

The well-posedness of the Saint-Venant is a difficult question that can be investigated using two different approaches depending on the importance of the viscosity terms. When viscosity terms cannot be neglected, see [70] and the references therein. In the other situation, the paper [50] and the references therein is interesting. Because the homogenous Saint-Venant system can also be seen as a particular form of the Euler system for gaz dynamics[1], the reader can refer to [90, 91, 114, 92].

3.7 Particular solutions

3.7.1 Stationary solutions

We are now interested in particular situations of the non homogenous Saint-Venant system. The homogenous situation i.e. when $\frac{\partial}{\partial x} z_b \equiv \mathbf{0}$ and $\mathbf{f} \equiv \mathbf{0}$ is, to some extent, classical since it corresponds to the isentropic Euler system.

Hereafter, we study several stationary solutions also called equilibrium states by analogy with dynamical systems. These solutions satisfy the system

$$\frac{\partial}{\partial x} F(X) = S_b(X) + S_{v,f}(X), \tag{II.60}$$

in the distributional sense. The system (II.60) is completed with the entropy inequality

$$\frac{\partial}{\partial x}(\bar{u}(E + gH^2/2)) \leqslant 0.$$

In the homogenous case, it is well-known that the stationary solutions consist in *constant states* connected each other by *stationary entropic shocks*. In the presence of sources, the situation is more complex even if stationary entropic shocks (the same as in the homogenous case) are admissible. Indeed, it is easy to see that the presence of enough regular source terms does not modifiy the derivation of the Rankine-Hugoniot jump condition (II.57) **[EX]**. In the following paragraph we first propose the construction of stationary smooth solutions for the Saint-Venant system then we investigate the construction of piecewise smooth stationary solutions connected with entropic stationary shocks.

[1] The analogy between the isentropic Euler equations and the Saint-Venant system appears replacing $H, gH^2/2$ by $\rho, p(\rho) = g\rho^\gamma/2$ (adiabatic coefficient $\gamma = 2$).

The lake at rest The first case consists in looking for solutions of (II.60) with $H\mathbf{u} \equiv \mathbf{0}$. The first equation is trivially satisfied and the second one gives for smooth solutions

$$H\frac{\partial H}{\partial x} = H\frac{\partial z_b}{\partial x}.$$

Two situations are possible. Either $H \equiv 0$, corresponding to a dry area, or $\frac{\partial}{\partial x}(H+z_b) = 0$ meaning the free surface of the water is flat. Notice stationary shocks with $H\mathbf{u} \equiv \mathbf{0}$ are not possible. Therefore we have the following characterization of the solutions at rest

$$H \in \mathscr{C}^0(\mathbb{R}^2) \text{ such that } \begin{cases} H = 0 \\ \text{or} \\ \frac{\partial}{\partial x}(H+z_b) = 0 \end{cases} \tag{II.61}$$

These solutions correspond to the situation of a lake at rest, see Fig. II.3. Even if the lake at rest solution

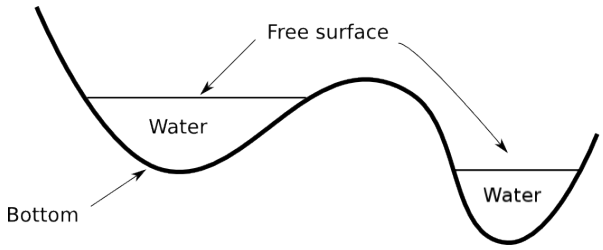

Figure II.3: Stationary solution corresponding to the lake at rest.

is very simple, it has a crucial interest. Indeed, the lake at rest solution is often the initial condition for a simulation and we will see that in practice i.e. at the discrete level, it is not so easy to maintain this solution.

Équilibrium without friction and viscosity : Bernoulli's theorem We consider now the case where $H\mathbf{u} \not\equiv \mathbf{0}$ but without friction nor viscosity. Simple manipulations show that stationary solutions satisfy

$$\begin{aligned} &\frac{\partial}{\partial x}(H\overline{u}) = 0, \\ &\overline{u}\frac{\partial \overline{u}}{\partial x} + g\frac{\partial}{\partial x}(H+z_b) = 0, \end{aligned} \tag{II.62}$$

or equivalently

$$\frac{\partial}{\partial x}\left(u^2/2 + g(H+z_b)\right) = 0,$$

that is exactly the *Bernouilli's theorem* where the pressure is hydrostatic. The Bernouilli's theorem can also be formulated in 2d (along the streamlines) **[EX]**.

Hereafter, we illustrate these particular solutions for the 1d Saint-Venant system with topography (without friction/viscosity) in three typical cases

- Bernoulli's equilibrium in fluvial regime

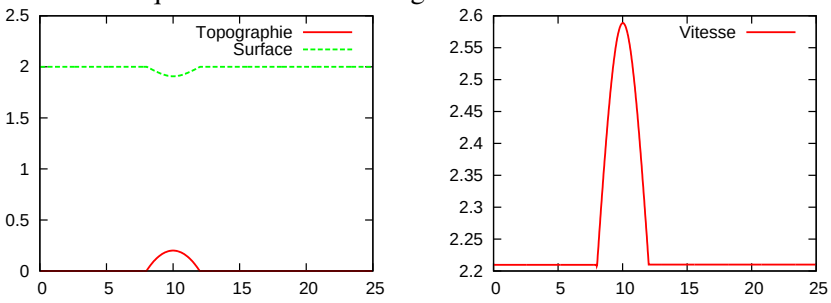

- Bernoulli's equilibrium fluvial (left part of the channel) and torrential (right part of the channel)

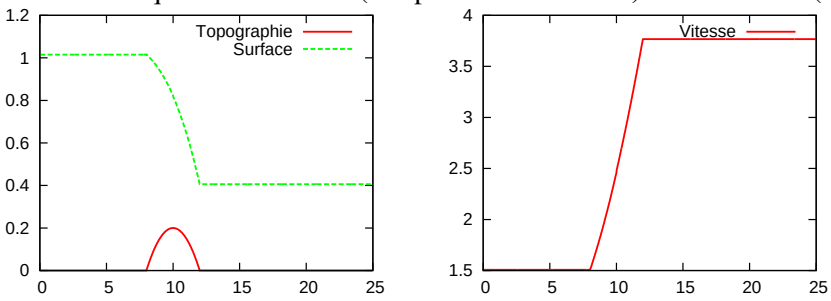

- Bernoulli's equilibrium and hydraulic jump

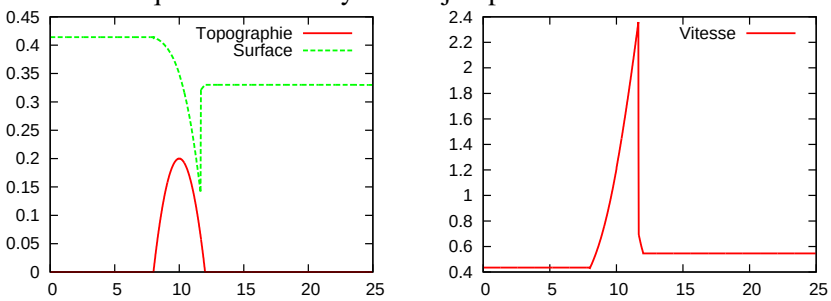

A study of these types of equilibria can be found in [43]. These typical situations often appear as long time solutions of the Saint-Venant system and strongly depend on the imposed boundary conditions. Notice that the three stationary states given above have been obtained with the same initial conditions.

3.7.2 Time dependent solutions

Now we propose some examples of non stationary solutions of the Saint-Venant system in 1d.

Roll waves Roll waves are periodic solutions moving at constant speed. They can appear in very particular situations but once the conditions are satisfied, the roll waves are very stable solutions. These solutions contain a smooth part and a shock, both propagating at the same speed [53, 79, 107], see Fig. II.4 for an illustration.

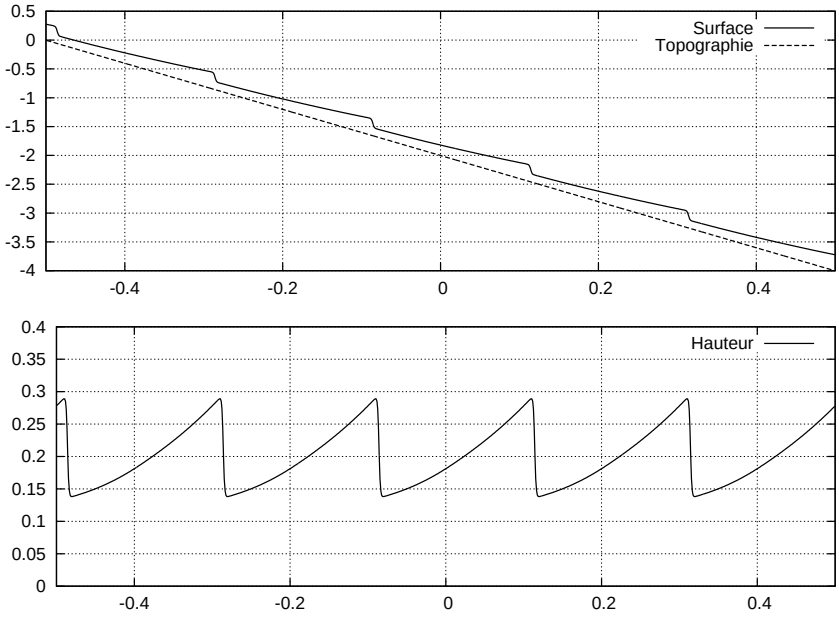

Figure II.4: Simulation de roll waves

Friction dominated flows When a dam break occurs, a wave floods a large area, typically dry, downstream the dam. Instead of taking into account the description of this flooded region, it is possible to model their influence by the means of additional terms or by a modification of existing terms. When the flooded region is a forest or typically a area with a lot of obstacles, its influence can be modeled by a significant increase in the friction coefficient.

Therefore, we consider the 1d system

$$\begin{aligned} &\frac{\partial H}{\partial t} + \frac{\partial H\bar{u}}{\partial x} = 0, \\ &\frac{\partial H\bar{u}}{\partial t} + \frac{\partial}{\partial x}\left(Hu^2 + gH^2/2\right) = -gH\frac{\partial z_b}{\partial x} - \kappa H\bar{u}. \end{aligned} \tag{II.63}$$

Other friction laws than $-\kappa H\bar{u}$ could have been used. In the following we denote

$$s(x) = \frac{\partial z_b}{\partial x}.$$

Let us denote T, L_0, H_0, $S = H_0/L_0$ and $U = L_0/T$ the characteristic quantities respectively corresponding to time, length, water depth, slope and velocity. Since κ corresponds to a frequency, we introduce a dimensionless friction coefficient κ_0 so that $\kappa = \kappa_0/T_\kappa$. And hence, denoting with˜the dimensionless variables, the system (II.63) becomes **[EX]**

$$\begin{aligned} &\frac{H_0}{T}\left[\partial_{\tilde{t}}\tilde{H} + \partial_{\tilde{x}}(\tilde{H}\tilde{u})\right] = 0, \\ &\frac{H_0L_0}{T^2}\left[\partial_{\tilde{t}}(\tilde{H}\tilde{u}) + \partial_{\tilde{x}}(\tilde{H}\tilde{u}^2) + \frac{1}{\mathsf{Fr}^2}\partial_{\tilde{x}}(\tilde{H}^2/2)\right] = -\frac{1}{\mathsf{Fr}^2}\frac{H_0L_0}{T^2}\tilde{H}\tilde{s} - \frac{H_0L_0}{T^2}\kappa_0\tilde{H}\tilde{u}, \end{aligned}$$

where $\mathsf{Fr} = U/\sqrt{gH_0}$ is the Froude number. A friction dominated flow is characterized by the fact that κ_0 is much larger than the other dimensions. Here, this means $\tilde{u} = \mathscr{O}(1/\kappa_0)$. Moreover the characteristic time associated with the friction is T/κ_0, that is very small compared to T. These two estimates induce a new definition for the dimensionless quantities $\tilde{t}$ and $\tilde{u}$ under the form

$$\tilde{t} = \frac{t}{\kappa_0 T} \quad \text{and} \quad \tilde{u} = \frac{\kappa_0 u}{U}, \tag{II.64}$$

that is compatible with the relation $U = L_0/T$. Therefore, the system becomes

$$\begin{aligned} &\begin{cases} \dfrac{H_0}{\kappa_0 T}\left[\partial_{\tilde{t}}\tilde{H} + \partial_{\tilde{x}}(\tilde{H}\tilde{u})\right] = 0, \\ \dfrac{H_0L_0}{(\kappa_0 T)^2}\left[\partial_{\tilde{t}}(\tilde{H}\tilde{u}) + \partial_{\tilde{x}}(\tilde{H}\tilde{u}^2) + \dfrac{\kappa_0^2}{\mathsf{Fr}^2}\partial_{\tilde{x}}(\tilde{H}^2/2)\right] = -\dfrac{1}{\mathsf{Fr}^2}\dfrac{H_0L_0}{T^2}\tilde{H}\tilde{s} - \dfrac{H_0L_0}{T^2}\tilde{H}\tilde{u}, \end{cases} \\ \Longrightarrow &\begin{cases} \partial_{\tilde{t}}\tilde{H} + \partial_{\tilde{x}}(\tilde{H}\tilde{u}) = 0, \\ \partial_{\tilde{x}}(\tilde{H}^2/2) = -\tilde{H}\tilde{s} - \mathsf{Fr}^2\tilde{H}\tilde{u} + \mathscr{O}(1/\kappa_0^2), \end{cases} \\ \Longrightarrow &\begin{cases} \mathsf{Fr}^2\partial_{\tilde{t}}\tilde{H} - \partial_{\tilde{x}}(\tilde{H}\tilde{s} + \partial_{\tilde{x}}(\tilde{H}^2/2)) = \mathscr{O}(1/\kappa_0^2), \\ \mathsf{Fr}^2\tilde{H}\tilde{u} = -\tilde{H}\tilde{s} - \partial_{\tilde{x}}(\tilde{H}^2/2) + \mathscr{O}(1/\kappa_0^2). \end{cases} \end{aligned}$$

The last system has a nonlinear parabolic equation and a relation between the flow velocity, the water depth and the gradient of the water depth. In other words, the velocity is related to the external forcing – the slope $\tilde{s}$ – and the pressure gradient, that corresponds to the *Darcy law*.

It is important to notice that the asymptotic form of an initial hyperbolic system with source term – in the case of a friction dominated flow – is a parabolic equation. For more details, the reader can refer to [50, 100].

3.7.3 Construction of analytical solutions for the Saint-Venant system

The Saint-Venant system cannot be solved analytically for any topography profile and any initial or boundary conditions. But choosing e.g. a particular topography and/or particular boundary conditions, the Saint-Venant system (II.32)-(II.33) can be solved by hand. In this paragraph, we first propose time dependent analytical solutions, then we derive a large family of stationary analytical solutions and finally the case of stationary analytical solutions with shocks is studied.

We assume $p^a = p_0^a = cst$. We also neglect the friction and viscous effects i.e. $\kappa = \nu = 0$.

The parabolic bowl The idea presented in this paragraph is due to Thacker [128]. It consists in looking for analytical solutions the Saint-Venant system (II.32)-(II.33) with the particular velociy field

$$u = u(x,t) = f(t). \tag{II.65}$$

Then Eq. (II.32) becomes

$$\frac{\partial H}{\partial t} + f\frac{\partial H}{\partial x} = 0,$$

whose solution is given by

$$H = F_1(x - \int_0^t f(t_1)dt_1),$$

where F_1 is any given non negative function.

With the particular choices $b_0 > 0$

$$\begin{aligned} F_1(z) &= -\frac{b_0}{2}z^2, \\ z_b(x) &= \frac{b_0}{2}x^2, \end{aligned}$$

Eq. (II.33) reduces to

$$\frac{df}{dt} + gb_0 \int^t f(t_1)dt_1 = 0,$$

whose solution is given by

$$f(t) = C_1 \sin(\sqrt{gb_0}t) + C_2 \cos(\sqrt{gb_0}t).$$

Choosing appropriate initial conditions typically $f(0) = 1$, $f'(0) = 0$ gives

$$f(t) = \cos(\sqrt{gb_0}t),$$

and hence

$$\begin{aligned} H(x,t) &= \max\left(0, -\frac{b_0}{2}\left(x - \frac{1}{\sqrt{gb_0}}\sin(\sqrt{gb_0}t)\right)^2\right), \\ u(x,t) &= \cos(\sqrt{gb_0}t), \end{aligned}$$

are analytical solutions of the Saint-Venant system and periodic in time. Notice that the quantity $H + zb$ reads

$$H + z_b = \frac{b_0}{\sqrt{gb_0}}\sin(\sqrt{gb_0}t)x - \frac{1}{\sqrt{2g}}\sin^2(\sqrt{gb_0}t),$$

meaning the free surface remains a straight line with slope varying along time.

Stationary analytical solutions The system (II.62) can be rewritten under the form

$$\begin{aligned} &\frac{\partial}{\partial x}\left(\frac{Q_0^2}{2H^2}+g(H+z_b)\right)=0,\\ &\overline{u}=\frac{Q_0}{H}, \end{aligned} \tag{II.66}$$

Therefore, for any non negative and enough regular function $H_0(x)$ and any constant $z_{b,0}$, the system

$$\begin{aligned} H &= H_0,\\ \overline{u} &= \frac{Q_0}{H},\\ z_b &= z_{b,0}-H-\frac{Q_0^2}{2gH^2}, \end{aligned}$$

with Q_0 a constant – corresponding to the imposed flow at the entry – is an analytical solution of the Saint-Venant system with topography (without friction/viscosity).

Stationary analytical solutions with discontinuities The system (II.66) is equivalent to

$$\begin{aligned} &\left(g-\frac{Q_0^2}{H^3}\right)\frac{\partial H}{\partial x}=-g\frac{\partial z_b}{\partial x},\\ &\overline{u}=\frac{Q_0}{H}, \end{aligned} \tag{II.67}$$

meaning, starting from a boundary condition for H, the resolution of a simple first order ODE gives an analytical solution for the Saint-Venant system. But since the quantity

$$g-\frac{Q_0^2}{H^3},$$

can cross 0, the solution (II.67) can be discontinuous. This is what we investigate below.

Let us consider a closed basin with vertical shores of length L. At the inflow in $x=0$, the boundary condition is a given flux Q_0 and at the exit in $x=L$ we impose a given water depth H_L.

An integration of the system (II.66) between the current position x and the exit L gives (when there is no discontinuity over the interval (x,L))

$$\frac{Q_0^2}{2H^2}+g(H+z_b)=\frac{Q_0^2}{2H_L^2}+g(H_L+z_{b,L}). \tag{II.68}$$

Since the study of the function

$$F:H\mapsto\frac{Q_0^2}{2H^2}+g(H+z_b),$$

shows that

$$\min_{\mathbb{R}_+}F(H)=\frac{3}{2}\sqrt[3]{Q_0^2g^2}+gz_b,$$

we see that if

$$\min_{x\in[0,L]}\frac{3}{2}\sqrt[3]{Q_0^2g^2}+gz_b<\frac{Q_0^2}{2H_L^2}+g(H_L+z_{b,L}),$$

then Eq. (II.68) cannot be solved for any $x\in[0,L]$. In such a situation, we proceed as follows.

Firstly, we observe that the minimum of the function $F(H)$ is achieved for

$$H_{lim}=\frac{1}{g}\sqrt[3]{Q_0^2g^2}, \tag{II.69}$$

that exactly corresponds to a Froude number of 1. Indeed, the Froude number being defined as in Eq. (II.45) by

$$Fr = \frac{\overline{u}}{\sqrt{gH}},$$

we have in our situation

$$Fr = \frac{Q_0}{H\sqrt{gH}},$$

and the value of H_{lim} gives $Fr = 1$. Therefore, Eq. (II.68) admits either zero or two solutions and among these two solutions one belong to the fluvial regime and the other one to the torrential one.

Secondly, we assume Q_0 and H_L are such that the regime is fluvial at the entry $x = 0$ and at the exit $x = L$. We also consider the bottom topography has the shape of a bump e.g. something like

$$z_b(x) = e^{-(x-x_m)^2},$$

with $x_m \in]0, L[$.

Then, the analytical solution is obtained using the following process

1. due to the choice of the topography z_b with $z_b(x_m) = \max_{x\in[0,L]} z_b(x)$, H_{lim} the minimum of the function $F(H)$ is obtained in $x = x_m$ and it corresponds to the abscissa where the Froude number equals 1. This means that starting from $x = 0$ where the regime is fluvial, the transition towards the torrential regime occurs in $x = x_m$. For $x \in (x_m, x_c)$, x_c being the position of the shock, the flow is torrential. And $x \in (x_c, L)$ we end up with a fluvial regime.

2. Around the shock located in x_c we have the conservation of momentum

$$\left(\frac{Q_0^2}{H} + \frac{g}{2}H^2\right)\Big|_{x_c^-} = \left(\frac{Q_0^2}{H} + \frac{g}{2}H^2\right)\Big|_{x_c^+}.$$

In order to calculate the analytical solution, we have to find the location of the shock x_c that is obtained solving the following system

$$\begin{aligned}
&\frac{Q_0^2}{2H_0^2} + g(H_0 + z_{b,0}) = \frac{Q_0^2}{2H_{c^-}^2} + g(H_{c^-} + z_{b,c}) \\
&\frac{Q_0^2}{2H_{c^+}^2} + g(H_{c^+} + z_{b,c}) = \frac{Q_0^2}{2H_{lim}^2} + g(H_{lim} + z_{b,lim}) \\
&\frac{Q_0^2}{H_{c^-}} + \frac{g}{2}H_{c^-}^2 = \frac{Q_0^2}{H_{c^+}} + \frac{g}{2}H_{c^+}^2
\end{aligned}$$

with H_{lim} defined by (II.69) and whose unknown are H_{c^-}, H_{c^+} and $z_{b,c}$.

4 Kinetic approach

We briefly present the kinetic theory applied to the formulation/interpretation of conservation laws. For a complete overview, the reader can refer to [112].

The idea we would like to emphasize is that the kinetic approach has two levels. First, the *kinetic formulations* where a full description is given when a large enough family of entropies is available, and the more general *kinetic representation* which is based on a single entropy. Notice that the *kinetic formulation* is not restricted to hyperbolic problems, it can be obtained for parabolic problems such as parabolic scalar conservation laws, see [112, chap. 1].

The so-called kinetic formulation of nonlinear hyperbolic systems of conservation laws is a method which reduces them to a linear equation, with an additional kinetic variable, on a nonlinear quantity related to the conserved unknowns. It represents all the entropy inequalities in a single Boltzmann type equation depending on the kinetic variable. It was introduced by Lions, Perthame and Tadmor for

scalar conservation laws (see [90, 114]) and for isentropic gas dynamics (see [91]). It turns out to be a powerful tool to derive mathematical properties – and also numerical schemes.

A kinetic interpretation is much weaker than the kinetic formulation since it only uses a single entropy often given by the energy. Moreover in a kinetic representation, the collision term in the right hand side carries little information. And yet, kinetic interpretations are in practice very useful since it allows to construct efficient numerical schemes.

In the following paragraph, we present the kinetic interpretation of the Saint-Venant system allowing to reduce the nonlinear set of equations to a scalar, essentially linear equation.

4.1 Kinetic interpretation of the Saint-Venant system

We introduce a distribution function $M(x,t,\xi)$ of fictitious particles with microscopic velocity ξ in order to obtain a linear microscopic kinetic equation equivalent to the macroscopic model (II.28)-(II.29).

We also introduce a real function χ defined on $\mathbb{R}$, compactly supported and which has the following properties

$$\left\{ \begin{array}{l} \chi(-w) = \chi(w) \geqslant 0 \\ \int_{\mathbb{R}} \chi(w)\, dw = \int_{\mathbb{R}} w^2 \chi(w)\, dw = 1, \end{array} \right. \tag{II.70}$$

we also define $k_3 = \int_{\mathbb{R}} \chi^3(w)\, dw$. Among all the possible choices for χ, two are very interesting. In [113], the interest of the choice

$$\chi_0(z) = \frac{1}{\pi}\sqrt{1-\frac{z^2}{4}}\mathbb{1}_{|z|\leqslant 2}. \tag{II.71}$$

is explained. The simplest choice for χ is

$$\chi_1(z) = \frac{1}{2\sqrt{3}}\mathbb{1}_{|z|\leqslant\sqrt{3}}, \tag{II.72}$$

but with less theoretical properties [10].

Now let us construct the density of particles $M(x,t,\xi)$ defined by a Gibbs equilibrium: the microscopic density of particles present at time t, abscissa x and with velocity ξ is given by

$$M(x,t,\xi) = \frac{H}{c}\chi\left(\frac{\xi-\overline{u}}{c}\right), \tag{II.73}$$

with $c = \sqrt{\frac{gH}{2}}$. Then we have the following proposition

Proposition II.11. *The functions $(H,\overline{u})$ are strong solutions of the Saint-Venant system (without friction) described in (II.28)-(II.29) if and only if the equilibrium $M(x,t,\xi)$ is solution of the kinetic equation*

$$(\mathscr{B}) \qquad \frac{\partial M}{\partial t} + \xi\frac{\partial M}{\partial x} - g\frac{\partial z_b}{\partial x}\frac{\partial M}{\partial \xi} = Q(x,t,\xi), \tag{II.74}$$

where $Q(x,t,\xi)$ is a "collision term" satisfying

$$\int_{\mathbb{R}} Q\, d\xi = \int_{\mathbb{R}} \xi Q\, d\xi = 0. \tag{II.75}$$

The solution is an entropy solution if additionally

$$\int_{\mathbb{R}} \left(\xi^2 + \frac{3g^2}{4k_3}M^2\right) Q d\xi \leqslant 0. \tag{II.76}$$

Proof of Prop. II.11. The proof **[EX]** is very simple and relies on simple integrations of the Gibbs equilibrium (II.73) using the properties (II.70), leading to

$$\int_{\mathbb{R}} M\, d\xi = H, \qquad \int_{\mathbb{R}} \xi M\, d\xi = H\bar{u}, \tag{II.77}$$
$$\int_{\mathbb{R}} \xi^2 M\, d\xi = H\bar{u}^2 + \frac{g}{2}H^2.$$

□

5 The rotating Saint-Venant system

The 3d hydrostatic Euler with Coriolis and constant density is given by

$$\nabla \cdot \mathbf{U} = 0, \tag{II.78}$$
$$\rho_0 \left(\frac{\partial \mathbf{u}}{\partial t} + \nabla_{x,y} \cdot (\mathbf{u} \otimes \mathbf{u}) + \frac{\partial (\mathbf{u} w)}{\partial z} \right) + \nabla_{x,y} p = -\rho_0 \Omega \mathbf{u}^{\perp}, \tag{II.79}$$
$$\frac{\partial p}{\partial z} = -\rho_0 g, \tag{II.80}$$

where $\mathbf{U}(t,x,y,z) = (u,v,w)^T$ is the velocity, $\mathbf{u}(t,x,y,z) = (u,v)^T$ is the horizontal velocity, p is the fluid pressure, g represents the gravity acceleration and $\rho_0 = cst$ is the fluid density. The quantity ∇ denotes $\nabla = \left(\frac{\partial}{\partial x}, \frac{\partial}{\partial y}, \frac{\partial}{\partial z}\right)^T$, $\nabla_{x,y}$ corresponds to the projection of ∇ on the horizontal plane i.e. $\nabla_{x,y} = \left(\frac{\partial}{\partial x}, \frac{\partial}{\partial y}\right)^T$. The term $\Omega \mathbf{u}^{\perp} = \Omega(-v,u)^T$ denotes the Coriolis force with Ω the angular speed.

Is is easy to see that the shallow water approximation of the system (II.78)-(II.80) coupled with the 2d version of the boundary conditions (I.9),(I.11) and (I.20) under the form On the bottom we prescribe an impermeability condition

- kinematic boundary condition at the bottom $\mathbf{U}.\mathbf{n}_b = 0$,
- kinematic boundary condition at the free surface $\frac{\partial \eta}{\partial t} + \mathbf{u}(t,x,y,\eta) \cdot \nabla_{x,y}\eta - w(t,x,y,\eta) = 0$,
- dynamic boundary condition at the free surface $p(t,x,y,\eta(t,x,y)) = 0$,

leads to the 2d rotating Saint-Venant system defined by

$$\frac{\partial h}{\partial t} + \nabla_{x,y} \cdot (h\mathbf{u}) = 0, \tag{II.81}$$
$$\frac{\partial (h\mathbf{u})}{\partial t} + \nabla_{x,y} \cdot (h\mathbf{u} \otimes \mathbf{u}) + \nabla_{x,y}\left(\frac{g}{2}h^2\right) = -gh\nabla_{x,y} z_b - \Omega h \mathbf{u}^{\perp}, \tag{II.82}$$

with $\mathbf{u}^{\perp} = (-v,u)^T$ and where the variations of the atmospheric pressure, the rheology of the fluid and the friction at the bottom have been neglected. The energy balance satisfied by (II.81)-(II.82) is given by

$$\frac{\partial hE}{\partial t} + \nabla_{x,y} \cdot \mathbf{u}\left(hE + \frac{g}{2}h^2\right) = 0,$$

with $E = \frac{u^2+v^2}{2} + \frac{g}{2}(\eta^2 - z_b^2)$.

It is very important to notice that the Coriolis forcing has no influence over the energy balance (it is obvious since $\mathbf{u}^{\perp} \cdot \mathbf{u} = 0$). We are going to examine questions and difficulties arising when one wants to apprximate the rotating Saint-Venant system.

5.1 Stationary analytical solutions

We begin with simple results concerning the stationary solutions of the system (II.81)-(II.82).

The following proposition gives a family of analytical solutions for the system (II.81)-(II.82) with a non flat topography.

Proposition II.12. *Let f be any real value function, h_0 a non negative constant and z_b^0 a constant. Then the variables h,u,v,w,p defined by*

$$
\begin{aligned}
&h(t,x,y) = h_0 + \frac{1}{2g}\int_0^{x^2+y^2} f(z)(f(z)+\Omega)dz,\\
&u(t,x,y,z) = yf(x^2+y^2), \qquad \text{(II.83)}\\
&v(t,x,y,z) = -xf(x^2+y^2), \qquad \text{(II.84)}\\
&w(t,x,y,z) = -\partial_x\Big((z-z_b)yf(x^2+y^2)\Big) + \partial_y\Big((z-z_b)xf(x^2+y^2)\Big),\\
&p(t,x,y,z) = \frac{g}{\rho_0}(h+z_b-z),\\
&z_b(x,y) = z_b^0 - \frac{\Omega}{g}\int_0^{x^2+y^2} f(z)dz,
\end{aligned}
$$

are analytical solutions of the system (II.78)-(I.9).

Since the expressions (II.83) and (II.84) for u and v do not depend on the variable z, the proposed analytical solution is also an analytical solution for the Saint-Venant system (II.81)-(II.82) with Coriolis.

In the case of a flat topography, the following proposition gives an analytical solution for the system (II.78)-(I.9).

Proposition II.13. *Let $z \mapsto f(z)$ be any function then the variables h,u,v,w,p defined by*

$$
\begin{aligned}
&h(t,x,y) = h_0 + \frac{1}{2g}\int_0^{x^2+y^2} f(z)(f(z)-\Omega)dz, \qquad \text{(II.85)}\\
&u(t,x,y,z) = yf(x^2+y^2), \qquad \text{(II.86)}\\
&v(t,x,y,z) = -xf(x^2+y^2), \qquad \text{(II.87)}\\
&w(t,x,y,z) = 0,\\
&p(t,x,y,z) = g(h+z_b-z),
\end{aligned}
$$

with $h_0 = cst$, $h_0 \geqslant 0$ and $z_b(x,y) = z_{b,0} = cst$ are analytical solutions of the system (II.78)-(I.9).

Since the expressions (II.86) and (II.87) for u and v do not depend on the variable z, the proposed analytical solution is also an analytical solution for the Saint-Venant system (II.81)-(II.82) with Coriolis.

Remark 2. Notice that these analytical solution do not vanish when $\Omega = 0$. Moreover the expressions for u, v and w do not depend on Ω. Only the expression for h depends on Ω.

Remark 3. The choice $f(z) = c_1 e^{c_2 z}$ where c_1 and c_2 are constant allows to create vortex of arbitrary height and width. The figure II.5 illustrates the shape of these stationary analytical solutions.

Proof of Props. II.12 and II.13. The proofs rely on very simple computations. □

6 An exercice (in french)

On considère un écoulement 'shallow water' modélisé par les équations de Saint-Venant. L'écoulement a lieu sur une topographie donnée par $x \to z_b(x)$.

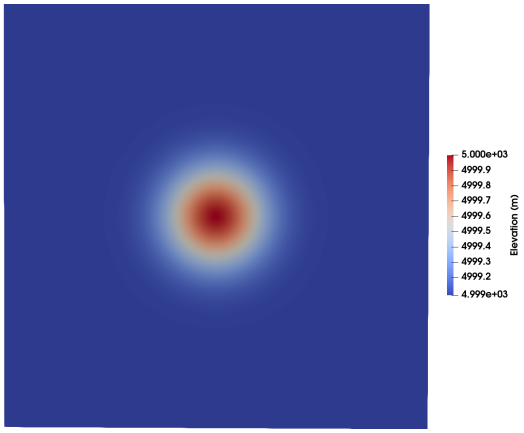

(a)

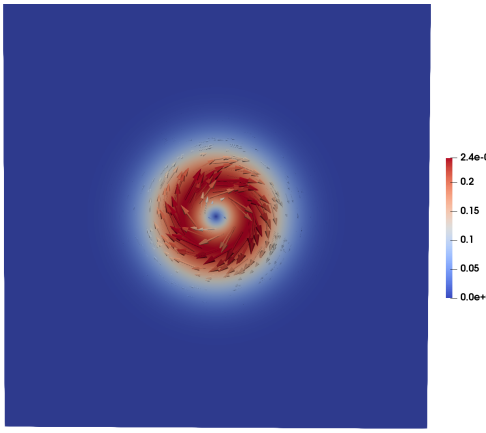

(b)

Figure II.5: A stationary vortex : *(a)* water depth and *(b)* velocity field.

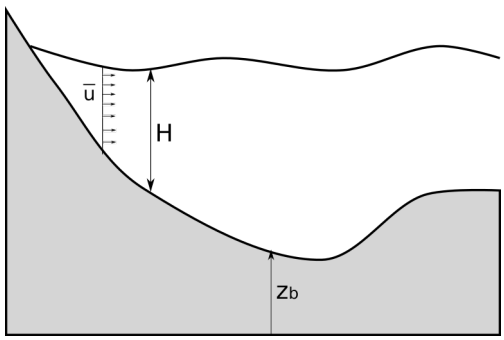

Figure II.6: Notations pour les équations de Saint-Venant.

On rappelle l'expression des équations de Saint-Venant

$$\frac{\partial H}{\partial t} + \frac{\partial (H\bar{u})}{\partial x} = 0, \tag{II.88}$$

$$\frac{\partial (H\bar{u})}{\partial t} + \frac{\partial}{\partial x}\left(H\bar{u}^2 + \frac{g}{2}H^2\right) = -gH\frac{\partial z_b}{\partial x}, \tag{II.89}$$

où $\rho_1 = cste$ est la densité du fluide, $H(x,t)$ est la hauteur d'eau du fluide et $\bar{u}(x,t)$ sa vitesse, voir figure II.6. On néglige les effets de la pression atmosphérique et de la viscosité du fluide.

1. Rappeler brièvement comment sont obtenues les équations de Saint-Venant.
2. Quelle est l'équation d'énergie vérifiée par le système (II.88)-(II.89) ? Comment est-elle obtenue ?
3. Quel est l'effet du frottement entre le fluide et la topographie ? Comment sont modifiées les équations (II.88)-(II.89) lorsqu'un frottement de type Navier est considéré entre le fluide et la topogrphie ?
4. On remplace l'équation (II.89) par

$$\frac{\partial (H\bar{u})}{\partial t} + \frac{\partial}{\partial x}\left(H\bar{u}^2 + \frac{g}{2}H^2\right) = -gH\frac{\partial z_b}{\partial x} + S_f(H,\bar{u}),$$

où le terme $S_f(H,\bar{u})$ correspond à un frottement entre le fluide et la topographie. A quelle condition le terme $S_f(H,\bar{u})$ correspond-il à une dissipation d'énergie ?

On considère maintenant la situation décrite par la figure II.7. La topographie $x \to z_b(x)$ est constituée d'un matériau 'très dur' qui ne se déforme pas au cours du temps. Un second fluide dénommé fluide 2, de densité $\rho_b = cste$, de hauteur $H_b(x,t)$ et ayant pour vitesse $u_b(x,t)$ est présent. Les fluides 1 et 2 ne sont pas miscibles.

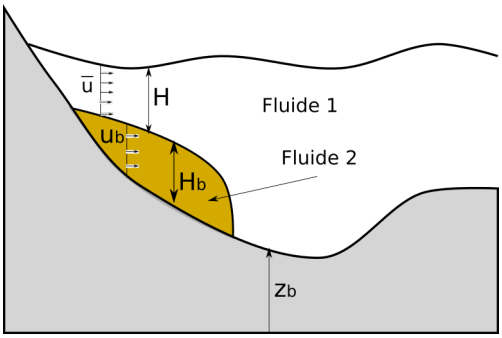

Figure II.7: Notations pour la modélisation du glissement de terrain.

5. Comment se réécrit le système (II.88)-(II.89) pour tenir compte de la nouvelle topographie $x \to z_b(x) + H_b(x,t)$
6. Rappeler ce que signifie l'hypothèse hydrostatique pour un écoulement gouverné par les équations de Navier-Stokes.
7. En supposant que l'écoulement dans le fluide 1 est hydrostatique, quelle est l'expression de la pression dans le fluide 1 ?
8. En supposant que l'écoulement dans le fluide 2 est hydrostatique, quelle est l'expression de la pression dans le fluide 2 ?
9. En supposant que l'écoulement dans le fluide 2 est de type 'shallow water', comment s'écrivent les équations de Saint-Venant dans le fluide 2 ?

10. On suppose que $\bar{u} \ll gH$ et $u_b \ll gH_b$, montrer que le système formé des équations (II.88)-(II.89) complété par le modèle obtenu à la question 9 s'écrit

$$\frac{\partial H}{\partial t} + \frac{\partial (H\bar{u})}{\partial x} = 0, \tag{II.90}$$

$$\frac{\partial (H\bar{u})}{\partial t} + \frac{\partial}{\partial x}\left(\frac{g}{2}H^2\right) = -gH\frac{\partial (z_b + H_b)}{\partial x}, \tag{II.91}$$

$$\frac{\partial H_b}{\partial t} + \frac{\partial (H_b u_b)}{\partial x} = 0, \tag{II.92}$$

$$\frac{\partial (H_b u_b)}{\partial t} + \frac{\partial}{\partial x}\left(\frac{g}{2}H_b^2\right) = -gH_b\frac{\partial z_b}{\partial x} - g\frac{\rho_1}{\rho_2}H_b\frac{\partial H}{\partial x}. \tag{II.93}$$

11. Montrer que le système (II.90)-(II.93) est hyperbolique si et seulement si

$$\frac{\rho_1}{\rho_2} < 1.$$

12. Proposer un schéma HLL pour approximer le système (II.90)-(II.93).

13. Simuler numériquement (II.90)-(II.91) dans le cas où H_b est connu, de la forme $F(x-ct)$.

14. Comment faudrait-il modifier les équations (II.91) et (II.93) pour modéliser un frottement de type Navier entre les fluides 1 et 2 ?

15. On suppose maintenant que $z_b = z_b^0 = cste$. Montrer que le fluide 1 vérifie l'équation des ondes

$$\frac{\partial^2 H}{\partial t^2} - \frac{\partial}{\partial x}\left(gH\frac{\partial H}{\partial x}\right) = g\frac{\partial}{\partial x}\left(H\frac{\partial H_b}{\partial x}\right). \tag{II.94}$$

16. Dans l'équation (II.94), on suppose $H = H_0 + h$ avec $H_0 = cste$ et $h \ll H_0$. De plus, on considère que $H_b = H_b(x,t)$ est de la forme

$$H_b = F(x-ct),$$

avec $c = cste$. Montrer que h satisfait l'équation

$$\frac{\partial^2 h}{\partial t^2} - gH_0\frac{\partial^2 h}{\partial x^2} = -gH_0F''(x-ct). \tag{II.95}$$

17. On cherche des solutions de l'équation (II.95) sous la forme $h(x,t) = \bar{h}(x-c_1t)$. A quelle condition sur c_1 peut-on avoir un effet de résonance ?

Remark 4. Pour répondre aux questions 12 et 13, il faut avoir vu le chapitre IV traitant de l'approximation numérique.

Chapter III

Around the Saint-Venant system

We will see in chapter V that even if the Saint-Venant system is a useful and efficient model, it fails to represent several type of complex flows, typically when the vertical acceleration is not small compared to the gravity effects or when the velocity field strongly varies along the vertical direction.

Despite some weaknesses, the Saint-Venant system remains a complex model to analyse and in several situations, simpler models than the Saint-Venant system can be useful. This is the objective of this chapter to present some of them.

1 Wave equation

1.1 Origins of the wave equation

Let us consider a string, its mass per unit length is denoted μ. It is stretched by a tension $T(x)$, which is much larger than the weight of the string, see Fig III.1. Applying the fondamental principle of dynamics to a small piece of the string of length dx and mass μdx we obtain over the axis x the balance

$$\mu dx \frac{\partial^2 y}{\partial t^2} = T(x+dx)\tan(\theta(x+dx)) - T(x)\tan(\theta(x)).$$

The length dx and the angle $\theta(x)$ being small, we can write

$$\tan\theta(x) \approx \theta(x) \approx \frac{\Delta y}{\Delta x} \approx \frac{\partial y}{\partial x},$$

and assuming $T(x+dx) = T(x) = T_0 = cst$, we get

$$T(x+dx)\tan(\theta(x+dx)) - T(x)\tan(\theta(x)) = T_0(\tan(\theta(x+dx) - \tan(\theta(x)) \approx T_0 \frac{\partial \theta}{\partial x} dx \approx T_0 \frac{\partial^2 y}{\partial x^2} dx.$$

Therefore the motion equation of the string is given by

$$\frac{\partial^2 y}{\partial t^2} = c_0^2 \frac{\partial^2 y}{\partial x^2}, \tag{III.1}$$

with

$$c_0 = \sqrt{\frac{T_0}{\mu}}.$$

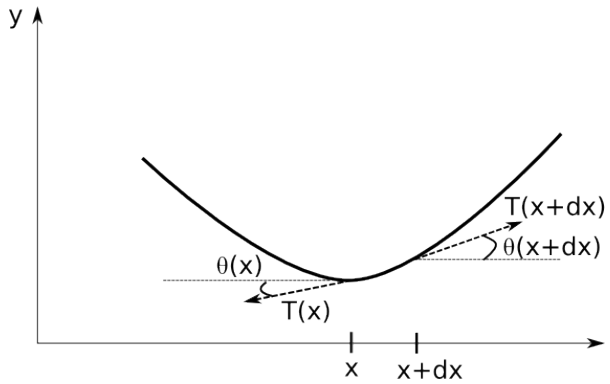

Figure III.1: Tension of the string between x and $x+dx$.

Equation (III.1) is called the `wave equation`. Depending on the imposed initial and boundary conditions, it admits two type of solutions, namely

- considering a very long string and imposing an initial condition at time t_0 of the form

$$y(x,t_0) = y_0(x),$$

then, far away from the boundary of the string, the d'Alembert solution of (III.1) can be written under the form

$$y(x,t) = \frac{1}{2}y_0(x - c_0(t-t_0)) + \frac{1}{2}y_0(x + c_0(t-t_0)t),$$

that consists in the propagation of two solitary waves one with velocity c_0 and the other with velocity $-c_0$.

1.2 From Saint-Venant to the wave equation

Let us recall the formulation of the Saint-Venant system (II.28)-(II.29)

$$\frac{\partial H}{\partial t} + \frac{\partial}{\partial x}\big(H\bar{u}\big) = 0, \tag{III.2}$$

$$\frac{\partial (H\bar{u})}{\partial t} + \frac{\partial (H\bar{u}^2)}{\partial x} + \frac{g}{2}\frac{\partial H^2}{\partial x} = -gH\frac{\partial z_b}{\partial x}, \tag{III.3}$$

without bottom friction and with $p^a = p_0^a = cst$, see Fig. I.1 for the notations.

Let us assume

$$\frac{\partial (H\bar{u}^2)}{\partial x} \ll \frac{g}{2}\frac{\partial H^2}{\partial x}, \tag{III.4}$$

then the Saint-Venant system becomes

$$\frac{\partial \eta}{\partial t} + \frac{\partial}{\partial x}\big(H\bar{u}\big) = 0, \tag{III.5}$$

$$\frac{\partial (H\bar{u})}{\partial t} + gH\frac{\partial \eta}{\partial x} = 0, \tag{III.6}$$

where we have used that the free surface η is defined by $\eta = H + z_b$ and since $z_b = z_b(x)$ we have

$$\frac{\partial \eta}{\partial t} = \frac{\partial H}{\partial t}.$$

Now differentiating (III.5) with respect to time t and (III.6) with respect to x leads to the equation

$$\frac{\partial^2 \eta}{\partial t^2} - \frac{\partial}{\partial x}\left(gH\frac{\partial \eta}{\partial x}\right) = 0, \tag{III.7}$$

that is nothing else than a 1d wave equation with the non-homogenous velocity $\sqrt{gH}$. When $H(x,t)$ slowly varies in space i.e.

$$H \approx H_0 = cst,$$

then Eq. (III.7) reduces to

$$\frac{\partial^2 \eta}{\partial t^2} - gH_0\frac{\partial^2 \eta}{\partial x^2} = 0, \tag{III.8}$$

Remark 5. The assumption (III.4) does not mean

$$H\bar{u}^2 \ll \frac{g}{2}H^2,$$

that is the assumption of low Froude flow. Indeed, we have

- for $x \approx 0$, $\sin(\frac{1}{x}) \ll \frac{1}{x}$, but $\frac{d}{dx}\left(\sin(\frac{1}{x})\right) \not\ll \frac{1}{x^2}$,

and conversely

- for $x \approx 0$, $\frac{d}{dx}\cos(x) \ll \frac{d}{dx}x$, but $\cos(x) \not\ll x$.

2 Potential flows

Starting from the Euler or Navier-Stokes equations, simplified models can also be derived using the assumption of potential flows. This assumption consists in considering the flow does not admit vortex. In other words, the fluid is supposed to be irrotational.

2.1 General formulation

The mathematical significance of the notion of irrotationality is given by the relation (in 2d with the velocity field (u,w))

$$\frac{\partial u}{\partial z} - \frac{\partial w}{\partial x} = 0. \tag{III.9}$$

For a 3d flow with the velocity field (u,v,w), the previous relation becomes

$$\nabla \wedge \begin{pmatrix} u \\ v \\ w \end{pmatrix} = 0$$

or equivalently

$$\begin{aligned} \frac{\partial w}{\partial y} - \frac{\partial v}{\partial z} &= 0, \\ \frac{\partial u}{\partial z} - \frac{\partial w}{\partial x} &= 0, \\ \frac{\partial v}{\partial x} - \frac{\partial u}{\partial y} &= 0. \end{aligned}$$

Starting from the 2d incompressible Euler equations (I.17)-(I.19), the assumption (III.9) ensures there exists a unique function Φ called the velocity potential and such that

$$\begin{aligned} u &= \frac{\partial \Phi}{\partial x}, \\ w &= \frac{\partial \Phi}{\partial z}. \end{aligned} \tag{III.10}$$

Thus, the divergence free condition becomes

$$\frac{\partial \Phi}{\partial x^2} + \frac{\partial \Phi}{\partial z^2} = 0, \tag{III.11}$$

that is a very famous partial differential equation called the *Laplace equation*. Moreover, using the expression (III.10) for u and w in Eqs. (I.18)-(I.19) leads to

$$\frac{\partial \Phi}{\partial t} + \left(\frac{\partial \Phi}{\partial x}\right)^2 + \left(\frac{\partial \Phi}{\partial z}\right)^2 + p + gz = C(t). \tag{III.12}$$

The system (III.11)-(III.12) is completed by the boundary conditions (I.9),(I.11). The boundary condition (I.20) means at the free surface we have

$$\frac{\partial \Phi}{\partial t} + \left(\frac{\partial \Phi}{\partial x}\right)^2 + \left(\frac{\partial \Phi}{\partial z}\right)^2 + g\eta = 0.$$

The analysis of the system (III.11)-(III.12) is a very difficult mathematical problem, but in simplified situations such as

- small waves amplitude,
- special form of the velocity potential,

the system can lead to interesting models.

2.2 The Airy wave model

Let us suppose the advection terms in (III.12) can be neglected and the topography is flat i.e. $z_b(x) = z_{b,0} = 0$. We introduce H_0 the typical water depth of the considered flow. We define a velocity potential of the form

$$\Phi = a\frac{\omega}{k}\frac{\cosh(k(z-z_{b,0}))}{\sinh(kz_{b,0})}\sin(kx-\omega t),$$

with $\omega^2 = gk\tanh(kH_0)$ and the free surface variations governed by

$$\frac{\partial H}{\partial t} + \left.\frac{\partial \Phi}{\partial z}\right|_{z=H(x,t)} = 0.$$

Then we have $\Delta\Phi = 0$ and

$$H = H_0 + \frac{a}{g^2}\frac{\sinh(kz)\cos(kx-\omega t)}{\left(\tanh^2(kH_0)\right)\sinh(kH_0)}. \tag{III.13}$$

This means that H defined by (III.13) and the velocities u, w defined by

$$u = \frac{\partial \Phi}{\partial x}, \qquad w = \frac{\partial \Phi}{\partial z},$$

are solutions of the approximate Euler system

$$\begin{aligned}
&\frac{\partial u}{\partial x} + \frac{\partial w}{\partial z} = 0,\\
&\frac{\partial u}{\partial t} + \frac{\partial p}{\partial x} = 0,\\
&\frac{\partial w}{\partial t} + \frac{\partial p}{\partial z} = -g,
\end{aligned}$$

completed with the boundary conditions

$$w_b = 0, \qquad \frac{\partial H}{\partial t} = w_s,$$

and $p_s = 0$.

Notice that when H_0 is small, the dispersion relation

$$c^2 = \frac{\omega^2}{k^2} = g\frac{\tanh(kH_0)}{k},$$

gives $c \approx \sqrt{gH_0}$ and we recover the wave velocity in the classical Saint-Venant system.

3 Erosion models

The main concern of morphodynamics is to determine the evolution of bed levels for hydrodynamic systems such as rivers, estuaries, bays and other nearshore regions where water flows interact with the bed geometry. Example of applications include among others, beach profile changes due to severe wave climates, seabed response to dredging procedures or imposed structures, and harbour siltation. The ability to design numerical methods able to predict the morphodynamic evolution of the coastal seabed has a clear mathematical and engineering relevances [116, 119, 65, 101, 48]. In practice, morphodynamic problems involve coupling between a hydrodynamic model, which provides a description of the flow field leading to a specification of local sediment transport rates, and an equation for bed level change which expresses the conservative balance of sediment volume and its continual redistribution with time. In the current study, the hydrodynamic model is described by a multi-layer shallow water equations and the sediment transport is modelled by the Exner equation. Morphodynamic coupling between classical shallow water system and Exner equation has been recently studied in some works [39, 40, 7].

3.1 Exner type models

Let us consider the Saint-Venant system (II.28)-(II.29). Since we consider a erodable bed, this means the bottom topography z_b also depends on time t i.e. $z_b = z_b(x,t)$. And the modelling of erosion processes require to find out the governing equation for the dynamical behavior of $z_b(x,t)$. To update the bed-load in the system (III.2)-(III.3), the Exner equation given by

$$(1-p)\frac{\partial z_b}{\partial t} + \frac{\partial Q_s}{\partial x} = 0, \tag{III.14}$$

is often used. In the preceding equation p denotes the sediment porosity assumed to be constant and the sediment discharge Q_s can be evaluated by the simple Grass formula introduced in [65]

$$Q(\overline{u}) = A\overline{u}\|\overline{u}\|^m,$$

with $\overline{u}$ is the fluid velocity in the Saint-Venant system, m and A are coefficients usually obtained from experiments taking into account the grain diameter and the kinematic viscosity of the sediment. In practice, the values of the coefficient A are between 0 and 1 depending on the interaction between the sediment transport and the water flow. Another formula, due to Meyer-Peter and Müller, frequently used for the sediment discharge Q_s is given in [101]

$$Q_s(h,\overline{u}) = 8\sqrt{g(s-1)d_{50}^3}\left(\frac{n_b^2\overline{u}^2}{(s-1)d_{50}\sqrt[3]{h}} - 0.047\right)^{\frac{3}{2}},$$

where we denote the grain specific gravity $s = \frac{\rho_s}{\rho_w}$ with ρ_w (resp. ρ_s) the water density (resp. the sediment density). Note that most of existing formulations for sediment transport models are empirical to differing extents and have been derived from experiments and measured data. Notice that the parameters n_b, d_{50}, s, p and A appeared in above equations are user-defined constants in the sediment transport model. In practice, the selection of these coefficients are problem dependent.

The calibration of the erosion models is a difficult question but the form of Eq. (III.14) raises another major issue. Indeed, the Saint-Venant system coupled with the Exner equation (III.14) does not admit any energy balance **[EX]**.

3.2 Derivation of the Exner model

Let us consider a two-layer fluid each layer being incompressible, inviscid. We also assume the two fluids are immiscible. They are characterized by their densities ρ_1, ρ_2, their water depths h_1, h_2 and their velocities u_1, u_2. The fluid densities are constant $\rho_1 = cst$, $\rho_2 = cst$ with $\rho_1 < \rho_2$. The bottom topography is $z_b = z_b(x)$, see Fig III.2. We propose to model this system using a shallow water type

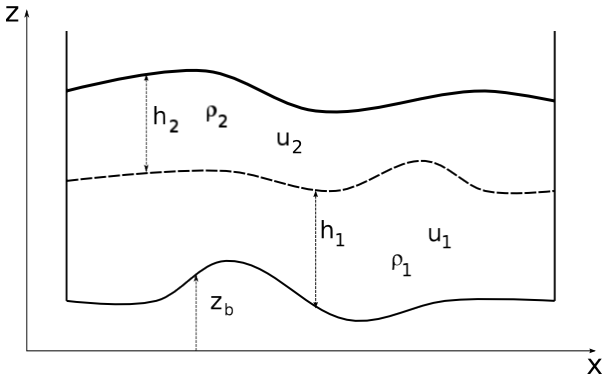

Figure III.2: A two-layer fluid.

model. It consists in the superposition of two Saint-Venant type systems

$$\begin{aligned}
&\frac{\partial(\rho_1 h_1)}{\partial t}+\frac{\partial(\rho_1 h_1 u_1)}{\partial x}=0,\\
&\frac{\partial(\rho_1 h_1 u_1)}{\partial t}+\frac{\partial}{\partial x}\left(\rho_1 h_1 u_1^2+\rho_2 g h_1 h_2+\frac{\rho_1 g}{2}h_1^2\right)=-g(\rho_1 h_1+\rho_2 h_2)\frac{\partial z_b}{\partial x}-\kappa u_1-\kappa_{1,2}(u_2-u_1),\\
&\frac{\partial(\rho_2 h_2)}{\partial t}+\frac{\partial(\rho_2 h_2 u_2)}{\partial x}=0,\\
&\frac{\partial(\rho_2 h_2 u_2)}{\partial t}+\frac{\partial}{\partial x}\left(\rho_2 h_2 u_2^2+\frac{\rho_2 g}{2}h_2^2\right)=-\rho_2 g h_2\frac{\partial}{\partial x}(z_b+h_1)+\kappa_{1,2}(u_2-u_1).
\end{aligned} \tag{III.15}$$

The derivation of the two-layer model (III.15) is a simple extension of the *one layer* Saint-Venant system (II.28)-(II.29). The main difficulty is the writting of the pressure. From the hydrostatic assumption, it is easy to see that in the layer 2, the expression of the fluid pressure is given by

$$p=\rho_2 g(h_1+h_2+z_b-z),$$

whereas in the layer 1, the fluid pressure is given by

$$p=\rho_2 g h_2+\rho_1 g(h_1+z_b-z).$$

The friction term between the two layers are given by $\kappa_{1,2}(u_2-u_1)$ and the bottom friction is κu_1.

If the fluid 1 corresponds to water and the fluid 2 models the bedload of a river, it is reasonable to assume $u_1 \ll \sqrt{g h_1}$ and the acceleration of the fluid is small i.e.

$$\frac{\partial(\rho_1 h_1 u_1)}{\partial t}\approx 0.$$

Therefore, the second equation of (III.15) reduces to

$$u_1=u_2+\mathscr{A}(\rho_1,\rho_2,h_1,h_2,z_b),$$

and replacing this expression for u_1 in the first equation of (III.15) leads to a relation of the form

$$\frac{\partial(h_1+z_b)}{\partial t}+\frac{\partial}{\partial x}(h_1\mathscr{B}(u_2,\rho_1,\frac{\rho_2}{\rho_1},h_1,h_2,z_b))=0, \tag{III.16}$$

where we have used the assumption $z_b=z_b(x)$ i.e.

$$\frac{\partial z_b}{\partial t}=0.$$

And in the simplified situation we have considered, we recover that the equation (III.16) has the form of the Exner equation (III.14).

4 A Saint-Venant system with complex rheology

In chapter II, we have derived the Saint-Venant system as an approximation of the Navier-Stokes equations considering a Newtonian fluid. When considering a fluid with a more complex rheology, as described in Section 7, the derivation of shallow water type models is often tricky. The main reason is that the constitutive laws for complex fluids are often based on sophisticated considerations and properties of the strain tensor that can hardly be reduced to 2d by the shallow water assumption when starting from the 3d Navier-Stokes system.

Nevertheless, there exist several shallow water type models derived for fluid with complex rheology, see [97, 93, 25, 115] and references therein. To illustrate this, we give below a model based on the Saint-Venant equations with a Coulomb type friction. The friction law is based on the empirical variable

friction coefficient proposed by Pouliquen and Forterre [115]. The model is used to simulate unconfined granular flow over an inclined plane [97] and it reads

$$\frac{\partial H}{\partial t} + \frac{\partial}{\partial x}\big(H\bar{u}\big) = 0, \tag{III.17}$$

$$\frac{\partial (H\bar{u})}{\partial t} + \frac{\partial (H\bar{u}^2)}{\partial x} + \frac{g}{2}\frac{\partial H^2}{\partial x} = -gH\frac{\partial z_b}{\partial x} + Hf, \tag{III.18}$$

where the friction force $f = f(x,t)$ must satisfy

$$\begin{cases} |f(x,t)| \leqslant g\mu, \\ \bar{u}(x,t) \neq 0 \;\Rightarrow\; f(x,t) = -g\mu \frac{\bar{u}(x,t)}{|\bar{u}(x,t)|} \end{cases} \tag{III.19}$$

The system (III.17)-(III.18) appears as a slight modification of the classical Saint-Venant system with friction (II.28)-(II.29). But the friction law (III.19) is singular (multivalued) when $\bar{u}$ tends to zero and this leads to significant difficulties. As an example, in the system (III.17)-(III.18) the steady states at rest play a crucial role since they describe the static/mobile transition and are not characterized by the "lake at rest" situation. Indeed they are given by

$$\bar{u} = 0, \qquad \frac{\partial}{\partial x}(H + z_b) = f,$$

or equivalently,

$$\bar{u} = 0, \qquad \frac{\partial}{\partial x}(H + z_b) \leqslant \mu.$$

Chapter IV

Numerical methods

In this chapter we are interested in the discretization of the Saint-Venant system using a finite volume approach. The numerical treatment of the conservative part is classical and can be used for various hyperbolic conservation laws. Even if efficient techniques exists for the discretization of the source terms, it remains tricky.

1 Numerical methods for the conservative system

We first introduce the notations for the discrete Saint-Venant system then we recall the basis properties for a finite volume scheme. In this section we consider the homogenous Saint-Venant system

$$\frac{\partial H}{\partial t} + \frac{\partial}{\partial x}\left(H\bar{u}\right) = 0,$$
$$\frac{\partial (H\bar{u})}{\partial t} + \frac{\partial (H\bar{u}^2)}{\partial x} + \frac{g}{2}\frac{\partial H^2}{\partial x} = 0,$$

the discretization of the source terms S_b and S_f (see (II.46)) that is often tricky is presented in Section 2.

1.1 Notations

To approximate the solution of the Saint-Venant system, we use a finite volume framework. We assume that the computational domain is discretised by I nodes x_i. We denote C_i the cell of length $\Delta x_i = x_{i+1/2} - x_{i-1/2}$ with $x_{i+1/2} = (x_i + x_{i+1})/2$. For the time discretization, we denote $t^n = \sum_{k\leqslant n} \Delta t^k$ where the time steps Δt^k will be precised later though a CFL condition. The ratio between the space and time steps is $\sigma_i^n = \Delta t^n / \Delta x_i$. We denote $X_i^n = (H_i^n, q_i^n)$ the approximate solution at time t^n on the cell C_i with $q_i^n = H_i^n u_i^n$ i.e.

$$X_i^n \approx \frac{1}{\Delta x_i}\int_{C_i} X(t^n, x)dx.$$

A finite volume conservative scheme for solving (II.28)-(II.29) (without source terms) is a formula of the form

$$X_i^{n+1} = X_i^n - \sigma_i^n \left(\mathscr{F}_{i+1/2}^n - \mathscr{F}_{i-1/2}^n\right), \tag{IV.1}$$

telling how to compute X_i^{n+1} at the next time level, knowing the values X_i^n at time t^n. In a first step, we consider only first-order three points schemes where

$$\mathscr{F}_{i+1/2}^n = \mathscr{F}(X_i^n, X_{i+1}^n). \tag{IV.2}$$

The function $\mathscr{F}(X_l, X_r)$ is called the numerical flux and determine the scheme.

It is important to say that it is always necessary to impose what is called a CFL condition (for Courant, Friedrichs, Levy) on the timestep so that the scheme does not blow up. A CFL condition has the form

$$\Delta t \leqslant a\Delta x_i,$$

where a is an approximation of the speed of propagation.

Remark 6. When source terms are considered, the scheme (IV.1) becomes

$$X_i^{n+1} = X_i^n - \sigma_i^n \left(\mathscr{F}_{i+1/2}^n - \mathscr{F}_{i-1/2}^n\right) + \Delta t^n S_{v.f}^{n/n+1} + \Delta t^n S_b^n,$$

corresponding to a discretization of (II.46).

1.2 Consistency and stability

Many methods exist to determine a numerical flux. The two main criteria that enter in its choice are its stability properties and the accuracy it has, which can be measured by the amount of viscosity it produces and by the property of exact computation of particular solutions to (II.46).

The consistency is the minimal property required for a scheme to ensure the approximation of the equation is correct. For a conservative scheme, we define it as follows

Definition IV.1. We say that the scheme (IV.1)-(IV.2) is consistent with (II.46) (without source terms) if the numerical flux satisfies

$$\mathscr{F}(X, X) = F(X).$$

We can see that this condition guarantees obviously that if for all i, $X_i^n = cst$ then also $X_i^{n+1} = cst$.

The stability of the scheme can be analysed in different ways, but we shall retain here the conservation of an invariant domain and the existence of a discrete entropy inequality. They are defined as follows.

Definition IV.2. We say that the scheme (IV.1)-(IV.2) preserves a convex invariant domain $\mathscr{X}$ (in the sense of (II.54)) if under a CFL condition,

$$X_i^n \in \mathscr{X} \text{ for all } i \;\Rightarrow\; X_i^{n+1} \in \mathscr{X} \text{ for all } i.$$

Definition IV.3. We say that the scheme (IV.1)-(IV.2) satisfies a discrete entropy inequality associated with the convex entropy ζ for (II.46), if there exists a numerical entropy flux function $\mathscr{G}$, consistent with the exact entropy flux G, such that under some CFL condition, the discrete values calculated in (IV.1)-(IV.2) automatically satisfies

$$\zeta(X_i^{n+1}) = \zeta(X_i^n) - \sigma_i^n \left(\mathscr{G}_{i+1/2}^n - \mathscr{G}_{i-1/2}^n\right). \tag{IV.3}$$

For the kinetic scheme presented in paragraph 3 (pages 69), we give a discrete entropy inequality.

Remark 7. For the stability analysis of a finite volume scheme, the flux definition has to rewritten so that the contribution of the cells i and $i+1$ clearly appears. Hence, the flux splitting that consists in being able to write

$$\mathscr{F}_{i+1/2}^n = \tilde{\mathscr{F}}(X_i^n) + \tilde{\mathscr{F}}(X_{i+1}^n).$$

is an important ingredient.

1.3 Godunov's scheme

Simple quadrature formula in space and time gives that the numerical fluxes in (IV.1) are defined by

$$\mathscr{F}_{i+1/2}^n = \int_{t^n}^{t^{n+1}} F(X_{i+1/2}) dt.$$

The Godunov method [61] consists in replacing the time integral with a forward Euler method

$$\int_{t^n}^{t^{n+1}} F(X_{i+1/2}) dt \approx \Delta t^n \mathscr{F}^{GOD}(X_i^n, X_{i+1}^n),$$

where $\mathscr{F}^{GOD}(X_i^n, X_{i+1}^n)$ is an approximation to the exact solution of the Riemann problem.

1.4 Approximate Riemann solver of Harten, Lax, Van Leer

The notion of approximate Riemann solver of Harten, Lax, Van Leer is the most general tool involved in the construction of numerical schemes. In fact, relaxation solvers, kinetic solvers and Roe solvers enter this framework.

We define the Riemann problem for the homogenous system (II.46) to be the problem of finding the solution of (II.46) with Riemann initial data

$$X^0(x) = \begin{cases} X_l & \text{if } x < 0, \\ X_r & \text{if } x > 0, \end{cases}$$

for two given constants X_l and X_r. By a simple rescaling this solution is indeed a function of x/t.

Definition IV.4. An approximate Riemann solver for (II.46) is a vector function $R(x/t, X_l, X_r)$ that is an approximation of the solution of the Riemann problem, in the sense that it must satisfy the consistency relation

$$R(x/t, X, X) = X,$$

and the conservativity identity

$$\mathscr{F}_l(X_l,X_r) = \mathscr{F}_r(X_l,X_r),$$

where the left and right numerical fluxes are defined by

$$\mathscr{F}_l(X_l,X_r) = F(X_l) - \int_{-\infty}^{0} (R(v,X_l,X_r) - X_l)\, dv, \tag{IV.4}$$

$$\mathscr{F}_r(X_l,X_r) = F(X_r) - \int_{0}^{+\infty} (R(v,X_l,X_r) - X_r)\, dv. \tag{IV.5}$$

It is possible to prove that the exact solution to the Riemann problem satisfies these properties. However, the above definition is rather motivated by numerical schemes. Indeed to an approximate Riemann solver we can associate a conservative numerical scheme as explained below.

We define an approximate solution $X(t,x)$ for $t^n < t < t^{n+1}$ by

$$X(t,x) = R\left(\frac{x - x_{i+1/2}}{t-t^n}, X_i^n, X_{i+1}^n\right), \quad \text{for } x_i < x < x_{i+1}.$$

According to (IV.4),(IV.5) we get

$$\begin{aligned}
X_i^{n+1} &= \frac{1}{\Delta x_i}\int_{x_{i-1/2}}^{x_{i+1/2}} X(t^{n+1},x)dx \\
&= \frac{1}{\Delta x_i}\int_{x_{i-1/2}}^{x_i} R\left(\frac{x-x_{i-1/2}}{\Delta t^n}, X_{i-1}^n, X_i^n\right)dx + \frac{1}{\Delta x_i}\int_{x_i}^{x_{i+1/2}} R\left(\frac{x-x_{i+1/2}}{\Delta t^n}, X_i^n, X_{i+1}^n\right)dx \\
&= \frac{1}{\Delta x_i}\int_{0}^{\frac{\Delta x_i}{2}} R\left(\frac{x}{\Delta t^n}, X_{i-1}^n, X_i^n\right)dx + \frac{1}{\Delta x_i}\int_{0}^{-\frac{\Delta x_i}{2}} R\left(\frac{x}{\Delta t^n}, X_i^n, X_{i+1}^n\right)dx \\
&= \frac{1}{\Delta x_i}\int_{0}^{\frac{\Delta x_i}{2}} \left(R\left(\frac{x}{\Delta t^n}, X_{i-1}^n, X_i^n\right) - X_i^n\right)dx + \frac{1}{\Delta x_i}\int_{0}^{-\frac{\Delta x_i}{2}} \left(R\left(\frac{x}{\Delta t^n}, X_i^n, X_{i+1}^n\right) - X_i^n\right)dx.
\end{aligned}$$

1.5 Two well-known fluxes

Several fluxes can be used in (IV.1) and we give the expression for two well-known fluxes namely, HLL (Harten, Lax, Van Leer) and Rusanov.

For the homogenous Saint-Venant system, we have

$$X = \begin{pmatrix} H \\ H\bar{u} \end{pmatrix}, \quad F(X) = \begin{pmatrix} H\bar{u} \\ H\bar{u}^2 + \frac{g}{2}H^2 \end{pmatrix},$$

and

$$\begin{aligned}
\lambda_1^n(X_i^n) &= u_i^n + \sqrt{gH_i^n}, \\
\lambda_2^n(X_{i+1}^n) &= u_{i+1}^n - \sqrt{gH_{i+1}^n},
\end{aligned}$$

then the Rusanov fluxes are defined by

$$\mathscr{F}^{Rus}(X_i^n, X_{i+1}^n) = \frac{F(X_i^n) + F(X_{i+1}^n)}{2} - \max_{k=1,2}\left(|\lambda_k^n(X_i^n)|, |\lambda_k^n(X_{i+1}^n)|\right)\frac{X_{i+1}^n - X_i^n}{2}.$$

Let

$$c_1^n = \min_{k=1,2}\left(\min_{X=X_i^n,X_{i+1}^n} \lambda_k^n(X)\right), \quad \text{and} \quad c_2^n = \max_{k=1,2}\left(\max_{X=X_i^n,X_{i+1}^n} \lambda_k^n(X)\right),$$

then the HLL fluxes is given by

$$\mathscr{F}^{HLL}(X_i^n, X_{i+1}^n) = \begin{cases} F(X_i^n) & \text{if } c_1^n \geqslant 0 \\ \frac{c_2^n F(X_i^n) - c_1^n F(X_{i+1}^n)}{c_2^n - c_1^n} + \frac{c_2^n c_1^n}{c_2^n - c_1^n}(X_{i+1}^n - X_i^n) & \text{if } c_1^n < 0 < c_2^n \\ F(X_{i+1}^n) & \text{if } c_2^n \leqslant 0 \end{cases}$$

Starting from a flux definition for the Saint-Venant system (II.28)-(II.29) (without source terms), propose a flux definition for the Saint-Venant with a passive tracer i.e. (II.28)-(II.29),(II.37) **[EX]**.

For the HLL and Rusanov fluxes, we have the following property

Proposition IV.5. *Under the CFL condition*

$$\Delta t^n \leqslant \frac{\min_{i\in I}\Delta x_i}{\max_{i\in I}(|\overline{u}_i^n| + \sqrt{gH_i^n})},$$

the finite volume scheme (IV.1) coupled with the HLL or Rusanov flux is positive.

The proof of the positivity of the kinetic scheme under a CFL condition is given in paragraph 3.3 (page 71).

2 Numerical treatment of the source terms

The solutions of the Saint-Venant system (II.38)-(II.39) can exhibit very particular solutions because of the source terms. In this paragraph, we present some aspects of the numerical methods allowing to deal in a more or less efficient and robust way – with these source terms. Notice that the derivation of acurate numerical schemes for conservation laws with source terms is far from being obvious.

2.1 Operator splitting

This method – also called fractional time step method – is the most simple for a numerical treatment of the source terms. The key idea is the following. Let us consider a Cauchy problem having the form

$$\begin{cases} \frac{\partial W}{\partial t} = A(W) + B(W), \quad t > 0, \\ W_{|t=0} = W_0, \end{cases}$$

where W_0 is the inital datum and A,B are operators, possibly differential operators. To approximate this system, we define the time step Δt and we define the sequence $(W^n)_{n\in\mathbb{N}}$ approximating $(W_{|t=n\Delta t})_{n\in\mathbb{N}}$ with the following iterative scheme

$$\begin{aligned} W^{n+1/2} &= W^n + \Delta t\ A(W^n), \\ W^{n+1} &= W^{n+1/2} + \Delta t\ B(W^{n+1/2}), \end{aligned}$$

Therefore, for a given time step Δt, each operator is solved separetely. And when another operator is added, it is only necessary to add the associated numerical discretization without any other modification. This technique is based on the Lie-Trotter-Kato formula, where $t = n\Delta t$,

$$e^{t(A+B)} = \lim_{n\to\infty}\left[e^{\Delta t A} \times e^{\Delta t B}\right]^n,$$

defining the convergence, in the sense of the semi-groups, of the operator splitting, see [130, 81].

In general, this method leads to a stable and consistent discretization. Indeed, the separation of each operator implies that each of them can be considered independantly from the others. And for each operator, an efficient numerical technique can be used. For the Saint-Venant system (II.63), the operator splitting can be written under the form

$$A = -\mathrm{div}F(X), \quad B = S_b(X) + S_{v,f}(X). \tag{IV.6}$$

The numerical resolution of the first step can be performed with a standard finite volume scheme

$$X_i^{n+1/2} = X_i^n - \frac{\Delta t}{\Delta x}\big(\mathscr{F}(X_i^n, X_{i+1}^n) - \mathscr{F}(X_{i-1}^n, X_i^n)\big), \tag{IV.7}$$

and the second step can be solved using the implicit Euler method e.g.

$$X_i^{n+1} = X_i^{n+1/2} + \Delta t\ B(X_i^{n+1}).$$

We do not discuss here the choice of $\mathscr{F}$ the fluxes for the homogenous part. This is detailed in paragraphs 3 (page 69) for the kinetic fluxes and in paragraph 1.5 (page 57) for HLL and Rusanov fluxes.

The operator splitting is easy to implement and generally gives satisfactory results but sometimes it fails... Even if the strategy seems to converge towards the expected solution, the lack of consistency can be very large even it tends to 0 when $\Delta t, \Delta x \to 0$, this corresponds to the constant coming from $\mathscr{O}(\Delta x + \Delta t)$.

The preservation of stationary states for the the Saint-Venant system (II.61) gives a well-known example of such a behavior. Let us introduce the following family of numerical scheme

Definition IV.6. A numerical scheme is said to be *well-balanced* for the stationary states (II.61) if it satisfies the following property

$$\begin{aligned}&\text{if } \forall i,j \in \mathbb{Z},\ (H\overline{u})_i^0 = 0 \text{ and } H_i^0 + z_{b_i} = H_j^0 + z_{b_j},\\ &\text{implies that } \forall n \geqslant 0 \text{ and } \forall i \in \mathbb{Z}, \text{ one has } H_i^n = H_i^0 \text{ and } (H\overline{u})_i^n = 0.\end{aligned}$$

(We omit the vaccum case $H_i^0 = 0$.)

This notion of *well-balanced* scheme defined in 1d remains valid in 2d and corresponds to a discrete version of (II.61).

Proposition IV.7. *Any numerical scheme obtained from a operator splitting (IV.6) is not* well-balanced *for the stationary states (II.61).*

Proof. We consider a stationary regime with a non constant topography i.e. $\exists i_0$ such that $z_{b_{i_0}} \neq z_{b_{i_0+1}}$. This implies $H_{i_0}^0 \neq H_{i_0+1}^0$. Consequently, in the finite volume scheme (IV.6), the flux calculated at the interface $i_0 + 1/2$ have different arguments, namely

$$H_{i_0}^{1/2} \neq H_{i_0}^0.$$

Now we consider the second step. The problem to solve is

$$\begin{aligned}&\frac{\partial H}{\partial t} = 0,\\ &\frac{\partial H\overline{u}}{\partial t} = -gH\frac{\partial z_b}{\partial x} - S_f.\end{aligned}$$

The discretization of the first equation gives $H_{i_0}^1 = H_{i_0}^{1/2} \neq H_{i_0}^0$ meaning the scheme is not *well-balanced*. □

2.2 Direct discretization of the source term

A very natural idea is to define a "one step" numerical scheme meaning the source term discretization is integrated in the scheme

$$X_i^{n+1} = X_i^n - \frac{\Delta t}{\Delta x}\big(\mathscr{F}(X_i^n, X_{i+1}^n) - \mathscr{F}(X_{i-1}^n, X_i^n)\big) + \Delta t\,\mathscr{S}(X_{i-1}^n, X_i^n, X_{i+1}^n; \Delta x) \tag{IV.8}$$

where $\mathscr{S}$ is a consistent discretization of the source term. Nevertheless, it is easy to see that such a formulation does not lead, for any $\mathscr{S}$, to a *well-balanced* scheme. Indeed, the computation of H_i^{n+1} is the same as the one obtained in the fractional time step strategy.

To avoid these difficulties, a strategy could be to consider implicit or semi-implicit discretization (in time) of the source term. Unfortunately, implicit schemes leads to costly numerical resolution since the the compactness of the stencil, when considering explicit time scheme, is lost.

2.3 *Well-balanced* schemes

The two previous praragraphs emphasize that in order to obtain a well-balanced scheme, the topography source term has also to appear to some extent, in the conservative part. Notice that, once a well-balanced scheme for the stationary states (II.61) without friction has been obtained, it can easily be extended using the splitting **[EX]**

$$A = -\mathrm{div}F(X) + S_b(X), \quad B = S_{v,f}(X).$$

Consequently, we only have to derive well-balanced scheme for the system

$$\begin{aligned} &\frac{\partial H}{\partial t} + \frac{\partial H\bar{u}}{\partial x} = 0, \\ &\frac{\partial H\bar{u}}{\partial t} + \frac{\partial}{\partial x}\left(H\bar{u}^2 + gH^2/2\right) = -gH\frac{\partial z_b}{\partial x}, \end{aligned}$$

Moreover, we assume a piecewise constant discretization of the topography under the form

$$z_{b_i} = \frac{1}{\Delta x}\int_{C_i} z_b(x)\, dx.$$

A general formulation of the schemes taking into account the source term can be written as follows

$$X_i^{n+1} = X_i^n - \sigma_i^n\left(\mathscr{F}^-(X_i^n, X_{i+1}^n, z_{b_{i+1}} - z_{b_i}) - \mathscr{F}^+(X_{i-1}^n, X_i^n, z_{b_i} - z_{b_{i-1}})\right), \tag{IV.9}$$

where the numerical fluxes $\mathscr{F}^-$ and $\mathscr{F}^+$ have to satisfy the following properties

- classical conservation : $\mathscr{F}^-(X,Y,0) = \mathscr{F}^+(X,Y,0)$,
- classical consistency : $\mathscr{F}^-(X,X,0) = F(X)$,
- consistency with the source term : $\mathscr{F}^+(X,Y,S) - \mathscr{F}^-(X,Y,S) \approx -gHS$.

The last properties is not clearly defined –see [24] for a discussion on this subject – it means the source term only appears at the interfaces of the mesh.

The notion of well-balanced scheme given in definition IV.6 corresponds to a definition "by cell". Using the writting (IV.9), we can deduce a necessary condition so that the scheme is well-balanced and this definition now corresponds to a characterization "by interface".

Proposition IV.8. *Let $(\bar{X}_i, \bar{z}_{b_i})_{i\in\mathbb{Z}}$ be the discretization of a stationary state (see the definition IV.6). If the numerical scheme (IV.9) satisfies $\forall i \in \mathbb{Z}$*

$$\mathscr{F}^-(\bar{X}_i, \bar{X}_{i+1}, \bar{z}_{b_{i+1}} - \bar{z}_{b_i}) = F(X_i) \quad et \quad \mathscr{F}^+(\bar{X}_i, \bar{X}_{i+1}, \bar{z}_{b_{i+1}} - \bar{z}_{b_i}) = F(X_{i+1}),$$

then it is a well-balanced scheme for the stationary state (II.61).

Proof. **[EX]** □

The question is now to derive a well-balanced scheme and this is far from being obvious. The first techniques proposed leading to well-balanced schemes appeared in the literature ten or fifteen years ago but some new results are regularly proposed. Let us examine some examples of the proposed techniques.

2.3.1 Godunov type schemes

The idea of these schemes relies on the formalism of Godunov's scheme. First, we introduce the discretized topography

$$z_{b_\Delta}(x) = \sum_{i\in\mathbb{Z}} z_{b_i} \mathbf{1}_{C_i}(x).$$

The topography z_b is replaced by z_{b_Δ} within the system (II.63) and an integration over $(n\Delta t,(n+1)\Delta t)\times C_i$ leads to

$$\int_{M_i} \big(X((n+1)\Delta t,x) - X(n\Delta t,x)\big)dx + \int_{n\Delta t}^{(n+1)\Delta t} \big(F(X(t,x_{i+1/2}^-)) - F(X(t,x_{i-1/2}^+))\big)dt = 0,$$

where $f(x_{i+1/2}^-)$ and $f(x_{i+1/2}^+)$ are the left and right traces of the function f at point $x_{i+1/2}$. As for the Godunov scheme in the conservative case, we deduce the scheme

$$X_i^{n+1/2} = X_i^n - \frac{\Delta t}{\Delta x}\big(F(\mathscr{X}(0^-;X_i^n,X_{i+1}^n,z_{b_{i+1}}-z_{b_i})) - F(\mathscr{X}(0^+;X_{i-1}^n,X_i^n,z_{b_i}-z_{b_{i-1}}))\big),$$

where $\mathscr{X}(x/t;X_g,X_d,z_{b_d}-z_{b_g})$ is the exact or approximated solution of the Riemann problem

$$\begin{cases} \frac{\partial X}{\partial t} + \frac{\partial F(X)}{\partial x} = \begin{pmatrix} 0 \\ -gH(z_{b_d}-z_{b_g})\delta_0(x) \end{pmatrix}, \\ X(0,x) = \begin{cases} X_g & \text{if } x<0, \\ X_d & \text{if } x>0. \end{cases} \end{cases} \tag{IV.10}$$

We will see later some aspects of the resolution of this problem. If there exists a solution to problem (IV.10) then we obtain, from the writting (IV.9), numerical fluxes having the form

$$F^\pm(X,Y,S) = F(\mathscr{X}(0^\pm;X,Y,S)). \tag{IV.11}$$

And hence, the following proposition holds.

Proposition IV.9. *If the Riemann solver $\mathscr{X}$ satisfies the property*

$$\begin{array}{l} \text{if } X_1,\ X_2 \text{ and } S \text{ satisfies } H_1 = H_2 + S \text{ and } \overline{u}_1 = \overline{u}_2 = 0, \\ \text{then } \mathscr{X}(0^-;X_1,X_2,S) = X_1 \text{ and } \mathscr{X}(0^+;X_1,X_2,S) = X_2, \end{array} \tag{IV.12}$$

then the scheme (IV.9)-(IV.11) is well-balanced for the stationary states (II.61).

Proof. **[EX]** □

In fact, the property (IV.12) means that if the initial datum of the Riemann problem (IV.10) corresponds to a stationary state having the form (II.61) then the solution of the Rieman problem is stationary i.e.

$$\mathscr{X}(\xi;X_1,X_2,S) = \begin{cases} X_1 & \text{if } \xi<0, \\ X_2 & \text{if } \xi>0. \end{cases} \quad \textbf{[EX]}$$

Linearized Riemann solver In a first step, we construct an approximated Riemann solver (IV.10). Let $\mathscr{X}_{\text{app}}(x/t;X_g,X_d,z_{b_d}-z_{b_g})$ be the exact solution of the Riemann problem

$$\begin{cases} \frac{\partial X}{\partial t} + F'(X_0)\frac{\partial X}{\partial x} = \begin{pmatrix} 0 \\ -gH(z_{b_d}-z_{b_g})\delta_0(x) \end{pmatrix}, \\ X(0,x) = \begin{cases} X_g & \text{if } x<0, \\ X_d & \text{if } x>0, \end{cases} \end{cases} \tag{IV.13}$$

where $X_0 = (X_g + X_d)/2$ et

$$F'(X) = \begin{pmatrix} 0 & 1 \\ gH - \overline{u}^2 & 2\overline{u} \end{pmatrix}.$$

Since this problem – corresponding to a linearized Riemann problem – is linear, it can be solved explicitely and it remains to prove $\mathscr{X}_{\text{app}}$ satisfies the property (IV.12), see [56] for more details about these numerical schemes **[EX]**.

Exact Riemann solver When resonant cases are excluded, we can propose a resolution technique for the Riemann problem. Let us define the sets

$$\mathscr{T}_-(X_g) = \{\mathscr{X}(0^-; X_g, X, 0), X \in \Omega\} \quad \text{and} \quad \mathscr{T}_+(X_d) = \{\mathscr{X}(0^+; X, X_d, 0), X \in \Omega\}$$

where $\mathscr{X}(x/t; X, Y, 0)$ is the exact solution of the Riemann problem associated with the Saint-Venant system without topography. Thus, $\mathscr{T}_-(X_g)$ (resp. $\mathscr{T}_+(X_d)$) is the set of reachable states at $x/t = 0^-$ (resp. $x/t = 0^+$) across non positive velocity waves (resp. non negative) from X_g (resp. X_d). Since the bottom is flat for $x/t < 0$ et $x/t > 0$, the resolution of the Riemann problem (IV.10) consists in finding two states $X_-, X_+ \in \Omega$ satisfying

$$\begin{cases} X_- \in \mathscr{T}_-(X_g) \\ X_+ \in \mathscr{T}_+(X_d) \end{cases} \quad \text{and} \quad \begin{cases} I_0^1(X_-) = I_0^1(X_+) \\ I_0^2(X_-, z_{b_g}) = I_0^2(X_+, z_{b_d}) \end{cases}. \tag{IV.14}$$

We do not discuss here the existence of X_- and X_+, the reader can refer to [77, 78, 84, 5, 58, 43]. Nevertheless, the following result holds Néanmoins, on peut vérifier le résultat qui nous intéresse :

Proposition IV.10. *The exact Riemann solver $\mathscr{X}$ based on the resolution of (IV.14) satisfies the property (IV.12). Therefore, the associated numerical scheme is a well-balanced scheme.*

Proof. It is enough to prove that $\mathscr{X}(\xi, X_1, X_2, S) = X_1 \mathbf{1}_{\xi<0} + X_2 \mathbf{1}_{\xi>0}$ satisfies the relations (IV.14). On the one hand, it is obvious that for any $X_1, X_2 \in \Omega$, $X_1 \in \mathscr{T}_-(X_1)$ and $X_2 \in \mathscr{T}_+(X_2)$. On the other hand, if X_1, X_2 and S satisfies $H_1 = H_2 + S$ and $\overline{u}_1 = \overline{u}_2 = 0$, one has

$$I_0^1(X_1) = I_0^1(X_2) = 0$$

and

$$\frac{u_1^2}{2} + gH_1 = \frac{u_2^2}{2} + gH_2 + gS,$$

therefore $I_0^2(X_1, \beta) = I_0^2(X_2, \beta + S)$ for all $\beta \in \mathbb{R}$. □

Notice that there exist other approximated Riemann solvers allowing to obtain well-balanced schemes. As an example, one may think to a HLL type scheme including the stationary wave. The use of another linearization in (IV.13) is also possible.

2.3.2 Schemes with reconstruction

Let us assume the equilibria we want to preserve can be defined by the means of two functions Ψ_- and Ψ_+ i.e.

$$\begin{aligned} X_1 \text{ and } X_2 \text{ satisfies an equilibrium} &\Longleftrightarrow X_1 = \Psi_-(X_2, S) \\ &\Longleftrightarrow X_2 = \Psi_+(X_1, S). \end{aligned} \tag{IV.15}$$

Then we can easily propose a well-balanced scheme [68, 63].

Proposition IV.11. *Let us consider the numerical scheme (IV.9) with the numerical scheme defined by*

$$\mathscr{F}^-(X, Y, S) = \mathscr{F}(X, \Psi_-(Y, S)) \quad \textit{and} \quad \mathscr{F}^+(X, Y, S) = \mathscr{F}(\Psi_+(X, S), Y),$$

where $\mathscr{F}$ is a numerical flux consistent with the Saint-Venant equations without topography. Then this is a well-balanced scheme.

Proof. If X and Y satisfies the equilibrium then $X = \Psi_-(Y,S)$. We deduce that

$$\mathscr{F}^-(X,Y,S) = \mathscr{F}(X,\Psi_-(Y,S)) = \mathscr{F}(X,X) = F(X).$$

Likewise we obtain

$$\mathscr{F}^+(X,Y,S) = \mathscr{F}(\Psi_+(X,S),Y) = \mathscr{F}(Y,Y) = F(Y),$$

and we conclude using prop. IV.8. □

Unfortunately, for the stationary states (II.61), it is not possible to find functions $\Psi_\pm$ satisfying (IV.15). Indeed, let us try to construct the function Ψ_-. From the first $\Longrightarrow$ in (IV.15), we necessarily have

$$\Psi_-(X_2,S) = \begin{pmatrix} H_2+S \\ 0 \end{pmatrix}. \tag{IV.16}$$

But if now we assume (IV.16) then (IV.15) does not hold (or only when $u_2 = 0$ inducing a lack of consistency).

Nevertheless, a modification of the numerical scheme proposed in prop. IV.11 can lead to a well-balanced scheme, it is detailed hereafter.

2.3.3 Hydrostatic reconstruction

The hydrostatic reconstruction proposed by Audusse *et al.* [8] is a very simple technique with reconstruction ensuring the equilibrium at rest, the positivity and the consistency starting from any solver for the homogenous system.

The idea is to propose and analyze a finite volume scheme with flux functions

$$\mathscr{F}^n_{i+1/2} = \mathscr{F}(X^n_{i+1/2-}, X^n_{i+1/2+}), \tag{IV.17}$$

where the interface values $X^n_{i+1/2-}, X^n_{i+1/2+}$ are derived from a local hydrostatic reconstruction to be described shortly, which is similar to second-order reconstructions in higher-order methods. The topography source term is discretized as

$$\mathscr{S}_{b,i} = \begin{pmatrix} 0 \\ \frac{g}{2}(H^n_{i+1/2-})^2 - \frac{g}{2}(H^n_{i-1/2+})^2 \end{pmatrix} \tag{IV.18}$$

This ansatz is motivated by the balancing requirement as follows. For nearly hydrostatic flows one has $\bar{u} \ll \sqrt{gH}$. In the associated asymptotic limit the leading order water depth H adjusts so as to satisfy the balance of momentum flux and momentum source terms, i.e.

$$\frac{\partial}{\partial x}\left(\frac{gH^2}{2}\right) = -gH\frac{\partial z_b}{\partial x}, \tag{IV.19}$$

Integrating over, say, the i^{th} grid cell we obtain an approximation to the source term as

$$-\int_{C_i} gH\frac{\partial z_b}{\partial x}dx = \frac{g}{2}(H^n_{i+1/2-})^2 - \frac{g}{2}(H^n_{i-1/2+})^2.$$

Thus we are able to locally represent the cell-averaged source term as the discrete gradient of the hydrostatic momentum flux, and this motivates the source term discretization in (IV.18). It is obvious now that any hydrostatic state is maintained exactly if, for such a state, the momentum fluxes in (IV.1) and the locally reconstructed heights satisfy $\mathscr{F}^q = \frac{1}{2}gH^2_{i+1/2-} = \frac{1}{2}gH^2_{i-1/2+}$. This is the motivation for (IV.17), which gives this property if for hydrostatic states we have $X^n_{i+1/2-} = X^n_{i+1/2+} = (H^n_{i+1/2-},0) = (H^n_{i+1/2+},0)$.

The hydrostatic balance in (IV.19) is equivalent to the "lake at rest" equation $H + z_b = cst$, so that the reconstruction of the leading order heights is straightforward,

$$H^n_{i+1/2-} = H^n_i + z_{b,i} - z_{b,i+1/2}, \quad H^n_{i+1/2+} = H^n_{i+1} + z_{b,i+1} - z_{b,i+1/2}. \tag{IV.20}$$

The evaluation of the cell interface height $z_{b,i+1/2}$ is somewhat subtle since the scheme shall also robustly capture dry regions where $H = 0$. The challenge is to design a scheme that guarantees nonnegativity of the water height even when cells begin to "dry out". We prove below that this can be achieved through a biased evaluation of the form

$$z_{b,i+1/2} = \max(z_{b,i}, z_{b,i+1}), \tag{IV.21}$$

and with a nonnegativity-preserving truncation of the leading order heights in (IV.19), $H^n_{i+1/2\pm} = \max(0, H^n_{i+1/2\pm})$.

With these rules in place we can now summarize the first-order well-balanced finite volume scheme by (IV.1),(IV.17),(IV.20) and

$$X^n_{i+1/2-} = \begin{pmatrix} H^n_{i+1/2-} \\ H^n_{i+1/2-}\overline{u}^n_i \end{pmatrix}, \quad X^n_{i+1/2+} = \begin{pmatrix} H^n_{i+1/2+} \\ H^n_{i+1/2+}\overline{u}^n_{i+1} \end{pmatrix}, \tag{IV.22}$$

$$H^n_{i+1/2\pm} = \max\left(0, H^n_{i+1/2\pm}\right), \tag{IV.23}$$

and

$$S^n_{b,i} = S^n_{b,i+1/2-} + S^n_{b,i-1/2+} = \begin{pmatrix} 0 \\ \frac{g}{2}\left(H^n_{i+1/2-}\right)^2 - \frac{g}{2}(H^n_i)^2 \end{pmatrix} + \begin{pmatrix} 0 \\ \frac{g}{2}(H^n_i)^2 - \frac{g}{2}\left(H^n_{i-1/2+}\right)^2 \end{pmatrix}. \tag{IV.24}$$

The latter expression for the source is equivalent to the earlier (IV.18), it shows that the source may be considered as being distributed to the cell interfaces. With this re-interpretation in mind, we may also rewrite the scheme as

$$X^{n+1}_i = X^n_i - \sigma^n_i\left(\mathscr{F}^n_l\left(X^n_i, X^n_{i+1}, z_{b,i}, z_{b,i+1}\right) - \mathscr{F}^n_r\left(X^n_{i-1}, X^n_i, z_{b,i-1}, z_{b,i}\right)\right), \tag{IV.25}$$

with left and right numerical fluxes

$$\mathscr{F}^n_l\left(X^n_i, X^n_{i+1}, z_{b,i}, z_{b,i+1}\right) = \mathscr{F}(X^n_{i+1/2-}, X^n_{i+1/2+}) + \begin{pmatrix} 0 \\ \frac{g}{2}(H^n_i)^2 - \frac{g}{2}\left(H^n_{i+1/2-}\right)^2 \end{pmatrix},$$
$$\mathscr{F}^n_r\left(X^n_i, X^n_{i+1}, z_{b,i}, z_{b,i+1}\right) = \mathscr{F}(X^n_{i+1/2-}, X^n_{i+1/2+}) + \begin{pmatrix} 0 \\ \frac{g}{2}\left(H^n_{i+1}\right)^2 - \frac{g}{2}\left(H^n_{i+1/2+}\right)^2 \end{pmatrix}.$$

Notice that (IV.21),(IV.23) and (IV.20) mean that we try to impose interface values satisfying some modified steady equations

$$H^n_{i+1/2-} + z_{b,i+1/2} = H^n_i + z_{b,i}, \quad \overline{u}^n_{i+1/2-} = \overline{u}^n_i,$$
$$H^n_{i+1/2+} + z_{b,i+1/2} = H^n_{i+1} + z_{b,i+1}, \quad \overline{u}^n_{i+1/2+} = \overline{u}^n_{i+1},$$

i.e. $H + z_b = cst, \overline{u} = cst$ instead of Bernoulli's law $\overline{u}^2/2 + g(H + z_b) = cst, H\overline{u} = cst$. Our construction, combined with a centered value of $z_{b,i+1/2}$, is not stable. The upwind value proposed in (IV.21), and the truncation of negative values in (IV.23) have the advantage of giving nonnegative values of $H^n_{i+1/2\pm}$ and of being stable, as we state it now.

Theorem IV.12. *Consider a consistent numerical flux $\mathscr{F}$ for the homogeneous problem that preserves nonnegativity of $H_i(t)$ and satisfies an in-cell entropy inequality corresponding to the entropy ζ in (II.58). Then the finite volume scheme (IV.25) with (IV.21),(IV.17),(IV.20),(IV.22),(IV.23)*

(i) preserves the nonnegativity of $H_i(t)$,

(ii) preserves the steady state of a lake at rest $H + z_b = cst$,

(iii) is consistent with the Saint-Venant system (II.28)-(II.29),

(iv) satisfies an in-cell entropy inequality associated to the entropy ζ in (II.58)

$$\frac{d}{dt}\tilde{\zeta}(X_i(t),z_{b,i})+\sigma_i^n\left(\tilde{G}^n_{i+1/2}-\tilde{G}^n_{i-1/2}\right)\leqslant 0.$$

Proof. The statement that $\mathscr{F}$ preserves the nonnegativity of $H_i(t)$ means exactly that

$$\mathscr{F}^H(H_i^n=0,\overline{u}_i^n,H_{i+1}^n,\overline{u}_{i+1}^n)-\mathscr{F}^H(H_{i-1}^n,\overline{u}_{i-1}^n,H_i^n=0,\overline{u}_i^n)\leqslant 0,$$

for all choices of the other arguments. Since the sources in (IV.18) have no contribution to the first component, $H_i^n(t)$ in our scheme satisfies a conservative equation with flux $\mathscr{F}^H(X^n_{i+1/2-},X^n_{i+1/2+})$. Therefore we need to check that $\mathscr{F}^H(X^n_{i+1/2-},X^n_{i+1/2+})-\mathscr{F}^H(X^n_{i-1/2-},X^n_{i-1/2+})\leqslant 0$ whenever $H_i^n=0$. Our construction (IV.20),(IV.21),(IV.23) (and this is the motivation for (IV.21)), gives $H^n_{i+1/2-}=H^n_{i-1/2+}=0$ when $H_i^n=0$, and this gives *(i)*. Then we prove statement *(ii)*. On a steady state of a lake at rest, we have $H^n_{i+1/2-}=H^n_{i+1/2+},\overline{u}^n_{i+1}=\overline{u}^n_i=0$, thus $X^n_{i+1/2-}=X^n_{i+1/2+}$ and by consistency of $\mathscr{F}$

$$\mathscr{F}^n_{i+1/2}=\begin{pmatrix}0\\ \frac{g}{2}(H^n_{i+1/2-})^2\end{pmatrix}=\begin{pmatrix}0\\ \frac{g}{2}(H^n_{i+1/2+})^2\end{pmatrix},$$

and this proves *(ii)*. The proofs of *(iii)* and *(iv)* are rather technical, the reader can refer to [8]. □

2.4 Schémas préservant l'asymptotique

On va maintenant étudier la possibilité de construire un schéma numérique permettant d'approcher correctement les écoulements à friction dominante présentés en 3.7.2 (page 36). Cela signifie que la précision du schéma ne doit pas être dépendante de la friction. C'est assez dur à quantifier et les démonstrations ne sont basées en général que sur des analyses de type différences finies, comme on va le voir par la suite.

Pour simplifier les calculs, on va restreindre la présentation à l'équation des ondes linéaire avec amortissement. Celle-ci correspond aux équations de Saint-Venant sans topographie avec une pression cubique et une friction linéaire en coordonnées lagrangiennes ($\mathrm{D}_t=\frac{\partial}{\partial t}+\bar{u}\frac{\partial}{\partial x}$, $-H\partial_m=\frac{\partial}{\partial x}$ et $r=1/H$). On regarde donc le système

$$\begin{aligned}&\mathrm{D}_t r+\partial_m u=0,\\ &\mathrm{D}_t u+\partial_m r=-\kappa u.\end{aligned}\tag{IV.26}$$

L'asymptotique à laquelle on s'intéresse apparaît après avoir introduit $s=t/\kappa$ et $v=\kappa u$, à la manière de (II.64). À $\mathscr{O}(\kappa^{-1})$ près, on a

$$\begin{aligned}&v=-\partial_m r,\\ &\mathrm{D}_s r-\partial^2_{mm} r=0.\end{aligned}\tag{IV.27}$$

Du point de vue du schéma numérique, on va faire l'analyse dans le cas d'un schéma semi-discret (continu en temps) pour simplifier les notations mais tout fonctionne de la même manière dans le cas totalement discret. Le schéma que l'on va d'abord étudier correspond au schéma de Godunov pour la partie EDP avec un terme source centré (celui-ci pourrait être interprété comme la version continue en temps du splitting...). Cela donne **[EX]**

$$\begin{aligned}&\mathrm{D}_t r_i+\frac{u_{i+1/2}-u_{i-1/2}}{\Delta m}=0,\\ &\mathrm{D}_t u_i+\frac{r_{i+1/2}-r_{i-1/2}}{\Delta m}=-\kappa u_i,\end{aligned}\tag{IV.28}$$

où

$$\begin{aligned}r_{i+1/2}&=(r_i+r_{i+1})/2-(u_{i+1}-u_i)/2,\\ u_{i+1/2}&=(u_i+u_{i+1})/2-(r_{i+1}-r_i)/2.\end{aligned}\tag{IV.29}$$

Pour alléger un peu les notations, on introduit $D_i(z) = (z_{i+1} - 2z_i + z_{i-1})/(\Delta m^2)$ et donc le schéma numérique s'écrit

$$\begin{aligned} \mathrm{D}_t r_i + \frac{u_{i+1} - u_{i-1}}{2\Delta m} - \frac{\Delta m}{2} D_i(r) = 0, \\ \mathrm{D}_t u_i + \frac{r_{i+1} - r_{i-1}}{2\Delta m} - \frac{\Delta m}{2} D_i(u) = -\kappa u_i. \end{aligned} \tag{IV.30}$$

Appliquons maintenant l'asymptotique au schéma numérique. On définit naturellement $v_{i+1/2} = \kappa u_{i+1/2}$ et $v_i = \kappa u_i$:

$$\begin{aligned} \mathrm{D}_s r_i + \frac{v_{i+1} - v_{i-1}}{2\Delta m} - \frac{\kappa \Delta m}{2} D_i(r) = 0, \\ \frac{1}{\kappa^2} \mathrm{D}_s v_i + \frac{r_{i+1} - r_{i-1}}{2\Delta m} - \frac{\Delta m}{2\kappa} D_i(v) = -v_i. \end{aligned} \tag{IV.31}$$

La deuxième équation nous donne une discrétisation de la loi de Darcy

$$v_i = -\frac{r_{i+1} - r_{i-1}}{2\Delta m} + \mathscr{O}(\Delta m \kappa^{-1}) + \mathscr{O}(\kappa^{-2})$$

et la première équation devient une approximation de l'équation de la chaleur

$$\mathrm{D}_s r_i - \frac{r_{i+2} - 2r_i + r_{i-2}}{(2\Delta m)^2} - \frac{\kappa \Delta m}{2} D_i(r) + \mathscr{O}(\kappa^{-1}) + \mathscr{O}(\Delta m^{-1} \kappa^{-2}) = 0. \tag{IV.32}$$

Étudions plus précisément le schéma numérique obtenu par cette asymptotique. Pour que le schéma limite soit bien une approximation de (IV.27), il faut que

$$\kappa^{-2} \ll \Delta m \ll \kappa^{-1}.$$

Cette condition relie le pas d'espace et le coefficient de friction. Elle n'est pas satisfaisante en pratique puisqu'on désire en général obtenir un schéma numérique ayant une précision comparable à pas d'espace fixé quelle que soit la friction. On voit en particulier dans (IV.32) que plus le coefficient est grand, plus la diffusion numérique est grande.

Pour remédier à ce problème on va de nouveau intégrer le terme source dans le calcul des flux numériques. On opère de la même manière que pour les schémas équilibres de type Godunov (section 2.3.1) en concentrant le terme source au niveau des interfaces. Pour cela, on introduit la fonction identité $\mathbf{I}(x) = x$ et on interprète le terme source de friction comme $\kappa u \mathbf{I}(x)$. Tout comme on avait remplacé la topographie z_b par sa discrétisation z_{b_Δ}, on remplace $\mathbf{I}$ par $\mathbf{I}_\Delta$, sa discrétisation constante par maille. On doit donc résoudre le problème de Riemann

$$\begin{cases} \mathrm{D}_t r + \partial_m u = 0, \\ \mathrm{D}_t u + \partial_m r = -\kappa u \Delta m \delta_0(x), \\ (r,u)(0,x) = \begin{cases} (r,u)_g & \text{si } x < 0, \\ (r,u)_d & \text{si } x > 0. \end{cases} \end{cases}$$

Après quelques calculs **[EX]**, on aboutit au schéma numérique

$$\begin{aligned} \mathrm{D}_t r_i + \frac{u_{i+1/2} - u_{i-1/2}}{\Delta m} = 0, \\ \mathrm{D}_t u_i + \frac{r^-_{i+1/2} - r^+_{i-1/2}}{\Delta m} = 0, \end{aligned} \tag{IV.33}$$

où, en notant $K = 1/(1 + \kappa \Delta m/2)$, les valeurs d'interface sont

$$\begin{aligned} (1 + \kappa \Delta m/2) u_{i+1/2} &= \big[(u_i + u_{i+1})/2 - (r_{i+1} - r_i)/2\big], \\ r^-_{i+1/2} &= r_i - u_{i+1/2} + u_i, \\ r^+_{i-1/2} &= r_i - u_i + u_{i-1/2}. \end{aligned} \tag{IV.34}$$

On définit $v_{i+1/2} = \kappa u_{i+1/2}$ et $v_i = \kappa u_i$, donc

$$\begin{aligned} v_{i+1/2} &= \frac{\kappa}{1+\kappa\Delta m/2}\left[(v_i+v_{i+1})/(2\kappa) - (r_{i+1}-r_i)/2\right] \\ &= \frac{1}{1+\kappa\Delta m/2}(v_i+v_{i+1})/2 - \frac{\kappa}{1+\kappa\Delta m/2}(r_{i+1}-r_i)/2 \\ &= \frac{1}{1+\kappa\Delta m/2}(v_i+v_{i+1})/2 - \left(1-\frac{1}{1+\kappa\Delta m/2}\right)(r_{i+1}-r_i)/\Delta m \\ &= -(r_{i+1}-r_i)/\Delta m + \mathscr{O}((\kappa\Delta m)^{-1}) \end{aligned}$$

On peut donc déduire le schéma numérique asymptotique :

$$\begin{aligned} &\mathrm{D}_s r_i - D_i(r) = \mathscr{O}(\kappa^{-1}), \\ &v_{i+1/2} = -(r_{i+1}-r_i)/\Delta m + \mathscr{O}((\kappa\Delta m)^{-1}). \end{aligned}$$

On voit que ce schéma est précis même pour $\kappa \gg 1$. De plus, si $\kappa = 0$, on retombe sur le schéma de Godunov classique **[EX]**. On dit alors que ce schéma numérique préserve l'asymptotique (IV.27) (*asymptotic preserving* en anglais).

Comme on l'a dit plus haut, ce type de schéma peut être développé pour le modèle complet (II.63). Pour illustrer le propos ci-dessus, on présente dans les figures IV.1 et IV.2 des résultats obtenus pour les équations d'Euler avec friction et gravité (la gravité étant dans la direction de l'écoulement cette fois), avec le schéma préservant l'asymptotique et la méthode de splitting d'opérateur, voir [41]. Ces figures représentent des tests avec un coefficient de friction très grand et permettent d'étudier la sensibilité à la finesse du maillage des deux méthodes numériques. On voit nettement qu'un maillage très fin (10000 mailles) est nécessaire pour la méthode de splitting pour avoir des résultats comparables au schéma préservant l'asymptotique sur maillage grossier.

Par ailleurs, on pourra retrouver dans [80] des discussions très intéressantes et les prémices de la notion de schéma préservant l'asymptotique.

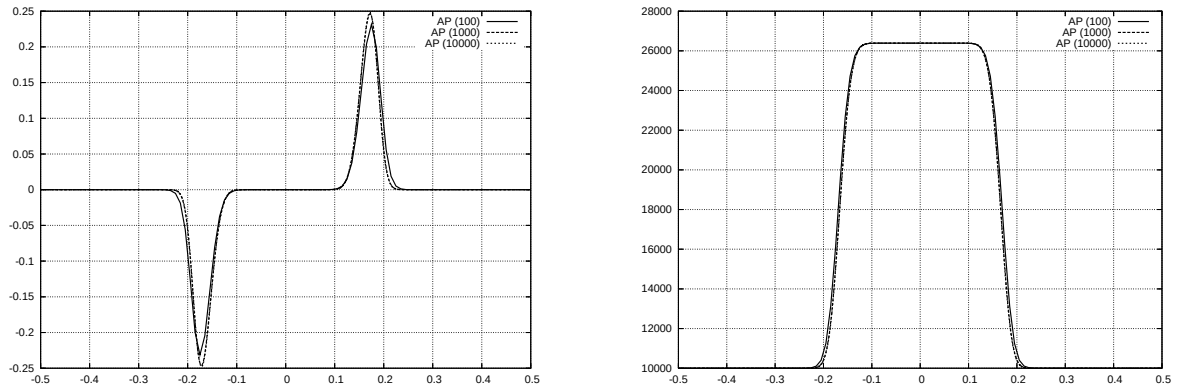

Figure IV.1: Résultats avec le schéma préservant l'asymptotique

2.5 Pour aller plus loin...

Nous allons évoquer brièvement les extensions possibles, ou non, des schémas présentés à des configurations plus complexes.

2.5.1 Passage au 2D

La première généralisation des questions précédentes concerne le passage au 2D. Pour la problématique des schémas équilibres, la généralisation est standard, quel que soit le type de maillage considéré. Le

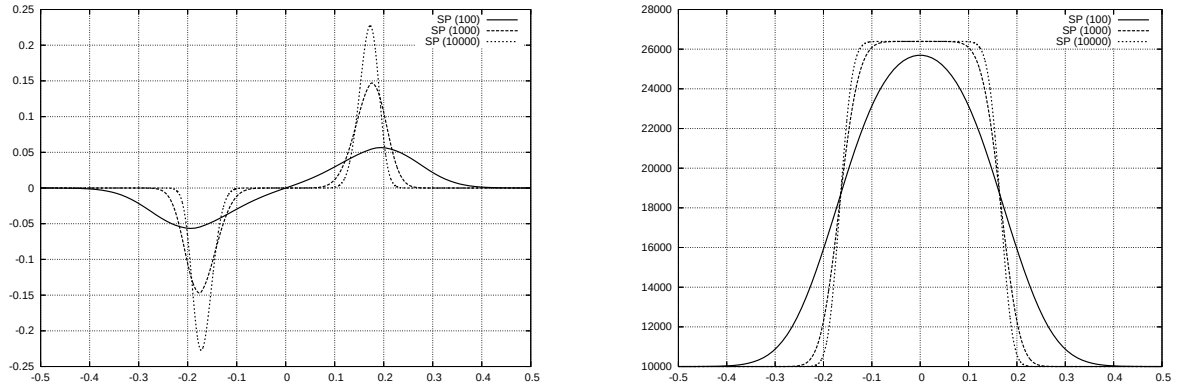

Figure IV.2: Résultats de la méthode de splitting d'opérateur

calcul est standard, ce qui est en grande partie due au fait que les états stationnaires (II.61) sont très simples et à vitesse nulle.

Concernant l'asymptotique, le développement pour obtenir le modèle parabolique avec une loi de Darcy reste valable. D'un point de vue numérique, c'est plus compliqué. Il est possible d'étendre l'analyse présentée dans le cas de maillage cartésiens mais, dans le cas de maillages non structurés, la question reste ouverte : il est maintenant à peu près clair que le schéma "limite" basé sur celui introduit ici n'est pas consistant avec le bon système. Des techniques plus évoluées doivent alors être utilisées pour obtenir à nouveau un bon comportement.

2.5.2 Termes sources plus compliqués

Dans le cas du terme source dû à la topographie, on peut imaginer le cas d'un fond variable en temps, par exemple quand on prend en compte un transport de sédiments. Mais comme le fond varie en temps, la notion d'état stationnaire n'a plus vraiment d'intérêt. Néanmoins, les schémas équilibres ont des comportements bien souvent meilleurs que les schémas standards (splitting ou discrétisation directe) dans les configurations transitoires. Il est donc naturel de se baser sur ces schémas pour proposer des extensions à des termes sources plus compliqués.

Des termes de friction plus compliqués (Darcy-Weisbach ou Manning notamment) peuvent être pris en compte de la même manière, mais la vitesse $u_{i+1/2}$ dans (IV.34) peut n'être définie qu'implicitement (et donc nécessiter une résolution itérative).

Il est important de noter que pour le schéma (IV.33-IV.34), le terme source a été concentré aux interfaces, en coordonnées *lagrangiennes*. Cela signifie qu'en coordonnées *eulériennes*, il aurait été concentré sur une discontinuité de contact additionnelle de vitesse u. En effet, à la lecture de [27], on peut se rendre compte que concentrer un terme source de friction en coordonnées eulériennes sur les interfaces du maillage (donc sur des discontinuités de contact de vitesse nulle) nécessite l'introduction d'hypothèse additionnelle sur la méthode numérique pour qu'elle préserve l'asymptotique choisie. Cependant c'était le choix effectué pour le terme source de topographie dans le schéma équilibre (IV.9-IV.11). La raison de ce traitement différent est simple : contrairement au terme source de topographie, le terme source de friction est invariant galiléen. Il est donc naturel d'avoir une discrétisation qui soit, autant que possible, invariante galiléenne. C'est bien sûr impossible puisque le maillage est fixe, mais le solveur de Riemann "doit" l'être. Ainsi, la concentration du terme source de topographie se fait à l'aide de l'équation $\frac{\partial z_{b_\Delta}}{\partial t} = 0$ alors que celle du terme source de friction se fait à l'aide de l'équation

$$\frac{\partial \mathbf{I}_\Delta}{\partial t} + u\frac{\partial \mathbf{I}_\Delta}{\partial x} = 0.$$

A noter que la problématique de l'approximation des *roll waves* n'a pas été évoquée. En effet, la plupart des schémas numériques, dont le splitting d'opérateur, fournit une approximation tout-à-fait convenable de ce type de solutions.

3 Kinetic scheme

The numerical scheme detailed in this section is based on the kinetic interpretation of the Saint-Venant system given in Section 4 (page 39). To have the notation in mind, we recall the main part of the proposition II.11 that is the fundation of the scheme.

Proposition IV.13. *The functions $(H,\overline{u})$ are strong solutions of the Saint-Venant system (without friction) described in (II.28)-(II.29) if and only if the equilibrium $M(x,t,\xi)$ is solution of the kinetic equation*

$$(\mathscr{B}) \qquad \frac{\partial M}{\partial t}+\xi\frac{\partial M}{\partial x}-g\frac{\partial z_b}{\partial x}\frac{\partial M}{\partial \xi}=Q(x,t,\xi), \tag{IV.35}$$

where $Q(x,t,\xi)$ is a "collision term" satisfying

$$\int_{\mathbb{R}} Q\,d\xi=\int_{\mathbb{R}}\xi Q\,d\xi=0. \tag{IV.36}$$

In a first step, we present the numerical scheme for the conservative part i.e. for

$$\frac{\partial z_b}{\partial x}=0.$$

Then using the hydrostatic reconstruction technique ([8]) presented in paragraph 2.3.3, the discretization of the topography source term id added.

To precise the numerical scheme, we deduce a finite volume kinetic scheme from the previous kinetic interpretation of the Saint-Venant system. The main interest of the kinetic interpretation is to transform the nonlinear Saint-Venant system into a simple linear advection equation. First, we define the discrete densities of particles M_i^n by

$$M_i^n=M_i^n(\xi)=\frac{H_i^n}{c_i^n}\chi\left(\frac{\xi-u_i^n}{c_i^n}\right), \tag{IV.37}$$

with $c_i^n=\sqrt{\frac{gH_i^n}{2}}$.

Using a simple upwing formula, we are now able to propose a finite volume scheme for the discretization of the Boltzmann equation (IV.35) under the form

$$M_i^{n+1-} \;=\; M_i^n-\sigma_i^n\xi\left(M_{i+1/2}^n-M_{i-1/2}^n\right), \tag{IV.38}$$

with

$$M_{i+1/2}^n \;=\; M_i^n\mathbb{1}_{\xi\geqslant 0}+M_{i+1}^n\mathbb{1}_{\xi\leqslant 0}. \tag{IV.39}$$

The discrete scheme (IV.38) does not take into account the collision term which makes relax M_i^{n+1-} to a Gibbs equilibrium so the quantity M_i^{n+1-} can not be written under the form (IV.37). The collision term is used in a second step introducing a discontinuity at time t^{n+1} on M and replacing M_i^{n+1-} by an equilibrium

$$M_i^{n+1}=M_i^{n+1}(\xi)=\frac{H_i^{n+1}}{c_i^{n+1}}\chi\left(\frac{\xi-u_i^{n+1}}{c_i^{n+1}}\right).$$

Notice that M_i^{n+1} is discontinuous in the sense that $M_i^{n+1}\neq M_i^{n+1-}$ whereas the macroscopic variables remain continuous $X_i^{n+1}=X_i^{n+1-}$.

By analogy with (II.77), H_i^{n+1} and $\overline{u}_i^{n+1}$ are calculated by

$$X_i^{n+1}=\begin{pmatrix} H_i^{n+1} \\ H_i^{n+1}u_i^{n+1}\end{pmatrix}=\int_{\mathscr{R}}\mathscr{K}(\xi)M_i^{n+1-}(\xi)\,d\xi, \tag{IV.40}$$

and where $\mathscr{K}(\xi)$ is the vector $\mathscr{K}(\xi)=(1,\xi)^T$.

3.1 Fluxes calculus

Using (IV.40), we are now able to precise the numerical scheme for the homogenous Saint-Venant system (II.28)-(II.29)

$$X_i^{n+1} = X_i^n - \sigma_i^n \left(\mathscr{F}_{i+1/2}^n - \mathscr{F}_{i-1/2}^n \right), \tag{IV.41}$$

with (using (IV.38))

$$\mathscr{F}_{i+1/2}^n = \int_{\mathscr{R}} \xi \mathscr{K}(\xi) M_{i+1/2}^n(\xi)\, d\xi. \tag{IV.42}$$

We also have

$$E_i^{n+1} = \int_{\mathscr{R}} \left(\frac{\xi^2}{2} + \frac{g^2}{8k_3}(M_i^{n+1})^2 + g z_{b,i} \right) M_i^{n+1} d\xi.$$

Now, using (IV.38), we are able to precise the computation of the fluxes introduced in the discrete macroscopic equations (IV.41). If we denote

$$\mathscr{F}_{i+1/2}^n = \mathscr{F}(X_i^n, X_{i+1}^n) = \mathscr{F}^+(X_i^n) + \mathscr{F}^-(X_{i+1}^n), \tag{IV.43}$$

following (IV.42),(IV.39) we define

$$\mathscr{F}^-(X_{i+1}^n) = \int_{\xi \leqslant 0} \xi \mathscr{K}(\xi) M_{i+1}^n(\xi)\, d\xi,$$
$$\mathscr{F}^+(X_i^n) = \int_{\xi \geqslant 0} \xi \mathscr{K}(\xi) M_i^n(\xi)\, d\xi.$$

More precisely the expression of $\mathscr{F}^+(X_i^n)$ can be written

$$\mathscr{F}^+(X_i^n) = \left(\mathscr{F}_H^+(X_i^n), \mathscr{F}_q^+(X_i^n) \right)^T,$$

with

$$\mathscr{F}_H^-(X_{i+1}^n) = H_{i+1}^n \int_{z \leqslant -\frac{\bar{u}_{i+1}^n}{c_{i+1}^n}} (\bar{u}_{i+1}^n + z c_{i+1}^n) \chi(z)\, dz, \tag{IV.44}$$

$$\mathscr{F}_H^+(X_i^n) = H_i^n \int_{z \geqslant -\frac{\bar{u}_i^n}{c_i^n}} (\bar{u}_i^n + z c_i^n) \chi(z)\, dz, \tag{IV.45}$$

$$\mathscr{F}_q^-(X_{i+1}^n) = H_{i+1}^n \int_{z \leqslant -\frac{\bar{u}_{i+1}^n}{c_{i+1}^n}} (\bar{u}_{i+1}^n + z c_{i+1}^n)^2 \chi(z)\, dz, \tag{IV.46}$$

$$\mathscr{F}_q^+(X_i^n) = H_i^n \int_{z \geqslant -\frac{\bar{u}_i^n}{c_i^n}} (\bar{u}_i^n + z c_i^n)^2 \chi(z)\, dz. \tag{IV.47}$$

Using χ_1 defined by (II.72), the previous integrations can be done analytically

$$\begin{aligned}
\int_{\xi \geqslant 0} \xi^p \frac{H}{c} \chi_1 \left(\frac{\xi - u}{c} \right) d\xi &= H \int_{z \geqslant -\frac{u}{c}} (cz+u)^p \chi_1(z)\, dz \\
&= \frac{H}{pc} \left[(cz+u)^{p+1} \right]_{\max(-\frac{u}{c}, -\sqrt{3})}^{\max(-\frac{u}{c}, \sqrt{3})}, \\
\int_{\xi \leqslant 0} \xi^p \frac{H}{c} \chi_1 \left(\frac{\xi - u}{c} \right) d\xi &= \frac{H}{pc} \left[(cz+u)^{p+1} \right]_{\min(-\frac{u}{c}, -\sqrt{3})}^{\min(-\frac{u}{c}, \sqrt{3})}.
\end{aligned}$$

3.2 The topography source term

The hydrostatic technique presented in paragraph 2.3.3 implies a reconstruction of the variables at the interfaces, this means $X_{i+1/2-}^n \neq X_i^n$ and $X_{i+1/2+}^n \neq X_{i+1}^n$. So we proceed as follows.

Using the definitions (IV.20),(IV.21),(IV.22) and (IV.23), we calculate the fluxes

$$\mathscr{F}(X_{i+1/2-}^n, X_{i+1/2+}^n),$$

as previously but with the reconstructed variables. Then adding the source term (IV.24), that is done.

3.3 Stability of the scheme

We now establish the stability property of the kinetic scheme. Classically for the Saint-Venant system, a CFL condition ensures the water height is non negative. This CFL condition means that the quantity of water leaving a given cell during a time step Δt^n is less than the actual water in the cell.

Proposition IV.14. *Assume that the function χ has a compact support of length $2w_M$ then under the CFL condition*

$$\Delta t^n \leqslant \min_{i\in I} \frac{\Delta x_i}{(|\bar{u}_i^n| + w_M c_i^n)} \tag{IV.48}$$

the kinetic scheme (IV.41) and (IV.42) keeps the water height positive i.e. $\mathscr{S}_i^n \geqslant 0$ and $H_i^n \geqslant 0$ if it is true initially. Notice that this condition does not depend on the bottom profile varitions $\frac{\partial z_b}{\partial x}$.

Proof. The proof has been adapted from those given in [11, 113]. To prove the stability property of the scheme, we come back to the kinetic interpretation and we proceed by induction. We assume that $H_i^n \geqslant 0$, $\forall i$ and we prove that $H_i^{n+1} \geqslant 0$, $\forall i$.

From the definition of the functions M in (IV.37) and the positivity of the function χ, we deduce $M_i^n \geqslant 0$ $\forall i$. We now introduce the quantities

$$[\xi]_+ = \max(0,\xi), \quad [\xi]_- = \max(0,-\xi),$$

and so we can write the upwind microscopic scheme (IV.38)

$$M_i^{n+1-} \quad = \quad (1-\sigma_i^n|\xi|)M_i^n + \sigma_i^n[\xi]_+ M_{i-1}^n + \sigma_i^n[\xi]_- M_{i+1}^n. \tag{IV.49}$$

The quantity $\sigma_i^n|\xi|M_j^n$ represents, at the microscopic level, the water leaving the cell C_i during Δt^n. A sufficient condition to obtain the stability property, i.e.

$$H_i^{n+1} = \int_{\mathscr{R}} M_i^{n+1-} d\xi \geqslant 0, \qquad \forall i, \tag{IV.50}$$

is then

$$\int_{\mathscr{R}} \sigma_i^n|\xi|M_i^n \leqslant \int_{\mathscr{R}} M_i^n d\xi, \tag{IV.51}$$

and this requirement is satisfied when $\sigma_i^n(|\bar{u}_i^n| + w_M c_i^n) \leqslant 1$. If Δt^n satisfies (IV.48), then the condition (IV.50) is satisfied and that completes the proof. □

3.4 Boundary conditions

The treatment of the boundary conditions is presented hereafter. For a complete description – especially in 2d – the reader can refer to Bristeau and Coussin, see [34].

In practice, 2 types of boundary conditions are used:

- given water depth H,
- given flux q.

The difficulty lies in the following. When the flow is supercritic at one of the boundary, the boundary condition when corresponding to a fluvial regime cannot be satisfied and hence we propose the following approach.

A ghost cell towards each boundary cell is added and using Riemann invariants, we build a numerical flux on each ghost cell satisfying – when possible – the boundary conditions.

For the sake of simplicity, we often assume

$$\frac{\partial z_b}{\partial x} = 0,$$

at the boundaries and hence only the fluxes of the conservative part are non zero. Such an assumption is not easily possible in 2d.

3.4.1 Given water depth

Let $H_e(t^n)$ be the given water depth. Then we have to define the velocity $\bar{u}_e(t^n)$ so that the numerical fluxes can be calculated over the ghost cell. Using the Riemann invariants (see (II.52)) we define

$$\bar{u}_e(t^n) + 2\sqrt{gH_e(t^n)} = \bar{u}_1^n + 2\sqrt{gH_1^n},$$

and

$$\bar{u}_e(t^n) - 2\sqrt{gH_e(t^n)} = \bar{u}_N^n - 2\sqrt{gH_N^n}.$$

This means we assume the continuity of the Riemann invariants though the boundaries.

3.4.2 Given flux

Let $q_e(t^n)$ be the given flux. Then we are looking for $H_e(t^n)$,$\bar{u}_e(t^n)$ such that $\mathscr{F}_{H,1/2}^n = q_e(t^n)$ or equivalently

$$H_e^n \int_{z \geqslant -\frac{\bar{u}_e^n}{c_e^n}} (\bar{u}_e^n + zc_e^n)\chi(z)\, dz + H_1^n \int_{z \leqslant -\frac{\bar{u}_1^n}{c_1^n}} (\bar{u}_1^n + zc_1^n)\chi(z)\, dz = q_e(t^n). \tag{IV.52}$$

Using the Riemann invariant

$$\bar{u}_e(t^n) + 2\sqrt{gH_e(t^n)} = \bar{u}_1^n + 2\sqrt{gH_1^n} = l_1^n,$$

we get

$$\bar{u}_e(t^n) = l_n^1 - 2\sqrt{2}c_e^n.$$

Then the equation (IV.52) becomes

$$H_e^n \int_{z \geqslant -\frac{l_n^1 - 2\sqrt{2}c_e^n}{c_e^n}} (l_1^n + (z - 2\sqrt{2})c_e^n)\chi(z)\, dz = a^n, \tag{IV.53}$$

that only depends on H_e and with

$$a^n = q_e(t^n) - H_1^n \int_{z \leqslant -\frac{\bar{u}_1^n}{c_1^n}} (\bar{u}_1^n + zc_1^n)\chi(z)\, dz.$$

It can be proved that, in fluvial regime, Eq. (IV.53) admits one and only one solution H_e^n, see [34].

3.5 Friction terms

Even if the bottom friction corresponds to dissipative and hence stabilizing effects, its numerical discretization is not always straightforward. In practice in cases of dry areas, large Froude numbers or when dealing with large friction effects, a stable treatment of the friction source term is necessary and hence an implicit scheme is often used.

3.5.1 Implicit treatment

Since the friction terms only appear in the momentum equation, this implicit step does not affect the discrete water depth. So the computation of the new velocitiy $\bar{u}^{n+1}$ leads to solve the discrete equation

$$q_i^{n+1} = q_i^n - \Delta t^{n+1} S_{f,i}^{n+1}. \tag{IV.54}$$

Several friction laws can be used among which are Navier, Chezy, Darcy-Weisbach, Manning and Strickler laws.

Unfortunately, such a centered discretization is not fully consistent e.g. for stationnary states. In such situations, the apparent topography procedure proposed by Bouchut [28] can be used. An explicit treatment of the friction with a modified CFL condition can also be used.

3.5.2 Kinetic description of the friction terms

Let us consider the Saint-Venant sytem with topography and a Navier type friction law corresponding to (II.28)-(II.29) with $p^a = cst$. The kinetic interpretation of this system – extending (II.74) – is

$$(\mathscr{B}) \qquad \frac{\partial M}{\partial t} + \xi \frac{\partial M}{\partial x} - g \frac{\partial z_b}{\partial x} \frac{\partial M}{\partial \xi} - \kappa \frac{\partial \tilde{M}}{\partial \xi} = Q(x,t,\xi), \tag{IV.55}$$

with

$$\tilde{M} = \frac{\overline{u}}{H} M.$$

The discretization of

$$\frac{\partial \tilde{M}}{\partial \xi},$$

is straightforward using the quadrature formula

$$\int_{C_i} \frac{\partial \tilde{M}}{\partial \xi} dx = \frac{\Delta x_i}{2} \left(\frac{\partial \tilde{M}_{i-1/2}}{\partial \xi} + \frac{\partial \tilde{M}_{i+1/2}}{\partial \xi} \right),$$

and gives

$$\int_{C_i} \mathscr{K}(\xi) \frac{\partial \tilde{M}}{\partial \xi} dx = \frac{\Delta x_i}{2} \begin{pmatrix} \tilde{M}^n_{i+1}(0) - \tilde{M}^n_{i-1}(0) \\ -\left(\overline{u}^n_i + \int_{\xi \leqslant 0} \tilde{M}^n_{i+1} d\xi + \int_{\xi \geqslant 0} \tilde{M}^n_{i-1} d\xi \right) \end{pmatrix}.$$

3.6 Second order scheme

The second-order accuracy in time is usually recovered by the Heun method [23] that is a slight modification of the second order Runge-Kutta method. The advantage of the Heun scheme is that it preserves the invariant domains without any additional limitation on the CFL.

We also apply a formally second order scheme in space by a limited reconstruction of the variables [9]. These new variables are classically obtained with three ingredients: prediction of the gradients in each cell, linear extrapolation, and limitation procedure.

The reconstructed values at interface $i+1/2-$ and $i+1/2+$ are respectively $X_{i,r}$ and $X_{i+1,l}$. This gives the second order scheme

$$X^{n+1}_i = X^n_i - \sigma^n_i \left(\mathscr{F}^n_{i+1/2} - \mathscr{F}^n_{i-1/2} \right),$$

where

$$\mathscr{F}^n_{i+1/2} = \mathscr{F}(X^n_{i,r}, X^n_{i+1,l}),$$
$$X^n_{i,r} = \begin{pmatrix} H_{i,r} \\ H_{i,r}\bar{u}_{i,r} \end{pmatrix}, \quad X_{i+1,l} = \begin{pmatrix} H_{i+1,l} \\ H_{i+1,l}\bar{u}_{i+1,l} \end{pmatrix}.$$

4 Simulation results

4.1 Analytical solutions

As already mentioned in this document, models arising in fluid dynamics often based on the Navier-Stokes equations are generally difficult to analyze both at the mathematical or numerical level. As a consequence the derivation of efficient numerical schemes and their validations are complex. A way to circumvent this difficulty is to have access to analytical solutions of the considered problem and to confront the simulated solutions with them. Even if this approach is not a complete validation of the numerical schemes, it enables to have a good knowledge of the behavior of the discrete schemes in front of typical and complex situations particularly when the family of analytical solutions is large enough. Moreover it makes possible the study of the convergence order of a simulated solution towards the reference one.

For shallow water flows, analytical solutions are available in various situations, see also paragraph 3.7.3 - page 37. In a chronological order, the most famous contributions are: analytical solutions for the dam break situation by Ritter [118], the nonlinear wave propagation in Shallow water open channels by Stoker [126], solutions of the Saint-Venant system for a flow respectively over a ridge and in parabolic bowl by Houghton [74] and Thacker [128]. MacDonald *et al.* [94, 95] have proposed a wide family of analytical solutions with bottom friction, hydraulic jumps and various open-channel cross-sections, see also [2].

Stationary solutions of the Saint-Venant system have to fulfill (see paragraph 3.7.1, page 34)

$$\left\{ \begin{array}{l} \frac{\partial}{\partial x}(H\bar{u}) = 0, \\ \bar{u}\frac{\partial \bar{u}}{\partial x} + g\frac{\partial (H+z_b)}{\partial x} = 0. \end{array} \right. \tag{IV.56}$$

Let $H_0(x)$ a non negative and enough smooth function then z_b defined by

$$z_b = cst - H_0 - \frac{Q_0^2}{2gH_0^2},$$

with $Q_0 = H\bar{u} = cst$ and $H = H_0$ satisfy (IV.56).

Now, we confront the kinetic scheme for the Saint-Venant system depicted in paragraph 3 with three typical test cases for which analytical solutions are available.

4.2 Fluvial regime

We consider a 1d rectangular basin of length L with vertical shores. At the entry $x = 0$, we impose an inflow Q_0 and at the exit we impose the water depth H_L. Let us consider the function H_0 given by

$$H_0(x) = 1 - 0.2\, e^{-\alpha \frac{(x-L/2)^2}{L^2}},$$

for $x \in [0, L]$ with $\alpha = 50$ and $L = 20$. Then for the bottom geometry

$$z_b(x) = -\frac{1}{g}\left(\frac{Q_0^2}{2H_0(x)^2} + gH_0(x)\right),$$

the water depth satisfies $H = H_0$ (see paragraph 4.1).

For $Q_0 = 1.7$ m^2.s^{-1}, we have a fluvial regime and we compare the convergence orders of the kinetic scheme described above to the theoretical one. In Fig. IV.3-*(a)*, we have plotted the bottom topography, the water depth and the velocity field $\bar{u}$ simulated with the prescribed initial and boundary conditions. In Fig. IV.3-*(b)*, we plot the rate of error versus the horizontal discretization, namely the number of nodes. We have plotted the $\log(L^1 - error)$ of the water height versus $\log(h_0/h_i)$. We denote by h_i the average cell length, h_0 is the average cell of the coarser mesh. These errors have been computed on 5 meshes with 30, 50, 100, 200 and 400 nodes. The convergence rates for the first and second order schemes are plotted.

4.3 Comparison with other solvers

For the test case depicted in the previous paragraph, we compare the convergence order of the kinetic, HLL and Rusanov solvers, see fig IV.4.

4.4 Transcritical regime with shock

We consider the same geometry as previously but with $Q_0 = 2.057447$ m^2.s^{-1}. The flow exhibits a shock located at the abscissa $x = 15$ m. As in paragraph 4.2, the obtained solution and the convergence orders of the proposed schemes are depicted over Fig. IV.5.

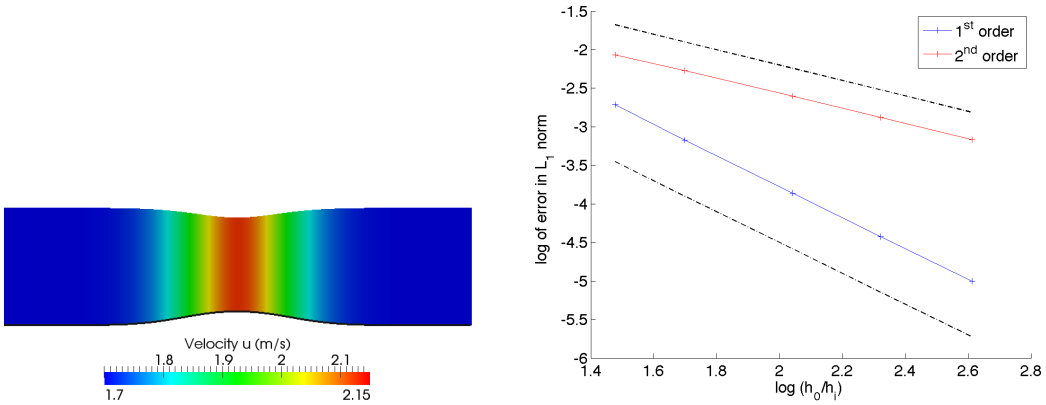

(a) *(b)*

Figure IV.3: *(a)* The simulated flow with the bottom topography and the water depth, *(b)* convergence rates to the reference solution, 1^{st} and 2^{nd} order schemes, '-.' theoretical order.

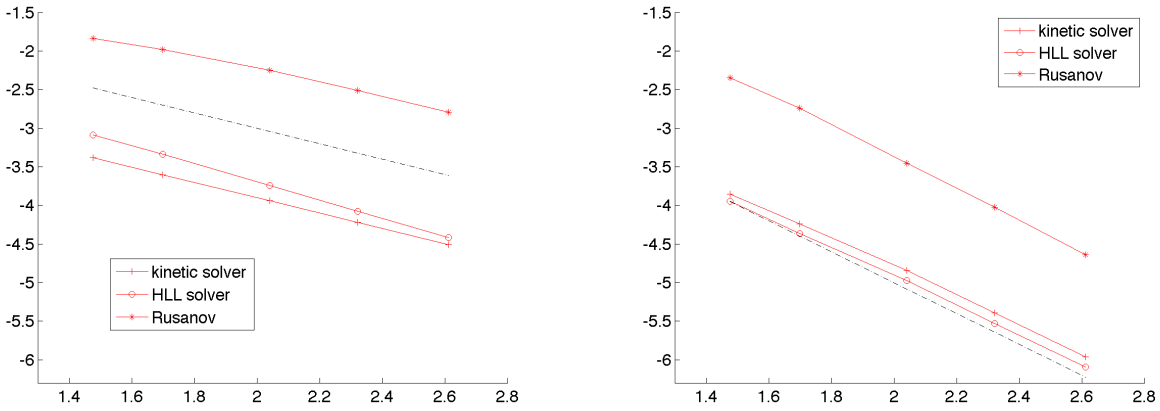

(a) *(b)*

Figure IV.4: Convergence rates to the reference solution. Comparison between the kinetic, HLL and Rusanov solvers. *(a)* 1^{st} order schemes and *(b)* 2^{nd} order schemes, '-.' theoretical order.

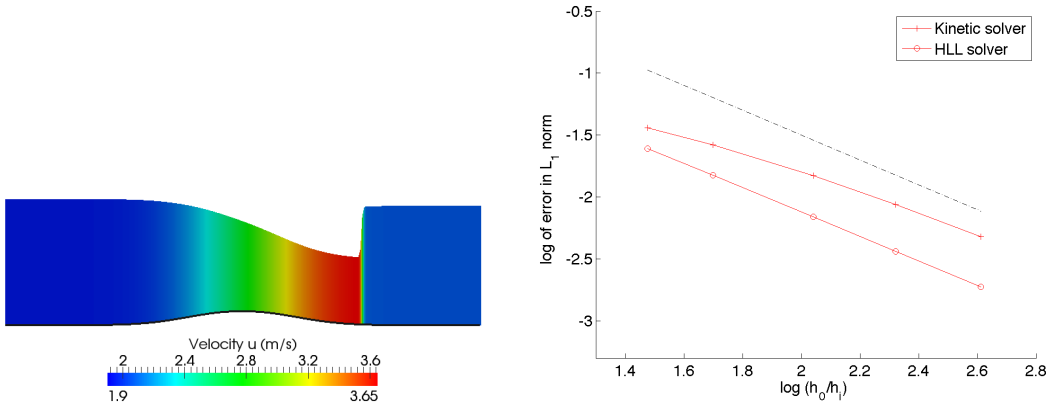

(a) *(b)*

Figure IV.5: *(a)* The simulated flow with the bottom topography and the water depth, *(b)* convergence rate to the reference solution. Comparison between the kinetic and HLL solvers. 1^{st} order schemes, '-.' theoretical order.

4.5 Parabolic bowl

We confront our numerical scheme with the analytical solutions proposed by Thacker [128], see paragraph 3.7.3 - page 37. This case provides us with a relevant test for the 1d Saint-Venant system because it deals with a sloping bed as well as with wetting and drying. The topography is a parabolic bowl given by

$$z_b(x) = h_0 \left(\frac{1}{a^2} \left(x - \frac{L}{2} \right)^2 - 1 \right).$$

Starting from the initial conditions $u(x,0) = 0$ and

$$H(x,0) = \begin{cases} \max\left\{0, -\frac{h_0}{a^2}\left(\left(x+\frac{1}{2}\right)^2 - a^2\right)\right\} \\ 0 \quad \text{else} \end{cases}$$

Thacker's analytic solution is a periodic solution and given by

$$H(x,t) = \begin{cases} \max\left\{0, -\frac{h_0}{a^2}\left(\left(x+\frac{1}{2}\cos(\omega t)\right)^2 - a^2\right)\right\} \\ 0 \quad \text{else} \end{cases}$$

We consider $a = 1$ m, $h_0 = 0.5$ m, $L = 4$ m. We compare the analytical solution and the computed ones for $t = T = 2\pi/\omega = 10.0303$ s that corresponds to 5 periods.

For this test case, the errors due to the time and space schemes are combined so the convergence rate of the simulated solution towards the analytical one is more difficult to analyse. In Fig. IV.6 we consider the kinetic solver with the hydrostatic reconstruction. The upper curve corresponds to the 1^{st} order scheme in space and time whereas the other curve corresponds to the 2^{nd} order scheme in space and time. As mentionned by several authors, the 1^{st} order in space version of the hydrostatic reconstruction technique is not very accurate for situations with large slopes, small water depths and coarse meshes.

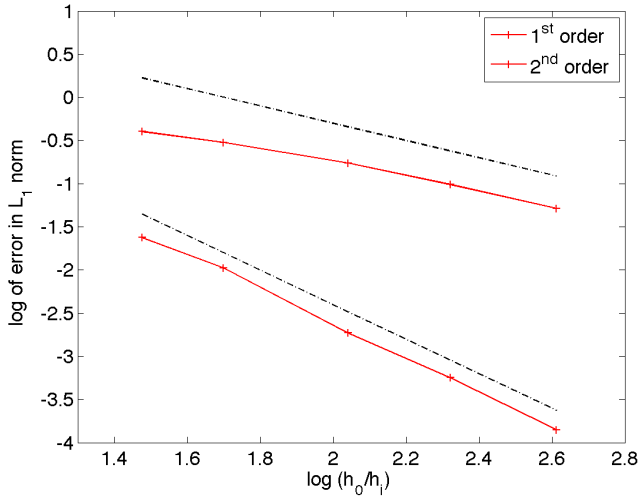

Figure IV.6: Convergence rates to the reference solution. Comparison between the proposed source term discretization and the hydrostatic reconstruction, 1^{st} order schemes (space and time) and 2^{nd} order schemes (space and time), '-.' theoretical order.

4.6 Numerical approximation of the 2d rotating Saint-Venant system

We recall the formulation of the 2d rotating Saint-Venant system (II.81)-(II.82) under the form

$$\frac{\partial h}{\partial t} + \nabla_{x,y} \cdot (h\mathbf{u}) = 0, \tag{IV.57}$$

$$\frac{\partial (h\mathbf{u})}{\partial t} + \nabla_{x,y} \cdot (h\mathbf{u} \otimes \mathbf{u}) + \nabla_{x,y}\big(\frac{g}{2}h^2\big) = -gh\nabla_{x,y} z_b - \Omega h\mathbf{u}^{\perp}, \tag{IV.58}$$

with $\mathbf{u}^{\perp} = (-v,u)^T$

Let us introduce the notations are depicted over Fig. IV.7. Using the notations of Fig. IV.7, the

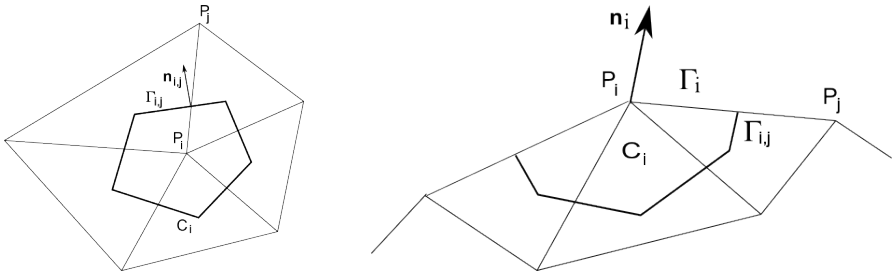

Figure IV.7: *(a)* Dual cell C_i and *(b)* Boundary cell C_i.

space approximation of the system (IV.57)-(IV.58) gives

$$|C_i|\frac{\partial \mathbf{X}_i}{\partial t} + \int_{\partial C_i} \mathbf{F}(\mathbf{X}_i) \cdot \mathbf{n} dl = \int_{C_i} \mathbf{S}_b(\mathbf{X}_i) dxdy + \int_{C_i} \mathbf{S}_\Omega(\mathbf{X}_i) dxdy, \tag{IV.59}$$

with

$$\mathbf{S}_b(\mathbf{X}) = \begin{pmatrix} 0 \\ -gh\nabla_{x,y} z_b \end{pmatrix}, \quad \mathbf{S}_\Omega(\mathbf{X}) = \begin{pmatrix} 0 \\ -\Omega h\mathbf{u}^{\perp} \end{pmatrix} \quad \text{and} \quad \int_{\partial C_i} \mathbf{F}(\mathbf{X}_i) \cdot \mathbf{n} dl = \sum_{j \in K_i} \int_{\Gamma_{i,j}} \mathbf{F}_{i,j} \cdot \mathbf{n}_{i,j} dl.$$

More precisely, formula (IV.59) corresponds to

$$|C_i|\frac{\partial h_i}{\partial t} + \sum_{j \in K_i} \int_{\Gamma_{i,j}} \mathbf{F}_{h,i,j} \cdot \mathbf{n}_{i,j} dl = 0,$$

$$|C_i|\frac{\partial (hu)_i}{\partial t} + \sum_{j \in K_i} \int_{\Gamma_{i,j}} \Big(\Big(hu^2 + \frac{g}{2}h^2\Big)n_{1,i,j} + huv\, n_{2,i,j}\Big) dl = \sum_{j \in K_i} \int_{\Gamma_{i,j}} \frac{g}{2}\big(h_i^2 - (h_{i,j})^2\big) n_{1,i,j} dl + \int_{C_i} \Omega (hv)_i dxdy,$$

$$|C_i|\frac{\partial (hv)_i}{\partial t} + \sum_{j \in K_i} \int_{\Gamma_{i,j}} \Big(huv\, n_{1,i,j} + \Big(hv^2 + \frac{g}{2}h^2\Big)n_{2,i,j}\Big) dl = \sum_{j \in K_i} \int_{\Gamma_{i,j}} \frac{g}{2}\big(h_i^2 - (h_{i,j})^2\big) n_{2,i,j} dl - \int_{C_i} \Omega (hu)_i dxdy,$$

with $\mathbf{n}_{i,j} = (n_{1,i,j}, n_{2,i,j})^T$ and where for the approximation of the topography source term $\mathbf{S}_b(\mathbf{X})$ over the cell i we use the 2d extension of the hydrostatic reconstruction technique written under the form

$$\int_{C_i} \mathbf{S}_b(\mathbf{X}_i) dxdy \approx \sum_{j \in K_i} \int_{\Gamma_{i,j}} \frac{g}{2}\big(h_i^2 - h_{i,j}^2\big) \mathbf{n}_{i,j} dl,$$

and

$$h_{i,j} = \max(h_i - \max(\Delta z_{b,i,j}, 0), 0), \qquad h_{j,i} = \max(h_j - \max(-\Delta z_{b,i,j}, 0), 0), \tag{IV.60}$$

and $\Delta z_{b,i,j} = z_{b,j} - z_{b,i}$, see paragraph 2.3.3. The previous system also writes

$$|C_i|\frac{\partial h_i}{\partial t} + \sum_{j\in K_i}\int_{\Gamma_{i,j}} hU\,dl = 0, \tag{IV.61}$$

$$|C_i|\frac{\partial (hu)_i}{\partial t} + \sum_{j\in K_i}\int_{\Gamma_{i,j}} \Big(huU + \frac{g}{2}h^2 n_{1,i,j}\Big)\,dl = \sum_{j\in K_i}\int_{\Gamma_{i,j}} \frac{g}{2}\big(h_i^2 - h_{i,j}^2\big)n_{1,i,j}dl + \sum_{j\in K_i}|C_{i,j}|\Omega(hv)_i, \tag{IV.62}$$

$$|C_i|\frac{\partial (hv)_i}{\partial t} + \sum_{j\in K_i}\int_{\Gamma_{i,j}} \Big(hvU + \frac{g}{2}h^2 n_{2,i,j}\Big)\,dl = \sum_{j\in K_i}\int_{\Gamma_{i,j}} \frac{g}{2}\big(h_i^2 - h_{i,j}^2\big)n_{2,i,j}dl - \sum_{j\in K_i}|C_{i,j}|\Omega(hu)_i, \tag{IV.63}$$

with $U = un_{1,i,j} + vn_{2,i,j}$ and $V = -un_{2,i,j} + vn_{1,i,j}$. After the following manipulations

- Eq. (IV.62)$_{i,j}$ becomes $(IV.62)_{i,j} \times n_{1,i,j} + (IV.63)_{i,j} \times n_{2,i,j}$,
- Eq. (IV.63)$_{i,j}$ becomes $(IV.62)_{i,j} \times (-n_{2,i,j}) + (IV.63)_{i,j} \times n_{1,i,j}$,

where $(.)_{i,j}$ denotes the spatial contribution corresponding the sub-triangle $C_{i,j}$ or the edge $\Gamma_{i,j}$, the system (IV.61)-(IV.63) corresponding to the contributions of $C_{i,j}$ or $\Gamma_{i,j}$ writes

$$|C_i|\frac{\partial h_{i,j}}{\partial t} + \int_{\Gamma_{i,j}} hU\,dl = 0, \tag{IV.64}$$

$$|C_i|\frac{\partial (hU)_{i,j}}{\partial t} + \int_{\Gamma_{i,j}} \Big(hU^2 + \frac{g}{2}h^2\Big)\,dl = \int_{\Gamma_{i,j}} \frac{g}{2}\big(h_i^2 - h_{i,j}^2\big)dl + |C_{i,j}|\Omega(hV)_i, \tag{IV.65}$$

$$|C_i|\frac{\partial (hV)_{i,j}}{\partial t} + \int_{\Gamma_{i,j}} hUV\,dl = -|C_{i,j}|\Omega(hU)_i, \tag{IV.66}$$

where the contribution of the Coriolis force in Eq. (IV.65) can be discretized using the apparent topography technique but the Coriolis term in Eq. (IV.66) is more difficult to approximate. In order to circumvent this difficulty, we propose the following reformulation.

The interpretation the Coriolis forcing as a gradient of a potential i.e. the existence of φ such that

$$\nabla_{x,y}\varphi = \mathbf{u}^{\perp},$$

requires that $\nabla_{x,y}\cdot\mathbf{u} = 0$ that is not ensured at the continuous level. But let us consider the discrete level. Over the cell $C_{i,j}\cup C_{j,i}$ (see Fig. IV.7), it is possible to choose

$$\varphi(x,y) = \frac{u_i+u_j}{2}y - \frac{v_i+v_j}{2}x,$$

satisfying

$$\nabla_{x,y}\varphi = \frac{\mathbf{u}_i^{\perp}+\mathbf{u}_j^{\perp}}{2}, \qquad \forall (x,y)\in C_{i,j}\cup C_{j,i}. \tag{IV.67}$$

Hence the right hand side of (IV.59) becomes

$$\int_{C_{i,j}} \Big(\mathbf{S}_b(\mathbf{X}_i) + \mathbf{S}_\Omega(\mathbf{X}_i)\Big)dxdy = \int_{C_{i,j}} \begin{pmatrix} 0 \\ -gh\nabla_{x,y}\Big(z_b + \frac{\Omega}{g}\varphi\Big)\end{pmatrix} dxdy,$$

allowing to use the hydrostatic reconstruction strategy by defining

$$h_{i,j}^{\Omega} = \max(h_i - \big(\Delta z_{b,i,j} + \Delta B_{i,j}\big), 0), \tag{IV.68}$$

with $\Delta z_{b,i,j} + \Delta B_{i,j} = z_{b,i,j} - z_{b,i} + \frac{\Omega}{g}\big(\varphi_{i,j} - \varphi(x_i,y_i)\big)$, $z_{b,i,j} + \frac{\Omega}{g}\varphi_{i,j} = \max\{z_{b,i} + \frac{\Omega}{g}\varphi(x_i,y_i), z_{b,j} + \frac{\Omega}{g}\varphi(x_j,y_j)\}$ and

$$\Delta z_{b,i,j} + \Delta B_{i,j} = \max\Big\{z_{b,j} - z_{b,i} + \frac{\Omega}{g}\Big(\frac{u_i+u_j}{2}(y_j-y_i) - \frac{v_i+v_j}{2}(x_j-x_i)\Big), 0\Big\}. \tag{IV.69}$$

This definition allows to preserve the equilibrium (when $h_{i,j}^{\Omega} \geqslant 0$)

$$\sum_{j\in K_i} l_{i,j}\Big(h_{i,j}^{\Omega}\Big)^2 \mathbf{n}_{i,j} = cst,$$

and we have the approximation formula

$$\int_{C_i}\Big(\mathbf{S}_b(\mathbf{X}_i)+\mathbf{S}_{\Omega}(\mathbf{X}_i)\Big)dxdy \approx \sum_{j\in K_i} l_{i,j}\frac{g}{2}\big(h_i^2-(h_{i,j}^{\Omega})^2\big)\mathbf{n}_{i,j}.$$

Therefore, the scheme (IV.64)-(IV.66) writes

$$|C_i|\frac{\partial h_{i,j}}{\partial t}+\int_{\Gamma_{i,j}} hU\,dl = 0, \tag{IV.70}$$

$$|C_i|\frac{\partial (hU)_{i,j}}{\partial t}+\int_{\Gamma_{i,j}}\Big(hU^2+\frac{g}{2}h^2\Big)\,dl = \int_{\Gamma_{i,j}}\frac{g}{2}\big(h_i^2-(h_{i,j}^{\Omega})^2\big)dl, \tag{IV.71}$$

$$|C_i|\frac{\partial (hV)_{i,j}}{\partial t}+\int_{\Gamma_{i,j}} hUV\,dl = 0. \tag{IV.72}$$

4.6.1 Preservation of stationary solutions

In oceanography, long-term simulations are carrried out and it is possible to consider that ocean dynamics is a fluctuation arround a stationary regime. Hence it is mandatory to be able to preserve, at the discrete level, the relevant stationary states.

The hydrostatic reconstruction technique is a very useful tool to preserve the equilibrium at rest i.e. when $u = v = 0$, see paragraph 2.3.3. But in the presence of the Coriolis force, the relevant equilibria are characterized by

$$g\nabla_{x,y}(h+z_b) = -\Omega\mathbf{u}^{\perp},$$

when the Rossby number

$$R_0 = \frac{U_0}{\Omega L_0},$$

is assumed to be $\ll 1$. But, because of the upwinding (necessary to obtain stable discretization), finite volume schemes contains numerical dissipation. More precisely, let us assume that the discrete scheme (IV.59) with topography and Coriolis effect satisfy a discrete energy balance under the form

$$\mathbf{E}_i^{n+1}-\mathbf{E}_i^n+\sigma_{i,j}^n\sum_{j\in K_i}\mathscr{G}_{i,j}^* \leqslant -C\sigma_{i,j}^n\sum_{j\in K_i}|X_{i,j}^*-X_i|^2, \tag{IV.73}$$

where $C = cst$, $X_{i,j}^*$ is the reconstructed vector X_i and the stationary solution of the considered system satisfy $\forall\, i$

$$X_{i,j}^* = X_i, \quad \forall\, j\in K_i.$$

In this paragraph, we investigate the stability of the stationary solutions when a discrete energy balance having the form (IV.73) holds.

From (IV.73), we get the global energy balance under the form

$$\sum_i \mathbf{E}_i^{n+1}-\sum_i \mathbf{E}_i^n \leqslant -\sum_i C\sigma_{i,j}^n\sum_{j\in K_i}|X_{i,j}^*-X_i|^2, \tag{IV.74}$$

that can be seen as a discrete version of

$$\frac{\partial E(X)}{\partial t} = -\delta|\nabla X|^2. \tag{IV.75}$$

Let us consider the simple situation where the previous equation reduces to

$$\frac{\partial |u|^2}{\partial t} = -\delta|\nabla u|^2.$$

In a 1d case, it corresponds to the situation

$$\frac{\partial u^2}{\partial t} = -\delta \left(\frac{\partial u}{\partial x} \right)^2, \tag{IV.76}$$

for which all the solutions $u = u_0 = cst$ are stationary solutions. And we are interested in the study of the stable stationary solutions of (IV.76).

The solution of Eq. (IV.76) are given by

$$u(t,x) = ae^{-\frac{2b}{\delta}(x+bt)},$$

where a, b are two constants. This seems to prove that the only stable stationary solutions is $u = u_0 = 0$. In other words, it seems that the reconstruction of variables in order to preserve stationary equilibria is only able to preserve in practice the stationary state at rest.

4.7 High order schemes

The use of high order schemes (especially in space) is a way to cirmcumvent the difficulty raised by the dissipation appearing in the r.h.s. of Eqs. (IV.74) and (IV.75).

Indeed the P_0 approximation of a continuous function necessarily leads to dissipation due to the discontinuity of the approximated solution at the edge of the mesh whereas a continuous approximation drastically reduces the numerical diffusion. More precisely, let us consider a stationary solution $\bar{u} = \bar{u}(x,y)$ of a PDE admitting a discrete entropy inequality having the form (IV.73). With obvious notations, starting at the initial instant from the P_0 apprroximation of $\bar{u}$ under the form

$$\bar{u} \approx \sum_{i \in C_i} \bar{u}(x_i, y_i) \mathbf{1}_{(x,y) \in C_i},$$

the dissipation

$$-\sum_i C \sigma_{i,j}^n \sum_{j \in K_i} |X_{i,j}^* - X_i|^2,$$

will not allow to preserve the stationary solution.

Chapter V

Beyond the Saint-Venant system

The derivation of the Saint-Venant system from the Navier-Stokes equations (see Chapter II) is based on two main approximations – valid because of the shallow water assumption $\varepsilon \ll 1$ – namely

- the horizontal fluid velocity is well approximated by its vertical mean i.e.

$$u(x,z,t) = \bar{u}(x,t) + \mathscr{O}(\varepsilon).$$

- the pressure is hydrostatic or equivalently the vertical acceleration of the fluid can be neglected compared to the gravitational effects. This means the z-momentum equation of the Navier-Stokes system

$$\frac{\partial w}{\partial t} + \frac{\partial uw}{\partial x} + \frac{\partial w^2}{\partial z} + \frac{\partial p}{\partial z} = -g + \frac{\partial \Sigma_{zx}}{\partial x} + \frac{\partial \Sigma_{zz}}{\partial z}.$$

  reduces to

$$\frac{\partial p}{\partial z} = -g + \frac{\partial \Sigma_{zx}}{\partial x} + \frac{\partial \Sigma_{zz}}{\partial z}.$$

But in practice, these two assumptions can be restrictive and in this chapter we propose two models extending the Saint-Venant system.

Firstly, we examine the situation where the fluid surface is only partially free. Then, we propose a non-hydrostatic Saint-Venant system i.e. a model where the hydrostatic pressure assumption is relaxed. Finally, we derive a model with a distributed velocity field in the z direction. For this last model, numerical simulations are presented.

In this chapter, we present an original derivation process of a non-hydrostatic shallow water-type model [32] which aims at approximating the incompressible Euler and Navier-Stokes systems with free surface. The closure relations are obtained by a minimal energy constraint instead of an asymptotic expansion. The model slightly differs from the well-known Green-Naghdi model and is confronted with stationary and analytical solutions of the Euler system corresponding to rotational flows.

Notice that the modeling of the non-hydrostatic effects for shallow water flows does not raise insuperable difficulties [67, 36, 20, 108, 111, 33] but the analysis [3, 88] of the resulting models and their discretization become tough.

1 Vertically averaged Euler systems

Neglecting the viscous effects, we consider the Euler equations written in a conservative form

$$\begin{cases} \dfrac{\partial \varphi}{\partial t} + \dfrac{\partial \varphi u}{\partial x} + \dfrac{\partial \varphi w}{\partial z} = 0, & \text{(V.1a)} \\ \dfrac{\partial \varphi u}{\partial t} + \dfrac{\partial \varphi u^2}{\partial x} + \dfrac{\partial \varphi uw}{\partial z} + \varphi \dfrac{\partial p}{\partial x} = 0, & \text{(V.1b)} \\ \dfrac{\partial \varphi w}{\partial t} + \dfrac{\partial \varphi uw}{\partial x} + \dfrac{\partial \varphi w^2}{\partial z} + \varphi \dfrac{\partial p}{\partial z} = -\varphi g, & \text{(V.1c)} \end{cases}$$

with φ defined by (I.7). The energy equation writes

$$\frac{\partial}{\partial t}\int_{z_b}^{\eta} (E + p^a)\, dz + \frac{\partial}{\partial x}\int_{z_b}^{\eta} u\big(E + p\big) = H\frac{\partial p^a}{\partial t} + (p|_b - p^a)\frac{\partial z_b}{\partial t}, \tag{V.2}$$

with E defined by (I.21). This system is completed with the boundary conditions (I.9),(I.10) and (I.11). In our case, (I.10) reduces to

$$p|_s = p^a. \tag{V.3}$$

For the sake of simplicity, in the following we neglect the variations of the atmospheric pressure p^a i.e. $p^a = p_0^a$ with $p_0^a = 0$.

1.1 Non negativity of the pressure

We also suppose in each point of the fluid region – including at the bottom – we have

$$p - p^a \geqslant 0.$$

The analysis below and especially the kinetic interpretation is restricted to this situation. Notice that in the case of hydrostatic Euler equations since we have

$$p - p^a = g(\eta - z),$$

this assumption reduces to the non-negativity of the water height H.

2 Depth-averaged solutions of the Euler and Navier-Stokes systems

In this section we take the vertical average of the Euler system and study the necessary closure relations for this system.

Let us denote $\langle f \rangle$ the average along the vertical axis, the so-called *depth-average*, of the quantity $f = f(z)$ i.e.

$$\langle f \rangle(x,t) = \int_{\mathscr{R}} f(x,z,t)\, dz. \tag{V.4}$$

During the derivation process of the model, we assume the bottom topography does not depend on time t, i.e.

$$\frac{\partial z_b}{\partial t} = 0.$$

The contribution of the time variations of the bottom topography is given in remark 9.

2.1 Depth-averaging of the Euler solution

The goal is to transpose the entropy-based moment closures proposed by Levermore in [86] for kinetic equations to our framework. In such a way, we obtain a nonperturbative derivation of shallow-water models which is justified by an entropy minimization process under constraint. The constraints concern the moments of the solution of the Euler equation, which are here the depth-averaged variables.

Taking into account the kinematic boundary conditions (I.9) and (I.11), the depth-averaged form of the Euler system (V.1) writes

$$\begin{cases} \dfrac{\partial}{\partial t}\langle\varphi\rangle + \dfrac{\partial}{\partial x}\langle\varphi u\rangle = 0, & \text{(V.5a)} \\ \dfrac{\partial}{\partial t}\langle\varphi u\rangle + \dfrac{\partial}{\partial x}\langle\varphi u^2\rangle + \langle\varphi\dfrac{\partial p}{\partial x}\rangle = 0, & \text{(V.5b)} \\ \dfrac{\partial}{\partial t}\langle\varphi w\rangle + \dfrac{\partial}{\partial x}\langle\varphi uw\rangle + \langle\varphi\dfrac{\partial p}{\partial z}\rangle = -\langle\varphi g\rangle, & \text{(V.5c)} \\ \dfrac{\partial}{\partial t}\langle\varphi z\rangle + \dfrac{\partial}{\partial x}\langle\varphi zu\rangle = \langle\varphi w\rangle, & \text{(V.5d)} \end{cases}$$

where the last equation is a rewriting of

$$\langle\int_{z_b}^{z}\left(\frac{\partial\varphi}{\partial t}+\frac{\partial\varphi u}{\partial x}+\frac{\partial\varphi w}{\partial z}\right)dz\rangle = \langle z\left(\frac{\partial\varphi}{\partial t}+\frac{\partial\varphi u}{\partial x}+\frac{\partial\varphi w}{\partial z}\right)\rangle = 0,$$

using again the kinematic boundary conditions. Notice that using the definition (I.7), we have

$$\langle\varphi\rangle = H, \quad \text{and } \langle\varphi z\rangle = \frac{\eta^2 - z_b^2}{2}. \tag{V.6}$$

Simple manipulations allow to obtain the system (V.5) from the Euler system (V.1),(I.9) and (I.11) e.g. for Eq. (V.5a), starting from (V.1a) we write

$$\langle\frac{\partial\varphi}{\partial t}+\frac{\partial\varphi u}{\partial x}+\frac{\partial\varphi w}{\partial z}\rangle = 0,$$

and permuting the derivative with the integral using the Leibniz rule directly gives (V.5a).

We decompose the pressure p under the form

$$p = g(\eta - z) + p_{nh},$$

i.e. the sum of the hydrostatic and non-hydrostatic parts of the pressure. Hence, the system (V.5) becomes

$$\begin{cases} \dfrac{\partial}{\partial t}\langle\varphi\rangle + \dfrac{\partial}{\partial x}\langle\varphi u\rangle = 0, & \text{(V.7a)} \\ \dfrac{\partial}{\partial t}\langle\varphi u\rangle + \dfrac{\partial}{\partial x}\left(\langle\varphi u^2\rangle + g\langle\varphi(\eta - z)\rangle + \langle\varphi p_{nh}\rangle\right) = -\left(g\langle\varphi\rangle + p_{nh}|_b\right)\dfrac{\partial z_b}{\partial x}, & \text{(V.7b)} \\ \dfrac{\partial}{\partial t}\langle\varphi w\rangle + \dfrac{\partial}{\partial x}\langle\varphi uw\rangle = p_{nh}|_b, & \text{(V.7c)} \\ \dfrac{\partial}{\partial t}\langle\varphi z\rangle + \dfrac{\partial}{\partial x}\langle\varphi zu\rangle = \langle\varphi w\rangle, & \text{(V.7d)} \end{cases}$$

where the boundary condition (V.3) has been used. The energy equation (V.2) gives

$$\frac{\partial}{\partial t}\langle\varphi E\rangle + \frac{\partial}{\partial x}\langle\varphi u(E+p)\rangle = 0, \tag{V.8}$$

where $E(z;u,w)$ is defined by (I.21).

Therefore the system (V.7) has four equations with four unknowns, namely $\langle\varphi\rangle$, $\langle\varphi u\rangle$, $\langle\varphi w\rangle$ and $\langle\varphi p_{nh}\rangle$ and closure relations are needed to define $\langle\varphi u^2\rangle$, $\langle\varphi uw\rangle$, $\langle\varphi zu\rangle$ and $p_{nh}|_b$.

If u',w' are defined as the deviations of u,w with respect to their depth-averages, then it comes

$$\varphi u = \varphi \frac{\langle \varphi u \rangle}{\langle \varphi \rangle} + \varphi u', \quad \varphi w = \varphi \frac{\langle \varphi w \rangle}{\langle \varphi \rangle} + \varphi w', \tag{V.9}$$

with $\langle \varphi u' \rangle = \langle \varphi w' \rangle = 0$. Following the moment closure proposed by Levermore [86], we study the minimization problem

$$\min_{u',w'} \langle \{ \varphi E(z;u,w) \} \rangle. \tag{V.10}$$

The energy $E(z;u,w)$ being quadratic with respect to u we notice

$$\begin{aligned} \langle \varphi u^2 \rangle &= \frac{\langle \varphi u \rangle^2}{\langle \varphi \rangle} + 2\langle \varphi u u' \rangle + \langle \varphi (u')^2 \rangle \\ &= \frac{\langle \varphi u \rangle^2}{\langle \varphi \rangle} + \langle \varphi (u')^2 \rangle \\ &\geqslant \frac{\langle \varphi u \rangle^2}{\langle \varphi \rangle}, \end{aligned} \tag{V.11}$$

and similarly, we obtain

$$\langle \varphi w^2 \rangle \geqslant \frac{\langle \varphi w \rangle^2}{\langle \varphi \rangle}. \tag{V.12}$$

Eqs. (V.11) and (V.12) mean that the solution of the minimization problem (V.10) is given by

$$\langle \varphi E\left(z; \frac{\langle \varphi u \rangle}{\langle \varphi \rangle}, \frac{\langle \varphi w \rangle}{\langle \varphi \rangle}\right) \rangle = \min_{u',w'} \langle \{ \varphi E(z;u,w) \} \rangle, \tag{V.13}$$

and

$$\langle \varphi E\left(z; \frac{\langle \varphi u \rangle}{\langle \varphi \rangle}, \frac{\langle \varphi w \rangle}{\langle \varphi \rangle}\right) \rangle = \frac{\langle \varphi u \rangle^2 + \langle \varphi w \rangle^2}{2\langle \varphi \rangle} + g\langle \varphi z \rangle, \tag{V.14}$$

Since the only choice leading to equalities in relations (V.11) and (V.12) corresponds to

$$u = \frac{\langle \varphi u \rangle}{\langle \varphi \rangle}, \quad \text{and } \ w = \frac{\langle \varphi w \rangle}{\langle \varphi \rangle},$$

this allows to precise the closure relations associated to a minimal energy, namely

$$\begin{cases} \langle \varphi u^2 \rangle = \dfrac{\langle \varphi u \rangle^2}{\langle \varphi \rangle}, & \text{(V.15a)} \\ \langle \varphi u w \rangle = \dfrac{\langle \varphi u \rangle \langle \varphi w \rangle}{\langle \varphi \rangle}, & \text{(V.15b)} \\ \langle \varphi z u \rangle = \langle \varphi z \rangle \dfrac{\langle \varphi u \rangle}{\langle \varphi \rangle}. & \text{(V.15c)} \end{cases}$$

Replacing (V.15) into Eqs. (V.7) leads to the system

$$\begin{cases} \dfrac{\partial}{\partial t}\langle \varphi \rangle + \dfrac{\partial}{\partial x}\langle \varphi u \rangle = 0, & \text{(V.16a)} \\ \dfrac{\partial}{\partial t}\langle \varphi u \rangle + \dfrac{\partial}{\partial x}\left(\dfrac{\langle \varphi u \rangle^2}{\langle \varphi \rangle} + g\langle \varphi(\eta - z) \rangle + \langle \varphi p_{nh} \rangle \right) = -\left(g\langle \varphi \rangle + p_{nh}|_b \right) \dfrac{\partial z_b}{\partial x}, & \text{(V.16b)} \\ \dfrac{\partial}{\partial t}\langle \varphi w \rangle + \dfrac{\partial}{\partial x}\langle \varphi w \rangle \dfrac{\langle \varphi u \rangle}{\langle \varphi \rangle} = p_{nh}|_b, & \text{(V.16c)} \\ \dfrac{\partial}{\partial t}\langle \varphi z \rangle + \dfrac{\partial}{\partial x}\langle \varphi z \rangle \dfrac{\langle \varphi u \rangle}{\langle \varphi \rangle} = \langle \varphi w \rangle, & \text{(V.16d)} \end{cases}$$

but it remains to find the closure relation for the non-hydrostatic pressure terms. As proved in the following proposition, the only possible choice is

$$p_{nh}|_b = 2\frac{\langle \varphi p_{nh} \rangle}{\langle \varphi \rangle}. \tag{V.17}$$

Proposition V.1. *The solutions of the Euler system (V.1)-(V.3),(I.11),(I.9) satisfying the closure relations (V.15),(V.17) are also solutions of the system*

$$\begin{cases} \dfrac{\partial}{\partial t}\langle\varphi\rangle + \dfrac{\partial}{\partial x}\langle\varphi u\rangle = 0, & \text{(V.18a)} \\ \dfrac{\partial}{\partial t}\langle\varphi u\rangle + \dfrac{\partial}{\partial x}\left(\dfrac{\langle\varphi u\rangle^2}{\langle\varphi\rangle} + g\langle\varphi(\eta - z)\rangle + \langle\varphi p_{nh}\rangle\right) = -\left(g\langle\varphi\rangle + 2\dfrac{\langle\varphi p_{nh}\rangle}{\langle\varphi\rangle}\right)\dfrac{\partial z_b}{\partial x}, & \text{(V.18b)} \\ \dfrac{\partial}{\partial t}\langle\varphi w\rangle + \dfrac{\partial}{\partial x}\langle\varphi w\rangle\dfrac{\langle\varphi u\rangle}{\langle\varphi\rangle} = 2\dfrac{\langle\varphi p_{nh}\rangle}{\langle\varphi\rangle}, & \text{(V.18c)} \\ \dfrac{\partial}{\partial t}\langle\varphi z\rangle + \dfrac{\partial}{\partial x}\langle\varphi z\rangle\dfrac{\langle\varphi u\rangle}{\langle\varphi\rangle} = \langle\varphi w\rangle. & \text{(V.18d)} \end{cases}$$

This system is a depth-averaged approximation of the Euler system and admits – for smooth solutions – an energy balance under the form

$$\begin{aligned} &\frac{\partial}{\partial t}\langle\varphi E\left(z;\frac{\langle\varphi u\rangle}{\langle\varphi\rangle},\frac{\langle\varphi w\rangle}{\langle\varphi\rangle}\right)\rangle \\ &\qquad + \frac{\partial}{\partial x}\langle\frac{\langle\varphi u\rangle}{\langle\varphi\rangle}\left(\varphi E\left(z;\frac{\langle\varphi u\rangle}{\langle\varphi\rangle},\frac{\langle\varphi w\rangle}{\langle\varphi\rangle}\right) + \langle\varphi p_{nh}\rangle\right)\rangle = 0. \end{aligned} \tag{V.19}$$

Remark 8. It is important to notice that whereas the solution H,u,w,p of the Euler system (V.1)-(V.3),(I.11),(I.9) also satisfies the system (V.7), only the solutions H,u,w,p of the Euler system (V.1)-(V.3),(I.11),(I.9) satisfying the closure relations (V.15),(V.17) are also solutions of the system (V.18)-(V.19). On the contrary, any solutions $\langle\varphi\rangle$, $\langle\varphi u\rangle$, $\langle\varphi w\rangle$ and $\langle p_{nh}\rangle$ of (V.18)-(V.18d) with $p_{nh}|_b$ defined by (V.17) are also solutions of (V.7)-(V.8).

Proof of prop. V.1. Only the manipulations allowing to obtain (V.19) have to be detailed. More precisely, we have to prove that, in (V.16), the relation (V.17) is needed in order to obtain (V.19).

For that purpose, we multiply (V.16b) by $\frac{\langle\varphi u\rangle}{\langle\varphi\rangle}$ and we rewrite each of the obtained terms. For the terms also appearing in the Saint-Venant system i.e. corresponding to the hydrostatic part of the model, we easily obtain

$$\begin{aligned} &\left(\frac{\partial}{\partial t}\langle\varphi u\rangle + \frac{\partial}{\partial x}\left(\frac{\langle\varphi u\rangle^2}{\langle\varphi\rangle} + g\langle\varphi(\eta - z)\rangle\right) + g\langle\varphi\rangle\frac{\partial z_b}{\partial x}\right)\frac{\langle\varphi u\rangle}{\langle\varphi\rangle} = \\ &\qquad \frac{\partial}{\partial t}\langle\varphi E\left(z;\frac{\langle\varphi u\rangle}{\langle\varphi\rangle},0\right)\rangle + \frac{\partial}{\partial x}\langle\frac{\langle\varphi u\rangle}{\langle\varphi\rangle}\varphi E\left(z;\frac{\langle\varphi u\rangle}{\langle\varphi\rangle},0\right)\rangle. \end{aligned} \tag{V.20}$$

Multiplying (V.16c) by $\frac{\langle\varphi w\rangle}{\langle\varphi\rangle}$ and using (V.16a), we obtain the relation

$$\frac{\partial}{\partial t}\frac{\langle\varphi w\rangle^2}{2\langle\varphi\rangle} + \frac{\partial}{\partial x}\frac{\langle\varphi u\rangle\langle\varphi w\rangle^2}{2\langle\varphi\rangle^2} = \frac{\langle\varphi w\rangle}{\langle\varphi\rangle}\,p_{nh}|_b\,. \tag{V.21}$$

And for the contribution of the non-hydrostatic pressure terms of Eq. (V.16b) over the energy balance, it comes

$$\begin{aligned} \left(\frac{\partial}{\partial x}\langle\varphi p_{nh}\rangle + p_{nh}|_b\frac{\partial z_b}{\partial x}\right)\frac{\langle\varphi u\rangle}{\langle\varphi\rangle} &= \frac{\partial}{\partial x}\frac{\langle\varphi p_{nh}\rangle\langle\varphi u\rangle}{\langle\varphi\rangle} - \langle\varphi p_{nh}\rangle\frac{\partial}{\partial x}\frac{\langle\varphi u\rangle}{\langle\varphi\rangle} \\ &\quad + p_{nh}|_b\frac{\langle\varphi u\rangle}{\langle\varphi\rangle}\frac{\partial z_b}{\partial x} \\ &= \frac{\partial}{\partial x}\frac{\langle\varphi p_{nh}\rangle\langle\varphi u\rangle}{\langle\varphi\rangle} - \frac{\langle\varphi p_{nh}\rangle}{\langle\varphi\rangle}\frac{\partial\langle\varphi u\rangle}{\partial x} \\ &\quad + \frac{\langle\varphi p_{nh}\rangle\langle\varphi u\rangle}{\langle\varphi\rangle^2}\frac{\partial\langle\varphi\rangle}{\partial x} \\ &\quad + p_{nh}|_b\frac{\langle\varphi u\rangle}{\langle\varphi\rangle}\frac{\partial z_b}{\partial x}. \end{aligned} \tag{V.22}$$

Since the identity

$$\langle \varphi z \rangle = \frac{\langle \varphi \rangle}{2} \left(\langle \varphi \rangle + 2 z_b \right),$$

holds, relation (V.16d) coupled with (V.16a) reduces to

$$\langle \varphi w \rangle = -\frac{\langle \varphi \rangle}{2} \frac{\partial \langle \varphi u \rangle}{\partial x} + \frac{\langle \varphi u \rangle}{2} \frac{\partial (\langle \varphi \rangle + 2 z_b)}{\partial x}, \tag{V.23}$$

and we can rewrite (V.22) under the form

$$\begin{aligned} \left(\frac{\partial}{\partial x} \langle \varphi p_{nh} \rangle + p_{nh}|_b \frac{\partial z_b}{\partial x} \right) \frac{\langle \varphi u \rangle}{\langle \varphi \rangle} = & \frac{\partial}{\partial x} \frac{\langle \varphi p_{nh} \rangle \langle \varphi u \rangle}{\langle \varphi \rangle} + 2 \frac{\langle \varphi p_{nh} \rangle}{\langle \varphi \rangle^2} \langle \varphi w \rangle \\ & + \left(p_{nh}|_b - 2 \frac{\langle \varphi p_{nh} \rangle}{\langle \varphi \rangle} \right) \frac{\langle \varphi u \rangle}{\langle \varphi \rangle} \frac{\partial z_b}{\partial x}. \end{aligned} \tag{V.24}$$

Adding (V.20),(V.21) and (V.24) gives

$$\begin{aligned} \frac{\partial}{\partial t} \langle \varphi E \left(z; \frac{\langle \varphi u \rangle}{\langle \varphi \rangle}, \frac{\langle \varphi w \rangle}{\langle \varphi \rangle} \right) \rangle + \frac{\partial}{\partial x} \langle \frac{\langle \varphi u \rangle}{\langle \varphi \rangle} \left(\varphi E \left(z; \frac{\langle \varphi u \rangle}{\langle \varphi \rangle}, \frac{\langle \varphi w \rangle}{\langle \varphi \rangle} \right) + \langle \varphi p_{nh} \rangle \right) \rangle \\ = \left(p_{nh}|_b - 2 \frac{\langle \varphi p_{nh} \rangle}{\langle \varphi \rangle} \right) \left(\frac{\langle \varphi w \rangle}{\langle \varphi \rangle} + \frac{\langle \varphi u \rangle}{\langle \varphi \rangle} \frac{\partial z_b}{\partial x} \right). \end{aligned} \tag{V.25}$$

Using (V.23) we have

$$\frac{\langle \varphi w \rangle}{\langle \varphi \rangle} + \frac{\langle \varphi u \rangle}{\langle \varphi \rangle} \frac{\partial z_b}{\partial x} = -\frac{1}{2} \frac{\partial \langle \varphi u \rangle}{\partial x} + \frac{\langle \varphi u \rangle}{2 \langle \varphi \rangle} \frac{\partial \langle \varphi \rangle}{\partial x} = -\frac{\langle \varphi \rangle}{2} \frac{\partial}{\partial x} \left(\frac{\langle \varphi u \rangle}{\langle \varphi \rangle} \right),$$

and therefore the right hand side of (V.25) vanishes iff (V.17) holds that concludes the proof. □

2.2 The proposed non-hydrostatic averaged model and other writings

In the following, we no more handle variables corresponding to vertical means of the solution of the Euler equations (V.1). We adopt the notation $\overline{f} = f(x,t)$. By analogy with (V.18)-(V.19), we consider as non-hydrostatic averaged model the following system

$$\begin{cases} \dfrac{\partial H}{\partial t} + \dfrac{\partial}{\partial x} \left(H \overline{u} \right) = 0, & \text{(V.26a)} \\ \dfrac{\partial}{\partial t} (H \overline{u}) + \dfrac{\partial}{\partial x} \left(H \overline{u}^2 + \dfrac{g}{2} H^2 + H \overline{p}_{nh} \right) = -(gH + 2 \overline{p}_{nh}) \dfrac{\partial z_b}{\partial x}, & \text{(V.26b)} \\ \dfrac{\partial}{\partial t} (H \overline{w}) + \dfrac{\partial}{\partial x} (H \overline{w} \overline{u}) = 2 \overline{p}_{nh}, & \text{(V.26c)} \\ \dfrac{\partial}{\partial t} \left(\dfrac{\eta^2 - z_b^2}{2} \right) + \dfrac{\partial}{\partial x} \left(\dfrac{\eta^2 - z_b^2}{2} \overline{u} \right) = H \overline{w}. & \text{(V.26d)} \end{cases}$$

The smooth solutions H, $\overline{u}$, $\overline{w}$, $\overline{p}_{nh}$ of the system (V.26) also satisfies the energy balance

$$\frac{\partial \overline{E}}{\partial t} + \frac{\partial}{\partial x} \left(\overline{u} \left(\overline{E} + \frac{g}{2} H^2 + H \overline{p}_{nh} \right) \right) = 0, \tag{V.27}$$

where

$$\overline{E} = \frac{H(\overline{u}^2 + \overline{w}^2)}{2} + \frac{gH(\eta + z_b)}{2}. \tag{V.28}$$

Notice that simple manipulations of Eqs. (V.26) lead to the relation

$$H \overline{w} = -\frac{H}{2} \frac{\partial (H \overline{u})}{\partial x} + \frac{H \overline{u}}{2} \frac{\partial (H + 2 z_b)}{\partial x}, \tag{V.29}$$

corresponding to a shallow water expression of the divergence free condition.

The system (V.26)-(V.27) has been obtained by one of the authors in [121] but in the framework of asymptotic expansion. In this case, the justification of the closure relations is less obvious than using the energy-based optimality criterion (V.13).

Simple manipulations in the equations of (V.26) lead to different formulations of the model which are given in the two following corollaries.

Corollary V.2. *The system (V.26) can be rewritten under the form*

$$\begin{cases} \dfrac{\partial H}{\partial t} + \dfrac{\partial}{\partial x}\big(H\overline{u}\big) = 0, & \text{(V.30a)} \\ \dfrac{\partial}{\partial t}(H\overline{u}) + \dfrac{\partial}{\partial x}\left(H\overline{u}^2 + \dfrac{g}{2}H^2 + H\overline{p}_{nh}\right) = -(gH + 2\overline{p}_{nh})\dfrac{\partial z_b}{\partial x}, & \text{(V.30b)} \\ \dfrac{\partial}{\partial t}(H\overline{w}) + \dfrac{\partial}{\partial x}(H\overline{w}\,\overline{u}) = 2\overline{p}_{nh}, & \text{(V.30c)} \\ H\overline{w} = -\dfrac{H}{2}\dfrac{\partial(H\overline{u})}{\partial x} + \dfrac{H\overline{u}}{2}\dfrac{\partial(H+2z_b)}{\partial x}, & \text{(V.30d)} \end{cases}$$

and for smooth solutions Eq. (V.27) remains valid.

Corollary V.3. *The system (V.26) can be rewritten under the form*

$$\begin{cases} \dfrac{\partial H}{\partial t} + \dfrac{\partial}{\partial x}\big(H\overline{u}\big) = 0, & \text{(V.31a)} \\ \dfrac{\partial}{\partial t}(H\overline{u}) + \dfrac{\partial}{\partial x}\left(H\overline{u}^2 + \dfrac{g}{2}H^2 + H\overline{p}_{nh}\right) = -(gH + 2\overline{p}_{nh})\dfrac{\partial z_b}{\partial x}, & \text{(V.31b)} \\ \dfrac{\partial}{\partial t}\left(\dfrac{H^2}{2}\overline{w}\right) + \dfrac{\partial}{\partial x}\left(\dfrac{H^2}{2}\overline{w}\,\overline{u}\right) = H\overline{p}_{nh} + H\overline{w}^2 - H\overline{u}\,\overline{w}\dfrac{\partial z_b}{\partial x}, & \text{(V.31c)} \\ \dfrac{\partial}{\partial t}\left(\dfrac{H^2}{2}\right) + \dfrac{\partial}{\partial x}\left(\dfrac{H^2}{2}\overline{u}\right) = H\overline{w} - H\overline{u}\dfrac{\partial z_b}{\partial x}, & \text{(V.31d)} \end{cases}$$

and for smooth solutions Eq. (V.27) remains valid.

Corollary V.4. *The system (V.26) can be rewritten under the form*

$$\begin{cases} \dfrac{\partial H}{\partial t} + \dfrac{\partial}{\partial x}\big(H\overline{u}\big) = 0, & \text{(V.32a)} \\ \dfrac{\partial}{\partial t}(H\overline{u}) + \dfrac{\partial}{\partial x}(H\overline{u}^2) + \dfrac{\partial}{\partial x}(H\overline{p}) = -2\overline{p}\dfrac{\partial z_b}{\partial x}, & \text{(V.32b)} \\ \dfrac{\partial}{\partial t}\left(\dfrac{\eta^2 - z_b^2}{2}\overline{w}\right) + \dfrac{\partial}{\partial x}\left(\dfrac{\eta^2 - z_b^2}{2}\overline{w}\,\overline{u}\right) = (H + 2z_b)\overline{p} + H\overline{w}^2 - g\dfrac{\eta^2 - z_b^2}{2}, & \text{(V.32c)} \\ \dfrac{\partial}{\partial t}\left(\dfrac{\eta^2 - z_b^2}{2}\right) + \dfrac{\partial}{\partial x}\left(\dfrac{\eta^2 - z_b^2}{2}\overline{u}\right) = H\overline{w}, & \text{(V.32d)} \end{cases}$$

and for smooth solutions Eq. (V.27) remains valid.

Proofs of corollaries V.2, V.3 and V.4. Equation (V.31c) can be obtained multiplying Eq. (V.26c) by $\frac{H}{2}$ and using (V.29) and simple manipulations allow to obtain (V.31d) from (V.26d). Equation (V.32c) can be obtained multiplying Eq. (V.26c) by $\frac{H+2z_b}{2}$ and using (V.29). □

Remark 9. When considering the bottom z_b can vary w.r.t. time t, the system (V.26) remains unchanged only the energy balance (V.27) is modified and becomes

$$\frac{\partial \overline{E}}{\partial t} + \frac{\partial}{\partial x}\left(\overline{u}\big(\overline{E} + \frac{g}{2}H^2 + H\overline{p}_{nh}\big)\right) = (gH + 2\overline{p}_{nh})\frac{\partial z_b}{\partial t}, \tag{V.33}$$

with $\overline{E}$ defined by (V.28). Since $\overline{p}|_b = gH + 2\overline{p}_{nh}$, the contributions of the time variations of z_b in Eq. (V.33) are consistent with those appearing in (V.2).

2.3 About asymptotic expansion

For shallow water flows, the model derivation is often carried out using the shallow water assumption. Indeed, introducing the small parameter

$$\varepsilon = \frac{h}{\lambda},$$

where h and λ, two characteristic dimensions along the z and x axis respectively, an asymptotic expansion of the Euler or Navier-Stokes system leads to simplified averaged models such as the Saint-Venant system. As in [57, 51, 98, 121] and neglecting the viscous and friction effects, the shallow water assumption allows to justify the estimate

$$u = \overline{u} + \mathscr{O}(\varepsilon^2), \tag{V.34}$$

leading, using the divergence free condition, to

$$w = -(z - z_b)\frac{\partial \overline{u}}{\partial x} + \overline{u}\frac{\partial z_b}{\partial x} + \mathscr{O}(\varepsilon^2). \tag{V.35}$$

Inserting (V.34) and (V.35) in the momentum equation (V.1c) implies that the non-hydrostatic part of the pressure is linear in the variable z

$$\frac{\partial p_{nh}}{\partial z} = \alpha(x,t)(z - z_b) + \beta(x,t) + \mathscr{O}(\varepsilon^2).$$

Unfortunately, the preceding relation is not compatible with the closure relation for the pressure (V.17). And it is then necessary to add a scaling coefficient over the non-hydrostatic pressure terms in order to ensure the existence of an energy balance.

Notice that the energy balance obtained using the rescaled non-hydrostatic pressure terms differ from (V.19) and (V.27). The Green-Naghdi [67] can be derived using such an asymptotic expansion strategy.

2.4 Comparison with Green-Naghdi model

One of the most popular models for the description of long, dispersive water waves is the Green-Naghdi model. Several derivations of the Green-Naghdi model have been proposed in the litterature [67, 66, 127, 102]. For the mathematical justification of the model, the reader can refer to [3, 96] and for its numerical approximation to [83, 21, 42, 31].

Following [83] and with $z_b = cst$, the Green-Naghdi model reads

$$\begin{cases} \dfrac{\partial H}{\partial t} + \dfrac{\partial}{\partial x}\big(H\overline{u}\big) = 0, & \text{(V.36a)} \\ \dfrac{\partial (H\overline{u})}{\partial t} + \dfrac{\partial}{\partial x}\left(H\overline{u}^2 + \dfrac{g}{2}H^2 + H\overline{p}_{gn}\right) = 0, & \text{(V.36b)} \end{cases}$$

with $\overline{p}_{gn} = \frac{1}{3}H\ddot{H}$ and the "dot" notation means the material derivative

$$\dot{H} = \frac{\partial H}{\partial t} + \overline{u}\frac{\partial H}{\partial x}. \tag{V.37}$$

When $z_b = cst$, the Green-Naghdi model and the non-hydrostatic model (V.26) are identical up to a multiplicative constant for the non-hydrostatic pressure. Indeed starting from the expression of $\overline{p}_{gn}$, the relations (V.36a) and (V.37) give

$$\begin{aligned} \overline{p}_{gn} =& \frac{1}{3}H\left(\frac{\partial \dot{H}}{\partial t} + \overline{u}\frac{\partial \dot{H}}{\partial x}\right) \\ =& \frac{1}{3}H\left(\frac{\partial}{\partial t}\left(-H\frac{\partial \overline{u}}{\partial x}\right) + \overline{u}\frac{\partial}{\partial x}\left(-H\frac{\partial \overline{u}}{\partial x}\right)\right). \end{aligned}$$

If we denote, as in (V.29)

$$\overline{w} = -\frac{H}{2}\frac{\partial \overline{u}}{\partial x}, \tag{V.38}$$

it comes

$$\overline{p}_{gn} = \frac{2}{3}H\left(\frac{\partial \overline{w}}{\partial t} + \overline{u}\frac{\partial \overline{w}}{\partial x}\right) = \frac{2}{3}\left(\frac{\partial}{\partial t}(H\overline{w}) + \frac{\partial}{\partial x}(H\overline{uw})\right).$$

Therefore, the Green-Naghdi can also be written under the form

$$\begin{cases} \dfrac{\partial H}{\partial t} + \dfrac{\partial}{\partial x}\big(H\overline{u}\big) = 0, & \text{(V.39a)} \\ \dfrac{\partial (H\overline{u})}{\partial t} + \dfrac{\partial}{\partial x}\left(H\overline{u}^2 + \dfrac{g}{2}H^2 + H\overline{p}_{gn}\right) = 0, & \text{(V.39b)} \\ \dfrac{\partial}{\partial t}(H\overline{w}) + \dfrac{\partial}{\partial x}(H\overline{uw}) = \dfrac{3}{2}\overline{p}_{gn}, & \text{(V.39c)} \end{cases}$$

with the constraint (V.38) and completed, for smooth solutions, by the energy balance

$$\frac{\partial \overline{E}_{gn}}{\partial t} + \frac{\partial}{\partial x}\overline{u}\left(\overline{E}_{gn} + H\overline{p}_{gn}\right) = 0, \tag{V.40}$$

with

$$\overline{E}_{gn} = \frac{H}{2}\left(\overline{u}^2 + \frac{2}{3}\overline{w}^2\right) + \frac{g}{2}H^2. \tag{V.41}$$

The energy balance (V.40) illustrates the main difference between the Green-Nagdhi model and the proposed non-hydrostatic model (V.26)-(V.27). In the case of a flat bottom, (V.28) and (V.41) only differ by the coefficient $\frac{2}{3}$ in the vertical part of the kinetic energy.

To summarize, for flat bottom, choosing either $\gamma = 2$ or $\gamma = \frac{3}{2}$, the system

$$\begin{cases} \dfrac{\partial H}{\partial t} + \dfrac{\partial}{\partial x}\big(H\overline{u}\big) = 0, & \text{(V.42a)} \\ \dfrac{\partial (H\overline{u})}{\partial t} + \dfrac{\partial}{\partial x}\left(H\overline{u}^2 + \dfrac{g}{2}H^2 + H\overline{p}\right) = 0, & \text{(V.42b)} \\ \dfrac{\partial}{\partial t}(H\overline{w}) + \dfrac{\partial}{\partial x}(H\overline{uw}) = \gamma\overline{p}, & \text{(V.42c)} \\ \overline{w} = -\dfrac{H}{2}\dfrac{\partial \overline{u}}{\partial x}, & \text{(V.42d)} \end{cases}$$

corresponds to the depth-averaged system (V.26) or to the Green-Naghdi system (V.38)-(V.39), respectively. The system (V.42) is completed with the energy balance

$$\frac{\partial \overline{E}_{\gamma}}{\partial t} + \frac{\partial}{\partial x}\overline{u}\left(\overline{E}_{\gamma} + H\overline{p}\right) = 0, \tag{V.43}$$

with

$$\overline{E}_{\gamma} = \frac{H}{2}\left(\overline{u}^2 + \frac{1}{\gamma}\overline{w}^2\right) + \frac{g}{2}H^2. \tag{V.44}$$

Despite its similarities with the Green-Naghdi model, the non-hydrostatic model (V.26)-(V.27) has several advantages

- its derivation is more simple than the Green-Naghdi model (see [67, 66]),
- the topography source terms appear quite naturally (that is not the case for most of the versions available in the literature [35, 106]),
- the model formulation is written under the form of an advection-reaction set of PDE and does not contain high order derivatives.

A comparison between the solutions of the two non-hydrostatic models is obviously a key point but it requires a numerical scheme for their discretization that is not in the scope of this paper. We illustrate in paragraphs 4.1 and 4.2 the differences between the two non-hydrostatic models in the case of analytical solutions.

2.5 Hydrostatic case

The process used for the derivation of the non-hydrostatic model in paragraph 2.1 can also be used for the derivation of shallow water hydrostatic models.

The hydrostatic assumption in (V.1) that means that the contribution of the vertical acceleration in the pressure p can be neglected, leads to the classical model

$$\begin{cases} \dfrac{\partial \varphi}{\partial t} + \dfrac{\partial \varphi u}{\partial x} + \dfrac{\partial \varphi w}{\partial z} = 0, & \text{(V.45a)} \\ \dfrac{\partial u}{\partial t} + \dfrac{\partial u^2}{\partial x} + \dfrac{\partial uw}{\partial z} + \dfrac{\partial p}{\partial x} = 0, & \text{(V.45b)} \\ \dfrac{\partial p}{\partial z} = -g. & \text{(V.45c)} \end{cases}$$

This hydrostatic model – or some variants with horizontal and vertical viscosity or other specific terms – is often used in geophysical flows studies and it has been widely studied, let us mention some important contributions [30, 69, 99].

Starting from Eqs. (V.45), the shallow water assumption allows to derive the classical Saint-Venant system (see also [55, 57, 98])

$$\begin{cases} \dfrac{\partial H}{\partial t} + \dfrac{\partial}{\partial x}\big(H\overline{u}\big) = 0, & \text{(V.46a)} \\ \dfrac{\partial (H\overline{u})}{\partial t} + \dfrac{\partial (H\overline{u}^2)}{\partial x} + \dfrac{g}{2}\dfrac{\partial H^2}{\partial x} = -gH\dfrac{\partial z_b}{\partial x}. & \text{(V.46b)} \end{cases}$$

The smooth solutions of (V.46) satisfy the energy equality

$$\frac{\partial E_h}{\partial t} + \frac{\partial}{\partial x}\left(\overline{u}\big(E_h + g\frac{H^2}{2}\big)\right) = 0, \tag{V.47}$$

with the energy

$$E_h = \frac{H\overline{u}^2}{2} + \frac{gH(\eta + z_b)}{2}. \tag{V.48}$$

Notice that (V.47),(V.48) corresponds to (I.21),(V.2) where the hydrostatic and shallow water assumptions are made.

2.6 A depth-averaged Navier-Stokes system

In Section 1, we have started from the Euler system to obtain its depth-averaged version. In this section, we use the same process as in paragraphs 2 to obtain a depth-averaged Navier-Stokes system. And we have the following proposition

Proposition V.5. *A depth-averaged version of the free surface Navier-Stokes system leads to the model*

$$\begin{cases} \dfrac{\partial H}{\partial t} + \dfrac{\partial}{\partial x}\big(H\overline{u}\big) = 0, & \text{(V.49a)} \\ \dfrac{\partial}{\partial t}(H\overline{u}) + \dfrac{\partial}{\partial x}\left(H\overline{u}^2 + \dfrac{g}{2}H^2 + H\overline{p}_{nh}\right) = -(gH + 2\overline{p}_{nh})\dfrac{\partial z_b}{\partial x} + \dfrac{\partial}{\partial x}\left(2\mu H\dfrac{\partial \overline{u}}{\partial x}\right) - \kappa\overline{u}, & \text{(V.49b)} \\ \dfrac{\partial}{\partial t}(H\overline{w}) + \dfrac{\partial}{\partial x}(H\overline{w}\overline{u}) = 2\overline{p}_{nh} + \dfrac{\partial}{\partial x}\left(\mu H\dfrac{\partial \overline{w}}{\partial x}\right), & \text{(V.49c)} \\ \dfrac{\partial}{\partial t}\left(\dfrac{\eta^2 - z_b^2}{2}\right) + \dfrac{\partial}{\partial x}\left(\dfrac{\eta^2 - z_b^2}{2}\overline{u}\right) = H\overline{w}. & \text{(V.49d)} \end{cases}$$

Moreover the smooth solutions of (V.49) satisfy the energy balance

$$\begin{aligned} \frac{\partial \overline{E}}{\partial t} + \frac{\partial}{\partial x}\left(\overline{u}\left(\overline{E} + \frac{g}{2}H^2 + H\overline{p}_{nh} - 2\mu H\frac{\partial \overline{u}}{\partial x}\right) - \mu H\overline{w}\frac{\partial \overline{w}}{\partial x}\right) \\ = -\mu H\left(2\left(\frac{\partial \overline{u}}{\partial x}\right)^2 + \left(\frac{\partial \overline{w}}{\partial x}\right)^2\right) - \kappa\overline{u}^2, \end{aligned} \tag{V.50}$$

with $\overline{E}$ defined by (V.28).

Proof of proposition V.5. Compared to the derivation of the model (V.26)-(V.27), only the treatment of the viscous terms has to be precised and we have

$$\int \left(\frac{\partial \Sigma_{xx}}{\partial x} + \frac{\partial \Sigma_{xz}}{\partial z} \right) \varphi dz = \frac{\partial}{\partial x} \int 2\mu \frac{\partial u}{\partial x} \varphi dz - \kappa \overline{u},$$

where the boundary conditions (I.10),(I.14) have been used. And replacing u by $\overline{u}$ in the r.h.s. of the preceding relation gives the expression of the viscous term in (V.49b). Likewise, using (I.10),(I.14), we have

$$\int \left(\frac{\partial \Sigma_{zx}}{\partial x} + \frac{\partial \Sigma_{zz}}{\partial z} \right) \varphi dz = \frac{\partial}{\partial x} \int \mu \frac{\partial w}{\partial x} \varphi dz,$$

and replacing w by $\overline{w}$ gives the expression of the viscous term in (V.49c). Multiplying (V.49b) by $\overline{u}$ and (V.49c) by $\overline{w}$ and after simple manipulations, we obtain the relation (V.50) that completes the proof. □

3 Some properties of the non-hydrostatic model

3.1 Expression for $\overline{p}_{nh}$

Equation (V.26d) – that is equivalent to (V.29) – is not a dynamical equation but a constraint ensuring a shallow water version of the divergence free condition. And hence it plays a specific role in the non-hydrostatic model. We try to reformulate Eq. (V.29) in order to obtain an equation satisfied by the pressure $\overline{p}_{nh}$. The process used is similar to Chorin solenoidal decomposition of the velocity field [44] for Navier-Stokes equations.

The derivative w.r.t. time t of the shallow water form of the divergence free condition (V.29) gives

$$\frac{\partial (H\overline{w})}{\partial t} + \frac{H}{2} \frac{\partial^2 (H\overline{u})}{\partial x \partial t} - \frac{1}{2} \frac{\partial (H + 2z_b)}{\partial x} \frac{\partial (H\overline{u})}{\partial t} = -\frac{H\overline{u}}{2} \frac{\partial^2 (H\overline{u})}{\partial x^2} + \frac{1}{2} \left(\frac{\partial (H\overline{u})}{\partial x} \right)^2,$$

where relation (V.26a) has been used. Now substituting the expressions (V.26b),(V.26c) for

$$\frac{\partial (H\overline{u})}{\partial t}, \quad \text{and} \quad \frac{\partial (H\overline{w})}{\partial t},$$

in the previous relation gives

$$2\overline{p}_{nh} - \frac{H}{2} \frac{\partial^2 (H\overline{p}_{nh})}{\partial x^2} + \frac{\partial (H + 2z_b)}{\partial x} \left(\frac{1}{2} \frac{\partial (H\overline{p}_{nh})}{\partial x} + \overline{p}_{nh} \frac{\partial z_b}{\partial x} \right) - H \frac{\partial}{\partial x} \left(\overline{p}_{nh} \frac{\partial z_b}{\partial x} \right) = B, \qquad \text{(V.51)}$$

with

$$B = \frac{1}{2} \left(\frac{\partial (H\overline{u})}{\partial x} \right)^2 - \frac{H\overline{u}}{2} \frac{\partial^2 (H\overline{u})}{\partial x^2} + \frac{\partial (H\overline{w}\overline{u})}{\partial x} + \frac{H}{2} \left(\frac{\partial^2}{\partial x^2} \left(H\overline{u}^2 + \frac{g}{2} H^2 \right) + g \frac{\partial}{\partial x} \left(H \frac{\partial z_b}{\partial x} \right) \right)$$
$$- \frac{1}{2} \frac{\partial (H + 2z_b)}{\partial x} \left(\frac{\partial}{\partial x} \left(H\overline{u}^2 + \frac{g}{2} H^2 \right) + gH \frac{\partial z_b}{\partial x} \right).$$

From (V.29), we get

$$\frac{\partial (H\overline{w}\overline{u})}{\partial x} = -\frac{1}{2} \frac{\partial}{\partial x} \left(H\overline{u} \frac{\partial (H\overline{u})}{\partial x} \right) + \frac{\partial}{\partial x} \left(\frac{H\overline{u}^2}{2} \frac{\partial (H + 2z_b)}{\partial x} \right),$$

leading to

$$\begin{aligned} B &= -H\overline{u}\frac{\partial^2(H\overline{u})}{\partial x^2} + \frac{H}{2}\left(\frac{\partial^2}{\partial x^2}\left(H\overline{u}^2 + \frac{g}{2}H^2\right) + g\frac{\partial}{\partial x}\left(H\frac{\partial z_b}{\partial x}\right)\right) \\ &\quad + \frac{H\overline{u}^2}{2}\frac{\partial^2(H+2z_b)}{\partial x^2} - \frac{1}{2}\frac{\partial(H+2z_b)}{\partial x}\left(\frac{\partial}{\partial x}\left(\frac{g}{2}H^2\right) + gH\frac{\partial z_b}{\partial x}\right) \\ &= H\left(-\overline{u}\frac{\partial^2(H\overline{u})}{\partial x^2} + \frac{1}{2}\frac{\partial^2(H\overline{u}^2)}{\partial x^2} + \frac{\overline{u}^2}{2}\frac{\partial^2(H+2z_b)}{\partial x^2}\right) \\ &\quad + \frac{gH}{2}\left(H\frac{\partial^2(H+z_b)}{\partial x^2} - 2\frac{\partial z_b}{\partial x}\frac{\partial(H+z_b)}{\partial x}\right). \end{aligned}$$

Introducing the new variable

$$\overline{q}_{nh} = \sqrt{H}\overline{p}_{nh},$$

relation (V.51) becomes

$$-4H^2\frac{\partial^2\overline{q}_{nh}}{\partial x^2} + \Lambda\overline{q}_{nh} = 8\sqrt{H}B, \tag{V.52}$$

that is an non-homogeneous differential equation with

$$\Lambda = 16\left(1 + \left(\frac{\partial z_b}{\partial x}\right)^2\right) - 8H\frac{\partial^2 z_b}{\partial x^2} + 16\frac{\partial H}{\partial x}\frac{\partial z_b}{\partial x} - 2H\frac{\partial^2 H}{\partial x^2} + 3\left(\frac{\partial H}{\partial x}\right)^2.$$

And the sign of Λ in Eq. (V.52) gives interesting informations about the influence of the non-hydrostatic terms. Indeed, for smooth/small variations of z_b and H, we have $\Lambda > 0$ whereas large variations of z_b and H can lead to the situation where $\Lambda < 0$.

When $\Lambda > 0$, Eq. (V.52) corresponds to a diffusion type equation and when $\Lambda < 0$, Eq. (V.52) corresponds to an Helmholtz type equation. This remark is very important since situations where $\Lambda < 0$ may correspond to areas where the non-hydrostatic effects can be significant

3.2 Requirements for the pressure $\overline{p}$

The positivity of the pressure p for the incompressible Euler equations (see paragraph 1.1) is an acute problem. On the one hand, the Euler system allows the pressure p to be non-positive, on the other hand $p < 0$ means that the fluid is no more in contact with the bottom and the system (V.1)-(V.3),(I.9),(I.11) has to be reformulated, especially its boundary conditions.

This problem vanishes when considering the Saint-Venant system. Indeed in this situation, the pressure term corresponds to

$$\frac{g}{2}H^2,$$

that is always non-negative.

When $H \to 0$ the Euler equations, the proposed non-hydrostatic model but also the Saint-Venant system are no more physically relevant. We would like in this situation, as for the Saint-Venant system, that the model (V.26)-(V.27) well behaves both at the continuous and discrete level.

4 Analytical solutions

The analysis of the proposed non-hydrostatic model being very complex, the knowledge of analytical solutions allows to examine the behavior of the model in particular situations. Moreover, analytical solutions are an important tool for the validation of numerical schemes.

In the following, we propose different analytical solutions for the averaged non-hydrostatic model (V.26)-(V.27).

4.1 Time dependent analytical solutions

In this paragraph we consider the Euler system (V.1) with the boundary conditions (I.9),(I.11) and (V.3). This system can also be written under the form

$$\begin{cases} \dfrac{\partial H}{\partial t} + \dfrac{\partial}{\partial x}\displaystyle\int_{z_b}^{\eta} u\, dz = 0, & \text{(V.53a)} \\ w = -\dfrac{\partial}{\partial x}\displaystyle\int_{z_b}^{z} u\, dz, & \text{(V.53b)} \\ \dfrac{\partial u}{\partial t} + u\dfrac{\partial u}{\partial x} + w\dfrac{\partial u}{\partial z} + \dfrac{\partial p}{\partial x} = 0, & \text{(V.53c)} \\ \dfrac{\partial w}{\partial t} + u\dfrac{\partial w}{\partial x} + w\dfrac{\partial w}{\partial z} + \dfrac{\partial p}{\partial z} = -g + s, & \text{(V.53d)} \end{cases}$$

coupled with the boundary condition (V.3) where s is an external forcing term.

And we have the following proposition.

Proposition V.6. *Let us consider the variables u, w, H, z_b, p defined by*

$$\begin{cases} H(x,t) = \max\left(H_0 - \dfrac{b_2}{2}\left(x - \displaystyle\int_{\tilde{t}^0}^{t} f(t_1)dt_1\right)^2, 0\right), & \text{(V.54a)} \\ u(x,z,t) = f(t)\mathbb{1}_{H>0}, & \text{(V.54b)} \\ w(x,z,t) = b_2 x f(t)\mathbb{1}_{H>0}, & \text{(V.54c)} \\ z_b(x) = b_1 + \dfrac{b_2}{2}x^2, & \text{(V.54d)} \\ p(x,z,t) = (g + b_2 f^2)(H + z_b - z)\mathbb{1}_{H>0}, & \text{(V.54e)} \\ s(x,z,t) = b_2 x \dfrac{df}{dt}, & \text{(V.54f)} \end{cases}$$

where $H_0 > 0, b_1, b_2$ are constants and the function f satisfies the ODE

$$\frac{df}{dt} + b_2(g + b_2 f^2)\int_{\tilde{t}^0}^{t} f(t_1)dt_1 = 0, \quad f(t_0) = f^0,\ \tilde{t}^0 \in \mathscr{R}. \tag{V.55}$$

Then u, w, H, z_b, p as defined previously satisfy the 2d incompressible Euler equations with free surface (V.53) with the boundary condition (V.3) where $p^a = 0$.

Proof. The proof relies on simple manipulations. Replacing (V.54) in (V.53) shows the solution is analytic when (V.55) is satisfied. □

Remark 10. Analytical solutions without the source term s in (V.53d) would have been a stronger result. Nevertheless, since we only consider a source term for one of the four equations (V.53), it remains an interesting result for numerical validations.

These analytical solutions generalize the solutions obtained by Thacker [128] for the shallow water equations. The analysis of the ODE (V.55) is not in the scope of this paper. Notice that the change of variables

$$h(t) = \int_{\tilde{t}^0}^{t} f(t_1)dt_1,$$

allows to rewrite (V.55) under the form

$$\begin{aligned} &\frac{d^2h}{dt^2} + b_2\left(g + b_2\left(\frac{dh}{dt}\right)^2\right)h = 0, \\ &h(t_0) = \int_{\tilde{t}^0}^{t^0} f(t_1)dt_1,\ \ \dot{y}(t_0) = f(t_0) = f^0. \end{aligned} \tag{V.56}$$

It is worth noticing that when $H > 0$ the free surface is a straight line varying with time. Indeed, from the definitions of prop. V.6 and when $H > 0$, we get that for any t

$$H + z_b = b_1 - \frac{b_2}{2}\left(-2x\int_{\tilde{t}^0}^{t} f(t_1)dt_1 + \left(\int_{\tilde{t}^0}^{t} f(t_1)dt_1\right)^2\right),$$

that is a linear function of the x variable.

The analytical solution depicted in prop. (V.6) is interesting for two reasons. First, it allows to confront a numerical scheme with behaviors difficult to capture typically drying and flooding. The second reason is explained in the following proposition.

Proposition V.7. *The variables H, $\overline{u}$, $\overline{w}$, z_b defined as in Eqs. (V.54a)-(V.54d) and $\overline{p}$ defined by*

$$\overline{p} = \frac{g}{2}H + \overline{p}_{nh} = \frac{1}{H}\int_{z_b}^{\eta} p(x,z,t)dz,$$

with p given in (V.54e) are analytical solutions of the depth-averaged Euler system (V.26) completed with the source term s.

The propositions V.6 and V.7 produce a very important consequence. Taking into account the source term s, we have exhibited an analytical solution for the 2d Euler system (V.1)-(V.2) with free surface which is also an analytical solution for the non-hydrostatic model (V.26)-(V.27) we propose. This a strong argument proving our model is a good approximation of the Euler system for shallow water flows. And this is reinforced by the following proposition.

Proposition V.8. *When f satisfies (V.55), the solution (V.54) is not an analytical solution of the Green-Naghdi model (V.39)-(V.40). If f satisfies the ODE*

$$\frac{df}{dt} + b_2\left(g + \frac{4b_2}{3}f^2\right)\int_{\tilde{t}^0}^{t} f(t_1)dt_1 = 0, \quad f(t_0) = f^0,\ \tilde{t}^0 \in \mathscr{R}, \tag{V.57}$$

then (V.54) is an analytical solution of the Green-Naghdi model (V.39)-(V.40). But the energy balance (V.40) is not consistent with the energy equation (V.2) of the Euler system.

Proof of prop. V.8. The proof relies on simple calculations. Since from (V.54) we have

$$\begin{aligned}
\int_{z_b}^{\eta} E\,dz &= \int_{z_b}^{\eta}\left(\frac{u^2+w^2}{2} + gz\right)dz = -\frac{b_0 f^2}{4}\left(x - \int_{\tilde{t}^0}^{t} f(t_1)dt_1\right)^2\left(1 + b_0^2x^2\right) \\
&\quad + \frac{gb_0^2}{8}\left(\left(x^2 - \left(x - \int_{\tilde{t}^0}^{t} f(t_1)dt_1\right)^2\right)^2 - x^4\right) \\
&= \overline{E} \\
&\neq \overline{E}_{gn},
\end{aligned}$$

this proves the result. □

To illustrate the difference between the solutions having the form (V.54) for the two non-hydrostatic models (V.26) and (V.39), we plot on Fig. V.1 the solutions of (V.55) and (V.57). The solutions have been obtained using an implicit first order Euler scheme solving (V.55) and (V.57). Over Fig. V.1, the solid lines (resp. the dashed lines) correspond to solutions of (V.55) (resp. (V.57)). The two curves with amplitude 1 have been obtained with $b_0 = 15$, $\tilde{t}_0 = t_0 = 0$ s, $f(t_0) = 1$ and the two curves with amplitude $\frac{1}{2}$ have been obtained with $b_0 = 10$, $\tilde{t}_0 = t_0 = 0$ s, $f(t_0) = \frac{1}{2}$. We observe that whenever the solutions of (V.55) and (V.57) remain periodic, the period differs especially for large values of b_0.

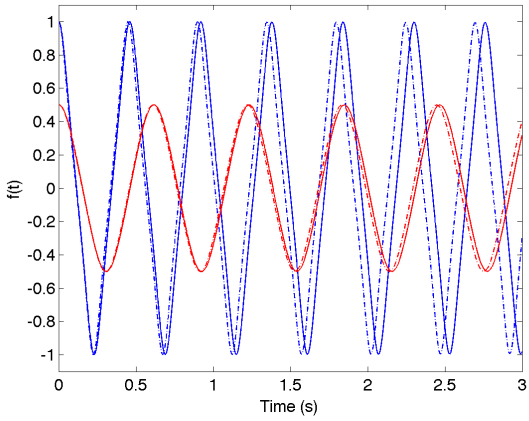

Figure V.1: Comparison of the solutions of (V.55) (solid lines) and (V.57) (dashed lines).

4.2 Solitary wave solutions

Using a process similar to what is done in [83, 42], in the case where $z_b = cst$, we can exhibit solitary waves for the system (V.26) under the form

$$\begin{cases} H = H_0 + a\left(\operatorname{sech}\left(\dfrac{x-c_0t}{l}\right)\right)^2, & \text{(V.58a)} \\ \overline{u} = c_0\left(1-\dfrac{d}{H}\right), & \text{(V.58b)} \\ \overline{w} = -\dfrac{ac_0d}{lH}\operatorname{sech}\left(\dfrac{x-c_0t}{l}\right)\operatorname{sech}'\left(\dfrac{x-c_0t}{l}\right), & \text{(V.58c)} \\ \overline{p}_{nh} = \dfrac{ac_0^2d^2}{2l^2H^2}\left((2H_0-H)\left(\operatorname{sech}'\left(\dfrac{x-c_0t}{l}\right)\right)^2\right. \\ \qquad \left. +H\operatorname{sech}\left(\dfrac{x-c_0t}{l}\right)\operatorname{sech}''\left(\dfrac{x-c_0t}{l}\right)\right), & \text{(V.58d)} \end{cases}$$

where f' denotes the derivative of function f and

$$c_0 = \frac{l}{d}\sqrt{\frac{gH_0^3}{l^2-H_0^2}}, \quad \text{and} \quad a = \frac{H_0^3}{l^2-H_0^2},$$

and $(d,l,H_0) \in \mathscr{R}^3$ with $l > H_0 > 0$.

The system (V.58) also gives analytical solutions for the Green-Naghdi system. Indeed, replacing a and c_0 by a_γ and $c_{0,\gamma}$ defined by

$$\begin{aligned} a_\gamma &= \frac{H_0^3}{\frac{\gamma}{2}l^2-H_0^2}, \\ c_{0,\gamma} &= \sqrt{\frac{\gamma}{2}}\frac{l}{d}\sqrt{\frac{gH_0^3}{\frac{\gamma}{2}l^2-H_0^2}}, \end{aligned}$$

with $(d,l,H_0) \in \mathscr{R}^3$ and $l > H_0 > 0$, the system (V.58) gives an analytical solution for the general system (V.42). Therefore, we are able to compare the analytical solutions of the two non-hydrostatic system. On Fig. V.2, we have plotted the water depth at three different instants $t_0 = 0$ s, $t_1 = 4$ s and $t_2 = 12$ s corresponding to the propagation of the two analytical solitary waves with $H_0 = 1$ m and $d = 2$ m. Fig. V.2-*(a)*, the analytical solutions of the depth-averaged model and the Green-Naghdi model are

depicted by the solid and dashed lines, respectively. The solutions correspond to the choice $l = 2$ m and the corresponding values of a_2 and $c_{0,2}$ for the depth-averaged model and the corresponding values of $a_{3/2}$ and $c_{0,3/2}$ for the Green-Naghdi model. We see on Fig. V.2-*(a)* that starting from the same physical parameters H_0, d, l, the two non-hydrostatic models propagate two solitons but with different amplitudes and propagation velocities. On the contrary, we can choose the physical parameters, typically l, so that the two solitons have the same amplitude and propagation velocities. Indeed, choosing for the depth-averaged system $l = 2$ m and the corresponding values of a_2 and $c_{0,2}$ and for the Green-Naghdi model $l = \frac{4}{\sqrt{3}}$ m and the corresponding values of $a_{3/2}$ and $c_{0,3/2}$ we obtained on Fig. V.2-*(b)* two solitons with the same amplitude and propagation velocities but a slightly different shape.

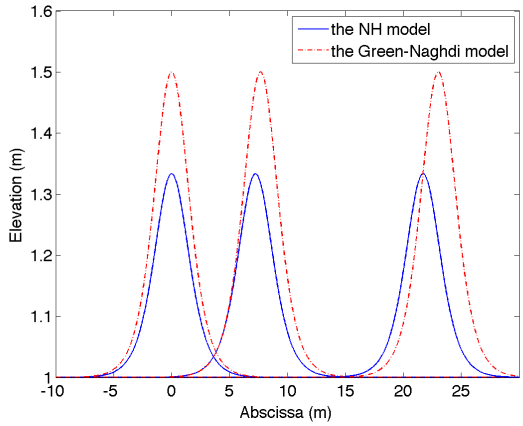

(a)

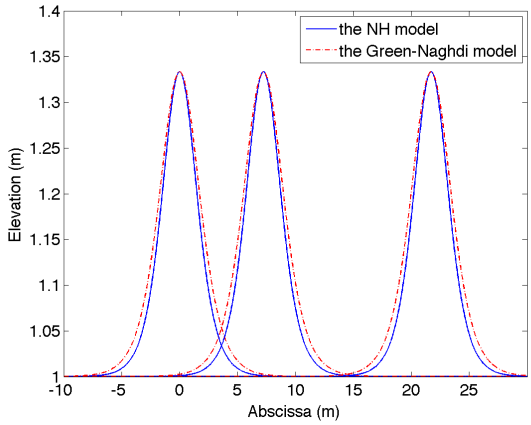

(b)

Figure V.2: Comparaison of analytical solutions of the depth-averaged model (NH) (solid lines) and of the Green-Naghdi (dashed lines) in the case of a solitary wave: *(a)* same values of l *(b)* same amplitude and propagation velocity.

4.3 Stationary solutions

4.3.1 Regularity of stationary solutions

Simple manipulations show that stationary analytical solutions of (V.26) have to satisfy

$$\begin{cases} H\overline{u} = Q_0 = Cst, & \text{(V.59a)} \\ \dfrac{\partial}{\partial x}\left(\dfrac{Q_0^2}{H} + \dfrac{g}{2}H^2 + H\overline{p}_{nh}\right) = -\left(gH + 2\overline{p}_{nh}\right)\dfrac{\partial z_b}{\partial x}, & \text{(V.59b)} \\ H\overline{w} = \dfrac{Q_0}{2}\dfrac{\partial}{\partial x}\left(H + 2z_b\right), & \text{(V.59c)} \\ \overline{p}_{nh} = \dfrac{Q_0}{2}\dfrac{\partial \overline{w}}{\partial x}, & \text{(V.59d)} \end{cases}$$

or equivalently

$$\begin{cases} \dfrac{\partial H}{\partial x} = \dfrac{2}{Q_0}H\overline{w} - 2\dfrac{\partial z_b}{\partial x} \\ \dfrac{\partial \overline{w}}{\partial x} = \dfrac{2}{Q_0}\overline{p}_{nh}, \\ \dfrac{\partial \overline{p}_{nh}}{\partial x} = \left(\dfrac{Q_0^2}{H^2} - gH - \overline{p}_{nh}\right)\left(\dfrac{2}{Q_0}\overline{w} - \dfrac{2}{H}\dfrac{\partial z_b}{\partial x}\right) - \left(g + \dfrac{2\overline{p}_{nh}}{H}\right)\dfrac{\partial z_b}{\partial x}, \end{cases}$$

and $\overline{u} = \frac{Q_0}{H}$. Hence, as long as $H > 0$, we have $(H, \overline{w}, \overline{p}_{nh}) \in (C^k)^3$ if $z_b \in C^k$. This means that when z_b is at least continuous, the stationary solutions of the non-hydrostatic model are necessarily continuous and do not admit shocks.

4.3.2 Stationary quasi-analytical solutions

From the previous writing, we deduce the following proposition.

Proposition V.9. *Choosing Q_0, a boundary condition H_0 for H and a given function $f = f(x)$ corresponding to the desired vertical velocity i.e. $\overline{w} = f$, then the variables $\overline{p}_{nh}, H, z_b, \overline{u}$, defined by*

$$\begin{cases} \overline{p}_{nh} = \dfrac{Q_0}{2}\dfrac{\partial f}{\partial x}, & \text{(V.61a)} \\ \left(\dfrac{g}{2}H - \dfrac{Q_0^2}{H^2}\right)\dfrac{\partial H}{\partial x} = -\dfrac{H}{Q_0}\left(gH + Q_0\dfrac{\partial f}{\partial x}\right)f - \dfrac{Q_0}{2}H\dfrac{\partial^2 f}{\partial x^2}, & \text{(V.61b)} \\ \dfrac{\partial z_b}{\partial x} = -\dfrac{1}{2}\dfrac{\partial H}{\partial x} + \dfrac{Hf}{Q_0}, & \text{(V.61c)} \\ \overline{u} = \dfrac{Q_0}{H}, & \text{(V.61d)} \end{cases}$$

are stationary quasi-analytical of the system (V.26).
The word "quasi-analytical" refers to the fact that the previous set of equations only contains two simple ODEs that have to be solved numerically.

Proof of proposition V.9. The proof is very simple, it only consists in a reformulation of the system (V.59a)-(V.59c) with the assumption $\overline{w} = f$, f given. □

Remark 11. Since the quantity

$$\frac{g}{2}H - \frac{Q_0^2}{H^2},$$

appears in the ODE to solve (V.61d), it is possible to obtain solutions for H with discontinuities. But necessarily, due to the second equation to solve, discontinuities also appears over z_b. Thus, this is not contradictory with the results in paragraph 4.3.

As in paragraphs 4.1 and 4.2, we compare the stationary solutions for the depth-averaged model (V.26) and the Green-Naghdi system (V.39). Following prop. V.9, we can also exhibit stationary quasi-analytical solutions for the Green-Naghdi system (V.39). For any given enough smooth function, f and the solutions of the system

$$\begin{cases} \overline{p}_{nh} = \dfrac{Q_0}{2}\dfrac{\partial f}{\partial x}, & \text{(V.62a)} \\ \left(\dfrac{g}{2}H - \dfrac{Q_0^2}{H^2}\right)\dfrac{\partial H}{\partial x} = -\dfrac{H}{Q_0}\left(gH + \dfrac{4Q_0}{3}\dfrac{\partial f}{\partial x}\right) f - \dfrac{2}{3}Q_0 H\dfrac{\partial^2 f}{\partial x^2}, & \text{(V.62b)} \\ \dfrac{\partial z_b}{\partial x} = -\dfrac{1}{2}\dfrac{\partial H}{\partial x} + \dfrac{Hf}{Q_0}, & \text{(V.62c)} \\ \overline{u} = \dfrac{Q_0}{H}, & \text{(V.62d)} \end{cases}$$

are analytical solutions of the Green-Naghdi system (V.39). Numerical comparisons between the solutions of systems (V.61) and (V.62) are given in the following paragraph.

4.3.3 Numerical illustrations

To illustrate the analytical solutions described by prop. V.9, we give below two typical examples. The analytical solutions are obtained choosing

$$f(x) = 2c(x-a)e^{-b(x-a)^2}, \tag{V.63}$$

and correspond to a channel of length $L = 10\ m$ where we impose the inflow $Q_0 > 0$ at the entrance (left boundary) and the water depth H_0 at the exit (right boundary). For Fig. V.3, the following parameters values $Q_0 = 1.8\ m^2.s^{-1}$, $H_0 = 1\ m$, $a = 5\ m$, $b = 3.4\ m^{-2}$ and $c = 1.5\ s^{-1}$ are considered. On Fig. V.3-*(a)*, we compare the free surface $\eta = H + z_b$ obtained with the quasi-analytical solution (V.61b),(V.61d) of the non-hydrostatic model to the one obtained with the Saint-Venant system (with the same topography z_b and the same boundary conditions). Likewise on Fig. V.3-*(b)*, we compare the velocity field $\overline{u}$ obtained with the depth-averaged Euler model to the one obtained with the Saint-Venant system (with the same topography z_b and the same boundary conditions). The velocity field $\overline{w}$ corresponding to the depth-averaged system is also plotted on Fig. V.3-*(b)*. Over Fig. V.3-*(c)*, we compare the total pressure $gH/2 + \overline{p}_{nh}$ to its hydrostatic part $gH/2$.

Figure V.4 is similar to Figure V.3 but has been obtained with the parameters values $Q_0 = 1.35\ m^2.s^{-1}$, $a = 5\ m$, $b = 4.6\ m^{-2}$ and $c = 1.0\ m^{-1}$. Figures V.3 and V.4 emphasize the influence of the non-hydrostatic effects.

On Fig. V.5, we compare the quasi-analytical solutions of the systems (V.61) and (V.62). The definition of the function f is still given by (V.63). For the inflow Q_0, we have chosen $Q_0 = 1.3\ m^2.s^{-1}$, the boundary condition H_0 and the parameters a, b and c have the same values as for Fig. V.4. Notice that the resolution of (V.62) with exactly the same parameters values as those used for Fig. V.4 i.e. with $Q_0 = 1.35\ m^2.s^{-1}$ instead of $Q_0 = 1.3\ m^2.s^{-1}$ leads to a discontinuous solution (see remark 11). In the Green-Naghdi model, the amplitude of the waves is higher than in the depth-averaged model.

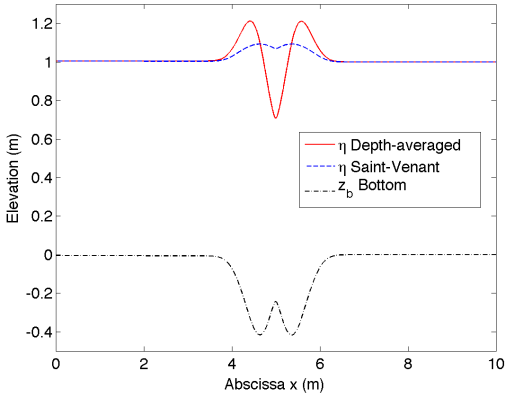

(a)

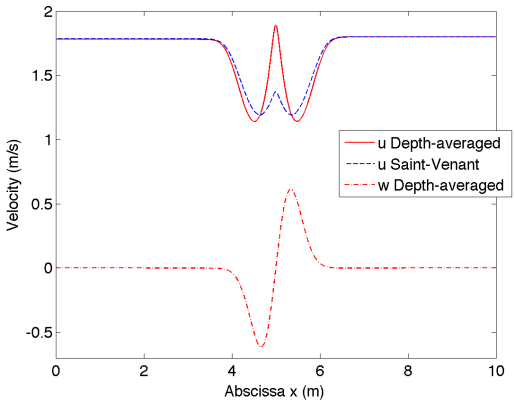

(b)

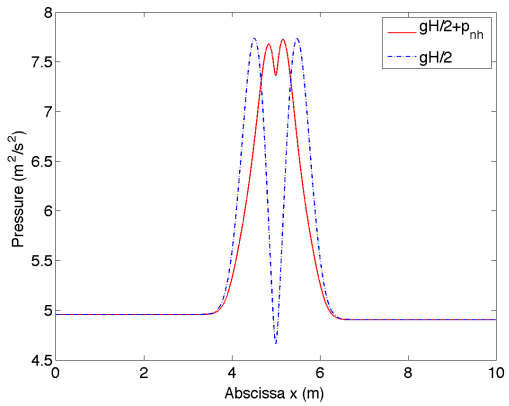

(c)

Figure V.3: Analytical solutions - Comparison of Saint-Venant and depth-averaged Euler solutions: *(a)* free surface $H + z_b$ and bottom profile z_b, *(b)* velocities $\overline{u}$ and $\overline{w}$ and *(c)* total pressure $gH/2 + \overline{p}_{nh}$ and hydrostatic part of the pressure $gH/2$.

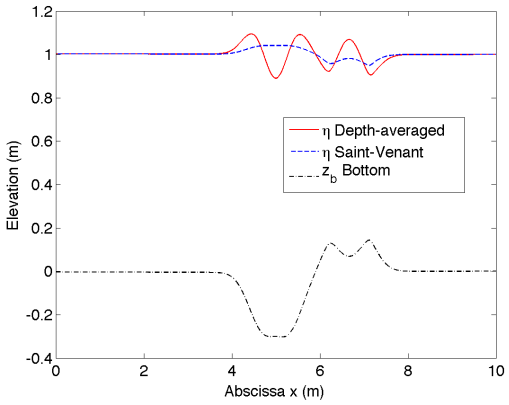

(a)

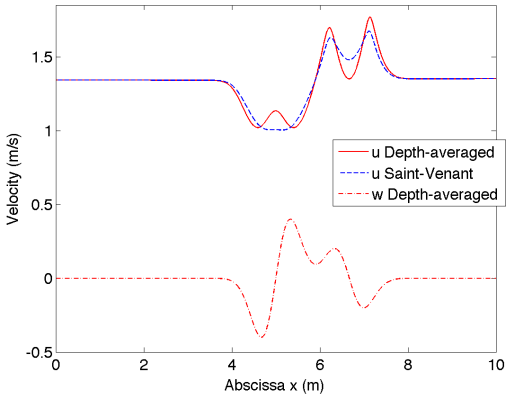

(b)

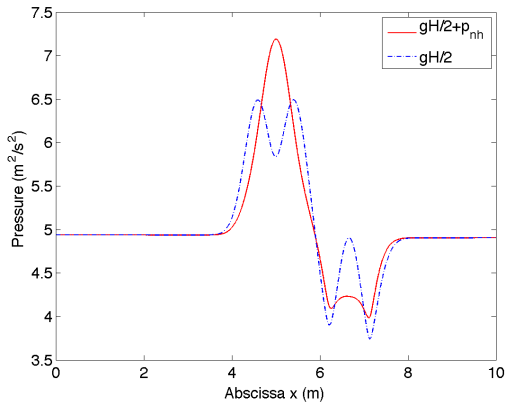

(c)

Figure V.4: Analytical solutions- Comparison of Saint-Venant and depth-averaged Euler solutions: *(a)* free surface $H + z_b$ and bottom profile z_b, *(b)* velocities $\overline{u}$ and $\overline{w}$ and *(c)* total pressure $gH/2 + \overline{p}_{nh}$ and hydrostatic part of the pressure $gH/2$.

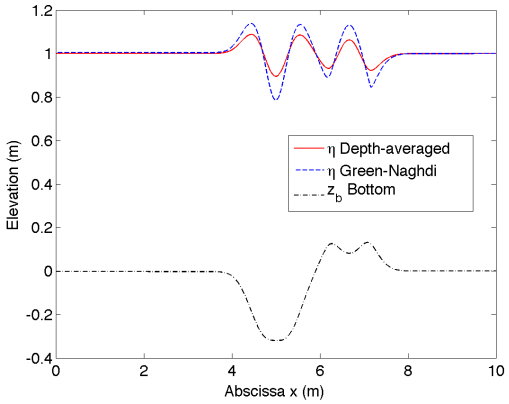

(a)

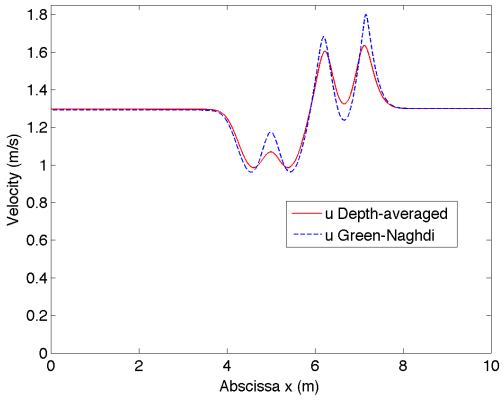

(b)

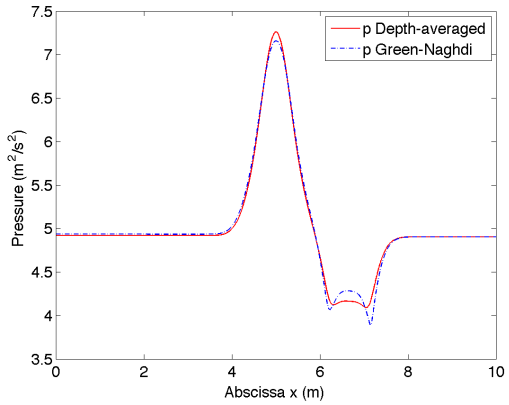

(c)

Figure V.5: Analytical solutions- Comparison of Green-Naghdi and depth-averaged Euler solutions: *(a)* free surface $H + z_b$ and bottom profile z_b, *(b)* velocities $\overline{u}$ and *(c)* total pressures $gH/2 + \overline{p}_{nh}$.

5 Hydrostatic Navier-Stokes (Euler) equations

In this section, we focus on flows with large friction coefficients, with significant water depth or with important wind effects i.e. where the horizontal velocity can hardly be approximated – as in Saint-Venant type systems – by a vertically constant velocity [122]. To drop this limitation multilayer Saint-Venant models are often used. In these models each layer is described by its own height, its own velocity and is advected by the flow (see [6, 13, 14] and the references therein). This advection property induces that there is no mass exchanges between neighborhing layers and makes a close relation to models for non-miscible fluids (see [26, 38, 37] for instance). In [6], introducing a vertical partitioning of the water height, a multilayer strategy was formally derived from the 2d Navier-Stokes system with hydrostatic hypothesis and it is extended to 3d computations in [14].

Here, we derive another and simpler multilayer model where we prescribe the vertical discretization of the layers taking into account the (unknown) total water height. Using a Galerkin approximation in lagrangian formulation, we obtain a system where the only additional unknowns are the layers velocities. This leads to a global continuity equation and allows mass exchanges between layers. This model is interesting since it has the structure of a classical multilayer type Saint-Venant system with mass exchanges but it is also an approximation –without any Shallow Water assumption – of the hydrostatic Navier-Stokes system. The technique we propose is also simpler than methods involving moving meshes and sigma transform [52] since we only use here fixed meshes.

We briefly present the main steps of this approximation of the hydrostatic Navier-Stokes system and recall its main properties (hyperbolicity, energy equality,...). The kinetic interpretation of the model and some simulations in various situations are presented in paragraphs 6.1 where we demonstrate the accuracy and robustness of this model in-between the Navier-Stokes and Saint-Venant systems. The numerical scheme is not described here, the reader can refer to [16, 15].

5.1 Model derivation

We start from the hydrostatic free surface Navier-Stokes equations corresponding to

$$\frac{\partial u}{\partial x}+\frac{\partial w}{\partial z}=0, \tag{V.64}$$

$$\frac{\partial u}{\partial t}+\frac{\partial u^2}{\partial x}+\frac{\partial uw}{\partial z}+\frac{\partial p}{\partial x}=\frac{\partial \Sigma_{xx}}{\partial x}+\frac{\partial \Sigma_{xz}}{\partial z}, \tag{V.65}$$

$$\frac{\partial p}{\partial z}=-g+\frac{\partial \Sigma_{zx}}{\partial x}+\frac{\partial \Sigma_{zz}}{\partial z}, \tag{V.66}$$

completed with the bondary conditions given in paragraph 3.2 (p. 11).

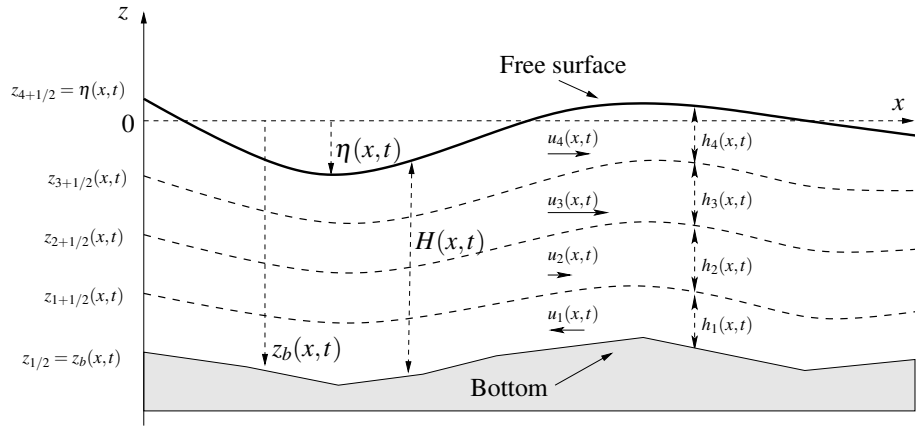

Figure V.6: Notations for the multilayer approach.

The interval $[z_b,\eta]$ is divided into N layers $\{L_\alpha\}_{\alpha\in\{1,\dots,N\}}$ of thickness $l_\alpha H(x,t)$ where each layer L_α corresponds to the points satisfying $z\in L_\alpha(x,t)=[z_{\alpha-1/2},z_{\alpha+1/2}]$ with

$$\left\{\begin{array}{l} z_{\alpha+1/2}(x,t)=z_b(x,t)+\displaystyle\sum_{j=1}^{\alpha} l_j H(x,t),\\ h_\alpha(x,t)=z_{\alpha+1/2}(x,t)-z_{\alpha-1/2}(x,t)=l_\alpha H(x,t),\end{array}\right. \tag{V.67}$$

with $l_j>0,\quad \sum_{j=1}^{N} l_j=1$, see Fig. V.6. Such a partitioning can also be found in [117] but leading to a different model.

Now let us consider the space $\mathbb{P}_{0,H}^{N,t}$ of piecewise constant functions defined by

$$\mathbb{P}_{0,H}^{N,t}=\left\{\mathbf{1}_{z\in L_\alpha(x,t)}(z),\quad \alpha\in\{1,\dots,N\}\right\}, \tag{V.68}$$

where $\mathbf{1}_{z\in L_\alpha(x,t)}(z)$ is the characteristic function of the interval $L_\alpha(x,t)$. Using this formalism, the projection of u and w onto $\mathbb{P}_{0,H}^{N,t}$ is a piecewise constant function defined by

$$X^N(x,z,\{z_\alpha\},t)=\sum_{\alpha=1}^{N}\mathbf{1}_{[z_{\alpha-1/2},z_{\alpha+1/2}]}(z)X_\alpha(x,t), \tag{V.69}$$

for $X\in(u,w)$. We have the following result where for the sake of simplicity, we omit the viscous and friction terms, we refer to [16] for the treatment of these terms.

Proposition V.10. *The weak formulation of Eqs. (V.64)-(V.66) on $\mathbb{P}_{0,H}^{N,t}$ leads to a system of the form*

$$\sum_{\alpha=1}^{N}\frac{\partial h_\alpha}{\partial t}+\sum_{\alpha=1}^{N}\frac{\partial h_\alpha u_\alpha}{\partial x}=0, \tag{V.70}$$

$$\begin{aligned}\frac{\partial h_\alpha u_\alpha}{\partial t}+\frac{\partial}{\partial x}\left(h_\alpha u_\alpha^2+h_\alpha p_\alpha\right)&=u_{\alpha+1/2}G_{\alpha+1/2}-u_{\alpha-1/2}G_{\alpha-1/2}\\ &\quad+\frac{\partial z_{\alpha+1/2}}{\partial x}p_{\alpha+1/2}-\frac{\partial z_{\alpha-1/2}}{\partial x}p_{\alpha-1/2},\end{aligned} \tag{V.71}$$

for $\alpha\in[1,\dots,N]$. The definitions of $p_\alpha,p_{\alpha+1/2},u_{\alpha+1/2},G_{\alpha+1/2}$ are given in the following. The system (V.70)-(V.71) results from a formal asymptotic approximation in $\mathcal{O}(\varepsilon^2)$ (see (II.1)) coupled with a vertical discretization of the Navier-Stokes equations (V.64)-(V.66) with hydrostatic pressure.

Without entering in details, we give hereafter a proof of this proposition since it allows to give the expression of the source terms in the right hand side of Eq. (V.71).

Proof of Prop. V.10. Using the Leibniz rule, the Galerkin approximation of Eq. (V.64) on $\mathbb{P}_{0,H}^{N,t}$ gives the set of equations

$$\frac{\partial h_\alpha}{\partial t}+\frac{\partial}{\partial x}\left(h_\alpha u_\alpha\right)=G_{\alpha+1/2}-G_{\alpha-1/2},\qquad \alpha\in[1,\dots,N] \tag{V.72}$$

with

$$G_{\alpha+1/2}=\left(\frac{\partial z_{\alpha+1/2}}{\partial t}+u_{\alpha+1/2}\frac{\partial z_{\alpha+1/2}}{\partial x}-w_{\alpha+1/2}\right), \tag{V.73}$$

$$G_{1/2}=G_{N+1/2}=0. \tag{V.74}$$

The relations (V.73) give the mass flux leaving/entering each layer α whereas the relations (V.74) just express that the bottom and the top are interfaces without loss/supply of mass (see the boundary conditions (I.9),(I.11)).

Let us notice that the layer mass equation (V.72) can not be used per se since the layer height h_α is not an independent variable but is defined as a part of the whole water height $H(t,x)$, see relation

(V.67). But using the first condition of (V.74), one can compute $G_{\alpha+1/2}$ just adding up the equations (V.72)

$$G_{\alpha+1/2} = \sum_{j=1}^{\alpha} \frac{\partial h_j}{\partial t} + \sum_{j=1}^{\alpha} \frac{\partial h_j u_j}{\partial x}, \quad ,\alpha = 1,\ldots,N. \tag{V.75}$$

Then the equation (V.75) written for $\alpha = N$ and the second condition of (V.74) give the equation (V.70). The need to consider only the global mass equation (V.70) is related to the fact that we consider a single fluid and not several layers of non-miscible fluids as in some other multilayer models [110, 131, 37, 29]. Then it is physically relevant to consider a single mass equation that authorizes in some sense a circulation of the fluid between the layers introduced in the discretization process. In the following, we use the formula (V.75) rather than (V.73), and thus we have not to define $w_{\alpha+1/2}$.

Similarly, the $\mathbb{P}^{N,t}_{0,H}$-approximation of the x-momentum equation (V.65) leads to (V.71). Indeed from (V.66) we can compute

$$p(x,z,t) = \int_z^{\eta} g\, dz,$$

so we have for $z \in L_\alpha$

$$p(x,z,t) = g\left(\sum_{j=\alpha+1}^{N} h_j + (z_{\alpha+1/2} - z)\right).$$

Using the notations

$$p_\alpha = \frac{1}{h_\alpha}\int_{z_{\alpha-1/2}}^{z_{\alpha+1/2}} p(x,z,t)dz, \qquad p_{\alpha+1/2} = p(x,z_{\alpha+1/2},t), \tag{V.76}$$

we have

$$p_\alpha = g\left(\frac{h_\alpha}{2} + \sum_{j=\alpha+1}^{N} h_j\right), \qquad p_{\alpha+1/2} = \rho_0 g \sum_{j=\alpha+1}^{N} h_j \tag{V.77}$$

and applying the Leibniz rule to the pressure term of equation (V.65), we can write

$$\int_{z_{\alpha-1/2}}^{z_{\alpha+1/2}} \frac{\partial p}{\partial x} dz \;\; = \frac{\partial h_\alpha p_\alpha}{\partial x} - \frac{\partial z_{\alpha+1/2}}{\partial x} p_{\alpha+1/2} + \frac{\partial z_{\alpha-1/2}}{\partial x} p_{\alpha-1/2}. \tag{V.78}$$

To complete the definition of equation (V.71), the quantities $u_{\alpha+1/2}$, $\alpha = 1,\ldots,N-1$ are defined using an upwinding

$$u_{\alpha+1/2} = \begin{cases} u_\alpha & \text{if } G_{\alpha+1/2} \leqslant 0 \\ u_{\alpha+1} & \text{if } G_{\alpha+1/2} > 0. \end{cases} \quad \square \tag{V.79}$$

5.2 Energy

It is straightforward to obtain an energy equality for the model depicted in Prop. V.10. Considering smooth solutions and multiplying the x-momentum equation (V.65) by u and performing the Galerkin approximation on $\mathbb{P}^{N,t}_{0,H}$.

For the layer α we have

$$\begin{aligned} \frac{\partial}{\partial t}E^N_{sv,\alpha} + \frac{\partial}{\partial x}\left(u_\alpha\left(E^N_{sv,\alpha} + \frac{g}{2}h_\alpha H\right)\right) = \\ + \left(\frac{u^2_{\alpha+1/2}}{2} + p_{\alpha+1/2} + g z_{\alpha+1/2}\right) G_{\alpha+1/2} \\ - \left(\frac{u^2_{\alpha-1/2}}{2} + p_{\alpha-1/2} + g z_{\alpha-1/2}\right) G_{\alpha-1/2} \\ - p_{\alpha+1/2}\frac{\partial z_{\alpha+1/2}}{\partial t} + p_{\alpha-1/2}\frac{\partial z_{\alpha-1/2}}{\partial t}, \end{aligned} \tag{V.80}$$

with $E^N_{sv,\alpha} = \frac{h_\alpha u_\alpha^2}{2} + \frac{g(z^2_{\alpha+1/2} - z^2_{\alpha-1/2})}{2}$. Adding the preceding relations for $\alpha = 1,\ldots,N$, we obtain the global balance

$$\frac{\partial}{\partial t}\left(\sum_{\alpha=1}^{N} E^N_{sv,\alpha}\right) + \frac{\partial}{\partial x}\left(\sum_{\alpha=1}^{N} u_\alpha \left(E^N_{sv,\alpha} + \frac{g}{2} h_\alpha H\right)\right) = 0.$$

5.3 Pressure source terms

As often when considering hyperbolic type problems, the treatment of the source terms is subtle. We have written in (V.78) the hydrostatic pressure terms of the layer α as the combination of a conservative part and two source terms, one for each interface.

It is obvious that (V.78) can be written under the simplified form

$$\int_{z_{\alpha-1/2}}^{z_{\alpha+1/2}} \frac{\partial p}{\partial x} dz \quad = g l_\alpha H \frac{\partial \eta}{\partial x} = \frac{g}{2}\frac{\partial h_\alpha H}{\partial x} + g h_\alpha \frac{\partial z_b}{\partial x}. \tag{V.81}$$

So the momentum equation (V.71) is equivalent to

$$\frac{\partial h_\alpha u_\alpha}{\partial t} + \frac{\partial}{\partial x}\left(h_\alpha u_\alpha^2 + \frac{g}{2} h_\alpha H\right) = u_{\alpha+1/2} G_{\alpha+1/2} - u_{\alpha-1/2} G_{\alpha-1/2} - g h_\alpha \frac{\partial z_b}{\partial x}.$$

The two writtings (V.78) and (V.81) are obviously equivalent but at the discrete level they differ since in (V.78) the conservative part of the pressure term nonlinearly depends on the elevation. Indeed for equally spaced layers i.e. $l_\alpha = 1/N$, we have

$$h_\alpha p_\alpha = \frac{g}{2}\frac{N-\alpha+1}{N^2} H^2,$$

that is very different from the corresponding expression in (V.81).

At the discrete level, we have singled out the formulation (V.78) that is more natural. For the discretization of the pressure source terms in (V.78), we have proposed an extension of the hydrostatic reconstruction technique proposed by Audusse *et al.* [8].

5.4 Comparison with other multilayer systems

To illustrate the formulation of the model, we compare it with the system proposed in [6] in the simple case of a two-layer formulation. Neglecting the viscosity and friction, the formulation obtained by Audusse [6] corresponds to (V.72),(V.71) with $G_{\alpha+1/2} \equiv 0$, i.e.

$$\frac{\partial h_1}{\partial t} + \frac{\partial h_1 u_1}{\partial x} = 0, \qquad \frac{\partial h_2}{\partial t} + \frac{\partial h_2 u_2}{\partial x} = 0, \tag{V.82}$$

$$\frac{\partial h_1 u_1}{\partial t} + \frac{\partial h_1 u_1^2}{\partial x} + g h_1 \frac{\partial (h_1 + h_2)}{\partial x} = -g h_1 \frac{\partial z_b}{\partial x}, \tag{V.83}$$

$$\frac{\partial h_2 u_2}{\partial t} + \frac{\partial h_2 u_2^2}{\partial x} + g h_2 \frac{\partial (h_1 + h_2)}{\partial x} = -g h_2 \frac{\partial z_b}{\partial x}, \tag{V.84}$$

with $h_1 + h_2 = H$. The preceding formulation corresponds to a superposition of two single layer Saint-Venant systems (see also [26, 38, 37] where a very similar model is considered in a bi-fluid framework).

With our approach (V.70),(V.71), the two-layer formulation reads

$$\frac{\partial H}{\partial t} + \frac{\partial h_1 u_1}{\partial x} + \frac{\partial h_2 u_2}{\partial x} = 0, \tag{V.85}$$

$$\frac{\partial h_1 u_1}{\partial t} + \frac{\partial h_1 u_1^2}{\partial x} + \frac{g}{2}\frac{\partial H h_1}{\partial x} = -g h_1 \frac{\partial z_b}{\partial x} + u_{3/2}\left(l\frac{\partial H}{\partial t} + l\frac{\partial H u_1}{\partial x}\right), \tag{V.86}$$

$$\frac{\partial h_2 u_2}{\partial t} + \frac{\partial h_2 u_2^2}{\partial x} + \frac{g}{2}\frac{\partial H h_2}{\partial x} = -g h_2 \frac{\partial z_b}{\partial x} - u_{3/2}\left(l\frac{\partial H}{\partial t} + l\frac{\partial H u_1}{\partial x}\right), \tag{V.87}$$

$$\text{where } h_1 = lH, \quad h_2 = (1-l)H, \tag{V.88}$$

with $l \in (0,1)$ prescribed. The velocity at the interface, denoted $u_{3/2}$, is calculated using upwinding, following the sign of the mass exchange between the layers. It is important to notice that, in the new formulation (V.85)-(V.88), we obtain directly a left hand side term written in conservative form with the topography and the mass exchange as source terms whereas the pressure term of (V.82)-(V.84) has to be modified [6] to get a conservative form. Moreover we prove in paragraph 5.5 that the system (V.85)-(V.88) is *often* hyperbolic, which is not the case for system (V.82)-(V.84).

The difference between (V.85)-(V.88) and (V.82)-(V.84) mainly comes from the physical definition of the layers. Audusse introduces a physical discretization where each layer has its own continuity equation. These N continuity equations mean the layers are isolated each other, this situation corresponds to the case of N non miscible fluids. In the formulation (V.85)-(V.88), the discretization corresponds to a semidiscretization in the vertical direction– of P_0 finite elements type – of the velocity u. In this case, the definition of the layers does not correspond to a physical partition of the flow but is related to the quality of the desired approximation over u. Thus we have only one continuity equation meaning the fluid can circulate from one layer to another.

5.5 Hyperbolicity

Let us first say some words about the two-layers case i.e. $N = 2$. It is proved in [16] that the two-layers version of the multilayer Saint-Venant system (V.70)-(V.71) is strictly hyperbolic when the total water height is strictly positive. When $N = 2$, the non-miscible multilayer system proposed by Audusse *et al.* [6] was proved to be non-hyperbolic.

In the general case, the system (V.70)-(V.71) approximates the hydrostatic free surface Euler system which in general is not an hyperbolic system. Thus this is not surprising that numerically, the quasilinear form of (V.70)-(V.71) can exhibit complex eigenvalues.

We have performed various numerical evaluations of the eigenelements of the jacobian of (V.70)-(V.71) with numerous choices of the variables H, u_α, $u_{\alpha+1/2}$ and l_α. When the chosen values correspond to physical values for geophysical flows, these tests have always shown that the matrix is diagonalizable on $\mathscr{R}$. But when considering shear flows with very large velocities e.g. $|u_{i_0}| \gg 1$, $|u_{j_0}| \gg 1$ and $u_{i_0}u_{j_0} < 0$ for some $i_0 \neq j_0$, complex eigenvalues can appear corresponding to vibrations of the interfaces $z_{\alpha+1/2}$, see [6, 38].

In the simple case where all the layers have the same velocity u, the barotropic eigenvalues $u+\sqrt{gH}$ and $u-\sqrt{gH}$ are simple and the baroclinic eigenvalue u has a multiplicity of $N-1$ but the matrix remains diagonalizable on $\mathscr{R}$.

Considering flows satisfying $u_\alpha \ll \sqrt{gH}$, it is observed numerically that the eigenvalues of the system belongs to the interval

$$\left[\min_\alpha\{|u_\alpha|\} - \sqrt{gH}, \max_\alpha\{|u_\alpha|\} + \sqrt{gH}\right].$$

The numerical discretization of the proposed model will be discussed later but we point out that the kinetic scheme instead of using discrete eigenvalues of the jacobian matrix, uses a continuum of eigenvalues and is able to deal with situations where some of the discrete eigenvalues are complex.

5.6 Vertical velocity

In Prop. V.10, the vertical velocity w no more appears, but performing the Galerkin approximation of the divergence free condition multiplied by z leads to **[EX]**

$$\frac{\partial}{\partial t}\left(\frac{z_{\alpha+1/2}^2 - z_{\alpha-1/2}^2}{2}\right) + \frac{\partial}{\partial x}\left(\frac{z_{\alpha+1/2}^2 - z_{\alpha-1/2}^2}{2}u_\alpha\right) = h_\alpha w_\alpha + z_{\alpha+1/2}G_{\alpha+1/2} - z_{\alpha-1/2}G_{\alpha-1/2}, \tag{V.89}$$

where the w_α, $\alpha = 1,\dots,N$ are the components of the Galerkin approximation of w on $\mathbb{P}_{0,H}^{N,t}$, see (V.69). And since all the quantities except w_α appearing in Eq. (V.89) are already defined by (V.70),(V.71), relation (V.89) allows to recover the value of w_α. Note that we use relation (V.89) rather than the divergence free condition for stability purpose. We refer the reader to [121] for more details.

5.7 Kinetic interpretation

In this paragraph we propose a kinetic interpretation of the system

$$\sum_{\alpha=1}^{N} \frac{\partial h_\alpha}{\partial t} + \sum_{\alpha=1}^{N} \frac{\partial h_\alpha u_\alpha}{\partial x} = 0, \tag{V.90}$$

$$\frac{\partial h_\alpha u_\alpha}{\partial t} + \frac{\partial}{\partial x}\left(h_\alpha u_\alpha^2 + \frac{g}{2} h_\alpha H\right) = u_{\alpha+1/2} G_{\alpha+1/2} - u_{\alpha-1/2} G_{\alpha-1/2} - g h_\alpha \frac{\partial z_b}{\partial x}, \tag{V.91}$$

$$\begin{aligned}\frac{\partial}{\partial t} E^N_{sv,\alpha} + \frac{\partial}{\partial x}\left(u_\alpha\left(E^N_{sv,\alpha} + \frac{g}{2} h_\alpha H\right)\right) &= \frac{u^2_{\alpha+1/2}}{2} G_{\alpha+1/2} - \frac{u^2_{\alpha-1/2}}{2} G_{\alpha-1/2} \\ &\quad - p_{\alpha+1/2} \frac{\partial z_{\alpha+1/2}}{\partial t} + p_{\alpha-1/2} \frac{\partial z_{\alpha-1/2}}{\partial t},\end{aligned} \tag{V.92}$$

that is equivalent to (V.70)-(V.71),(V.81). We assume $\frac{\partial z_b}{\partial t} = 0$.

Let us construct a density of particles $M_\alpha(x,t,\xi)$ defined by a Gibbs equilibrium: the microscopic density of particles present at time t in the layer α, in the vicinity Δx of the abscissa x and with velocity ξ given by

$$M_\alpha(x,t,\xi) = l_\alpha \frac{H(x,t)}{c} \chi\left(\frac{\xi - u_\alpha(x,t)}{c}\right), \qquad \alpha = 1,\dots,N, \tag{V.93}$$

where χ satisfies (II.70) with

$$c^2 = \frac{gH}{2}.$$

Likewise, we define $N_{\alpha+1/2}(x,t,\xi)$ by

$$N_{\alpha+1/2}(x,t,\xi) = G_{\alpha+1/2}(x,t)\ \delta\left(\xi - u_{\alpha+1/2}(x,t)\right), \qquad \alpha = 0,\dots,N, \tag{V.94}$$

where δ denotes the Dirac distribution. The quantities $G_{\alpha+1/2}, 0 \leqslant \alpha \leqslant N$ represent the mass exchanges between layers α and $\alpha+1$, they are defined in (V.75) and satisfy the conditions (V.74), so $N_{1/2}$ and $N_{N+1/2}$ also satisfy

$$N_{1/2}(x,t,\xi) = N_{N+1/2}(x,t,\xi) = 0. \tag{V.95}$$

We also introduce the densities $\widetilde{M}_\alpha(x,t,\xi)$ that will be used for the energy equations , they are defined by

$$\widetilde{M}_\alpha(x,t,\xi) = \frac{gH(x,t)h_\alpha(x,t)}{4c} \chi\left(\frac{\xi - u_\alpha(x,t)}{c}\right).$$

Notice that the introduction of this second family of densities is not needed when we consider the two dimensional shallow water system. Here they take into account some kind of transversal effect at the kinetic level that is implicitely included into the macroscopic one dimensional shallow water system. We refer the reader to [12, 113] for more details.

With the previous definitions, we write a kinetic representation of the multilayer Saint-Venant system described in proposition V.10 and we have the following proposition:

Proposition V.11. *The functions H and u^N (given by (V.69)) are strong solutions of the multilayer Saint-Venant system (V.90)-(V.91) if and only if the set of equilibria $\{M_\alpha(x,t,\xi)\}_{\alpha=1}^N$ is solution of the kinetic equations*

$$\begin{aligned}\frac{\partial M_\alpha}{\partial t} + \xi \frac{\partial M_\alpha}{\partial x} - g \frac{\partial z_b}{\partial x} \frac{\partial M_\alpha}{\partial \xi} - N_{\alpha+1/2}(x,t,\xi) + N_{\alpha-1/2}(x,t,\xi) &= Q_\alpha(x,t,\xi), \\ &\quad \alpha = 1,\dots,N,\end{aligned} \tag{V.96}$$

with $\{N_{\alpha+1/2}(x,t,\xi)\}_{\alpha=0}^N$ satisfying (V.94),(V.95). The set of equations (V.96) can also be written under the form

$$N_{\alpha+1/2}(x,t,\xi) = \sum_{i=1}^{\alpha} \left(\frac{\partial M_i}{\partial t} + \xi \frac{\partial M_i}{\partial x} - g \frac{\partial z_b}{\partial x} \frac{\partial M_i}{\partial \xi} - Q_i\right), \qquad \alpha = 1,\dots,N. \tag{V.97}$$

The quantities $Q_\alpha(x,t,\xi)$ are "collision terms" equals to zero at the macroscopic level i.e. which satisfy for a.e. values of (x,t)

$$\int_{\mathbb{R}} Q_\alpha d\xi = 0, \qquad \int_{\mathbb{R}} \xi Q_\alpha d\xi = 0.$$

The solution of (V.96),(V.97) is an entropy solution if additionally

$$\frac{\partial \widetilde{M}_\alpha}{\partial t} + \xi \frac{\partial \widetilde{M}_\alpha}{\partial x} = \widetilde{Q}_\alpha(x,t,\xi), \quad \alpha = 1,\ldots,N, \tag{V.98}$$

with

$$\int_{\mathbb{R}} \left(\frac{\xi^2}{2} Q_\alpha + \widetilde{Q}_\alpha \right) d\xi \leqslant 0.$$

Proof. As previously we denote $X = (H, q_1, \ldots, q_N)^T$ the vector of unknowns with $q_\alpha = l_\alpha H u_\alpha$. We introduce $M = (M_1, \ldots, M_N)^T$ and an $(N+1) \times N$ matrix $\mathscr{K}(\xi)$ defined by $\mathscr{K}_{1,j} = 1$, $\mathscr{K}_{i+1,j} = \delta_{i,j}\, \xi$ with $\delta_{i,j}$ the Kronecker symbol.

Using the definition (V.93) and the properties of the function χ, we have

$$l_\alpha H(x,t) = \int_{\mathscr{R}} M_\alpha(x,t,\xi) d\xi, \tag{V.99}$$

and

$$X(x,t) = \int_{\mathscr{R}} \mathscr{K}(\xi)\, M(x,t,\xi) d\xi. \tag{V.100}$$

The proof is obtained by a simple integration in ξ of the set of equations (V.96) against the matrix $\mathscr{K}(\xi)$. First, an integration in ξ of (V.96) gives the continuity equation (V.72) i.e.

$$\frac{\partial l_\alpha H}{\partial t} + \frac{\partial l_\alpha H u_\alpha}{\partial x} = G_{\alpha+1/2} - G_{\alpha-1/2}, \quad \alpha = 1,\ldots,N,$$

and by summation we have (V.90). Actually from the definition (V.94) of $N_{\alpha+1/2}$ we have

$$\int_{\mathscr{R}} N_{\alpha+1/2}(x,t,\xi) d\xi = G_{\alpha+1/2}(x,t),$$

and

$$\int_{\mathscr{R}} \xi N_{\alpha+1/2}(x,t,\xi) d\xi = u_{\alpha+1/2} G_{\alpha+1/2}.$$

Likewise for the energy balance of the layer α we proceed an integration in ξ of (V.96) against $\xi^2/2$. Since we have

$$\int_{\mathscr{R}} \left(\frac{\xi^2}{2} M_\alpha + \widetilde{M}_\alpha \right) d\xi = \frac{h_\alpha}{2} u_\alpha^2 + \frac{g}{2} h_\alpha H, \tag{V.101}$$

$$\int_{\mathscr{R}} \xi \left(\frac{\xi^2}{2} M_\alpha + \widetilde{M}_\alpha \right) d\xi = \frac{h_\alpha}{2} u_\alpha^3 + g h_\alpha H u_\alpha, \tag{V.102}$$

and for the source term

$$\begin{aligned} \int_{\mathscr{R}} \frac{\xi^2}{2} g \frac{\partial z_b}{\partial x} \frac{\partial M_\alpha}{\partial \xi} d\xi &= -g \frac{\partial z_b}{\partial x} h_\alpha u_\alpha \\ &= -g \frac{\partial}{\partial x}\left(z_b h_\alpha u_\alpha\right) + g z_b \frac{\partial h_\alpha u_\alpha}{\partial x} \\ &= -g \frac{\partial}{\partial x}\left(z_b h_\alpha u_\alpha\right) - g z_b \frac{\partial h_\alpha}{\partial t} \\ &\quad -g z_b G_{\alpha+1/2} + g z_b G_{\alpha-1/2}, \end{aligned} \tag{V.103}$$

we obtain the equality

$$\frac{\partial}{\partial t}\left(\frac{h_\alpha}{2}u_\alpha^2+\frac{g}{2}h_\alpha(\eta+z_b)+h_\alpha p^a\right)+\frac{\partial}{\partial x}\left[u_\alpha\left(h_\alpha u_\alpha^2+\frac{g}{2}h_\alpha H+\frac{g}{2}h_\alpha(\eta+z_b)+h_\alpha p^a\right)\right]$$
$$+\frac{u_{\alpha-1/2}^2}{2}G_{\alpha-1/2}-\frac{u_{\alpha+1/2}^2}{2}G_{\alpha+1/2}=\int_{\mathscr{R}}\left(\frac{\xi^2}{2}Q_\alpha+\widetilde{Q}_\alpha\right)d\xi. \tag{V.104}$$

The previous relation corresponds to (V.92). The sum of the equations (V.104) gives the energy equality for the global system and that completes the proof. □

The formulation (V.96) reduces the nonlinear multilayer Saint-Venant system to a linear transport system on nonlinear quantities $\{M_\alpha\}_{\alpha=1}^N$, $\{N_{\alpha+1/2}\}_{\alpha=0}^N$ for which it is easier to find a simple numerical scheme with good theoretical properties. In the case of a single layer, for a detailed proof of the kinetic interpretation refer to [12] and for the treatment of the source term at this microscopic level see [113]. Notice that the choice of the function χ remains quite open at this stage since several functions satisfy the requested properties. Following this choice the deduced kinetic scheme will have different properties.

5.8 Numerical scheme

The numerical scheme is not described in this course, the reader can refer to [16].

5.9 Variable density case

We now consider the two-dimensional hydrostatic Navier-Stokes system with variable density

$$\frac{\partial\rho}{\partial t}+\frac{\partial\rho u}{\partial x}+\frac{\partial\rho w}{\partial z}=0, \tag{V.105}$$
$$\frac{\partial\rho u}{\partial t}+\frac{\partial\rho u^2}{\partial x}+\frac{\partial\rho uw}{\partial z}+\frac{\partial p}{\partial x}=\frac{\partial\Sigma_{xx}}{\partial x}+\frac{\partial\Sigma_{xz}}{\partial z}, \tag{V.106}$$
$$\frac{\partial p}{\partial z}=-\rho g+\frac{\partial\Sigma_{zx}}{\partial x}+\frac{\partial\Sigma_{zz}}{\partial z}, \tag{V.107}$$

where the fluid density $\rho(x,t)$ is assumed to depend on the spatial and temporal distribution of a given tracer $T(x,t)$, namely

$$\rho=\rho(T), \tag{V.108}$$

and T is governed by a transport-diffusion equation

$$\frac{\partial\rho T}{\partial t}+\frac{\partial\rho uT}{\partial x}+\frac{\partial\rho wT}{\partial z}=\mu_T\frac{\partial^2 T}{\partial x^2}+\mu_T\frac{\partial^2 T}{\partial z^2}, \tag{V.109}$$

where μ_T is the tracer diffusivity. As in paragraph 3.2, the system (V.105)-(V.109) is completed with appropriate kinematic and dynamical boundary conditions. The viscosity tensor corresponds to (I.5)-(I.6).

Then, with the notations of paragraph 5.1, we introduce the discretization

$$X^N(x,z,\{z_\alpha\},t)=\sum_{\alpha=1}^N\mathbf{1}_{[z_{\alpha-1/2},z_{\alpha+1/2}]}(z)X_\alpha(x,t), \tag{V.110}$$

for $X\in(u,w,T)$ and the density $\rho=\rho(T)$ inherits a discretization from the previous relation with

$$\rho^N(x,z,\{z_\alpha\},t)=\sum_{\alpha=1}^N\mathbf{1}_{[z_{\alpha-1/2},z_{\alpha+1/2}]}(z)\rho(T_\alpha(x,t)). \tag{V.111}$$

We have the following result.

Proposition V.12. *Omitting the viscosity terms, the weak formulation of Eqs. (V.105)-(V.107) and (V.109) on $\mathbb{P}^{N,t}_{0,H}$ leads to a system of the form*

$$\sum_{\alpha=1}^{N} \frac{\partial \rho_\alpha h_\alpha}{\partial t} + \sum_{\alpha=1}^{N} \frac{\partial \rho_\alpha h_\alpha u_\alpha}{\partial x} = 0. \tag{V.112}$$

$$\frac{\partial \rho_\alpha h_\alpha u_\alpha}{\partial t} + \frac{\partial}{\partial x}\left(\rho_\alpha h_\alpha u_\alpha^2 + h_\alpha p_\alpha\right) = u_{\alpha+1/2} G_{\alpha+1/2} - u_{\alpha-1/2} G_{\alpha-1/2} + \frac{\partial z_{\alpha+1/2}}{\partial x} p_{\alpha+1/2} - \frac{\partial z_{\alpha-1/2}}{\partial x} p_{\alpha-1/2}, \tag{V.113}$$

$$\frac{\partial \rho_\alpha h_\alpha T_\alpha}{\partial t} + \frac{\partial}{\partial x}\left(\rho_\alpha h_\alpha T_\alpha u_\alpha\right) = T_{\alpha+1/2} G_{\alpha+1/2} - T_{\alpha-1/2} G_{\alpha-1/2}, \tag{V.114}$$

$$\alpha \in [1, \ldots, N],$$

with $h_\alpha = l_\alpha H$. The definitions of $G_{\alpha+1/2}$, p_α, $p_{\alpha+1/2}$, $u_{\alpha+1/2}$, $T_{\alpha+1/2}$ are given by formula analogous to (V.75), (V.77) and (V.79).

Proof of Prop. V.12. The proof is rather similar to the one given for prop. V.10 (p. 103) and left to the reader **[EX]**. □

6 Numerical simulations

The simulations presented in this section have been obtained with numerical codes developed by the authors. For a complete description, the reader can refer to [16, 15].

6.1 Hydrostatic Navier-Stokes system

6.1.1 Comparison with a finite element simulations of the hydrostatic Navier-Stokes system

First we compare the simulations obtained with the model given in prop. V.10 – and the numerical scheme derived from the kinetic interpretation given in paragraph 5.7 – with results obtained using a finite element discretization of the hydrostatic Navier-Stokes system. The finite element formulation is P_1/P_1 for the velocity and the pressure and uses a stabilization technique. The formulation is available in the FreeFem++ code [1].

We consider a wind driven flow with vertical shores but with a non trivial bottom. The domain is 6 m long with an initial water height of 2 m. The mesh has 160 nodes in the x direction and 20 layers. The wind velocity (from left to right at the free surface) is 10 m.s^{-1}. We have used a viscosity of $\nu = 0.1$ m^2.s^{-1} and a Navier type bottom friction with $\kappa = 0.1$ m.s^{-1}. For each simulation (multilayer approach or finite elements approximation), the mesh has approximatively 1000 nodes. For the multilayer approach, the results on a postprocessing 2d mesh (see Fig. V.7) are presented in Fig. V.8 where we have plotted the two dimensional velocity vectors $(u,w)^T$. In Fig. V.9 the results obtained with the finite elements code are shown. The results exhibit a global recirculation that is combined with two local recirculations that are induced by the topography of the lake. The qualitative aspect of the solution is consistent with the previsions.

The FreeFem++ code, solving the full Navier-Stokes system serves as a reference. It is however not straightforward to analyze the origin of the differences because the boundary conditions are not imposed in the same way. But in the examples presented in Figs. V.8 and V.9 whereas the viscosity and the bottom friction are large, the simulations are in agreement. The vertical velocity w is overestimated by the multilayer code. This mainly comes from the fact that in the multilayer approach, w is calculated offline using u and the divergence free condition whereas in the finite element formulation, w follows a dynamical equation

$$\tilde{\varepsilon}\left(\frac{\partial w}{\partial t} + u\frac{\partial w}{\partial x} + w\frac{\partial w}{\partial z}\right) + \frac{\partial p}{\partial z} = -g + \tilde{\varepsilon}\frac{\partial \Sigma_{zx}}{\partial x} + \tilde{\varepsilon}\frac{\partial \Sigma_{zz}}{\partial z},$$

with $\tilde{\varepsilon} \ll 1$. Notice also that the difference of shape for the step in Figs. V.8 and V.9 only comes from the mesh reconstruction/interpolation procedure in the multilayer approach.

It is also difficult to compare the computational costs of the multilayer model and of the FE discretization since the simulations uses different tools. Nevertheless, if the simulation cost of a single layer Saint-Venant system is T, it is worth being noticed that without any parallelisation, the computational cost of a N layers system is only NT.

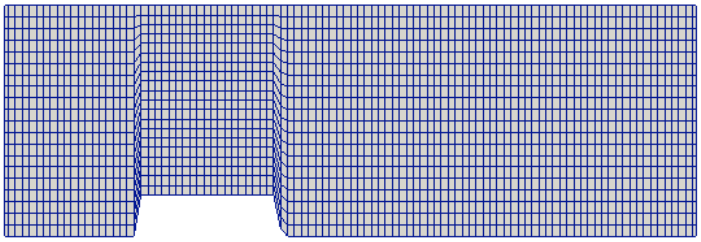

Figure V.7: The geometrical model with the horizontal mesh and the vertical discretization by layers.

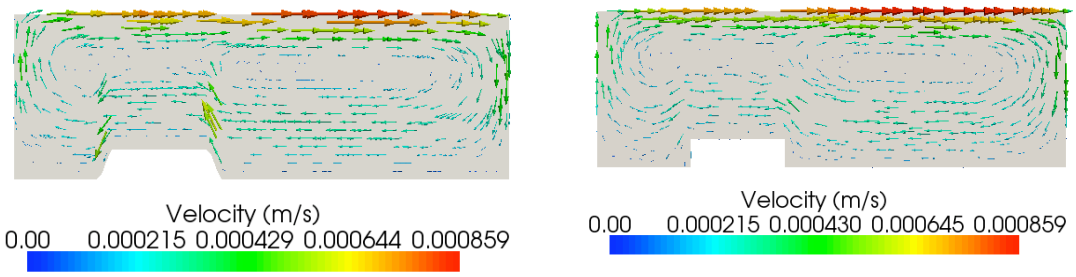

(a) *(b)*

Figure V.8: The wind blows from the left part of the domain to the right part. The arrows represent the velocity field in the lake. *(a)* multilayer code and *(b)* finite element code.

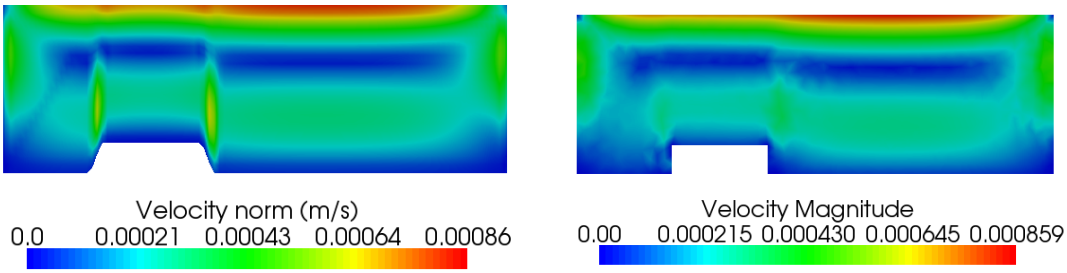

(a) *(b)*

Figure V.9: Same as Fig. V.8 but we plot the velocity norm $\sqrt{u^2+w^2}$.

6.2 Stratified flows

In this paragraph, we concentrate on situations where the density variations have crucial influence over the hydrodynamics. We consider the Navier-Stokes system with varying density described in paragraphs 5.9.

First we illustrate the behavior of the scheme in front of a non trivial static equilibria and then we present numerical experiments simulating density-stratified flows subjected to wind surface stress and internal waves. The density is considered a function of the water temperature, and we adopt the classical state equation (as in Eq. (V.108))

$$\rho(T) = \rho_0 \left(1 - \alpha (T - T_0)^2\right), \tag{V.115}$$

with $T_0 = 4\,^o\mathrm{C}$, $\alpha = 6.63\,10^{-6}\,^o\mathrm{C}^{-2}$ (volume coefficient of thermal expansion) and $\rho_0 = 10^3\,\mathrm{kg\,m}^{-3}$.

6.2.1 Static equilibria with non flat bottom

Here we illustrate the properties associated with the preservation of equilibria for stratified flows. When $\rho = \rho(T)$, the static equilibria correspond to situations where

$$\int_z^\eta \rho(T) dz = cst,$$

that is more complex to guarantee than in the constant density case where the static equilibrium reduces to $\eta = cst$.

When considering diffusion on the pollutant i.e. $\mu_T \neq 0$ in relation (V.109), the only possible static equilibria are trivial and correspond to

$$\frac{\partial T}{\partial x} = Cst, \quad \text{and} \quad \frac{\partial T}{\partial z} = Cst, \qquad \forall x, z, t.$$

To avoid these simplified situations, we consider in this paragraph $\mu_T = \nu_T = 0$. However our numerical schemes having small numerical dissipation, a Navier type bottom friction is considered in each simulation in order to reach a static equilibrium more quickly.

We consider a 3 meters long closed 1d basin with vertical shores and an initial water level of $H_0 + z_b = 1$ meter with the bottom geometry $z_b(x)$ defined by the parabolic bump

$$z_b(x) = \max(-1, -0.75 - 1.246(x - 1.2)^2),$$

The mesh has 100 nodes in the x direction.

In Figs. V.10 and V.11, we illustrate in the case of a non flat bottom the behavior of the scheme when starting from an unstable state. For the first example, presented in Fig. V.10, at $t = t_0$ the temperature is distributed as follows

$$T^0(x,z) = \begin{cases} 25^o C & \text{if } z - z_b \geqslant 2H_0(x)/3 \\ 8^o C & \text{otherwise} \end{cases}$$

$H_0(x)$ being the total water depth. For the simulation we have used a vertical discretization with 20 equally spaced layers i.e. $l_\alpha = 1/20$ for $\alpha = 1, \ldots, 20$. The postprocessing visualization tool performs a linear interpolation of the constant cell data that explains the small diffusion which is observed at initial time.

With the same geometry, still with a flow initially at rest but starting from an initial temperature distribution far from any equilibrium, see Fig. V.11-*(a)*, the system also reaches a stable static equilibrium, see Fig. V.11-*(b)*.

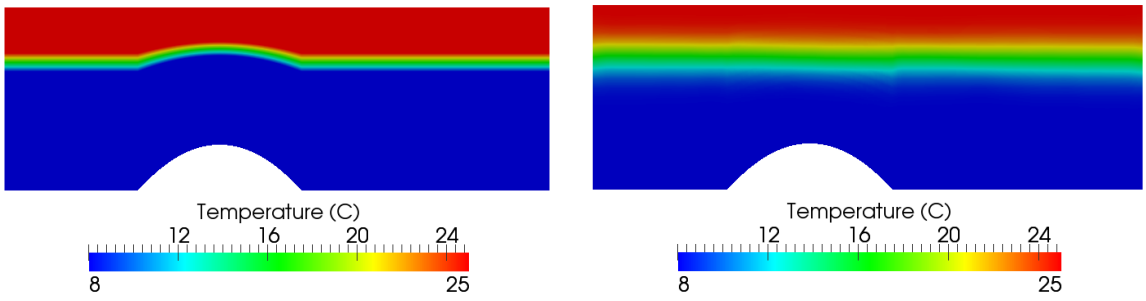

(a) *(b)*

Figure V.10: *(a)* initial state and *(b)* static equilibrium reached after 10 minutes.

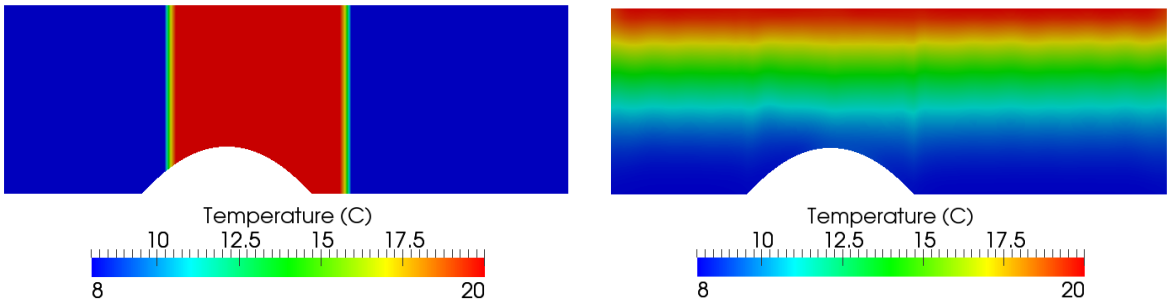

(a) *(b)*

Figure V.11: *(a)* initial state and *(b)* static equilibrium reached after 20 minutes.

6.2.2 Wind forced flows

The response of stratified flows to wind forcing is a typical situation in geophysical flows modeling. In this paragraph we first compare our numerical scheme to a local analytical solution then reproduce upwelling phenomena.

The typical thermal stratification of natural lakes and hydraulic reservoirs consists of a warmer less dense surface layer, a colder denser bottom layer, and a middle layer characterized by a steep vertical thermal gradient, the center of which is the thermocline. Thermo-hydrodynamical phenomena in lakes subject to the action of wind have been studied since a long time, by means of observations and measurements *in situ* [132, 105], laboratory experiments [105, 82, 104, 125], theoretical analysis [71, 103, 76], and, more recently, numerical simulations [129, 45, 73, 109]. Classically, in the literature the lake temperature distribution is schematized by a two-layer or three-layer thermal stratification.

When wind blows over these stratified systems, the thermocline is deflected upward in the upwind region. The thermocline behaves as a barrier between an upper region with circular fluid motion that has the same direction as the wind at the surface, and a lower region with fluid rotating in the opposite sense. If the wind is sufficiently strong then the thermocline reaches the surface at the upwind end of the basin and *upwelling* of deep fluid in the windward region occurs. This is quite different from the effect of wind forcing a homogeneous basin, where wind induces a simple circular motion of the fluid mass.

Analytical validation In this paragraph, we confront our numerical scheme to a local analytical solution. We consider a fluid in an enclosed rectangular basin, and we impose a constant uniform wind stress from left to right at the free surface. In order to take into account the wind effects, a modification of the bounadary condition (I.10) is necessary. We denote with τ_w the surface wind stress, for which the following expression [75] is considered

$$\tau_w = C_D \frac{\rho_a}{\rho_0} |V_w| V_w. \tag{V.116}$$

Here V_w is the wind velocity, ρ_a the air density, ρ_0 a reference water density, and C_D the wind drag coefficient (taken as $C_D = 1.3 \times 10^{-3}$ in the numerical experiments). Assuming negligible the air viscosity, the continuity of stresses at the free boundary imposes

$$\Sigma_T \mathbf{n}_s = \tau_w \mathbf{t}_s, \tag{V.117}$$

where $\mathbf{t}_s$ is the unit vector orthogonal to $\mathbf{n}_s$. Relation (V.117) is equivalent to

$$\mathbf{n}_s \cdot \Sigma_T \mathbf{n}_s = 0, \quad \text{and} \quad \mathbf{t}_s \cdot \Sigma_T \mathbf{n}_s = \tau_w.$$

The simulations start with a basin at rest with the following two-layer temperature distribution (see Fig. V.12)

$$T_0(x,z) = \begin{cases} 25^o C \text{ if } z - z_b \geqslant 2H_0(x)/3 \\ 8^o C \text{ else} \end{cases}$$

where H_0 is the initial water height. Notice that since at $t_0 = 0$ we have

$$\frac{\partial \rho}{\partial z} \leqslant 0,$$

the initial state corresponds to a stable equilibrium. In such a situation, the system is supposed to reach a stationary regime described schematically by Fig. V.12.

In the case of constant density, there exists an analytical solution of the horizontal velocity vertical profile at mid-length of the lake that is compatible with stationary Navier-Stokes equations. This calculation is detailed in [124]. Here we extend this local analytical solution to the case of varying density. The calculus of this analytical solution is described in Appendix A, see also [15].

We have used a viscosity of $\nu = 0.003$ m^2.s^{-1}, a Navier friction coefficient of $\kappa = 0.1$ m.s^{-1} and a wind velocity of 6 m.s^{-1}.

Notice that we have $\frac{\partial H}{\partial x}\frac{\partial H_1}{\partial x} < 0$ meaning the slope of the interface $z = H_1$ is significant and in the opposite direction compared to the free surface variations.

In Fig. V.13-*(a)* we compare the analytical solution with the results obtained with the multilayer model for different vertical discretizations. Fig. V.13-*(a)* presents the results obtained with 10, 30

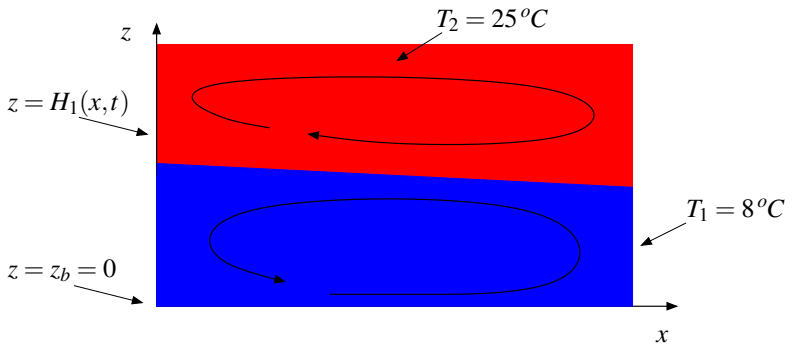

Figure V.12: Flow domain with water height $H(x,t)$, interface $H_1(x,t)$ and with the double-gyre phenomenon.

and 50 layers. For each mesh, the horizontal discretization is taken very precise meaning the error associated with this discretization can be neglected. The results presented in Fig. V.13-*(a)* are in good agreement with the analytical solution.

In Fig. V.13-*(b)*, we plot the rate of error versus the vertical discretization, namely the number of layers. We have plotted the $\log(L^1 - error)$ of the horizontal velocity – at mid-length of the domain – versus $\log(h_0/h_i)$. We denote by h_i the average cell height, h_0 is the average cell height of the coarser mesh. These errors have been computed on 5 meshes with 5, 10, 20, 30 and 50 layers. It has to be noticed that the expression of the analytical solution gives $\frac{\partial H_1}{\partial x} < 0$. But since the velocity at the interface is tangent to $z = H_1$, this means we have $w \neq 0$ near $z = H_1$ so the initial assumption $w \approx 0$ is not completly true. For these reasons, the analytical solution and the simulated velocity at mid-length of the basin are not completly consistent and the convergence rate appearing in Fig. V.13-*(b)* is not completely meaningful.

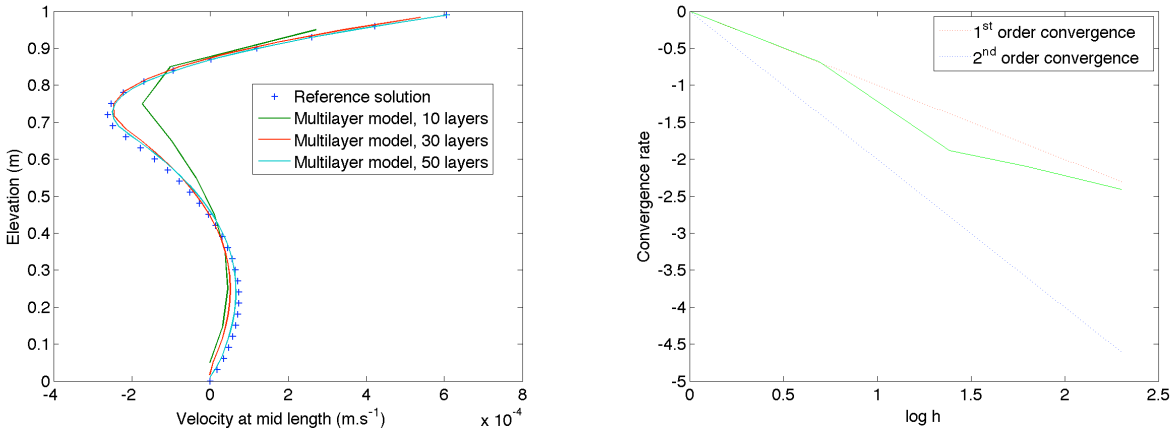

(a) *(b)*

Figure V.13: Comparison between the analytical and numerical velocities at mid length of the basin.

Response to wind stress and upwelling Here we consider the test case depicted in the previous paragraph but with a larger wind velocity. The domain is a closed basin of 3 meters long with an initial water height of 1 meter. The mesh has 100 nodes in the x direction and 30 layers. The wind velocity (from left to right) is $20\,\mathrm{m.s}^{-1}$. We have used a viscosity of $\nu = \nu_T = 0.001\,\mathrm{m}^2.\mathrm{s}^{-1}$ and a Navier type bottom friction with $\kappa = 0.1\mathrm{m.s}^{-1}$. In Fig. V.14, we show at different times the computed temperature distribution and the velocity field. The right column corresponds to the case of a variable density

obeying to the equation of state (see Eqs. (V.108) and (V.115)). The left column has been obtained with analogous configuration and initial conditions except that we have considered constant density: $\rho(T) \equiv \rho_0$. This means that T is merely a passive tracer that does not affect the density. Then, the differences between the right and left columns highlight the influence of the density variations on the flow response to wind forcing.

Notice that when the density variations are not considered the velocity profile along the vertical axis satisfies – far from the shores –

$$\frac{\partial^2 u}{\partial z^2} > 0,$$

whereas when the density variations are taken into account this quantity changes of sign when z varies from the bottom to the free surface. Because of the viscosity, this induces large dissipation and thus explains why the velocities are smaller on the left column than on the right one, see especially Fig. V.14 (last picture on the left column). In the varying density case, the velocity field of the flow has reached a stationary state after $t = t_2$. In the constant density case, it is clear that no stationary state exists for the temperature distribution except an homogenous situation $T(x,z,t) = \bar{T}$. The shear stress coming from the wind induces a gradient of the free surface. Since the corresponding deformations of the free surface are small, they are not visible in Fig. V.14.

Due to the simplicity of our physical model (uniform diffusivity, hydrostatic pressure), the aim of our numerical tests here is not attempting to reproduce realistic limnological processes on a long time scale. Rather, we emphasize the influence of density variations on the hydrodynamical response of the water body. In particular, the results of the simulations with variable density show that the numerical model is able to describe the tilting of the thermocline and upwelling of deeper fluid to the surface. Thus we are able to capture the essential features of the expected hydrodynamical behavior until the occurrence of upwelling. The post-upwelling flow dynamics cannot be modeled effectively by the present simplified model, mainly because of the lack of a turbulent mixing model.

6.3 3d simulations

We have claimed our model and numerical scheme can be extended to 3d flows. We present in this paragraph some 3d simulations with a 3d hydrostatic Navier-Stokes system with varying density. The 3d Navier-Stokes code has been built using a 3d extension of the model presented in paragraphs 5.

The derivation of the 3d model is straightforward. The discretization is more tricky to obtain and we have followed the results proposed by Audusse et al. [12]. The scheme we have used is positive, well-balanced and satisfies a maximum principle for the tracer.

Since analytical solutions of the 3d hydrostatic Navier-Stokes are hardly accessible, we have confronted our code with situations reducing to 2d phenomena

- in the directions (x,z) such as those given in paragraphs 6.1 and 6.2,
- in the directions (x,y). In this case, we use our 3d code with only 1 layer ($N = 1$) and we compare it with existing codes solving the (x,y) Saint-Venant system.

In these two situations, the 3d code gives results that are similar to those obtained with

- the code developed by the author for the other proposed models,
- the 2d Saint-Venant code presented in [12].

Obviously our 3d model with 1 layer reduces to the 2d (x,y) Saint-Venant system. The computational cost of the 3d model with N layers and constant density is exactly N times the cost of the simple 2d (x,y) Saint-Venant code.

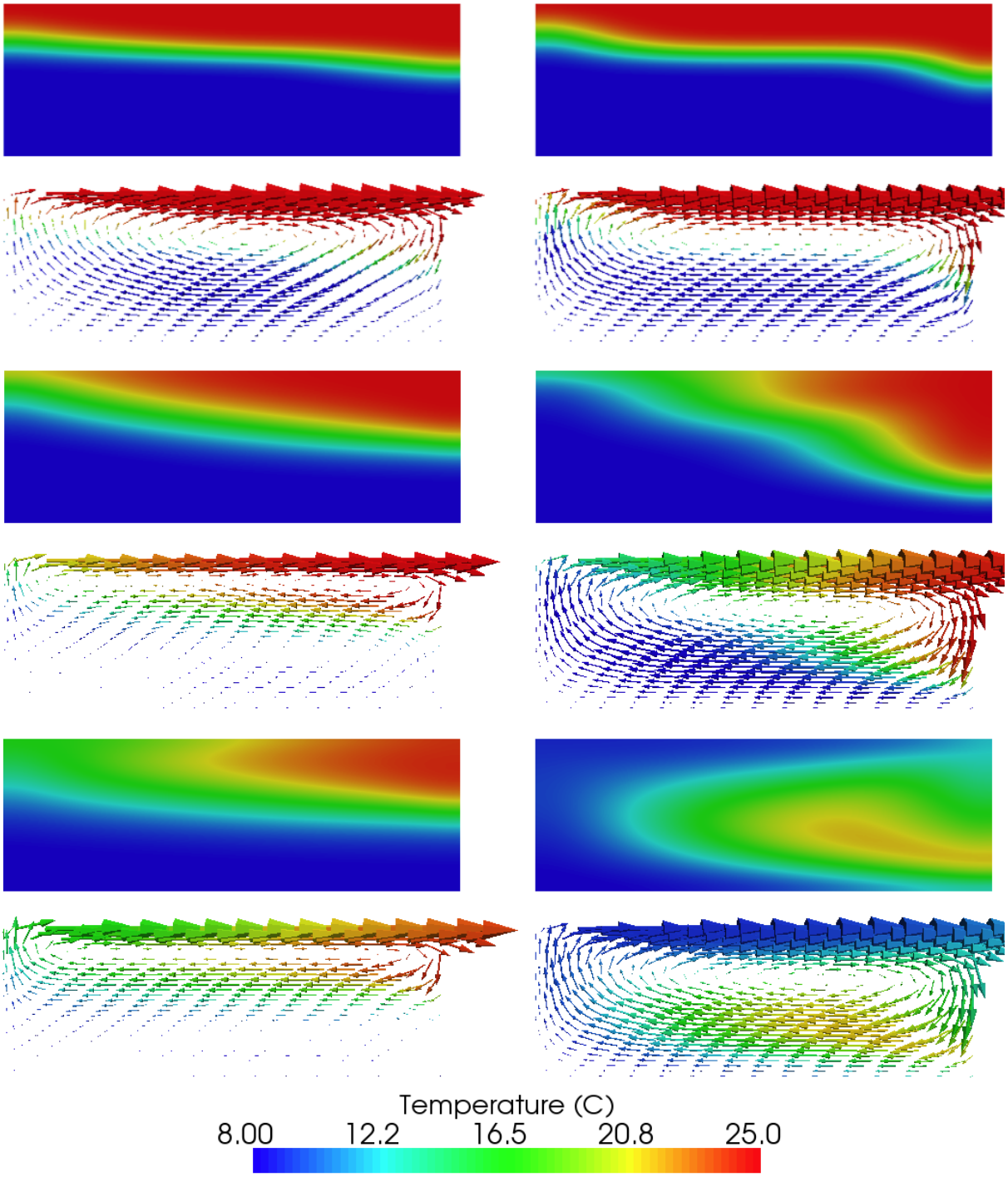

Figure V.14: Influence of the density variations, left column with $\rho = \rho(T)$, right : same simulation but with $\rho = \rho_0$. First line, at time $t_1 = 10\,\mathrm{s}$, second line at time $t_2 = 70\,\mathrm{s}$ and third line at time $t_3 = 140$ s.

6.3.1 Dam break simulation

We consider the case of a dam break in a channel with a locally rectangular section shortening and a bump before the shortening of the channel width (the bump is not in the middle of channel in the y direction), see Fig. V.15. The flow charateristics at four different instants are depicted in Fig. V.16. We have used the 3d model with 10 layers. The mesh has 3500 nodes. Initially the flow is at rest in the situation depicted over Fig. V.16 at time $t = 0\ s$.

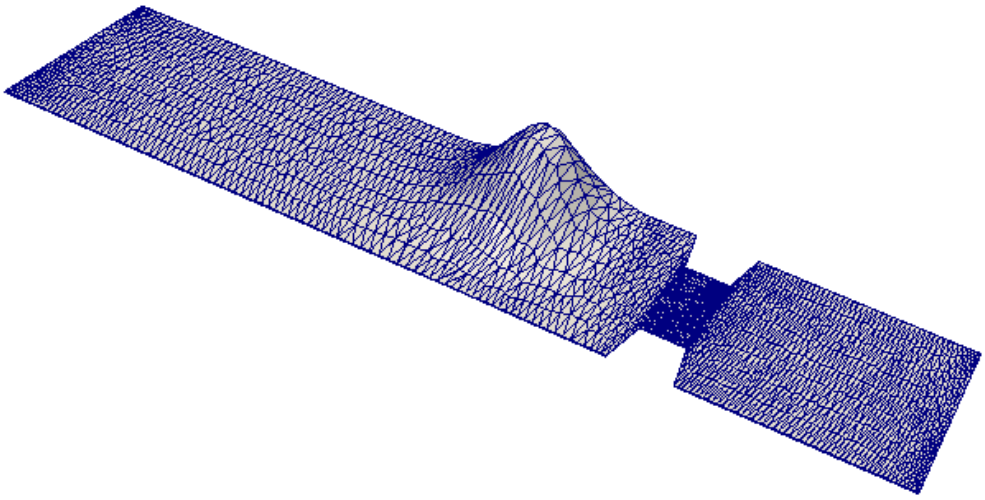

Figure V.15: Mesh representing the channel geometry.

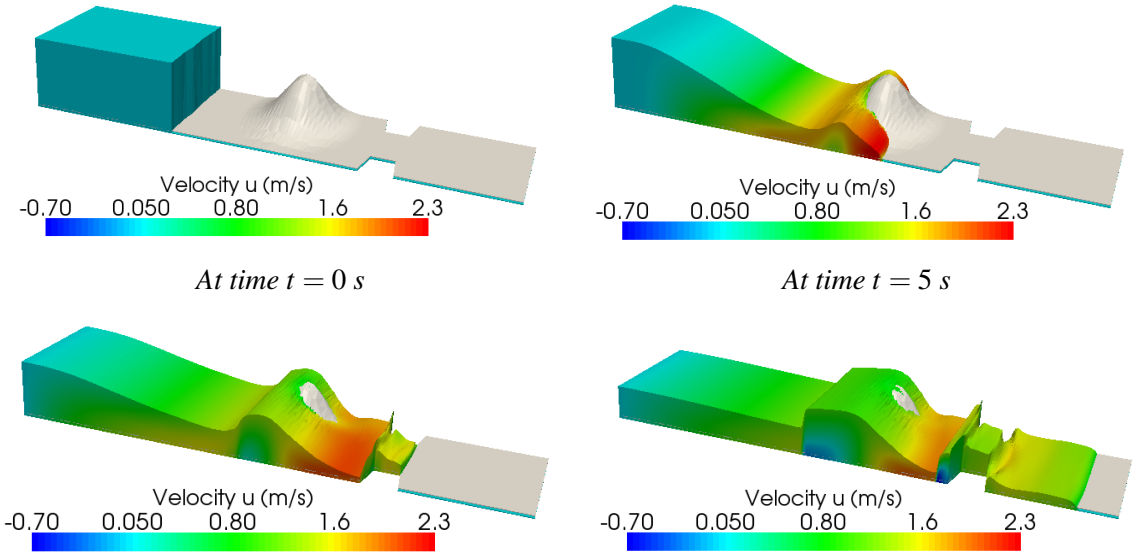

Figure V.16: Dam break simulation over dry bottom with an uneven topography. Water depth and velocity u at different instants.

When the bump is removed, the geometry corresponds exactly to a test case for which experimental measurements are available. Thus, considering a flat bottom we can compare the 3d results with the experimental data and with the results coming from the section-averaged Saint-Venant system. The comparison is given in Fig V.17 where we can see the 3d simulation is in good agreement with the experimental data and improves the results coming from the section-averaged system, see [64].

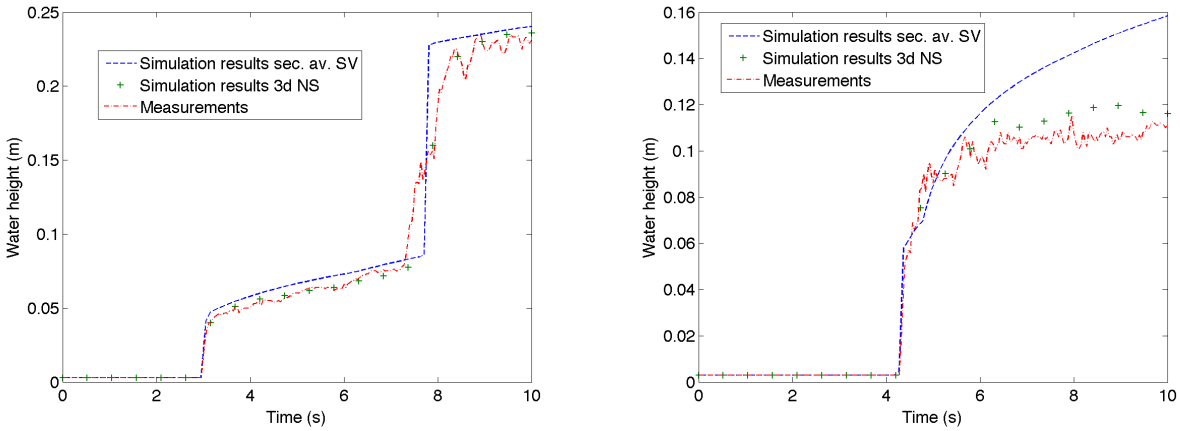

Sensor 2 *Sensor 3*

Figure V.17: Comparison of the simulations obtained with the 3d code and with the section-averaged code, results for sensors 2 and 3 located just before and in the middle of the shortening.

6.3.2 Wind driven stratified flows

In this test case, we consider the same channel geometry as depicted in Fig. V.15. The basin is initially at rest with hot water near the free surface and colder water near the bottom, see Fig. V.18.

The water density is kept constant i.e. it does not depend on the temperature. The wind blows (25 $m.s^{-1}$) parallel to the long axis of the basin (x-axis). At two different instants we give the temperature distribution and the velocity field, see Fig. V.19. In the case of a rectangular bassin with flat bottom, we recover that the velocity field corresponds to the analytical solution given in Appendix A (p. 129).

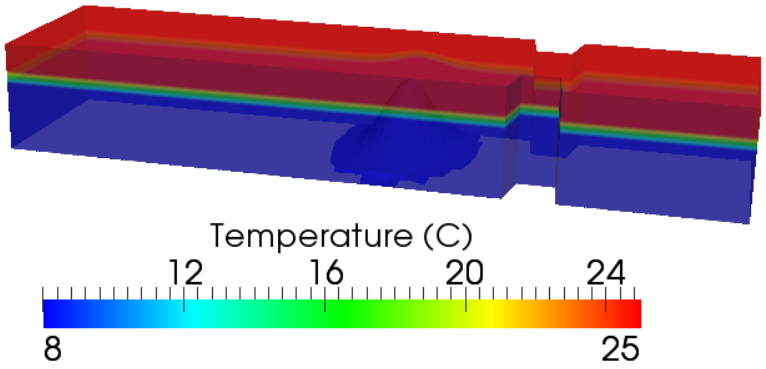

Figure V.18: Geometry and initial conditions.

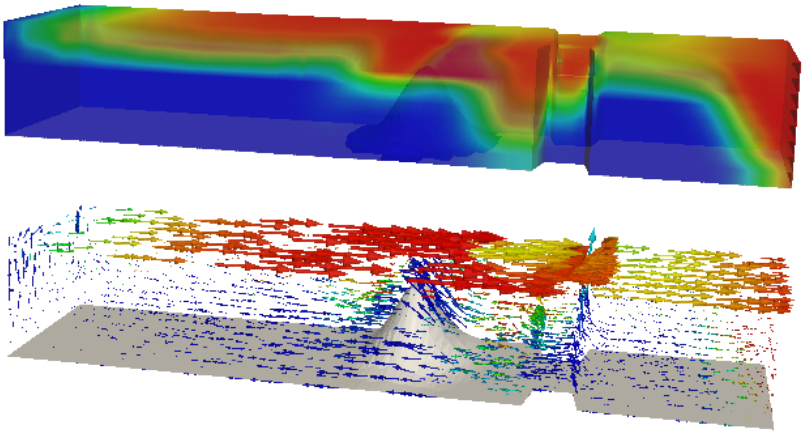

At time $t_1 = 100\ s$

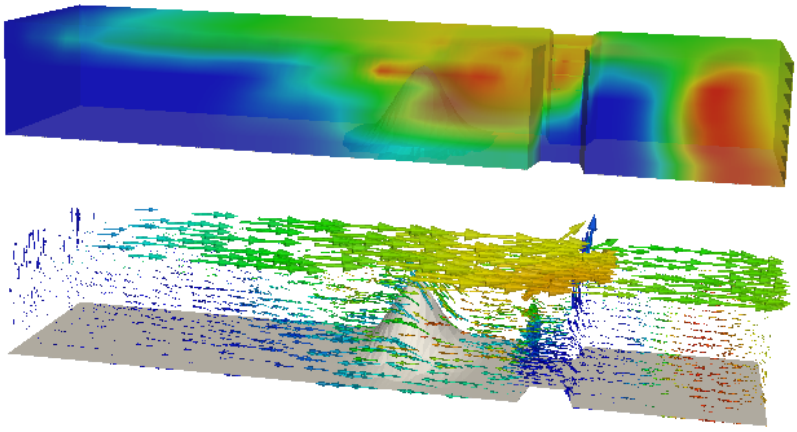

At time $t_2 = 200\ s$

Figure V.19: Wind driven flow. Temperature and velocity fields.

Bibliography

[1] *FreeFem++ home page*, http://www.freefem.org/ff++/index.htm, 2009.

[2] *Fullswof project home page*, http://www.univ-orleans.fr/mapmo/soft/FullSWOF/, 2011.

[3] B. Alvarez-Samaniego and D. Lannes, *Large time existence for 3D water-waves and asymptotics*, Invent. Math. **171** (2008), no. 3, 485–541. MR 2372806 (2009b:35324)

[4] Christophe Ancey, *Plasticity and geophysical flows: A review*, Journal of Non-Newtonian Fluid Mechanics **142** (2007), no. 1–3, 4 – 35, Viscoplastic fluids: From theory to application.

[5] F. Asakura, *Global solutions with a single transonic shock wave for quasilinear hyperbolic systems*, Methods Appl. Anal. **4** (1997), no. 1, 33–52. MR 1457203 (98d:35143)

[6] E. Audusse, *A multilayer Saint-Venant System : Derivation and Numerical Validation*, Discrete Contin. Dyn. Syst. Ser. B **5** (2005), no. 2, 189–214.

[7] E. Audusse, F. Benkhaldoun, J. Sainte-Marie, and M. Seaid, *Multilayer Saint-Venant Equations over movable beds*, Discrete Contin. Dyn. Syst. Ser. B **15** (2011), no. 4, 917–934.

[8] E. Audusse, F. Bouchut, M.-O. Bristeau, R. Klein, and B. Perthame, *A fast and stable well-balanced scheme with hydrostatic reconstruction for shallow water flows*, SIAM J. Sci. Comput. **25** (2004), no. 6, 2050–2065 (electronic). MR MR2086830 (2005f:76069)

[9] ———, *A fast and stable well-balanced scheme with hydrostatic reconstruction for Shallow Water flows*, SIAM J. Sci. Comput. **25** (2004), no. 6, 2050–2065.

[10] E. Audusse, F. Bouchut, M.-O. Bristeau, and J. Sainte-Marie, *Kinetic entropy inequality and hydrostatic reconstruction scheme for the Saint-Venant system*, September 2014.

[11] E. Audusse and M.-O. Bristeau, *Transport of pollutant in shallow water flows : A two time steps kinetic method*, ESAIM: M2AN **37** (2003), no. 2, 389–416.

[12] ———, *A well-balanced positivity preserving second-order scheme for shallow water flows on unstructured meshes.*, J. Comput. Phys. **206** (2005), no. 1, 311–333.

[13] ———, *Finite-volume solvers for a multilayer Saint-Venant system*, Int. J. Appl. Math. Comput. Sci. **17** (2007), no. 3, 311–319.

[14] E. Audusse, M.-O. Bristeau, and A. Decoene, *Numerical simulations of 3d free surface flows by a multilayer Saint-Venant model*, Internat. J. Numer. Methods Fluids **56** (2008), no. 3, 331–350.

[15] E. Audusse, M.-O. Bristeau, M. Pelanti, and J. Sainte-Marie, *Approximation of the hydrostatic Navier-Stokes system for density stratified flows by a multilayer model. Kinetic interpretation and numerical validation.*, J. Comp. Phys. **230** (2011), 3453–3478.

[16] E. Audusse, M.-O. Bristeau, B. Perthame, and J. Sainte-Marie, *A multilayer Saint-Venant system with mass exchanges for Shallow Water flows. Derivation and numerical validation.*, ESAIM: M2AN **45** (2011), 169–200.

[17] A.-J.-C. Barré de Saint-Venant, *Théorie du mouvement non permanent des eaux avec applications aux crues des rivières et à l'introduction des marées dans leur lit*, C. R. Acad. Sci. Paris **73** (1871), 147–154.

[18] O. Besson and M.R. Laydi, *Some estimates for the anisotropic Navier-Stokes equations and for the hydrostatic approximation*, M2AN **26** (1992), 855–865.

[19] E. C. Bingham, *An Investigation of the Laws of Plastic Flow*, U.S. Bureau of Standards Bulletin **13** (1916), 309–353.

[20] J.-L. Bona, T.-B. Benjamin, and J.-J. Mahony, *Model equations for long waves in nonlinear dispersive systems*, Philos. Trans. Royal Soc. London Series A **272** (1972), 47–78.

[21] P. Bonneton, E. Barthelemy, F. Chazel, R. Cienfuegos, D. Lannes, F. Marche, and M. Tissier, *Recent advances in Serre-Green Naghdi modelling for wave transformation, breaking and runup processes*, European Journal of Mechanics - B/Fluids **30** (2011), no. 6, 589 – 597, Special Issue: Nearshore Hydrodynamics. MR 2906225 (2012j:76018)

[22] Philippe Bonneton, *Note sur la propagation des vagues en zone de surf interne*, Comptes Rendus de l'Académie des Sciences - Series IIB - Mechanics **329** (2001), no. 1, 27 – 33.

[23] F. Bouchut, *An introduction to finite volume methods for hyperbolic conservation laws.*, ESAIM Proc. **15** (2004), 107–127.

[24] _____, *Nonlinear stability of finite volume methods for hyperbolic conservation laws and well-balanced schemes for sources*, Frontiers in Mathematics, Birkhauser Verlag, Basel, 2004. MR 2128209

[25] F. Bouchut and S. Boyaval, *Unified formal reduction for fluid models of free-surface shallow gravity-flows*, June 2013.

[26] F. Bouchut and T. Morales de Luna, *An entropy satisfying scheme for two-layer shallow water equations with uncoupled treatment*, M2AN Math. Model. Numer. Anal. **42** (2008), 683–698.

[27] F. Bouchut, H. Ounaissa, and B. Perthame, *Upwinding of the source term at interfaces for Euler equations with high friction*, Comput. Math. Appl. **53** (2007), no. 3-4, 361–375. MR MR2323698

[28] F. Bouchut and M. Westdickenberg, *Gravity driven shallow water models for arbitrary topography*, Comm. in Math. Sci. **2** (2004), 359–389.

[29] F. Bouchut and V. Zeitlin, *A robust well-balanced scheme for multi-layer shallow water equations*, Discrete Contin. Dyn. Syst. Ser. B **13** (2010), 739–758.

[30] Y. Brenier, *Homogeneous hydrostatic flows with convex velocity profiles*, Nonlinearity **12** (1999), no. 3, 495–512. MR 1690189 (2000b:35205)

[31] M.-O. Bristeau, N. Goutal, and J. Sainte-Marie, *Numerical simulations of a non-hydrostatic Shallow Water model*, Computers & Fluids **47** (2011), no. 1, 51–64. MR 2949395

[32] M. O. Bristeau, A. Mangeney, J. Sainte-Marie, and N. Seguin, *An energy-consistent depth-averaged euler system: derivation and properties.*, Discrete Contin. Dyn. Syst. Ser. B **20** (2015), no. 4, 961–988.

[33] M.-O. Bristeau and J. Sainte-Marie, *Derivation of a non-hydrostatic shallow water model; Comparison with Saint-Venant and Boussinesq systems*, Discrete Contin. Dyn. Syst. Ser. B **10** (2008), no. 4, 733–759.

[34] M.O. Bristeau and B. Coussin, *Boundary Conditions for the Shallow Water Equations solved by Kinetic Schemes*, Research Report RR-4282, INRIA, 2001.

[35] R. Camassa, D. D. Holm, and C. D. Levermore, *Long-time effects of bottom topography in shallow water*, Phys. D **98** (1996), no. 2-4, 258–286, Nonlinear phenomena in ocean dynamics (Los Alamos, NM, 1995). MR 1422281 (98a:76005)

[36] R. Camassa, D.D. Holm, and J.M. Hyman, *A new integrable shallow water equation*, Adv. Appl. Math. **31** (1993), 23–40.

[37] M.-J. Castro, J. Macías, and C. Parés, *A q-scheme for a class of systems of coupled conservation laws with source term. application to a two-layer 1-D shallow water system.*, M2AN Math. Model. Numer. Anal. **35** (2001), no. 1, 107–127.

[38] M.J. Castro, J.A. García-Rodríguez, J.M. González-Vida, J. Macías, C. Parés, and M.E. Vázquez-Cendón, *Numerical simulation of two-layer shallow water flows through channels with irregular geometry*, J. Comput. Phys. **195** (2004), no. 1, 202–235.

[39] M.-J. Castro Díaz, E.-D. Fernández-Nieto, and A.-M. Ferreiro, *Sediment transport models in shallow water equations and numerical approach by high order finite volume methods*, Computers & Fluids **37** (2008), no. 3, 299–316.

[40] M.J. Castro Díaz, E.D. Fernández-Nieto, A.M. Ferreiro, and C. Parés, *Two-dimensional sediment transport models in shallow water equations. a second order finite volume approach on unstructured meshes*, Computer Methods in Applied Mechanics and Engineering **198** (2009), no. 33-36, 2520 – 2538.

[41] C. Chalons, F. Coquel, E. Godlewski, P.-A. Raviart, and N. Seguin, *Godunov-type schemes for hyperbolic systems with parameter-dependent source. The case of Euler system with friction*, Math. Models Methods Appl. Sci. **20** (2010), no. 11, 2109–2166. MR 2740716

[42] F. Chazel, D. Lannes, and F. Marche, *Numerical simulation of strongly nonlinear and dispersive waves using a Green–Naghdi model*, J. Sci. Comput. **48** (2011), no. 1-3, 105–116. MR 2811693 (2012e:76015)

[43] A. Chinnayya, A.-Y. LeRoux, and N. Seguin, *A well-balanced numerical scheme for the approximation of the shallow-water equations with topography: the resonance phenomenon*, Int. J. Finite Volumes (2004), 1–33.

[44] A. J. Chorin, *Numerical solution of the Navier-Stokes equations*, Math. Comp. **22** (1968), 745–762. MR 0242392 (39 #3723)

[45] C. R. Chu and C. K. Soong, *Numerical simulation of wind-induced entrainment in a stably stratified water basin*, J. Hydraul. Research IAHR **35** (1997), 21–41.

[46] C. A. Coulomb, *Essai sur une application des règles des maximis et minimis à quelques problemes de statique relatifs à l'architecture*, .Mem. Acad. Roy. Div. Sav. **7** (1776), 343–387.

[47] R. V. Craster and O. K. Matar, *Dynamics and stability of thin liquid films*, Rev. Mod. Phys. **81** (2009), 1131–1198.

[48] A. Crotogino and K.P. Holz, *Numerical movable-bed models for practical engineering.*, Applied Mathematical Modelling **8** (1984), 45–49.

[49] C. Dafermos, *Hyperbolic conservation laws in continuum physics*, Springer Verlag, Berlin, 1999.

[50] C. M. Dafermos and R. Pan, *Global BV solutions for the p-system with frictional damping*, SIAM J. Math. Anal. **41** (2009), no. 3, 1190–1205. MR 2529961

[51] A. Decoene, L. Bonaventura, E. Miglio, and F. Saleri, *Asymptotic derivation of the section-averaged shallow water equations for river hydraulics*, M3AS **19** (2009), no. 3, 387–417.

[52] A. Decoene and J.-F. Gerbeau, *Sigma transformation and ALE formulation for three-dimensional free surface flows.*, Internat. J. Numer. Methods Fluids **59** (2009), no. 4, 357–386.

[53] R. F. Dressler, *Mathematical solution of the problem of roll-waves in inclined open channels*, Comm. Pure Appl. Math. **2** (1949), 149–194. MR 0033717 (11,480d)

[54] D. C. Drucker and W. Prager, *Soil mechanics and plastic analysis for limit design.*, Quarterly of Applied Mathematics **10** (1952), no. 2, 157–165.

[55] S. Ferrari and F. Saleri, *A new two-dimensional Shallow Water model including pressure effects and slow varying bottom topography*, M2AN Math. Model. Numer. Anal. **38** (2004), no. 2, 211–234.

[56] T. Gallouët, J.-M. Hérard, and N. Seguin, *Some approximate Godunov schemes to compute shallow-water equations with topography*, Comput. & Fluids **32** (2003), no. 4, 479–513. MR MR1966639 (2004a:76095)

[57] J.-F. Gerbeau and B. Perthame, *Derivation of Viscous Saint-Venant System for Laminar Shallow Water; Numerical Validation*, Discrete Contin. Dyn. Syst. Ser. B **1** (2001), no. 1, 89–102.

[58] P. Goatin and Philippe G. LeFloch, *The Riemann problem for a class of resonant hyperbolic systems of balance laws*, Ann. Inst. H. Poincaré Anal. Non Linéaire **21** (2004), no. 6, 881–902. MR 2097035 (2006i:35225)

[59] E. Godlewski and P.-A. Raviart, *Numerical approximation of hyperbolic systems of conservation laws*, Applied Mathematical Sciences, vol. 118, Springer-Verlag, New York, 1996. MR MR1410987 (98d:65109)

[60] E. Godlewski and P.-A. Raviart, *Numerical approximation of hyperbolic systems of conservation laws*, Springer Verlag, 1996.

[61] S. K. Godunov, *A difference method for numerical calculation of discontinuous solutions of the equations of hydrodynamics*, Mat. Sb. (N.S.) **47 (89)** (1959), 271–306. MR MR0119433 (22 #10194)

[62] L. Gosse, *Computing qualitatively correct approximations of balance laws*, SIMAI Springer Series, vol. 2, Springer, Milan, 2013, Exponential-fit, well-balanced and asymptotic-preserving. MR 3053000

[63] L. Gosse and A.-Y. LeRoux, *Un schéma-équilibre adapté aux lois de conservation scalaires non-homogènes*, C. R. Acad. Sci. Paris Sér. I Math. **323** (1996), no. 5, 543–546. MR MR1408992 (97i:35112)

[64] N. Goutal and J. Sainte-Marie, *A kinetic interpretation of the section-averaged Saint-Venant system for natural river hydraulics.*, Int. J. Numer. Meth. Fluids **67** (2011), no. 7, 914–938.

[65] A.J. Grass, *Sediment transport by waves and currents.*, Tech. Report FL29, SERC London Cent. Mar., 1981.

[66] A. E. Green, N. Laws, and P. M. Naghdi, *On the theory of water waves*, Proc. Roy. Soc. (London) Ser. A **338** (1974), 43–55. MR 0349127 (50 #1621)

[67] A.E. Green and P.M. Naghdi, *A derivation of equations for wave propagation in water of variable depth*, J. Fluid Mech. **78** (1976), 237–246.

[68] J. M. Greenberg and A.-Y. LeRoux, *A well-balanced scheme for the numerical processing of source terms in hyperbolic equations*, SIAM J. Numer. Anal. **33** (1996), no. 1, 1–16. MR MR1377240 (97c:65144)

[69] E. Grenier, *On the derivation of homogeneous hydrostatic equations*, ESAIM: M2AN **33** (1999), no. 5, 965–970. MR 1726718 (2000j:76051)

[70] B. Haspot, *Cauchy problem for viscous shallow water equations with a term of capillarity*, Math. Models Methods Appl. Sci. **20** (2010), no. 7, 1049–1087.

[71] N. S. Heaps and A. E. Ramsbottom, *Wind effects on water in a narrow two-layered lake*, Phil. Trans. R. Soc. London A **312** (1966), 391–430.

[72] R. Herschel, W.H.; Bulkley, *Konsistenzmessungen von Gummi-Benzollösungen*, Kolloid Zeitschrift **39** (1926), 291–300.

[73] R. Hodges, J. Imberger, A. Saggio, and K. B. Winters, *Modeling basin-scale internal waves in a stratified lake*, Limnol. Oceanogr. **45** (2000), no. 7, 1603–1620.

[74] D. D. Houghton and A. Kasahara, *Nonlinear shallow fluid flow over an isolated ridge*, Communications on Pure and Applied Mathematics **21** (1968), no. 1, 1–23.

[75] J. Imberger, *Physical processes in lakes and oceans*, American Geophysical Union, 1998.

[76] J. Imberger and J. C. Patterson, *Physical limnology*, Adv. Applied Mech. **27** (1990), 303–475.

[77] E. Isaacson and B. Temple, *Nonlinear resonance in systems of conservation laws*, SIAM J. Appl. Math. **52** (1992), no. 5, 1260–1278. MR MR1182123 (93f:35140)

[78] ———, *Convergence of the* 2×2 *Godunov method for a general resonant nonlinear balance law*, SIAM J. Appl. Math. **55** (1995), no. 3, 625–640. MR MR1331577 (96c:65146)

[79] S. Jin and M. A. Katsoulakis, *Hyperbolic systems with supercharacteristic relaxations and roll waves*, SIAM J. Appl. Math. **61** (2000), no. 1, 273–292 (electronic). MR 1776396 (2001h:35116)

[80] S. Jin and C. D. Levermore, *Numerical schemes for hyperbolic conservation laws with stiff relaxation terms*, J. Comput. Phys. **126** (1996), no. 2, 449–467. MR 1404381 (97g:65173)

[81] T. Kato, *Trotter's product formula for an arbitrary pair of self-adjoint contraction semigroups*, Topics in functional analysis (essays dedicated to M. G. Kreĭn on the occasion of his 70th birthday), Adv. in Math. Suppl. Stud., vol. 3, Academic Press, New York, 1978, pp. 185–195. MR 538020 (80i:47040)

[82] C. Kranenburg, *Mixed-layer deepening in lakes after wind set-up*, J. Hydraul. Div. ASCE **111** (1985), 334–354.

[83] O. Le Métayer, S. Gavrilyuk, and S. Hank, *A numerical scheme for the Green-Naghdi model*, J. Comp. Phys. **229** (2010), no. 6, 2034–2045. MR 2586235 (2010j:65134)

[84] A.-Y. LeRoux, *Riemann solvers for some hyperbolic problems with a source term*, Actes du 30ème Congrès d'Analyse Numérique: CANum '98 (Arles, 1998), ESAIM Proc., vol. 6, Soc. Math. Appl. Indust., Paris, 1999, pp. 75–90 (electronic). MR MR1689443 (2000h:65119)

[85] R. J. LeVeque, *Finite volume methods for hyperbolic problems*, Cambridge Texts in Applied Mathematics, Cambridge University Press, Cambridge, 2002. MR MR1925043 (2003h:65001)

[86] C. David Levermore, *Entropy-based moment closures for kinetic equations*, Proceedings of the International Conference on Latest Developments and Fundamental Advances in Radiative Transfer (Los Angeles, CA, 1996), vol. 26, 1997, pp. 591–606. MR 1481496

[87] C.D. Levermore and M. Sammartino, *A shallow water model with eddy viscosity for basins with varying bottom topography*, Nonlinearity **14** (2001), no. 6, 1493–1515.

[88] Yi A. Li, *A shallow-water approximation to the full water wave problem*, Comm. Pure Appl. Math. **59** (2006), no. 9, 1225–1285. MR 2237287 (2007d:76024)

[89] P.-L. Lions, *Mathematical Topics in Fluid Mechanics. Vol. 1: Incompressible models.*, Oxford University Press, 1996.

[90] P.-L. Lions, B. Perthame, and E. Tadmor, *A kinetic formulation of multidimensional scalar conservation laws and related equations*, J. Amer. Math. Soc. **7** (1994), no. 1, 169–191. MR 1201239 (94d:35100)

[91] ———, *Kinetic formulation of the isentropic gas dynamics and p-systems*, Commun. Math. Physics **163** (1994), 415–431.

[92] P.L. Lions, B. Perthame, and P.E. Souganidis, *Existence of entropy solutions to isentropic gas dynamics system.*, Comm. Pure Appl. Math. **49** (1996), 599–638. MR 97e:35107

[93] C. Lusso, F. Bouchut, A. Ern, and A. Mangeney, *A simplified model of thin layer static/flowing dynamics for granular materials with yield*.

[94] I. MacDonald, M.J. Baines, N.K. Nichols, and P.G. Samuels, *Comparisons of some steady state Saint-Venant solvers for some test problems with analytic solutions.*, Tech. Report 3/95, Dept of Mathematics, University of Reading, 1995, http://www.reading.ac.uk/maths/research/maths-numanalrpts.aspx#1995.

[95] ———, *Steady open channel test problems with analytic solutions.*, Tech. Report 2/95, Dept of Mathematics, University of Reading, 1995, http://www.reading.ac.uk/maths/research/maths-numanalrpts.aspx#1995.

[96] N. Makarenko, *A second long-wave approximation in the Cauchy-Poisson problem (in russian)*, Dyn. Contin. Media **77** (1986), 56–72.

[97] A. Mangeney-Castelnau, B. Bouchut, J.P. Vilotte, E. Lajeunesse, A. Aubertin, and M. Pirulli, *On the use of Saint-Venant equations for simulating the spreading of a granular mass*, J. Geophys. Res. **110** (2005), B09103.

[98] F. Marche, *Derivation of a new two-dimensional viscous shallow water model with varying topography, bottom friction and capillary effects*, Eur. J. Mech. B Fluids **26** (2007), no. 1, 49–63. MR 2281291

[99] N. Masmoudi and T. Wong, *On the Hs theory of hydrostatic Euler equations*, Archive for Rational Mechanics and Analysis **204** (2012), no. 1, 231–271 (English). MR 2898740

[100] Ming Mei, *Best asymptotic profile for hyperbolic p-system with damping*, SIAM Journal on Mathematical Analysis **42** (2010), no. 1, 1–23.

[101] E. Meyer-Peter and Müller R., *Formulas for bed-load transport*, 2nd meeting on international association on hydraulic structures research (Stockholm), 1948, pp. 39–64.

[102] J. Miles and R. Salmon, *Weakly dispersive nonlinear gravity waves*, J. Fluid Mech. **157** (1985), 519–531. MR 808127 (86m:76021)

[103] S. G. Monismith, *Wind-forced motions in stratified lakes and their effect on mixed-layer shear*, Limnol. Oceanogr. **30** (1985), no. 4, 771–783.

[104] ———, *An experimental study of the upwelling response of stratified reservoirs to surface shear stress*, J. Fluid Mech. **171** (1986), 407–439.

[105] C. H. Mortimer, *Water movements in lakes during summer stratification; evidence from the distribution of temperature in Windermere*, Phil. Trans. R. Soc. B **236** (1952), 255–404.

[106] B. T. Nadiga, L. G. Margolin, and P. K. Smolarkiewicz, *Different approximations of shallow fluid flow over an obstacle*, Phys. Fluids **8** (1996), no. 8, 2066–2077.

[107] P. Noble, Analyse d'écoulements en eaux peu profondes et stabilité de solutions périodiques pour les équations de SaintVenant et des systèmes hamiltoniens discrets, Habilitation à diriger des recherches, Université Claude Bernard (Lyon I), 2009.

[108] O. Nwogu, *Alternative form of Boussinesq equations for nearshore wave propagation*, Journal of Waterway, Port, Coastal and Ocean Engineering, ASCE **119** (1993), no. 6, 618–638.

[109] P. Okely and J. Imberger, *Horizontal transport induced by upwelling in a canyon-shaped reservoir*, Hydrobiologia **586** (2007), 343–355.

[110] L. V. Ovsyannikov, *Two-layer shallow water models*, Prikl. Mekh. Tekh. Fiz. **2** (1979), 3–14.

[111] D.H. Peregrine, *Long waves on a beach*, J. Fluid Mech. **27** (1967), 815–827.

[112] B. Perthame, *Kinetic formulation of conservation laws.*, Oxford University Press, 2002.

[113] B. Perthame and C. Simeoni, *A kinetic scheme for the Saint-Venant system with a source term*, Calcolo **38** (2001), no. 4, 201–231.

[114] B. Perthame and E. Tadmor, *A kinetic equation with kinetic entropy functions for scalar conservation laws*, Commun. Math. Phys. **136** (1991), 501–517.

[115] O. Pouliquen and Y. Forterre, *A non-local rheology for dense granular flows*, Phil. Trans. R. Soc. A **367** (2009), no. 1909, 5091–5107.

[116] D. Pritchard and A.J. Hogg, *On sediment transport under dam-break flow.*, J. Fluid Mech. **473** (2002), 265–274.

[117] M. Reggio, A. Hess, and A. Ilinca, *3-d multiple-level simulation of free surface flows*, J. Hyd. Res. **44** (2002), no. 2, 413–423.

[118] A. Ritter, *Die fortpflanzung der wasserwellen*, Vereine Deutscher Ingenieure Zeitswchrift (in German) **36** (1892), no. 33, 947–954.

[119] G. Rosatti and L. Fraccarollo, *A well-balanced approach for flows over mobile-bed with high sediment-transport.*, J. Comput. Phys. **220** (2006), 312–338.

[120] K. C. Sahu, P. Valluri, P. D. M. Spelt, and O. K. Matar, *Linear instability of pressure-driven channel flow of a Newtonian and a Herschel-Bulkley fluid*, Phys. of Fluids **19** (2007), no. 12, –.

[121] J. Sainte-Marie, *Vertically averaged models for the free surface Euler system. Derivation and kinetic interpretation.*, Math. Models Methods Appl. Sci. (M3AS) **21** (2011), no. 3, 459–490.

[122] M.J. Salençon and J.M. Thébault, *Simulation model of a mesotrophic reservoir (lac de pareloup, france): Melodia, an ecosystem reservoir management model*, Ecological modelling **84** (1996), 163–187.

[123] D. Serre, *Systèmes de lois de conservation. II*, Fondations. [Foundations], Diderot Editeur, Paris, 1996, Structures géométriques, oscillation et problèmes mixtes. [Geometric structures, oscillation and mixed problems]. MR MR1459989 (99e:35144)

[124] N. J. Shankar, H. F. Cheong, and S. Sankaranarayanan, *Multilevel finite-difference model for three-dimensional hydrodynamic circulation*, Ocean Engineering **24** (1997), no. 9, 785–816.

[125] C. Stevens and J. Imberger, *The initial response of a stratified lake to a surface shear stress*, J. Fluid Mech. **312** (1996), 39–66.

[126] J. J. Stoker, *Water waves*, Wiley Classics Library, John Wiley & Sons Inc., New York, 1992, The mathematical theory with applications, Reprint of the 1957 original, A Wiley-Interscience Publication. MR 92m:76029

[127] C. H. Su and C. S. Gardner, *Korteweg-de Vries equation and generalizations. III. Derivation of the Korteweg-de Vries equation and Burgers equation*, J. Mathematical Phys. **10** (1969), 536–539. MR 0271526 (42 #6409)

[128] W. C. Thacker, *Some exact solutions to the non-linear shallow- water wave equations*, J. Fluid Mech. **107** (1981), 499–508.

[129] R. O. R. Y. Thomson and J. Imberger, *Response of a numerical model of a stratified lake to wind stress*, Second International Symposium on Stratified Flows, IAHR, Trondheim, Norway (T. Carsten and T. McClimans, eds.), 1980, pp. 562–570.

[130] H. F. Trotter, *On the product of semi-groups of operators*, Proc. Amer. Math. Soc. **10** (1959), 545–551. MR 0108732 (21 #7446)

[131] C. B. Vreugdenhil, *Two-layer shallow-water flow in two dimensions, a numerical study*, J. Comput. Phys. **33** (1979), 169–184.

[132] E. M. Wedderburn, *Temperature observations in Loch Earn, with a further contribution to the hydrodynamical theory of the temperature seiche*, Trans. R. Soc. Edin. **48** (1912), 629–695.

Appendix

A Local analytical solution for a two-layered flow subject to wind stress

We start with the two-dimensional hydrostatic Navier–Stokes system (V.105)-(V.109), with the initial conditions and the notations defined in Fig. V.12. Since we have a two-layered basin, the density can be written:

$$\rho(z) = \rho_1 + (\rho_2 - \rho_1) H_e(z - H_1), \tag{A.1}$$

where H_e is the Heaviside function and $\rho_i = \rho(T_i)$ for $i = 1,2$.

We look for the stationary solution of this problem, by assuming $\mu_T = 0$, and by considering a vertical viscosity only for the x-momentum equation. Near the mid-length of the basin we can assume

$$\frac{\partial u}{\partial x} \approx 0, \quad \text{and} \quad w \approx 0. \tag{A.2}$$

Therefore, in this region, the stationary solution of the system (V.105)-(V.107), (V.109), neglecting nonlinear convective terms, satisfies

$$\nu \frac{\partial^2 u}{\partial z^2} - g \frac{\partial}{\partial x} \int_z^\eta \rho(T)\, d\tilde{z} = 0. \tag{A.3}$$

By using (A.1) in the equilibrium condition above, we obtain

$$\nu \frac{\partial^2 u}{\partial z^2} - g\rho_2 \frac{\partial H}{\partial x} - g(\rho_1 - \rho_2) \frac{\partial H_1}{\partial x} H_e(H_1 - z) = 0. \tag{A.4}$$

Let τ_w and τ_b denote respectively the shear stress at the free surface (wind stress) and at the bottom (Navier friction). A first integration of (A.4) from z_b to z gives

$$\begin{aligned} \nu \frac{\partial u}{\partial z} - \tau_b &= \rho_2 g (z - z_b) \frac{\partial H}{\partial x} + (\rho_1 - \rho_2) g (z - z_b) \frac{\partial H_1}{\partial x} H_e(H_1 - z) \\ &\quad + (\rho_1 - \rho_2) g H_1 \frac{\partial H_1}{\partial x} H_e(z - H_1), \end{aligned}$$

and a second integration from z_b to z gives

$$\begin{aligned} \nu(u - u_b) &= (z - z_b)\tau_b + \frac{\rho_2 g}{2}(z - z_b)^2 \frac{\partial H}{\partial x} \\ &\quad + g(\rho_1 - \rho_2) \frac{\partial H_1}{\partial x} \left(\frac{(z - z_b)^2}{2} H_e(H_1 - z) + H_1 \left(z - \frac{H_1}{2} \right) H_e(z - H_1) \right). \end{aligned}$$

Then, the mass conservation condition in the layer where $T = T_1$ gives

$$-\nu u_b = \frac{H_1}{2}\tau_b + \frac{\rho_2 g}{6} H_1^2 \frac{\partial H}{\partial x} + \frac{(\rho_1 - \rho_2) g}{6} H_1^2 \frac{\partial H_1}{\partial x},$$

while mass conservation in the layer where $T = T_2$ leads to

$$-\nu u_b = \frac{H + H_1}{2}\tau_b + \frac{\rho_2 g}{6}(H^2 + H H_1 + H_1^2) \frac{\partial H}{\partial x} + (\rho_1 - \rho_2) g \frac{H_1}{2} \frac{\partial H_1}{\partial x}.$$

From the two previous relations, since we have a Navier type friction law at the bottom, i.e. $\tau_b = \kappa u_b$, we obtain

$$u_b = -\frac{1}{\alpha_1}\left(\frac{\rho_2 g}{6}H_1^2\frac{\partial H}{\partial x} + \frac{(\rho_1-\rho_2)g}{6}H_1^2\frac{\partial H_1}{\partial x}\right) \tag{A.5}$$

$$(\rho_1-\rho_2)\left(\frac{H_1^2}{6\alpha_1} - \frac{H_1 H}{2\alpha_{1,0}}\right)\frac{\partial H_1}{\partial x} = \frac{\rho_2}{6}\left(\frac{H^2+HH_1+H_1^2}{\alpha_{0,1}} - \frac{H_1^2}{\alpha_1}\right)\frac{\partial H}{\partial x}, \tag{A.6}$$

with $\alpha_1 = \nu + \kappa H_1/2$, $\alpha_{1,0} = \nu + \kappa(H+H_1)/2$. Now, integration of (A.4) from z_b to η gives

$$\tau_w - \kappa u_b = \rho_2 g H\frac{\partial H}{\partial x} + (\rho_1-\rho_2)gH_1\frac{\partial H_1}{\partial x}.$$

Hence, with obvious notations, we finally have

$$\frac{\partial H_1}{\partial x} = a\frac{\partial H}{\partial x}, \quad u_b = \tilde{K}\frac{\partial H}{\partial x}, \quad \tau_w = \tau\frac{\partial H}{\partial x}, \tag{A.7}$$

and

$$\begin{aligned} u(z) &= \left(\tilde{K} + \kappa\tilde{K}\frac{z-z_b}{\nu} + \frac{\rho_2 g}{2\nu}(z-z_b)^2 + \frac{(\rho_1-\rho_2)g}{2\nu}a(z-z_b)^2 H_e(H_1-z)\right. \\ &\quad \left. + \frac{(\rho_1-\rho_2)g}{\nu}aH_1\left(z-\frac{H_1}{2}\right)H_e(z-H_1)\right)\frac{\tau_w}{\tau}. \end{aligned}$$